PHARMACOLOGICAL AND COLD-INDUCED ALTERATIONS IN GLUCOSE AND FAT UTILIZATION: IMPLICATIONS FOR TISSUE-SPECIFIC AND WHOLE-BODY ENERGY METABOLISM

DIANE MIEKO SEPA-KISHI

A DISSERTATION SUBMITTED TO THE FACULTY OF GRADUATE STUDIES IN PARTIAL FULFILMENT OF THE REQUIREMENTS FOR THE DEGREE OF

DOCTOR OF PHILOSOPHY

GRADUATE PROGRAM IN KINESIOLOGY AND HEALTH SCIENCE
YORK UNIVERSITY
TORONTO, ONTARIO
NOVEMBER 2017

Abstract

This dissertation presents two possible approaches to enhancing glucose utilization, improving insulin sensitivity and reducing fat mass that could have therapeutic value for the treatment of obesity and type 2 diabetes (T2D). The results of my first study showed that suppressing the import of long-chain fatty acids into the mitochondria improved glucose homeostasis while also reducing fat mass. A reduction in lipogenesis in the white adipose tissue (WAT) explained the reduction in fat mass as lipolysis was also reduced. Subsequent studies examined the effects that activation of cold-induced thermogenesis would have on whole-body and tissue-specific metabolism. I confirmed that cold exposure increases UCP1 content (induces browning) in the subcutaneous (Sc) inguinal (Ing) WAT, but it did not enhance substrate oxidation in this fat depot. Instead, cold acclimation activated a futile cycle of lipolysis and lipogenesis that contributed to increasing energy expenditure within this fat depot. This futile cycle was not activated in the epididymal (Epid) fat, confirming that cold induced a fat depot-specific browning adaptive response. I then studied the hormone fibroblast growth factor 21 (FGF21) as a factor that could explain this depot-specific difference. FGF21 content and secretion was enhanced in the Sc Ing WAT, but not the Epid WAT depot. The downstream signaling pathway was also only activated in the Sc Ing WAT depot, suggesting that FGF21 could be involved in the depot-specific browning that I observed. Additional studies showed that muscles rich in both type I and type II fibers enhanced their FA oxidation following cold exposure. However it was only muscles rich in type I fibers that enhanced expression of the glucose transporter *Glut4* while also reducing phosphorylation of glycogen synthase, leading to an increase in glycogen synthesis rate

and glycogen content after cold acclimation. Liver glycogen content was reduced following cold acclimation, while gluconeogenesis was enhanced in this organ. Despite a cold-induced increase in food intake and endogenous glucose production, and reduction in plasma insulin, circulating glucose remained unchanged. These results show that activation of cold-induced thermogenesis can enhance insulin sensitivity and could be a viable alternative treatment for diseases such as obesity and T2D.

Acknowledgements

Dr. Rolando Ceddia: None of this would have been possible without your guidance and support. These past 4 years have simultaneously been the toughest and most rewarding of my entire life. Since day 1 you've had my back and with you as my mentor I've managed to accomplish so much more than I ever thought I would during my PhD. Most importantly, our relationship has been one of collaboration and friendship, and I am grateful for that. A thank you doesn't even begin to express my gratitude. A large can of mixed nuts might…

Ceddia Lab members: Michelle, Abinas and Arta, we were the original 4. Thank you for making me laugh and making the long days bearable. Michelle especially, you will always be the best lab partner ever. Pauline, our friendship and collaborations have been such a blessing. Thank you for all types of science discussions and for taking care of me in Brazil. Ishvinder, thanks for being a buddy and accompanying me to conferences and presentations so I could be social my last year here. Dr. Ricardo Pinho, obrigada pela confiança e pela oportunidade de viajar e trabalhar no Brasil. It was an experience I will never forget! George, you are a PCR master and have taught me so much. There was never a dull day with you in the lab! And to every other volunteer and undergraduate student who graced the Ceddia Lab over the last 4 years- there are too many to list but thank you for every task you completed, big or small, that helped me complete my work.

My supervisory committee: Your guidance and support are much appreciated. Thank you for being thoughtful, critical, patient and encouraging at all the right times.

My family and friends: Mom, Dad, my brother Matt, my grandparents, friends, teammates and the countless cousins and Aunts and Uncles I have, thank you for always asking how research was going, even if you had no idea what it entailed. Thank you for the laughter, food, competition and company that provided such a balance to my life as a grad student and helped to keep me sane.

Peit: Nobody quite understands the stress of a grad student quite like their spouse. Thank you for being a sounding board for all my frustrations and for making me laugh or look at pictures of puppies when I really needed to. Thanks for your patience and understanding for every weekend or late night spent in the lab, for your pride in my work, and for loving me no matter what. And thank you for working so hard so that I never ever had to worry about paying bills while trying to complete my research.

The Elia Family: Thank you for your generous contribution to York University in the form of the Elia Scholars program that allowed me to invest all of my time and energy into my research. I'm proud to be part of such a prestigious group of individuals.

Lastly, thanks be to God, without whom none of this would be possible.

Table of Contents

List of Figures

List of Tables

List of Abbreviations

aBAT	Aortic brown adipose tissue
AC	Adenylyl cyclase
ACC	Acetyl-CoA carboxylase
Ach	acetylcholine
ACL	ATP-citrate lyase
ADP	Adenosine diphosphate
AMP	Adenosine monophosphate
AMPK	AMP-activated protein kinase
Apo	Apolipoprotein
AQP-7	Aquaporin-7
AS160	Akt substrate of 160 kDa
ATGL	Adipose triglyceride lipase
ATP	Adenosine triphosphate
β-Adr	Beta-adrenergic receptor
BAT	Brown adipose tissue
Bmp2, 4, 7	Bone morphogenetic protein 2, 4, 7
BSA	Bovine serum albumin
C/EBPα/β	CCAAT-enhancer binding protein alpha/beta
Ca^{2+}	Calcium ion
cAMP	Cyclic AMP
CD36	Cluster of differentiation 36
CGI-58	Comparative gene identification-58
CIDEA	Cell death-inducing DFFA-like effector A
CLAMS	Comprehensive laboratory animal monitoring system
CoA	Coenzyme A
Cox8b	Cytochrome c oxidase subunit VIIIb
CPT-1	Carnitine palmitoyltransferase-1
CRTC	CREB-regulated transcriptional coactivator
DAG	Diacylglycerol
DHPR	Dihydropyridine receptor
DIO2	Type 2 iodothyronine deiodinase
DIT	Diet-induced thermogenesis
EDL	Extensor digitorum longus
EE	Energy expenditure
EI	Energy intake
Elovl3,6	Elongation of very long chain fatty acids 3,6
Epid	Epididymal
Epit	Epitrochlearis
ERK1/2	Extracellular signal-regulated kinase 1/2
ETC	Electron transport chain
FA	Fatty acid (used interchangeably with free FA (FFA) and NEFA)
$FADH_2$	Flavin adenine dinucleotide
FAS	Fatty acid synthase
FI	Food intake

FGF21	Fibroblast growth factor 21
FGFR	FGF21 receptor
FNDC5	Fibronectin domain-containing protein 5
FoxO1	Forkhead box O 1
G1P	Glucose-1-phosphate
G3P	Glycerol-3-phosphate
G3PDH	G3P dehydrogenase
G6P	Glucose-6-phosphate
G6Pase	Glucose-6-phosphatase
GAP	Glyceraldehyde-3-phosphate
GAPDH	Glyceraldehyde-3-phosphate dehydrogenase
GLUT1/4	Glucose transporter isoform ¼
$GPCR_{s/i}$	Stimulatory or inhibitory G-protein coupled receptor
GS	Glycogen synthase
GSK3	Glycogen synthase kinase 3
GYK	Glycerol kinase
HDL	High density lipoprotein
HF	High fat
HNF-4α	Hepatocyte nuclear factor-4α
HSL	Hormone sensitive lipase
iBAT	Interscapular brown adipose tissue
INSIG	Insulin-induced gene
IRS-1	Insulin receptor substrate-1
KRB	Krebs Ringer buffer
LCFA	Long chain fatty acid
LDH	Lactate dehydrogenase
LF	Low fat
Lpl	Lipoprotein lipase
MAG	Monoacylglycerol
MAPK	Mitogen-activated protein kinase
MAGL	Monoacylglycerol lipase
MDH	Malate dehydrogenase
MEK1/2	MAPK/ERK kinase 1/2
miR	MicroRNA
MyHC	Myosin heavy chain
nAChRs	Nicotinic acetylcholine receptors
NADH	Nicotinamide adenine dinucleotide
NE	Norepinephrine
NEFA	Non-esterified fatty acid (used interchangeably with FA and FFA)
OAA	Oxaloacetate
PCr	Phosphocreatine
PDC	Pyruvate dehydrogenase complex
PDH	Pyruvate dehydrogenase
PDK-1	Phosphoinositide-dependent kinase-1
PDE3B	Phosphodiesterase 3B
PEPCK-C	Phosphoenolpyruvate carboxykinase (cytosolic isoform)

PFK	Phosphofructokinase
PGC-1α	Peroxisome proliferator-activated receptor gamma coactivator-1 alpha
PIP3	Phosphatidylinositol 3,4,5-triphosphate
PIP2	Phosphatidylinositol 4,5-bisphosphate
PI3K	Phosphoinositide 3 kinase
PK	Pyruvate kinase
PKA	Protein kinase A
PKB	Protein kinase B (AKT)
PKC	Protein kinase C
PLIN	Perilipin
PLN	Phospholamban
PP1,PP2A	Protein phosphatase 1, protein phosphatase 2A
PPARα	Peroxisome proliferator-activated receptor alpha
PPARγ	Peroxisome proliferator-activated receptor gamma
PRDM16	PRD1-BF1-RIZ1 homologous domain containing 16
RER	Respiratory exchange ratio
Retro	Retroperitoneal
RXR	Retinoid X receptor
RyR	Ryanodine receptor
Sc Ing	Subcutaneous inguinal
SCAP	SREBP cleavage-activating protein
Ser	Serine
SERCA	Sarco(endo)plasmic reticulum Ca^{2+}-ATPase
SLN	Sarcolipin
SNS	Sympathetic nervous system
Sol	Soleus
SR	Sarcoendoplasmic reticulum
SREBP-1c	Sterol regulatory element binding protein-1c
SVF	Stromal vascular fraction
T2D	Type 2 diabetes mellitus
TAG	Triacylglyceride
TCA	Tricarboxylic acid (cycle)
Thr	Threonine
TNF-α	Tumor necrosis factor-alpha
TZDs	Thiazylidinediones
UCP1	Uncoupling protein 1
VCO_2	Carbon dioxide production
VO_2	Oxygen consumption
WAT	White adipose tissue

CHAPTER 1: Introduction

There is currently a global epidemic of obesity with the highest prevalence of the disease in developed countries such as the United States and Canada (1). 26% of the Canadian adult population is classified as obese (body mass index (BMI) ≥30 kg/m^2), which is of significant concern as obesity is a major risk factor for the development of type 2 diabetes (T2D), cardiovascular disease and certain types of cancer (2). In addition to the impact on individuals' health, it has been estimated that obesity is responsible for an economic burden in Canada totaling $3.9 billion in direct medical costs that includes physician visits, hospitalizations, drug therapy and other treatment (2). Furthermore, obesity incurred an estimated $3.2 billion in indirect costs related to lost productivity and short- and long-term disability (2). The evidence clearly shows that obesity is a disease that significantly impacts the health care system and economy of the country.

A variety of hypotheses have been put forth to explain the increased prevalence of obesity with two of the main contributing factors being a reduction in physical activity levels and an increase in intake of calorie dense foods, particularly those with a high fat and high sucrose content (3). This decrease in energy expenditure and increase in energy intake leads to an energy imbalance that if sustained chronically results in excessive weight gain and obesity. The most common approach to treating obesity attempts to restore energy balance by using lifestyle intervention (ie. changes to the diet and exercise) to reduce energy intake and increase energy expenditure (4). Individuals participating in clinical weight loss programs are fairly successful at achieving a meaningful weight loss of 10% that significantly reduces their risk of development of

T2D and cardiovascular disease (4, 5). Importantly, significant weight loss activates energy sparing mechanisms that reduce basal metabolic rate in an attempt to counteract weight loss, making it increasingly difficult to continue to lose weight and maintain weight loss. Many individuals are unable to adhere to the lifestyle change required to maintain the weight loss under their new basal metabolic rate and many regain the lost weight within 5 years (4–6). Thus, it has become increasingly important to continue to develop novel methods to address energy imbalance, either through reducing food intake or increasing energy expenditure, to provide alternative therapies for individuals who need to lose weight and maintain weight loss.

It has been shown that some individuals require the assistance of a pharmacological agent to maintain successful weight loss (7). There have been a number of pharmacological agents developed and prescribed for the treatment of obesity; however, many act through the central nervous system to alter food intake and may result in serious side effects such as insomnia, anxiety, depression and suicidal thoughts (8). Orlistat (a gastrointestinal lipase inhibitor) and more recently liraglutide (a glucagon-like peptide 1 (GLP1) analog) are two pharmaceuticals prescribed specifically for weight loss that do not have such serious side effects (7, 9). However, these drugs may not be tolerated by all individuals who require the assistance of a pharmacological agent. Therefore, it is important to continue to investigate new drugs and other alternative non-pharmacological therapies that address energy imbalances with minimal side effects in order to assist all individuals suffering from obesity and its co-morbidities.

In this context, the work described in this dissertation focuses on two therapeutic

approaches that enhance glucose utilization, improve insulin sensitivity and reduce fat mass that could be beneficial for the treatment of obesity and type 2 diabetes (T2D).

CHAPTER 2: Literature Review

2.1. White Adipose Tissue (WAT)

2.1.1. Structure and depot-specific differences

The white adipose tissue (WAT) is a connective tissue composed of mature adipocytes and a stromal vascular fraction (SVF). Though the adipocytes make up between 35-70% of total adipose mass in adults, they only account for 25% of the total cell population in the WAT (10). The SVF accounts for the remaining 75% and contains a variety of cells including fibroblasts, endothelial cells, macrophages, pericytes, blood cells and preadipocytes (10, 11). Differentiation of preadipocytes into mature adipocytes is primarily controlled by peroxisome proliferator-activated receptor (PPAR)γ and a family of transcription factors known as CCAAT enhancer binding proteins (C/EPBs) (12) (Figure 2-5). C/EBPβ is important for the induction of *Pparγ* expression, while C/EBPα works with PPARγ to induce expression of adipocyte-specific genes (12). The fully mature adipocyte is characterized by a large lipid droplet (LD) (unilocular adipocyte) composed of triacylglyderides (TAGs). The cell nucleus is pushed to the side by the large LD that occupies the majority of the adipocyte cytoplasmic space (13) (Figure 2-1). The WAT has a low oxidative capacity as it contains a very small number of mitochondria which are thin and elongated, with randomly oriented cristae (13).

There are basically two types of WAT depots distributed throughout the body and they can be broadly classified as subcutaneous (Sc) and visceral (Vc) WAT. The Sc WAT is located beneath the skin and represents the majority (80%) of fat stored in the human body (10). The Sc WAT provides insulation and serves as a reservoir of energy

that can be mobilized under conditions of energy deficit (e.g. fasting) and increased energy expenditure (e.g. prolonged exercise) (14). The Vc WAT is located inside the abdominal cavity and provides support to internal organs (e.g. kidneys, pancreas, and intestines), but it can also be mobilized to provide substrate for energy production (14). Vc fat accounts for ~20% of total body fat and adipocytes in the Vc WAT are generally larger in diameter than the ones found in the Sc WAT (10). Additionally, Vc adipocytes are less insulin-sensitive and more lipolytic than adipocytes in the Sc WAT (14, 15). Importantly, lipid accumulation in the Sc WAT is associated with a healthy metabolic profile (16), whereas the expansion of the Vc WAT (termed Vc or central obesity) is associated with increased risk of dyslipidemia, T2D, cardiovascular disease, and certain types of cancer (16).

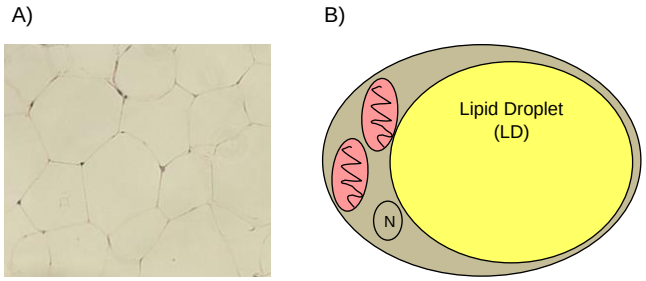

Figure 2-1: Unilocular whilte adipocyte. Microscopic image of subcutaneous WAT with hematoxylin and eosin (H&E) stain (A).Representation of a unilocular white adipocyte with one large lipid droplet (LD) and offset nucleus (B).

2.1.2. Function of the WAT and contribution to energy homeostasis

The WAT is integral to the maintenance of energy homeostasis at rest and during periods of increased energy demand. In the post-prandial state, the WAT synthesizes and stores excess lipids as TAGs, whereas during periods of fasting or increased

energy demand such as with exercise, it releases fatty acids through lipolysis and provides substrate for energy production in other organs and tissues (e.g. liver and skeletal and cardiac muscles). The WAT is also an important endocrine organ (17, 18). It produces and secretes hormones and proteins called adipokines. Therefore, through the actions of adipokines the WAT can affect the functions of several organs and tissues, and play an important role in the regulation of whole-body energy homeostasis. A typical example is leptin, a hormone that is secreted by the adipose tissue in proportion to its size (17, 18). As the adipose tissue expands, more leptin is released in the circulation, which, in turn, signals to specific hypothalamic regions and activates pathways that promote satiety and increased energy expenditure (19). The communication between the WAT and the brain through leptin allows the organism to control adiposity on a regular basis (17, 18). Other adipokines such as adiponectin (secreted from adipocytes), visfatin, TNF-α, interleukin (IL)-6, and monocyte chemoattractant protein-1 (secreted primarily from resident immune cells in the adipose tissue) have also been shown to regulate glucose and lipid metabolism (17, 18, 20).

2.1.2.1. Regulation of fatty acid synthesis and TAG formation

In the post-prandial state, the WAT stores excess energy in the form of TAGs. TAGs are made up of 3 fatty acids (FAs) esterified to glycerol-3-phosphate (G3P) (21, 22). The FAs are either taken up by the WAT from circulating chylomicrons or very low density lipoproteins (VLDLs), or are synthesized in the tissue from glucose (21). Fatty acid synthesis from glucose begins with the conversion of glucose into pyruvate (through the glycolytic pathway) and subsequent conversion of pyruvate into acetyl-CoA in the mitochondria (23). Acetyl-CoA is transported out of the mitochondria as citrate

where it is lysed into acetyl-CoA and oxaloacetate (OAA) by ATP-citrate lyase (ACL) (23). Subsequently, acetyl-CoA is carboxylated by acetyl-CoA carboxylase (ACC) to form malonyl-CoA, which is used to synthesize palmitic acid by fatty acid synthase (FAS) (23). NADPH provides the reducing power for fatty acid synthesis (23). Control of FAS occurs mainly at the transcriptional level. The promoter of the *Fas* gene contains a sterol regulatory element (SRE) which can be bound by sterol regulatory element binding protein (SREBP)-1 (23). SREBP-1c is the main isoform in AT and liver and its activity is controlled by insulin (23), providing a mechanism for the insulin-induced increase in *Fas* mRNA that has been previously described (24).

Because white adipocytes lack glycerol kinase (GYK) activity (25), the G3P moiety that forms the backbone of the TAG molecule has to be synthesized within the cell. This is accomplished through the breakdown of glucose in the glycolytic pathway in the post-prandial period when levels of insulin and glucose are elevated in the circulation (21) (Figure 2-2). Dihydroxyacetone phosphate (DHAP), a product in the glycolytic pathway, can be converted to G3P, a reaction that is catalyzed by the enzyme G3P dehydrogenase (G3PDH). In the fed state, insulin is the main regulator of the FA synthesis pathway as it stimulates glucose uptake into the cell, in addition to inhibiting lipolysis. The insulin signaling pathway in the adipose tissue is identical to that in skeletal muscles and is described in detail in Section 2.3.4. Briefly, insulin binds to the insulin receptor (IR) leading to auto-phosphorylation of the IR and subsequent phosphorylation of insulin receptor substrate (IRS) proteins (26). This leads to the

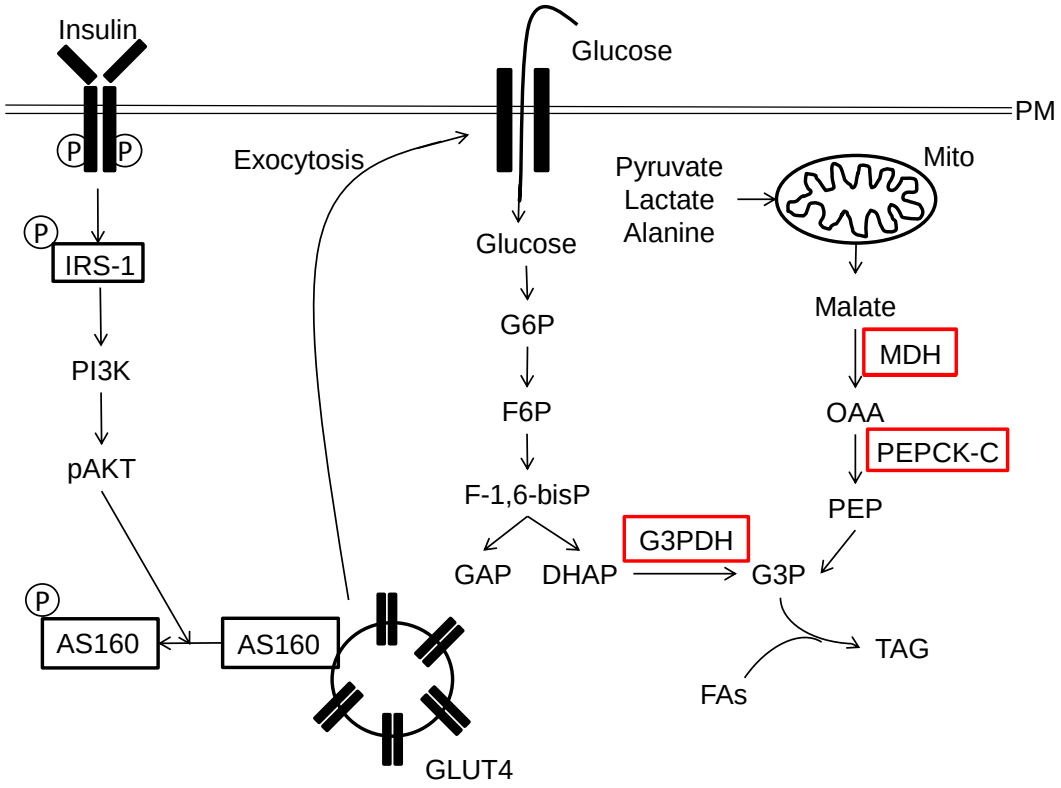

Figure 2-2: Synthesis of G3P for TAG formation. In the fed state, G3P is synthesized from glucose, beginning with insulin-stimulated glucose uptake. Insulin binds to the insulin receptor leading to auto-phosphorylation of the receptor and subsequent phosphorylation of IRS1. Phosphorylation leads to the recruitment of PI3K, which results in the recruitment of AKT and its phosphorylation by PDK1. Activated AKT subsequently phosphorylates and inactivates AS160, allowing for exocytosis of GLUT4 from intracellular vesicles and translocation to the plasma membrane (PM) to facilitate glucose uptake. Glucose is then converted to DHAP through the glycolytic pathway, and finally converted to G3P by G3PDH. In the fasted state, G3P in synthesized from non-glucose precursors (ie. pyruvate, lactate and alanine) through glyceroneogenesis. Glyceroneogenesis begins with the conversion of pyruvate into OAA in the mitochondria (Mito). OAA is converted into malate by MDH and malate is then shuttled out of the mitochondria and converted back into OAA by MDH. OAA is then converted into phosphoenolpyruvate (PEP), a reaction catalyzed by PEPCK-C. PEP can then be converted into DHAP through a general reversal of the steps of glycolysis. Finally DHAP is converted to G3P, a reaction that is catalyzed by the enzyme G3PDH. Three fatty acids can then be esterified to G3P to form a TAG.

activation of phosphoinositide 3-kinase (PI3K) and phosphorylation and activation of AKT by 3-phosphoinositide-dependent kinase (PDK1) (26). In its activated state, AKT phosphorylates and inactivates AKT substrate of 160 kDA (AS160). The latter step leads to the translocation of GLUT4-containing vesicles to the plasma membrane and enhanced glucose uptake (26, 27).

In the late 1960s, a separate pathway was discovered that provides the G3P for TAG synthesis. This additional synthesis pathway, termed glyceroneogenesis, is required in the fasted state, when glucose and insulin are low in the circulation. In this state, there is no stimulus for glucose uptake and glucose would be spared to fuel the metabolism of the brain and red blood cells (25). However, in the fasted state approximately 30% of the FAs released via lipolysis are re-esterified into TAG. Once again, due to the lack of GYK activity in adipocytes (25) the glycerol released from TAG hydrolysis cannot be the source of G3P required for re-esterification to occur. The majority of the glycerol released from lipolysis is transported out of the cell through plasma membrane aquaporin-7 (AQP-7) (28) and is used primarily by the liver for gluconeogenesis. G3P is instead produced from non-glucose precursors such as pyruvate, lactate and alanine through glyceroneogenesis (Figure 2-2). PEPCK is the main regulatory enzyme of the glyceroneogenesis pathway. This enzyme is found in two compartments of the cell: the mitochondria and the cytosol, with the AT expressing the cytosolic form of the enzyme (25). Increases in the mRNA expression of *Pepck* are closely linked to increases in enzyme content within the cell (21).

In the adipose tissue, the PEPCK gene has two PPARγ/retinoid X receptor (RXR) binding sites on its promoter region. A class of drugs known as

thiazolidinediones (TZDs) has been shown to activate PEPCK through this region of the promoter (21). The PEPCK promoter also contains a cyclic adenosine monophosphate (cAMP)-responsive element (CRE) and expression of *Pepck* can be induced by β-adrenergic agonists that increase intracellular cAMP levels (21). Interestingly, glucocorticoids reduce *Pepck* expression in the adipose tissue, but enhance it in the liver. The specific effect in the adipose tissue appears to be mediated by C/EBPs as content and nuclear binding of C/EBPα was reduced in adipocytes upon glucocorticoid treatment (29). The importance of an intact glyceroneogenesis pathway can be demonstrated using mice with a disrupted PPARγ binding site in the PEPCK promoter that significantly reduced *Pepck* expression in the adipose tissue (22). These mice were insulin resistant and showed a reduced uptake of glucose into skeletal muscle (22), highlighting the importance of TAG synthesis in the AT that would promote the proper storage of fat in this tissue and prevent ectopic lipid deposition and the development of FA-induced insulin resistance.

2.1.2.2. Regulation of lipolysis

During periods of increased energy demand, such as exercise, cold exposure or fasting, the adipose tissue releases its fatty acid content through lipolysis. Lipolysis is activated through the β-adrenergic signaling pathway. It begins with stimulus of the sympathetic nervous system (SNS) leading to release of norepinephrine (NE) that binds to a β-adrenergic receptor (β-Adr) (Figure 2-3). This activates stimulatory G-protein coupled receptors ($GPCR_s$), the alpha unit of which activates adenylyl cyclase (AC) (30) that produces cAMP (31), a second messenger involved in the signaling cascade for a multitude of physiological processes. In the lipolytic cascade, cAMP binds to the

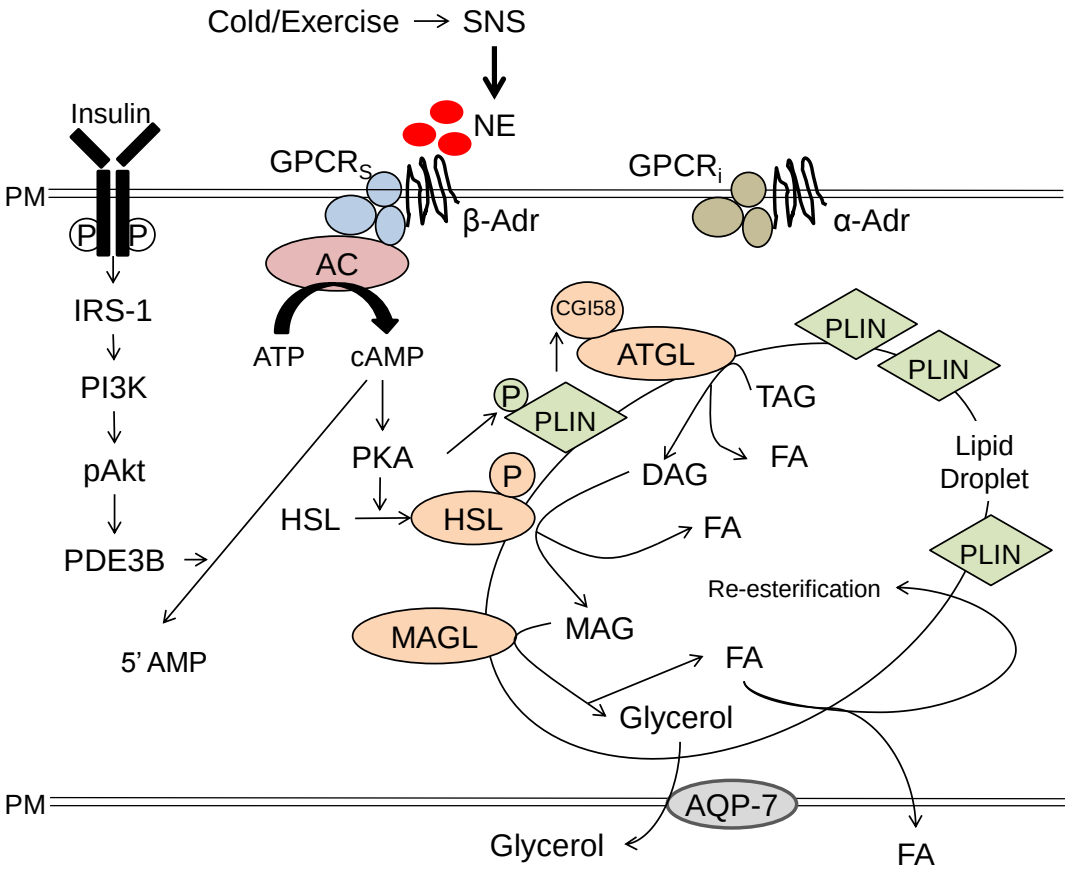

Figure 2-3: Schematic of the lipolytic signaling pathway. Stimulus of the SNS releases NE that binds to a β-Adr receptor, activating $GPCR_s$, the alpha unit of which activates AC, producing cAMP. cAMP is a second messenger that binds to the regulatory subunit of PKA that subsequently phosphorylates HSL and PLIN, a structural LD protein. The phosphorylation of PLIN alters the structure of the LD, giving the activated HSL access to the neutral LD in order to facilitate lipolysis. Phosphorylation of PLIN by PKA also leads to the dissociation of CGI-58 from PLIN, allowing CGI-58 to associate with ATGL and increase its hydrolase activity. Lipolysis proceeds with the stepwise hydrolyzation of a TAG. ATGL hydrolyzes the first ester bond, forming DAG and HSL hydrolyzes the next ester bond in DAG, forming MAG. Finally MAG is hydrolyzed by MAGL. A FA is released at each step that can be re-esterified in the adipocyte, or used as fuel in other peripheral tissues. The majority of the glycerol released is transported out of the adipocyte through AQP-7. Lipolysis is inhibited by insulin-induced activation of PDE3B that converts cAMP into 5' AMP, shutting down the lipolytic pathway. Binding of catecholamines to the α-Adr would activate $GPCR_i$, preventing the continuation of the downstream signaling cascade.

regulatory subunit of cAMP-dependent protein kinase A (PKA), allowing the release of the catalytic subunit that subsequently phosphorylates hormone sensitive lipase (HSL) and perilipin A (PLIN), a structural protein that coats the LD (31). The phosphorylation of PLIN alters the structure of the LD, giving the activated HSL access to the neutral LD in order to facilitate lipolysis. HSL specifically hydrolyzes DAG leading to the formation of MAG and the release of a FA (32). Though HSL has multiple phosphorylation sites, phosphorylation at serine residue 660 (Ser-660) by PKA is essential for HSL activation in rodents (33). Because HSL is essentially a DAG lipase (34), TAG hydrolysis needs to be initiated by a TAG lipase, so DAG is formed and the lipolytic process can effectively occur. This is possible because PKA is also important in the activation of adipose triglyceride lipase (ATGL), the rate limiting enzyme responsible for hydrolyzing the first ester bond in the TAG and for the formation of DAG. ATGL activation is strongly dependent on its interaction with comparative gene identification 58 (CGI-58) (35). Under basal non-stimulated conditions, CGI-58 is bound to PLIN on the surface of the LD, which prevents its interaction with ATGL. However, upon activation of the β-Adr, PLIN becomes phosphorylated by PKA and this leads to the dissociation of CGI-58 from PLIN and the LD surface. This now allows CGI-58 to interact with ATGL and increase its hydrolase activity (36–38). Granneman et al. suggest that there is a small amount of CGI-58 that is not bound to PLIN in the basal state (36), allowing for basal lipolysis to take place. ATGL has been shown to be the predominant lipase in basal lipolysis, whereas HSL is more important for stimulated lipolysis (39). Following hydrolysis by ATGL and HSL, the final step in lipolysis is the hydrolysis of MAG by the constitutively active monoacylglycerol lipase (MAGL) (40). The FAs released through lipolysis can be

re-esterified in the adipocyte, or used as fuel in other peripheral tissues, while the glycerol moiety is transported out of the cell and used primarily by the liver for gluconeogenesis.

Several factors alter the rate of lipolysis. α-adrenergic receptors (α-Adr) that also bind NE are associated with inhibitory GPCR ($GPCR_i$) that do not activate AC (41). Thus, the relative proportion of α-Adr and β-Adr determines lipolytic rates. Indeed, the adipose tissue from the femoral fat pad of humans (a Sc fat pad) has a much larger distribution of α-Adr than β-Adr (41), and also has the lowest lipolytic rate (42). Under post-prandial conditions, lipolysis is inhibited by the hormone insulin (34, 43, 44). Similarly to the insulin signaling pathway described earlier, insulin initiates the response by binding its receptor on the cell membrane resulting in a cascade of events that phosphorylates AKT/PKB (44). In addition to playing an important role in the signaling steps that promote the translocation of GLUT4 vesicles to the plasma membrane, AKT also phosphorylates phosphodiesterase 3B (PDE3B) (Figure 2-3). This activates PDE3B and leads to the conversion of cAMP into 5'-AMP. The reduction in cAMP by PDE3B causes deactivation of PKA and prevents the phosphorylation of HSL or PLIN, which ultimately inhibits lipolysis (34, 43, 45). Insulin can also act in a cAMP-independent manner by phosphorylating the regulatory subunit of protein phosphatase 1 (PP1) and activating it. Once activated, PP1 can dephosphorylate and deactivate HSL (34, 44, 46).

AMP-activated protein kinase (AMPK) is a cellular energy sensing protein that is activated under conditions that lead to a reduction in the intracellular AMP:ATP ratio. The exact mechanism of this activation is described in Section 2.3.4. With respect to the

regulation of WAT metabolism, AMPK has been shown to modulate mitochondrial oxidation, as well as lipolysis. AMPK modulates substrate oxidation by phosphorylating and inactivating ACC which results in a reduced production of malonyl-CoA (47) (Figure 2-8). This removes the inhibition of malonyl-CoA on carnitine palmitoyltransferase (CPT)-1, the protein responsible for transporting long-chain fatty acids (LCFAs) into the mitochondria (47). Removal of the inhibition thus allows for fatty acid transport into the mitochondria and for β-oxidation to proceed. AMPK activation also increases the expression of peroxisome proliferator-activated receptor gamma coactivator-1 alpha *(Pgc-1α*) (47), a transcription factor that drives mitochondrial biogenesis that is discussed in more detail in Section 2.2.2. AMPK has been proposed to modulate lipolysis by phosphorylating Ser-565 on HSL, preventing the phosphorylation of Ser-660 and Ser-563 on this lipase (48). Evidence has also been provided that AMPK is activated by lipolysis, a process that causes changes in the intracellular AMP:ATP ratio. In this context, AMPK activation has been demonstrated to actually inhibit lipolysis in order to limit TAG breakdown and curtail the high energy cost of fatty acid re-esterification in this tissue (48). It has also been reported that chronic pharmacological activation of AMPK leads to remodeling of WAT metabolism. In fact, under chronic activation of AMPK, adipocytes enhanced their fatty acid oxidation capacity, reduced lipogenesis, and increased ATGL content and NEFA release (49). These findings suggest that AMPK promotes energy dissipation within the WAT, despite inhibiting HSL. Through these effects, it has been proposed that AMPK regulates WAT lipolysis in a way that attenuates the costly process of fatty acid re-esterification within the tissue

while still allowing the exportation of fatty acids to provide substrate to meet the energy demands of other peripheral tissues.

Lipolysis is also modulated during mild- to moderate-intensity endurance exercise (45-65% VO_2 max) as fatty acids represent a large proportion of the substrate used to fuel this type of exercise (50). The majority of these fatty acids are provided by the adipose tissue where a single bout of exercise leads to 2-3 fold increases in catecholamine-stimulated lipolysis (50). However, there are conflicting reports as to the effect of chronic endurance training on rates of lipolysis. Studies completed in healthy humans examining whole body lipolysis showed a reduction in FFAs and glycerol release after training (51–55), whereas other studies examining lipolysis in isolated adipocytes from trained individuals and rodents found an increase in stimulated lipolysis (56–60). More recently Pistor et al. found that circulating NEFAs and glycerol were reduced in endurance-trained rats compared to controls following a bout of submaximal exercise of the same relative intensity (61). Furthermore, stimulated rates of lipolysis were reduced in adipocytes isolated from both the visceral and subcutaneous fat depots of endurance trained rats (61). Thus, it could be that as an adaptive response to chronic endurance training the organism modulates WAT lipolysis to match the rate of utilization by skeletal muscles and minimize the costly process of re-esterification of those non-used fatty acids that return to the WAT. The molecular mechanisms that could underlie a modulatory effect of endurance training on WAT lipolysis remain poorly understood. These could likely involve the regulation of ATGL and HSL activities, as well as the content and activity of other proteins involved in the lipolytic cascade, but this remains to be fully investigated in the adipose tissue.

2.2. Brown Adipose Tissue (BAT)

2.2.1. Structure and function

The brown adipose tissue (BAT) is a unique organ found in mammals that is specifically designed to produce heat, a process termed non-shivering thermogenesis (NST). In contrast to the WAT, the BAT is highly oxidative due to its abundance of large, spherical mitochondria that also give the BAT its distinctive brown colour (13). The BAT can also be characterized by its multilocular adipocytes, fat cells that store TAGs in smaller vacuoles as opposed to one single large LD (13) (Figure 2-4). These multiple LD have been shown to be tightly associated with mitochondria, providing an efficient means of transferring substrate for oxidation and NST (62). In addition, BAT is densely innervated and highly vascularized (63). It produces heat by uncoupling oxidative phosphorylation from ATP synthesis and by using the potential energy generated from the mitochondrial proton gradient to instead produce heat (63). It does so through the fact that BAT is unique in expressing uncoupling protein 1 (UCP1), a protein that is located on the inner mitochondrial membrane (13). UCP1 is 32 kDa protein that is a member of the mitochondrial carrier protein family. UCP1 is activated by FFAs and allows protons to leak across the membrane, bypassing ATP synthase and instead producing heat (63). This process is triggered by temperatures below thermoneutrality through the SNS. In rodents a large depot of BAT is located in between the scapula (interscapular BAT or iBAT) with other BAT depots located more centrally such as around the aorta (aortic BAT, aBAT) (13). In humans, BAT is found mainly in the supraclavicular region and the core (64, 65). The dense capillary network of the BAT ensures that blood is warmed as it flows through the activated BAT while its central

location in the body ensures that integral core regions are kept warm during exposure to temperatures below thermoneutrality (13).

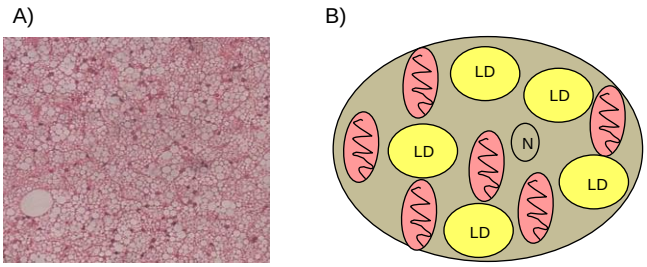

Figure 2-4: Multilocular brown adipocyte. Microscopic image of iBAT with H&E stain (A). Representation of a multilocular brown adipocyte with multiple small lipid droplets (LDs) and mitochondria (B). The nucleus is centrally located (B).

2.2.2. Development of BAT

There are a number of factors responsible for determining the ultimate fate of mesenchymal stem cells and their development into mature brown adipocytes (Figure 2-5). Bone morphogenetic proteins (BMPs) control stem cell commitment to various lineages (66). While BMP2 and 4 have been shown to promote white adipogenesis, brown pre-adipocytes treated with BMP7 were shown to differentiate into mature brown adipocytes (66). Importantly BMP7 was shown to induce expression of the transcriptional regulator PRD1-BF1-RIZ1 homologous domain containing 16 (PRDM16) (66). Brown adipocytes appear to share a common lineage with skeletal muscle, since both originate from $Myf5^{+}$ precursor cells (67). It is PRDM16 that directs the precursor cells to the brown adipocyte fate. PRDM16 interacts through its zinc finger (ZF1) domain with the MED1 subunit of the Mediator coactivator complex which enhances the transcriptional function of PPARγ and thyroid hormone receptor (TR) to increase the

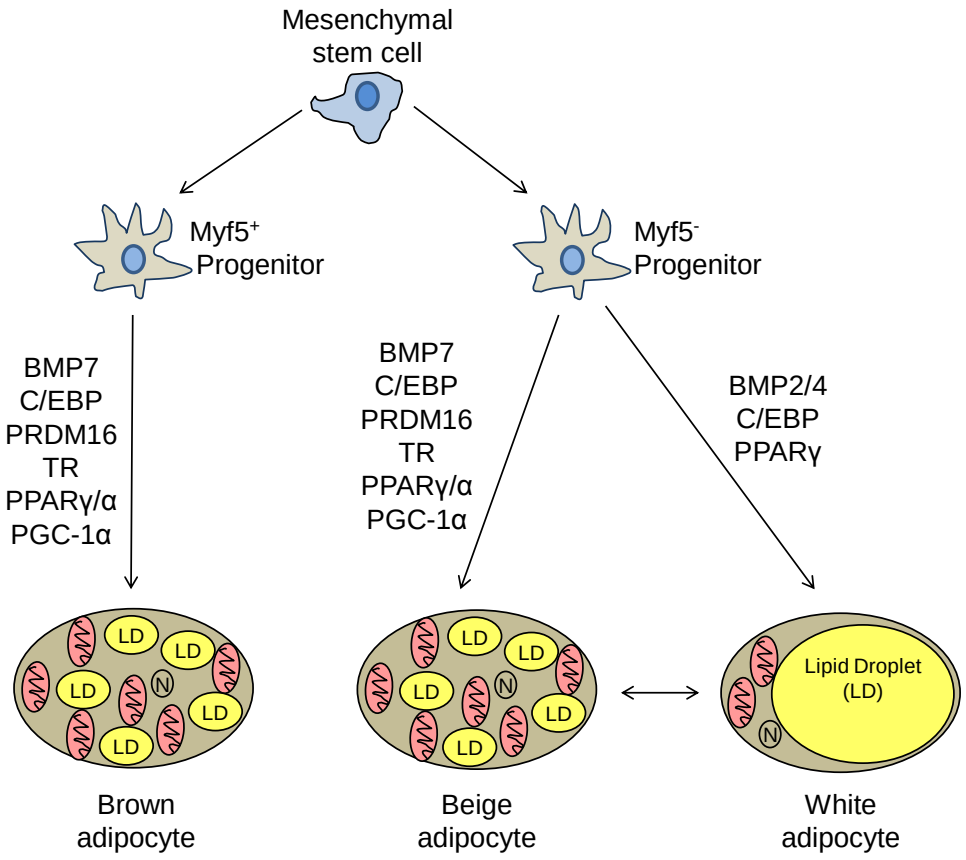

Figure 2-5: Brown, beige and white adipocyte origin and development. Brown adipocytes derive from Myf5^{+} while white and beige adipocytes derive from Myf5^{-} progenitor cells. BMP7, C/EBP, PRDM16, TR, PPARγ/α and PGC-1α are important regulators of brown and beige fat development. BMP2/4, C/EBP and PPARγ are essential to mature white adipocyte differentiation. Furthermore, it has been shown that white adipocytes can be stimulated to convert into beige adipocytes (a process known as “browning”).

expression of *Ucp1* (68, 69). Interestingly, PRDM16 specifically enhances the expression of BAT-specific genes such as *Ucp1,* cell death-inducing DFFA-like effector a *(Cidea),* elongation of very long chain fatty acids 3 *(Elovl3),* type 2 iodothyronine deiodinase *(Dio2),* and *Pgc-1α*, while also repressing the expression of WAT-specific genes during differentiation (70). Moreover expressing PRDM16 in C_2C_{12} myoblasts led to the development of adipocytes when the myoblasts were given an adipogenic

cocktail (67). PRDM16 is essential during the differentiation of brown preadipocytes into mature brown adipocytes, but is not required for the actual thermogenic activation of these cells (70). In addition to PPARγ and TR, PRDM16 also binds and enhances the transcriptional factors PPARα, PGC-1α and C/EBP (12). C/EBP was previously described in this review as a transcription factor that works with PPARγ to drive adipocyte differentiation (12), whereas PPARα is highly expressed in brown adipocytes and is principally involved in increasing the expression of *Ucp1* and genes involved in fatty acid oxidation (12, 71). PGC-1α is the master regulator of mitochondrial biogenesis. It was originally identified as a transcription factor that binds PPARγ and TR and enhances the expression of *Ucp1* in BAT (72). In fact, PGC-1α is the main transcription factor that controls thermogenic gene expression upon cold exposure or β-adrenergic stimulation and is essential for the activation of BAT (12). *Pgc-1α* expression is induced by cold exposure, and this protein is phosphorylated and activated by p38 mitogen-activated protein kinase (MAPK) following β-adrenergic stimulation (12). Furthermore, its transcriptional activity is increased upon deacetylation by Sirtuin 1 (SIRT1) (73).

Recently it has been shown that microRNAs (miRs), short non-coding RNAs, can regulate the expression of BAT-specific genes through their effects on SIRT1 and PGC-1α. Down-regulation of miR-34a led to increased expression of *Ucp1* and *Prdm16* in the BAT of high-fat fed mice as a result of enhanced protein levels of SIRT1 and reduced PGC-1α acetylation in these mice (74). In contrast, over-expression of miR-455 in brown pre-adipocytes led to the induction of *Pgc-1α*, *Prdm16*, *Ucp1* and *Cidea* in mature brown adipocytes (75).

2.2.3. Activation of the BAT

The activation of UCP1 and BAT thermogenic activity is controlled by the SNS through a lipolysis-induced increase in intracellular FAs levels. The signaling pathway is similar to the pathway of lipolytic activation beginning with a cold stimulus that activates the SNS causing the release of NE that subsequently binds β-Adr (63). It has been shown that the β3-Adr is the most significant for this response to cold in rodents. β1-Adr are also found in the brown adipocyte; however, they are not coupled to signaling processes in the cells. β2-Adr are more likely expressed in the vascular system and not in the adipocytes themselves (63); therefore, they do not seem to play a major role in BAT activation. Activation of lipolysis leads to the release of FFAs which activate UCP1 by removing the inhibitory effect of nucleotides on this protein. Fatty acids are essential for thermogenesis. In fact, simply providing fatty acids can increase thermogenesis (63), whereas blocking NE-induced lipolysis through the deletion of phosphorylation sites on PLIN significantly blunted the thermogenic response (76). Activation of the SNS also leads to activation of the transcription factor PGC-1α, as described earlier.

An important component of SNS-induced BAT activation is an increase in the activity of DIO2. DIO2 is the enzyme that converts intracellular tyroxine (T4) to the activated 3,5,3'-triiodothyronine (T3) (77). T3 binds TRs, transcriptional factors located on the UCP1 promoter that enhance its expression (63). DIO2 is essential for the activation of BAT as *Dio2*$^{-/-}$ mice showed a reduction in core body temperature upon acute cold exposure and a reduction in iBAT heat generation upon norepinephrine infusion (77). Isolated brown adipocytes from *Dio2*$^{-/-}$ mice also displayed reduced

oxygen consumption and glycerol release upon NE, CL 316,243 (β3-Adr agonist) or forskolin (activator of AC) treatment (77).

In response to BAT activation, there are a number of physiological adaptations that occur within the organism. Foremost is the increase in BAT mass and UCP1 protein content that enhance the capacity of the organism for NST (78). This is accompanied by an increase in food intake to fuel the increased demands in energy expenditure (78). The WAT and liver also supply substrate to fuel BAT thermogenesis, described in other sections of this review. As expected, glucose and fatty acid uptake and metabolism in the BAT are increased with activation as is total oxidative activity (78). Mechanistically, these changes occur as a result of increases in the expression, content and activity of a number of transporters and enzymes involved in glucose and fatty acid metabolism. GLUT4 content and expression is increased with cold exposure in both rats and mice, while GLUT1 content does not seem to be affected by cold (78, 79). GLUT4 content has also been shown to be enhanced in type 2 diabetic humans following short term cold exposure (80). Furthermore, the expression of enzymes involved in glycolysis (hexokinase, phosphofructokinase (*Pfk*) and pyruvate dehydrogenase (*Pdh*)) (78, 79) and *de novo* fatty acid and TAG synthesis (*Fas*, *Pepck*, *Gyk,* and diacylglycerol acyltransferase (*Dgat 1* and *2*)) (78) are also increased with cold exposure. Fat transporters such as cluster of differentiation *(Cd)36* (78, 81), *f*atty acid transport protein 1 *(Fatp 1)*, fatty acid binding protein 4 *(Fabp 4)*, lipoprotein lipase *(Lpl)* and *Cpt-1b* (78) have also been reported to increase with cold exposure.

2.2.4. Browning of the WAT

Recently, a third type of fat has been identified that is composed of BAT-like adipocytes within the WAT. These have been named brown-in-white (“brite”) (82, 83) or beige (84) adipocytes that can be induced by cold exposure or β-adrenergic stimulation (83, 85). In contrast to the brown adipocytes, beige adipocytes derive from a $Myf5^-$ lineage (86); however, similarly to brown adipocytes, they require PRDM16 for the induction of thermogenic genes such as *Ucp1*, *Cidea*, cytochrome c oxidase subunit VIIIb *(Cox8b)*, and *Pgc-1α* (86) (Figure 2-5). Beige adipocytes resemble brown adipocytes as they are multilocular in appearance, UCP1 positive and contain mitochondria densely filled with cristae (85, 87). Importantly, these adipocytes are thermogenically competent and capable of NST, despite having lower total mitochondrial content and lower capacity for NST when compared to classical brown adipocytes (88). Interestingly, the induction and appearance of beige adipocytes is depot specific with the Sc depot, particularly in the inguinal (Ing) region of rodents, being the most prone to browning compared to other Vc fat depots such as the Epid fat (83, 84, 86, 89–91). These differences may be due to each depot’s capacity to promote two processes currently being debated to explain the emergence of beige adipocytes. One refers to transdifferentiation, meaning that a pre-existing fully mature white adipocyte would acquire the features of a brown adipocyte. The other involves the stimulation of *de novo* adipogenesis to create new beige adipocytes (92). In favour of the latter theory, Wu et al. showed that the Sc Ing WAT contains two groups of progenitor cells, one with a gene expression profile similar to WAT and another with a gene expression profile similar to classical BAT that when stimulated with cAMP,

induced expression of *Ucp1* (84). In favour of the transdifferentiation theory, Barbatelli et al. showed that cold exposure did not increase pre-adipocyte density, despite stimulating the appearance of multilocular, UCP1 expressing adipocytes in the Sc Ing depot (93). Cold exposure also did not increase the expression of genes involved in cell cycling and proliferation in the Sc Ing depot (93). Moreover the researchers identified adipocytes that appeared to have characteristics in between that of white adipocytes and fully transdifferentiated brown adipocytes. These intermediate adipocytes were UCP1 positive, displayed a large, central LD along with some smaller LDs, and contained a larger number of mitochondria with fully developed transverse cristae than white adipocytes (93). It appeared that these intermediate cells were adipocytes undergoing the transdifferentiation process. Indeed, following some additional research, a model of multilocular adipocyte development through the process of transdifferentiation was proposed (87). This model suggests that under β-adrenergic stimulation, lipolysis would be increased in white adipocytes, releasing fatty acids and glycerol. Expression of *Gyk* would also be increased under these conditions, allowing for glycerol to be used as a substrate for re-esterification into TAG along with fatty acids. The newly synthesized TAG would form small LDs. Lastly, the β-adrenergically induced increase in CIDEA, a protein that promotes LD enlargement, would enlarge the small LDs, eventually leading to the multilocular appearance. Importantly, the futile cycle of TAG hydrolysis and re-esterification would consume a significant amount of substrate and be a source of energy dissipation by the beige adipose tissue (87). This is relevant as recent work has shown that neither chronic β-adrenergic stimulation nor cold exposure increased oxidative activity in the Sc Ing fat, despite increasing UCP1 content

(94), questioning the role that browning of the WAT could play in increasing energy expenditure (90, 91).

It is possible that a futile energy cycle could be the main contribution of beige adipocytes to increasing energy expenditure. Given the data showing the potential for browning to increase energy expenditure, researchers are currently studying multiple ways of stimulating the browning of WAT so that we may understand and potentially develop this new therapeutic approach to the treatment of obesity and T2D. Chronic endurance exercise has also been shown to induce the expression of thermogenic genes in the Sc Ing WAT depot of rodents (90, 91, 95). Notably, recent research identified a novel PGC-1α-dependent myokine, irisin, that is released during exercise (90). Irisin is cleaved from a larger protein named fibronectin domain-containing protein 5 (FNDC5) and induces the expression of *Ucp1*, *Prdm16*, *Pgc-1α*, *Cidea*, *Dio2* and *Elovl3* in Sc Ing adipocytes (90). The discovery of irisin provided a link between chronic endurance exercise and browning of WAT; however, a receptor for irisin has yet to be identified and details of its signaling pathway are largely unknown (96). Furthermore, it was recently discovered that the start codon of the human *Fndc5* gene differed from that of the conserved start codon in the rat, mouse, gorilla and chimp, and that this human transcript did not result in translation of a full-length FNDC5 protein (97). These data have questioned the importance or even the existence of irisin in humans and this continues to be a controversial research topic.

While chronic endurance exercise was shown to induce the expression of thermogenic genes in the Sc Ing WAT, the effect on whole-body energy expenditure remains debatable. Considering that exercise in itself is thermogenic, it seemed

counterintuitive that it would further contribute to the generation of heat through browning of the WAT. Indeed, further research provided evidence that chronic endurance exercise exerts an antagonistic effect on classical BAT and Sc Ing WAT in rats. Eight weeks of treadmill training at 75-85% of peak VO_2 reduced iBAT mass and iBAT PGC-1α and UCP1 contents, while increasing PGC-1α and UCP1 content in the Sc Ing WAT tissue (91). Importantly, exercise training resulted in a 14.2% increase in energy expenditure during the dark cycle compared to sedentary controls (91). These findings showed that the thermogenic capacity of iBAT was attenuated by chronic endurance exercise, reducing its potential contribution to energy expenditure. It also suggested that the exercise-induced browning effect promoted energy dissipation within the Sc Ing WAT tissue and compensated for the reduction in the thermogenic capacity of classical BAT thermogenesis. The mechanism(s) by which exercise regulates the thermogenic capacities of the BAT and Sc Ing WAT remains unknown. However, because during exercise catecholamine release is increased (98), it could be possible that chronic endurance training could induce browning of the WAT and promote thermogenesis in this tissue through transient SNS activation (63, 99, 100). What seems to contradict this hypothesis is the fact that the same rise in sympathetic activity has opposing effects on the thermogenic responses of classical BAT (iBAT and aBAT for instance) and the Sc Ing WAT under chronic exercise conditions (91). An alternative hypothesis is that locally produced factors could drive the adaptive thermogenic responses of the Sc WAT to chronic endurance training. This would be a cell autonomous mechanism that overrides the action of the SNS and provides selectivity to the adaptive responses of WAT and classical BAT to chronic endurance exercise.

Thus, further work is needed to test these hypotheses and identify the mechanisms by which exercise induces antagonistic alterations in the thermogenic capacities of BAT and WAT.

In addition to chronic endurance exercise, browning could be induced through the actions of hormones. Fibroblast growth factor-21 (FGF21) has recently been identified as a protein that induces browning of the WAT. It belongs to a subgroup of the FGF family that functions in an endocrine manner and is expressed in the liver, thymus, islet β-cells, as well as in BAT and WAT adipose tissues (101). FGF21 is most highly expressed in the liver where it can be induced by fasting and ketogenic diets in a PPARα-depending manner (102). FGF21 signaling requires the presence of β-klotho proteins and the FGF receptor (FGFR) in order to elicit a downstream response (103, 104). This limits the action of this hormone only to those tissues that express both the receptor and β-klotho, which is the case of the WAT adipose tissue (104). Binding of FGF21 to the FGFR-β-klotho complex leads to autophosphorylation of tyrosine residues on the FGFR (105) (Figure 2-6). This leads to recruitment of Ras-GDP and its phosphorylation and conversion to Ras-GTP by the FGFR (105, 106). Ras-GTP subsequently activates the Raf kinase family of proteins that catalyze the phosphorylation and activation of MAPK/ERK kinase (MEK)1/2 (106). MEK1/2 phosphorylate tyrosine and threonine (Thr) in extracellular signal-regulated kinase (ERK)1/2 that has multiple downstream targets (106).

FGF21 was first identified as a stimulator of glucose uptake into adipocytes (107) and was shown to improve whole-body insulin sensitivity in *ob/ob* mice (107). Furthermore, FGF21 has been shown to induce the expression of *Ucp1* and *Dio2* in

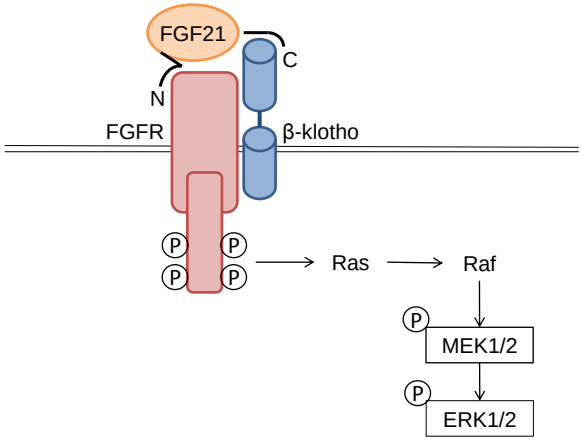

Figure 2-6: The FGF21 signaling pathway. FGF21 signaling requires both the receptor, FGFR, and the receptor co-factor, β-klotho. Binding of FGF21 to the FGFR-β-klotho complex leads to autophosphorylation of tyrosine residues on the FGFR. This leads to recruitment of Ras-GDP and its phosphorylation and conversion to Ras-GTP by the FGFR. Ras-GTP subsequently activates the Raf kinase family of proteins that catalyze the phosphorylation and activation of MEK1/2. MEK1/2 phosphorylate ERK1/2 that has multiple downstream targets.

BAT (108), which could increase energy expenditure through adaptive thermogenesis and utilize some of the excess calories that have accumulated in obesity. FGF21 could also be inducing browning in the WAT and further enhancing energy expenditure. Indeed, a 3-day infusion of FGF21 led to a 20-fold induction of *Ucp1* and 10-fold induction of *Dio2* in the Sc Ing WAT tissue in mice (108). Morphologically, there was also an increase in multilocular, UCP1 positive cells in the Sc Ing fat (108). Most importantly, genetic deletion of FGF21 resulted in an impaired induction of *Ucp1* and *Dio*2 in the Sc Ing adipose tissue following cold exposure, indicating the importance of FGF21 in the browning process (108). The effects of FGF21 were also dependent on PGC-1α (108). In addition, cold exposure and β3-Adr activation have been shown to

increase the mRNA expression and secretion of FGF21 from brown and Sc Ing adipocytes (108, 109). This response was mediated by a cAMP-responsive ATF2 binding site in the proximal region of the FGF21 gene promoter and was dependent on signaling through the cAMP, PKA, and p38 MAPK pathway (109). This data suggests the possibility of FGF21 acting in an autocrine manner in the adipose tissue. FGF21 could be produced by the BAT and Sc Ing WAT and exert an autocrine effect on these tissues to enhance thermogenesis and energy expenditure.

2.3. Skeletal muscle

2.3.1. Structure and excitation-contraction coupling

Skeletal muscle is the largest organ in the body, representing approximately 40% of total body weight in men and 30% in women (110). One of the main functions of skeletal muscle is to move or position the skeleton. Thus, each muscle is uniquely designed to perform its movement or stabilizing task (111). Movement is controlled by motor neurons (111). Each motor neuron in the muscle controls a cluster of multinucleated muscle cells or fibers. This unit of contraction is known as a motor unit and the force of contraction depends on the number of motor units recruited (111, 112). Individual fibers in the motor unit are each enclosed in a sarcolemma and contain a sarcoendoplasmic reticulum (SR), mitochondria, stored glycogen and lipid, and myofibrils made up of thick and thin filaments and their regulatory machinery. Neuronal signals from the brain initiate muscle contraction through the excitation-contraction coupling pathway (111). This pathway begins by the generation of an action potential in the α-motor neuron. The signal travels to the presynaptic neuron terminal, where it opens calcium (Ca^{2+}) voltage-gated channels, allowing Ca^{2+} to travel from the

extracellular space into the neuron. Ca^{2+} ions facilitate the interaction between nicotinic acetylcholine receptors (nAChRs) and soluble NSF attachment protein receptors (SNAREs), allowing for the fusion of the nACHRs to the presynaptic membrane and the release of acetylcholine (ACh) into the presynaptic cleft. nACHRs located on the sarcolemma of the muscle fiber bind ACh from the synaptic cleft. These receptors act as voltage gated channels and upon binding they open to allow for sodium (Na^{+}) influx leading to depolarization of the membrane. The local depolarization travels along the membrane to the t-tubule (an invagination of the sarcolemma located close to the terminal cisternae of the SR) where it causes a conformational change in the dihydropyridine receptor (DHPR) (111, 113). The DHPR is physically linked to a ryanodine receptor (RyR) on the SR and the conformational change results in the opening of the RyR and the release of Ca^{2+} into the sarcoplasm (111, 113). Ca^{2+} binds the regulatory protein troponin resulting in a removal of tropomyosin from the actin binding site, allowing for myosin to bind to actin. Lastly, myosin hydrolyzes an ATP, generating potential energy to mechanically move actin, resulting in muscle contraction. In order for muscle to relax, Ca^{2+} is removed from the sarcoplasm and pumped back in to the SR by sarco (endo) plasmic reticulum Ca^{2+}-ATPase (SERCA) pumps (114). This process requires ATP. SERCA pumps are expressed in cardiac and skeletal muscle and are inhibited by phospholamban (PLN) in the former and sarcolipin (SLN) in the latter tissue, respectively (114).

2.3.2. ATP production in skeletal muscle

Importantly, ATP is required both for myosin-actin binding in muscle contraction and muscle relaxation through the actions of the SERCA pumps. In the muscle ATP is

generated through one of three processes: phosphocreatine (PCr), glycolysis or oxidative phosphorylation. PCr generates ATP through the actions of creatine kinase donating a phosphate group to ADP (115). The reaction is quick however the muscle has a limited supply of PCr so there is a limited capacity to use and rely on this energy generating process (112).

Glycolysis is the breakdown of glucose into pyruvate, generating two ATP molecules per glucose molecule (116). The first step in the glycolytic pathway is the phosphorylation of glucose by hexokinase (glucokinase in the liver) to produce glucose-6-phosphate (G6P), a reaction that requires one ATP. The charged G6P is unable to travel back through the cell membrane and remains trapped inside the cell. G6P is then converted to fructose-6-phosphate, which is then phosphorylated by phosphofructokinase (PFK) to form fructose-1,6-bisphosphate. This reaction requires another ATP and is considered a rate limiting step in glycolysis. PFK is allosterically activated by AMP, an indication of low energy in the cell. In contrast, it is inhibited by ATP. Fructose-1,6-bisphosphate is split in to two compounds by aldolase, forming glyceraldehyde-3-phosphate (GAP) and DHAP. GAP is oxidized by glyceraldehyde-3-phosphate dehydrogenase (GAPDH), using NAD^+ as an electron acceptor and a phosphate group is also added to form 1,3-bisphosphoglycerate. As the GAP is constantly being used in the downstream step, DHAP is constantly being converted in to GAP by triose phosphate isomerase. The phosphate group on 1,3-bisphosphoglycerate is high in energy and is transferred to an ADP, forming ATP and 3-phosphoglycerate by the enzyme 3-phosphoglycerate kinase. In the final steps of glycolysis, 3-phosphoglycerate is converted into 2-phosphoglycerate and then water is removed by

an enolase, forming phosphoenolpyruvate PEP. The phosphate group on PEP is transferred to an ADP by pyruvate kinase (PK), forming ATP and pyruvate. The net yield of glycolysis from one extracellular glucose molecule is 2 ATP and 2 NADH. Glucose can also be obtained from stored glycogen. In this case, a glucose molecule on the nonreducing end of glycogen is phosphorylated by glycogen phosphorylase, producing glucose-1-phosphate (G1P), which is converted to G6P by phosphoglucomutase (116). The initial phosphorylation of glucose does not require an ATP and thus the net yield would be 3 ATP instead of 2. Glycolysis is an anaerobic pathway, not dependent on oxygen, and compared to PCr, has a larger capacity to produce ATP but requires more time to complete all of the steps (112). It is dependent on the availability of NAD^+.

Mitochondrial oxidative phosphorylation has the capacity to produce a large amount of ATP, using both glucose and fatty acids as substrates. The pathway is dependent on oxygen and requires significantly more time than ATP generation through PCr or glycolysis (112). Tissues with the most mitochondria and the most densely folded cristae have the highest capacity for oxidative phosphorylation (112). This pathway is a continuation of glycolysis (116). The final product of glycolysis, pyruvate, is transported into the mitochondria and converted to acetyl-CoA by the enzyme complex PDH. This complex is made up of three enzymes that each performs a step in the formation of acetyl-CoA. Pyruvate is first decarboxylated to form an acetyl group, which is then transferred to a coenzyme A to produce acetyl-CoA. NADH is also a product of this series of reactions. Acetyl-CoA then enters the tricarboxylic acid (TCA) cycle that is a series of reactions with the end products of 2 molecules of CO_2, 3 molecules of

NADH, and one molecule of $FADH_2$. NADH and $FADH_2$ are reducing agents that enter the electron transport chain to produce ATP. On the inner membrane of the mitochondria, a series of electron carrier complexes is arranged from highest to lowest redox potential (117). Complex I accepts electrons from NADH and complex II from $FADH_2$. These electrons are transported down the chain of complexes until complex IV where oxygen is the final acceptor of the electrons. Protons are transferred from the matrix to the inner membrane space by complexes I, II and IV, creating a proton gradient that drives the production of ATP by ATP synthase (117).

2.3.3. Skeletal muscle fiber type characterization

There are three types of skeletal muscle fibers characterized by their rate of contraction, their resistance to fatigue and their metabolism. Type I fibers are slow twitch fibers. They express the type I myosin heavy chair (MyHC) isoform (encoded for by the *Myh7* gene) (118). These fibers have the lowest maximum shortening velocity, peak power output, and rate of myofibrillar ATP hydrolysis (112). As such they do not generate a large amount of force, but are able to sustain contractions of lesser force over longer periods of time and do not fatigue quickly. ATP is generated for these longer periods of contractions through oxidative phosphorylation as type I fibers are highly oxidative and contain a larger number of capillaries and mitochondria (112). These fibers are also more sensitive to insulin and have a higher content of GLUT4 transporters that facilitate the increased insulin-stimulated glucose uptake rate found in type I fibers (112, 119). Type I fibers may be converted into type IIa fibers through high-frequency electrical stimulation and resistance training (112, 120). Interestingly, T2D patients have a decreased proportion of type I fibers and a decreased phosphorylation

of AKT in response to insulin (119) which may contribute to the impairments in glucose disposal in these patients.

Type IIa fibers express the type IIa MyHC isoform (encoded by the *Myh2* gene) (118) and are characterized by higher rates of shortening velocity, peak power output and myofibrillar ATP hydrolysis than type I fibers (112). They are able to generate more force in a shorter period of time and require a quicker source of ATP, mostly relying on glycolysis. These fibers fatigue more quickly than type I fibers (112). Interestingly, type IIa fibers may be converted into type I fibers through chronic low frequency stimulation and endurance exercise (112, 120). Adaptations in response to endurance exercise are mediated in part through the increased expression and activation of PGC-1α (121), the transcription factor that increases the expression of mitochondrial proteins and leads to an increase in mitochondrial density in the muscle, enhancing its capacity for oxidative phosphorylation. These adaptations allow the muscle to rely more on fat as a substrate for oxidation and rates of fat oxidation are increased with endurance exercise (121).

Type IIb fibers (type IIx in humans) express the type IIb MyHC isoform (encoded by the *Myh4* gene) (118) and have the highest rates of shortening velocity, myofibrillar ATP hydrolysis and peak power output (112). These fibers can generate a large amount of force in a short period of time and rely on PCr to generate ATP. As there are limited stores of PCr, there is limited capacity to produce ATP through this process and the muscle fatigues quickly (112). Type IIb fibers are able to contract and relax at higher rates because of an increased abundance of SERCA that facilitate movement of Ca^{2+} from the cytosol back into the SR (111). Type IIb fibers can be converted to type IIa

fibers through chronic low grade stimulation, however they cannot convert fully to type I fibers under this condition (120).

2.3.4. Skeletal muscle contribution to energy homeostasis

In the post-prandial state when circulating insulin levels are elevated, glucose uptake is stimulated in the skeletal muscle. As the skeletal muscle makes up approximately 30-40% of total body weight, it represents a significant site of glucose uptake and plays an important role in glucose homeostasis. While some of the glucose may be oxidized and used as fuel, the majority will be stored as glycogen in the muscle (122). Given the size of skeletal muscle, it represents the largest store of glycogen in the body (123). Furthermore, it has been shown that glycogen synthesis represents ~90% of non-oxidative glucose disposal and ~70% of whole-body glucose metabolism (124), demonstrating the importance of insulin-stimulated glycogen synthesis in the maintenance of whole-body glucose homeostasis. Individuals who are insulin resistant or who have T2D have a significantly reduced rate of insulin-stimulated glycogen synthesis (124) and this defect is considered to be the main contributor to the impaired glucose tolerance observed in these individuals (124, 125). Thus, studying the insulin signaling pathway in skeletal muscle is integral to understanding the mechanisms underlying these defects in order for effective therapies to be developed. The insulin-stimulated uptake of glucose begins with the binding of insulin to the IR located on the plasma membrane, leading to autophosphorylation of the IR through the activation of tyrosine kinase located in the β-subunit of the receptor (26) (Figure 2-7). The receptor

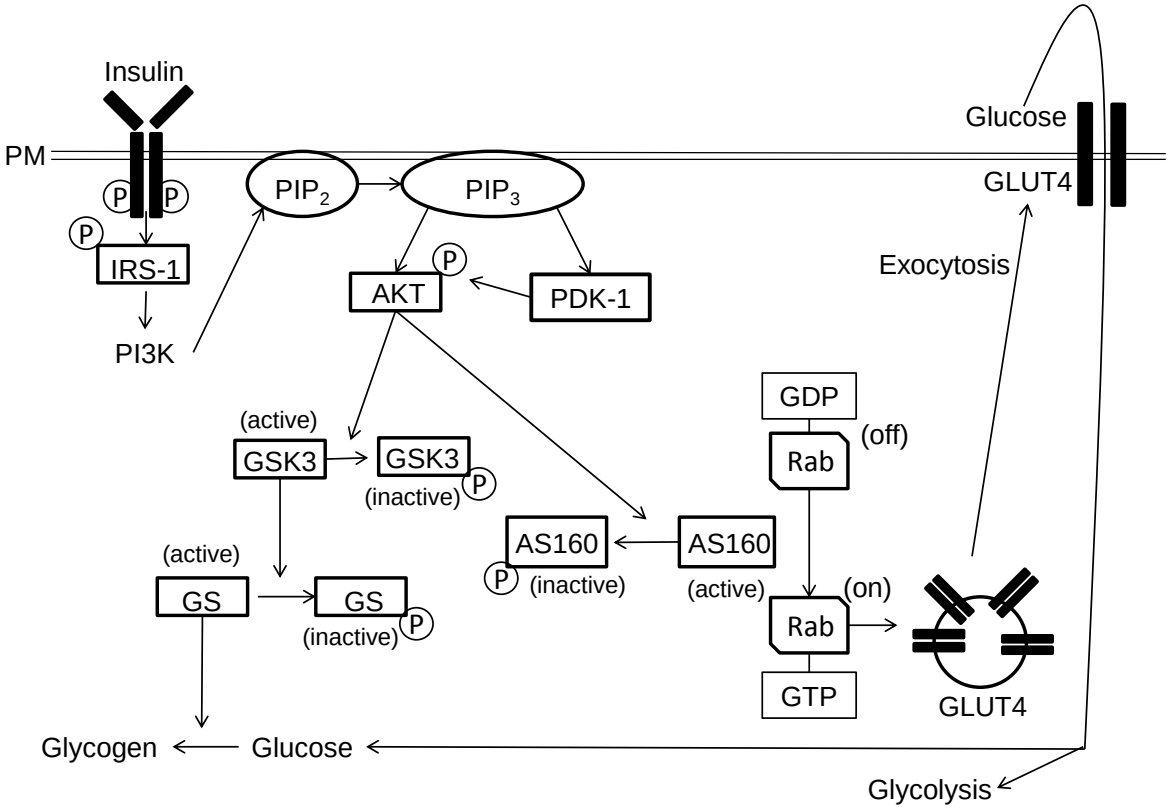

Figure 2-7: Schematic of glucose uptake into skeletal muscle. The insulin-stimulated uptake of glucose begins with the binding of insulin to the IR located on the plasma membrane (PM), leading to autophosphorylation of the IR through the activation of tyrosine kinase located in the β-subunit of the receptor. The receptor then catalyzes the tyrosine phosphorylation of IRS, leading to the recruitment of PI3K, which phosphorylates the membrane lipid PIP2 to form PIP3. The increase in PIP3 creates a lipid platform for proteins such as AKT where it is activated via phosphorylation by PDK1. pAKT subsequently phosphorylates and inactivates AS160, removing the inhibitory effect of AS160 on its Rab proteins and allowing for GLUT4 exocytosis and translocation to the PM to facilitate glucose uptake. Furthermore, pAKT phosphorylates GSK3α and β, which inactivates this enzyme. In its active form, GSK3 phosphorylates GS, inactivating the enzyme and reducing the rate of glycogen synthesis. With the binding of insulin, and the subsequent inactivation of GSK3, GS can be dephosphorylated and glycogen synthesis can proceed.

then catalyzes the tyrosine phosphorylation of the IRS protein, leading to the recruitment of PI3K, which phosphorylates the membrane lipid phosphatidylinositol-4,5-bisphosphate (PIP2) to form phosphatidylinositol-3,4,5-trisphosphate (PIP3) (26). The increase in PIP3 creates a lipid platform for proteins such as AKT and PDK1. AKT is activated via its phosphorylation on Thr 308 by PDK1 and serine (Ser) 473 residues by what is thought to be PDK2 (27). In its phosphorylated/activated state, AKT phosphorylates and inactivates AS160. This removes the inhibitory effect of AS160 on its target Rab proteins and allows for GLUT4-containing vesicles to translocate and fuse to the plasma membrane and enhance glucose uptake (26, 27). Furthermore, activated AKT phosphorylates glycogen synthase kinase 3α and β (GSK3α and GSK3β) on serine residues 21 and 9 respectively, which inactivates this enzyme (126). In its active form, GSK3 phosphorylates glycogen synthase (GS) at serine residues 641, 645, 649 and 653, inactivating the enzyme and reducing the rate of glycogen synthesis (123). With the binding of insulin, and the subsequent inactivation of GSK3, GS can be dephosphorylated and activated by PP1 (123).

Glucose uptake can also be stimulated in a non-insulin-dependent manner through the activation of AMPK. AMPK is a heterotrimeric protein composed of an α-catalytic subunit and two regulatory subunits (β and γ) (47). AMPK is activated with skeletal muscle contraction which causes a reduction in the AMP:ATP ratio as ATP is depleted. AMP binds cystathionine β-synthase sequence repeats (CBS domains) in the γ regulatory subunit of AMPK, directly activating it (47). Binding of AMP also leads to a conformational change in AMPK that allows for the phosphorylation of the α-catalytic subunit at Thr residue 172 by the upstream kinase LKB1. This further enhances AMPK

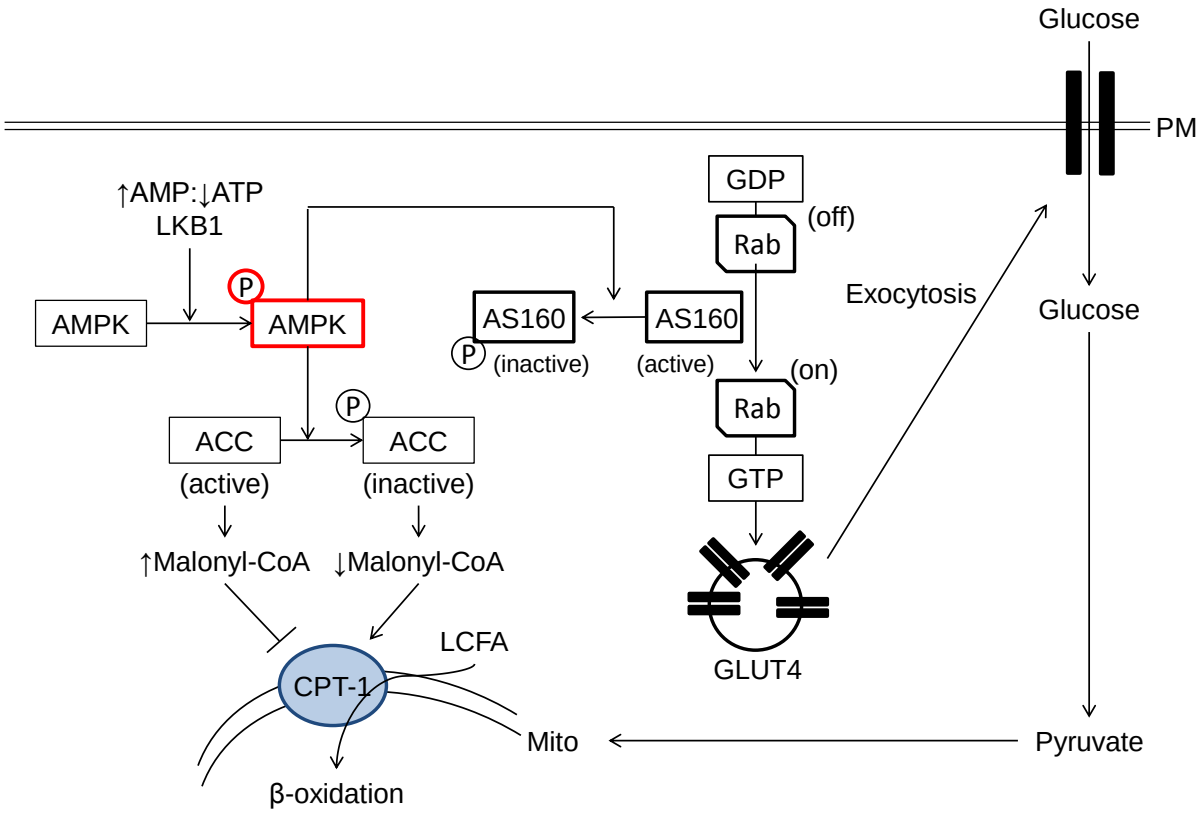

Figure 2-8: AMPK signaling pathway. AMPK is a cellular energy sensing protein that is activated by a reduction in the AMP:ATP ratio. Binding of AMP to AMPK leads to a conformational change that allows for the phosphorylation of AMPK by LKB1. AMPK modulates FA oxidation by phosphorylating and inactivating ACC which results in a reduced production of malonyl-CoA. This removes the inhibition of malonyl-CoA on CPT-1, the protein responsible for transporting LCFAs into the mitochondria. Removal of the inhibition thus allows for fatty acid transport into the mitochondria and for β-oxidation to proceed. AMPK also stimulates glucose uptake into the cell. Activated AMPK phosphorylates and inactivates AS160, removing the inhibitory effect of AS160 on its Rab proteins. This allows for GLUT4 exocytosis and translocation to the plasma membrane (PM) and for glucose uptake into the cell.

activity (47). Once activated, AMPK can then phosphorylate AS160 and remove the inhibitory effect of AS160 on its Rab proteins, which allows for GLUT4 translocation to the membrane and enhancement of glucose uptake (27) (Figure 2-8).

2.3.5. Skeletal muscle adaptation to cold

Skeletal muscle plays an important role in maintaining homeostasis upon exposure to cold. In mammals and adult humans, the initial response to acute cold exposure is the stimulation of shivering (muscle contraction) to generate heat (63). During this acute period, there is constant stimulation of the muscle fibers and adaptation to this stimulation is very similar to muscle adaptation to endurance exercise. Alterations include an increase in capillary density (127), an increase in mitochondrial oxidative capacity (128) and a shift in fiber composition, which has been shown in oxidative muscles only (128–130). Similarly to endurance exercise, cold exposure also increases glucose uptake in the skeletal muscle of rodents and humans. Glucose uptake is enhanced in the vastus lateralis, extensor digitorum longus, and soleus muscles of rats exposed to 4°C for two days (131). GLUT4 content has also been shown to be increased in the muscle of cold-exposed mice (132). Furthermore, glucose uptake and GLUT4 content was increased in the skeletal muscle of T2D humans after a 10-day cold acclimation protocol (80). With sufficient time, BAT is able to increase its UCP1 content and enhance its capacity for NST, which replaces the need for shivering thermogenesis (63). Recent research has shown that skeletal muscles also contribute to NST. They do so by generating heat through the uncoupling of SERCA ATP hydrolysis from Ca^{2+} transport, a process that is regulated by SLN (133–135). As alluded to earlier, SERCA is an integral membrane protein that transports or pumps Ca^{2+} from the cytoplasm into the SR, allowing muscle to relax (114). SERCA accomplishes this by going through a series of conformational changes (136, 137) (Figure 2-9). SERCA actually exists in two states: E1 and E2 (136, 137). In the E1 state,

SERCA Ca^{2+} binding sites face the cytosol and have a high affinity for Ca^{2+} (136, 137). Following Ca^{2+} binding, SERCA is autophosphorylated, becoming a high energy phosphoprotein intermediate (136). SERCA then transitions into its E2 conformation state, becoming a low energy phosphoprotein intermediate with Ca^{2+} binding sites facing the SR lumen that have a low affinity for Ca^{2+} (136). Ca^{2+} is subsequently released into the SR and the inorganic phosphate of the SERCA phosphoprotein intermediate is exchanged for water (136). SERCA transitions back to its E1 conformation (136). In skeletal muscle the transport of Ca^{2+} by SERCA is regulated by SLN, a protein of 31 amino acids in length that binds to SERCA in the SR membrane (138). SLN is highly expressed in rodent oxidative slow-twitch muscles such as the soleus, red gastrocnemius, and diaphragm (114). Binding of SLN does not inhibit the ATPase activity of SERCA, rather it promotes the early release of Ca^{2+} back into the cytosol after SERCA has been autophosphorylated and prior to SERCA transitioning to its E2 state (136, 137) (Figure 2-9B). This is referred to as slippage and it uncouples the actions of ATP hydrolysis from Ca^{2+} transport, producing heat instead (133, 137, 138). In fact, SLN has been shown to be an important regulator of body temperature during cold exposure. Recent research has shown that SLN-null mice had a reduced body temperature following 8 h of cold (4°C) exposure (135). Interestingly, wild-type mice that had their iBAT surgically removed were still able to maintain body temperature, whereas SLN-null mice that had their iBAT removed were unable to maintain their body

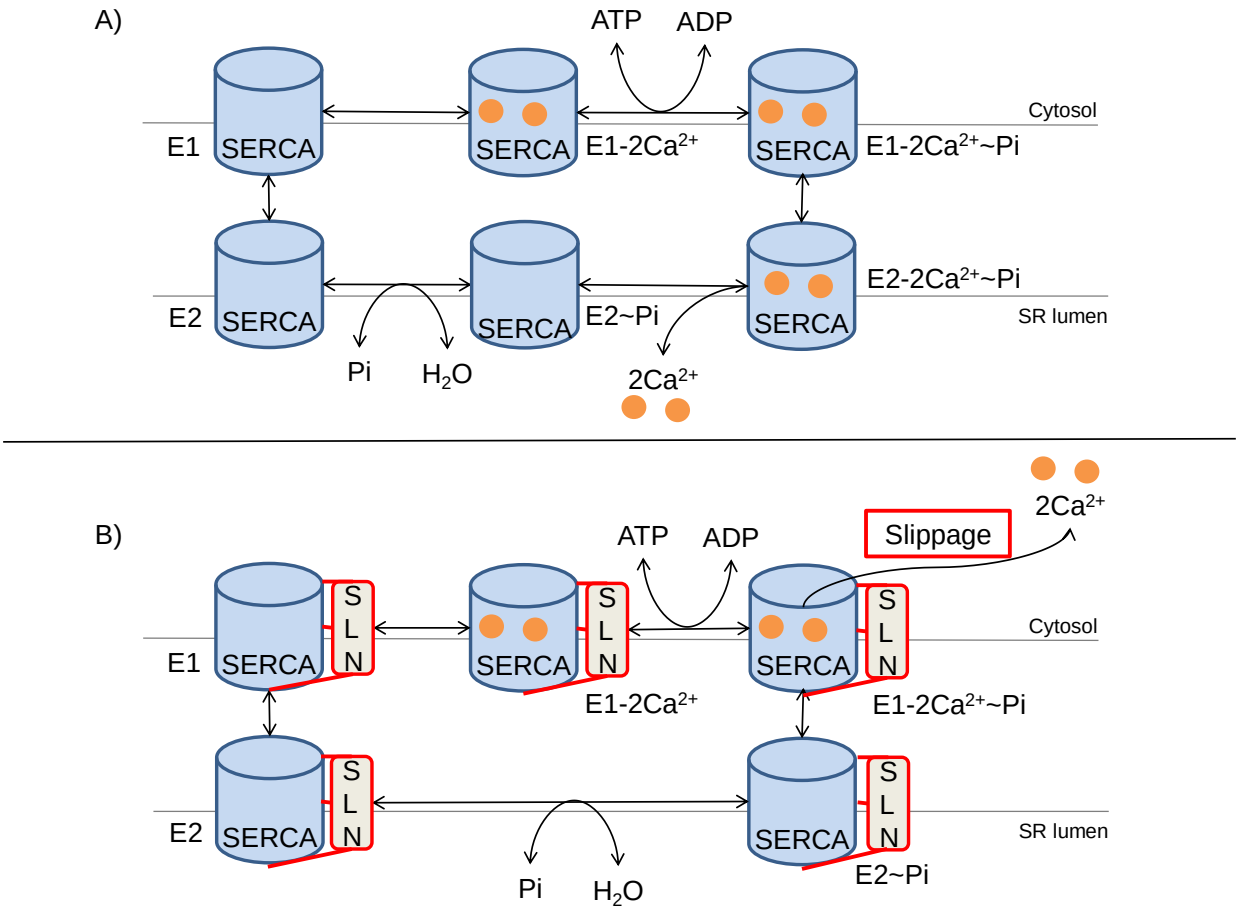

Figure 2-9: Regulation of SERCA by SLN. In the absence of SLN, SERCA pumps Ca^{2+} from the cytoplasm into the SR by going through a series of conformational changes (A). SERCA can exist in two states: E1 and E2. In the E1 state, SERCA Ca^{2+} binding sites face the cytosol and have a high affinity for Ca^{2+}. Following Ca^{2+} binding, SERCA is autophosphorylated, becoming a high energy phosphoprotein intermediate. SERCA then transitions into its E2 conformation state, becoming a low energy phosphoprotein intermediate with Ca^{2+} binding sites facing the SR lumen that have a low affinity for Ca^{2+}. Ca^{2+} is subsequently released into the SR and the inorganic phosphate of the SERCA phosphoprotein intermediate is exchanged for water. SERCA transitions back to its E1 conformation. In the presence of SLN, Ca^{2+} is released back into the cytosol after SERCA autophosphorylation and prior to SERCA transitioning to its E2 state (B). This is referred to as slippage and it uncouples the actions of ATP hydrolysis from Ca^{2+} transport, instead producing heat.

temperature and had to be removed from the cold to prevent death from hypothermia (135). These findings suggest that SLN-mediated NST can play a significant role in the maintenance of body temperature in the absence of BAT-mediated NST. Indeed, SLN was significantly upregulated in the gastrocnemius of cold-exposed iBAT-ablated mice compared to cold-exposed mice with intact iBAT (139). The increased SLN was accompanied by a significant increase in VO_2 upon initial exposure to 4°C and after 8 days of cold exposure (139). In order to provide the energy for this muscle-based NST, there was an increase in content of LPL and CD36 in the skeletal muscle (139), increasing the transport of fatty acids into the tissue. Furthermore, the content of mitochondrial complexes I, III and V, and staining intensity of succinate dehydrogenase were increased, providing evidence for an increase in mitochondrial oxidative capacity in the skeletal muscle (139).

Skeletal muscles can also contribute to maintaining energy homeostasis through muscle-based diet-induced thermogenesis (DIT) mediated by SLN (140). SLN content is increased in mice fed a HF diet for 12 weeks and this recruitment of SLN appears to be important in increasing energy expenditure and mitigating the effects of the HF diet as SLN-null mice gain significantly more weight on the HF diet than controls (135). SLN-null mice also displayed reduced insulin sensitivity following a glucose tolerance test (GTT) (135). These results were reproduced in a second study which showed a reduction in whole-body VO_2 during the dark cycle in HF-fed SLN-null mice (140). This reduction was accompanied by an increase in body weight and adiposity and a reduction in glucose tolerance (140).

2.4. Liver

The liver plays a critical role in the maintenance of energy homeostasis in the body, both in terms of glucose and lipid metabolism. In the fed state, glucose is transported directly from the intestine via the portal vein to the liver where it is either stored as glycogen or used to synthesize fatty acids (*de novo* lipogenesis) (141). GLUT2 is the main glucose transporter in the liver and is located at the membrane of hepatocytes. The uptake of glucose through GLUT2 is totally independent of insulin and allows a high influx of glucose into hepatocytes (141). The liver is a very versatile organ and has the capacity to store glucose as glycogen and release glucose to maintain blood glucose levels relatively constant despite variations is food availability. The liver is also capable of producing glucose from non-carbohydrate sources through a process called gluconeogenesis. This is very important for the maintenance of circulating glucose levels under conditions of fasting (141). These processes are described in detail below.

The transport of lipids proceeds in a very different manner (142). Following a meal, particles known as chylomicrons are formed in the enterocytes of the intestine. TAGs are the main component of chylomicrons, but these particles also contain cholesterol esters, phospholipids and apolipoprotein (Apo)A and B-48. From enterocytes, chylomicrons are absorbed first into the lymph vessels of the intestinal villi and enter the bloodstream via the thoracic duct. In the blood, chylomicrons acquire ApoC-II and ApoE from high density lipoproteins (HDL). ApoC-II activates LPL that is located at the capillary wall in peripheral tissues such as the skeletal muscle and adipose tissue. LPL hydrolyzes TAG from the chylomicrons, releasing FAs that may be

transported into these tissues for oxidation or storage. As chylomicrons donate their TAG content to peripheral tissues, ApoC-II and ApoA are transferred back to HDL and the chylomicrons become chylomicron remnants. Chylomicron remnants travel to the liver where they are removed from the blood through hepatocyte endocytosis, a process that requires interaction of chylomicron remnants with receptors for ApoE or ApoB/E on hepatocytes. Chylomicrons are degraded and their components reused by the liver. In the liver, remaining TAGs may be stored in hepatocytes, oxidized to produce ATP (described below) or repackaged into VLDLs and exported to the adipose tissue and other peripheral tissues to be stored or used as fuel (141).

2.4.1. Glucose metabolism in the liver

In the fed state, glucose travels to the liver by the portal vein and enters hepatocytes through GLUT2 transporters (141). As in the skeletal muscle, once glucose enters the tissue, it is then phosphorylated by a hexokinase (in the liver it is glucokinase) forming G6P (141). Unlike hexokinase in the skeletal muscle, glucokinase has a high Km and is not inhibited by G6P meaning that it remains active during periods of increased glucose concentration such as after a meal (116). G6P can be used by the liver to synthesize glycogen, or it can be converted to pyruvate through the glycolytic pathway (as described previously) and then be further used to synthesize FAs through lipogenesis.

2.4.1.1. Glycogen synthesis and breakdown

In the fed state, G6P can be used to synthesize glycogen. Importantly, even though hepatic glucose uptake does not require insulin, the storage of glucose into glycogen is largely dependent on this hormone (141). In fact, the liver is the organ that

receives the first bolus of insulin that is released by the pancreas. This is because endocrine pancreatic secretions are drained directly to the portal vein before reaching the systemic circulation to be distributed to other organs and tissues in the body (142). Therefore, as blood glucose levels rise after a meal, the pancreas releases insulin, which signals in the liver to promote glycogen storage. Under these circumstances, G6P is first converted into G1P by phosphoglucomutase and then into UDP-glucose by UDP-glucose pyrophosphorylase (143). UDP-glucose is transferred to the end of a pre-existing branch of glycogen (glycogenin) by GS to produce a new α1-4 glycosidic linkage (143). GS regulation in the liver and skeletal muscle is similar. As described earlier, GS is regulated in the fed state through the actions of insulin that lead to phosphorylation and inactivation of GSK3, which leaves GS in its dephosphorylated and active state (141, 143). GS can also be allosterically activated by G6P (126), which also promotes glycogen synthesis.

In the fasted state, when circulating insulin is low, glycogen is broken down into glucose through a process called glycogenolysis to help maintain circulating glucose levels. The removal of a glucose moiety from the non-reducing end of a glycogen molecule is catalyzed by glycogen phosphorylase (126, 143). Glycogen phosphorylase is activated following the binding of glucagon and epinephrine to glucagon and β-Adr, respectively. Binding to these G protein-coupled receptors activates AC and increases concentrations of cAMP. cAMP subsequently activates PKA which phosphorylates glycogen phosphorylase at serine residue 14, activating it (143). In the fed state, this signaling cascade is inactivated as there is a lack of glucagon and epinephrine. Furthermore, as previously mentioned, the increase in circulating insulin in the fed state

promotes the activation of PP1 that can dephosphorylate and inactivate glycogen phosphorylase (143).

2.4.1.2. Lipogenesis

In the fed state, glucose can also be used to synthesize fatty acids through *de novo* lipogenesis (141, 144). The process begins with the conversion of glucose into pyruvate (through the glycolytic pathway) and the transport of pyruvate into the mitochondria where it is converted into acetyl-CoA (Figure 2-10). Through a condensation reaction acetyl-CoA is combined with OAA to form citrate, which is catalyzed by citrate synthase (CS). Citrate is then exported out of the mitochondria where it is lysed into acetyl-CoA and OAA by ACL. Subsequently, acetyl-CoA is carboxylated by ACC to form malonyl-CoA, which is used to synthesize palmitic acid by FAS. NADPH provides the reducing power for fatty acid synthesis (141, 144). NADPH itself is produced via the pentose phosphate shuttle or the breakdown of malate into pyruvate through the action of malic enzyme. In addition to providing reducing equivalents, this reaction helps to maintain a source of pyruvate that is required for the initial step in fatty acid synthesis. Once palmitic acid is synthesized, it may be elongated by Elovl6 and desaturated by steroyl-CoA desaturase 1 (SCD1) (141, 144). These fatty acids can then be esterified to G3P (derived from glucose through the glycolytic pathway) forming a TAG, packaged into VLDL particles and transported to extrahepatic tissues such as the adipose tissue for storage.

Lipogenesis is primary controlled through the transcriptional regulation of lipogenic genes by carbohydrate response element binding protein (ChREBP), SREBP, and liver X receptor (LXR). ChREBP is a basic helix-loop-helix-leucine zipper

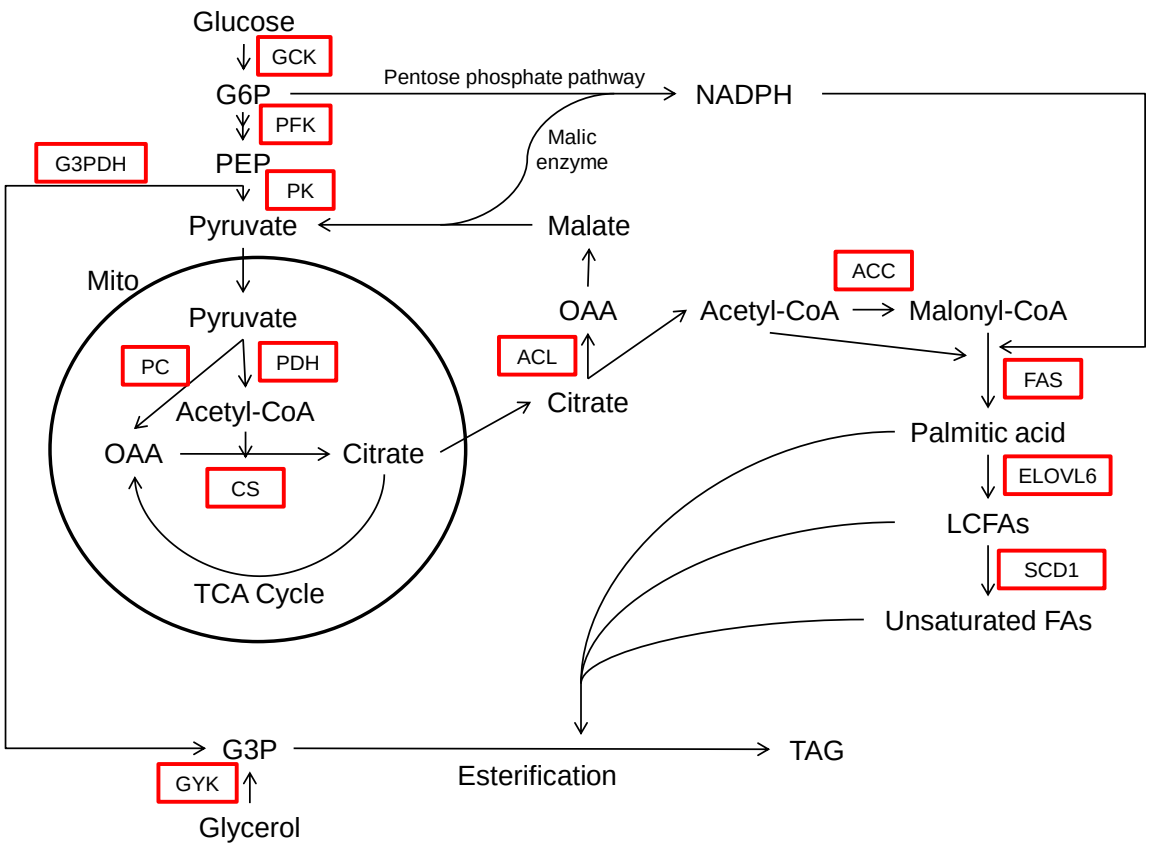

Figure 2-10: Schematic of the lipogenesis pathway. The process begins with the conversion of glucose into pyruvate (through the glycolytic pathway) and the transport of pyruvate into the mitochondria where it is converted into acetyl-CoA. Acetyl-CoA is combined with OAA to form citrate in a reaction catalyzed by CS. Citrate is then exported out of the mitochondria where it is lysed into acetyl-CoA and OAA by ACL. Subsequently, acetyl-CoA is carboxylated by ACC to form malonyl-CoA, which is used to synthesize palmitic acid by FAS. NADPH provides the reducing power for fatty acid synthesis. Once palmitic acid is synthesized, it may be elongated by Elovl6 and desaturated by SCD1. These fatty acids can then be esterified with G3P (derived from the glucose through the glycolytic pathway) into TAG.

transcription factor that forms a complex with Max-like protein that subsequently binds a carbohydrate response element at the promoter regions of target genes *Pk*, *Acl*, *Acc*, *Fas*, *Scd1* and *Elovl6* (144). Deletion of ChREBP results in the inhibition of glycolysis and lipogenesis (144). As the name suggests, ChREBP is regulated by glucose. Glucose metabolism to xylulose 5-phosphate through the pentose phosphate pathway activates PP2A, which dephosphorylates and activates ChREBP, promoting its translocation to the nucleus (145). In contrast, glucagon inhibits ChREBP via an increase in cAMP and activation of PKA that phosphorylates ChREBP at Ser 196 and Thr 666, deactivating it (146). ChREBP can also be phosphorylated by AMPK at Ser 568, reducing its DNA-binding activity (145).

SREBPs are categorized as basic helix-loop-helix-leucine zipper transcription factors (141, 144). SREBP-1c is the main isoform in the liver and it has been shown to regulate the lipogenic genes *Acl*, *Acc*, *Scd1* and glyceraldehyde-3-phosphate acyltransferase (an enzyme involved in esterification for TAG synthesis) (141, 144). It also regulates genes that produce NADPH, the reducing equivalent required for fatty acid synthesis (144). SREBPs exist in the cell as large precursor proteins complexed to SREBP cleavage-activating protein (SCAP) in the endoplasmic reticulum that must be transported to the Golgi apparatus for processing (147). Under conditions where there is an abundance of sterols, SCAP binds sterols, undergoes a conformational change and subsequently binds insulin-induced gene (INSIG) proteins (147). In the INSIG-bound state, the SREBP-SCAP complex remains sequestered in the endoplasmic reticulum (147). A low abundance of sterols removes this inhibition on SCAP and the SCAP-SREBP complex can be transported to the Golgi. SREBP is cleaved to its mature

N-terminal SREBP-1c form that can translocate to the nucleus and bind SREs and enhance transcription (147). Insulin regulates the expression and activity of SREBP in several ways. Insulin-induced activation of AKT leads to phosphorylation of SREBP-1c, increasing the affinity of SCAP-SREBP for coatomer protein II-coated vesicles that transport the complex to the Golgi apparatus for cleavage (144). In cell culture, activated AKT also phosphorylates and deactivates GSK3, reducing this kinase's ability to phosphorylate the N-terminal region of SREBP-1c, leaving the transcription factor is its activated state (144). AKT also activates mammalian target of rapamycin complex 1 (mTORC1), which has been shown to increase mRNA of *Srebp-1c* (147). Furthermore, insulin-induced activation of AKT can act independently of mTORC1, decreasing expression of *Insig2* and removing the inhibition on SCAP-SREBP transport (147). In contrast to insulin, increases in expression and processing of SREBP are inhibited by glucagon in a cAMP-dependent manner (144). The activity of SREBP-1c can also be modulated through acetylation. p-300-cAMP response element-binding protein (p-300-CREB) has been shown to acetylate and activate SREBP-1c, whereas SIRT1 deacetylates and inhibits it (144). The expression of *Srebp-1c* can also be increased by the binding of the transcription factor LXR to the SREBP promoter (144).

2.4.1.3. Gluconeogenesis

In the fasted state the liver plays a key role in maintaining blood glucose levels, first by breaking down glycogen and then through the endogenous production of glucose by the process of gluconeogenesis. Gluconeogenesis is the synthesis of glucose from precursors such as lactate, pyruvate, glycerol and amino acids (141, 143). Pyruvate is generated by the liver itself, whereas other precursors are delivered to the

liver from peripheral tissues such as the skeletal muscle (providing lactate and amino acids) and adipose tissue (providing glycerol). These substrates are first converted to pyruvate or other gluconeogenic precursors before entering the gluconeogenic pathway (141). Glycerol is converted first into G3P and then DHAP by GYK and G3PDH, respectively (Figure 2-11). DHAP is an intermediate in the glycolytic pathway and can act as a gluconeogenic precursor. The amino acid alanine can be directly converted into pyruvate by alanine aminotransferase (ALT), while other amino acids can be converted into intermediates of the TCA cycle, which are converted to OAA or pyruvate. Lactate can also be converted directly into pyruvate, a reaction catalyzed by lactate dehydrogenase (LDH) (Figure 2-11). The pyruvate formed is then transported into the mitochondria where it is converted into OAA by pyruvate carboxylase (PC) (Figure 2-11). Once pyruvate has been converted into OAA, it is shuttled into the cytoplasm via the OAA-malate shuttle. OAA is then converted into PEP by the cytoplasmic form of PEPCK (PEPCK-C). This is a key step in the gluconeogenic pathway (141, 143). PEP is then converted into fructose-1,6-bisphosphate through the reversal of steps in the glycolytic pathway. Fructose-1,6-bisphosphate is then converted into fructose-6-phosphate by fructose-1,6-bisphosphatase (FBPase) and is then converted into G6P by an isomerase. Lastly, G6P is converted to glucose by glucose-6-phosphatase (G6Pase).

In the prolonged fasted state, gluconeogenesis is activated through the upregulation of gluconeogenic proteins such as PEPCK and G6Pase which are regulated by a number of transcription factors. Glucagon and epinephrine can both increase the expression of gluconeogenic enzymes by increasing cAMP concentrations

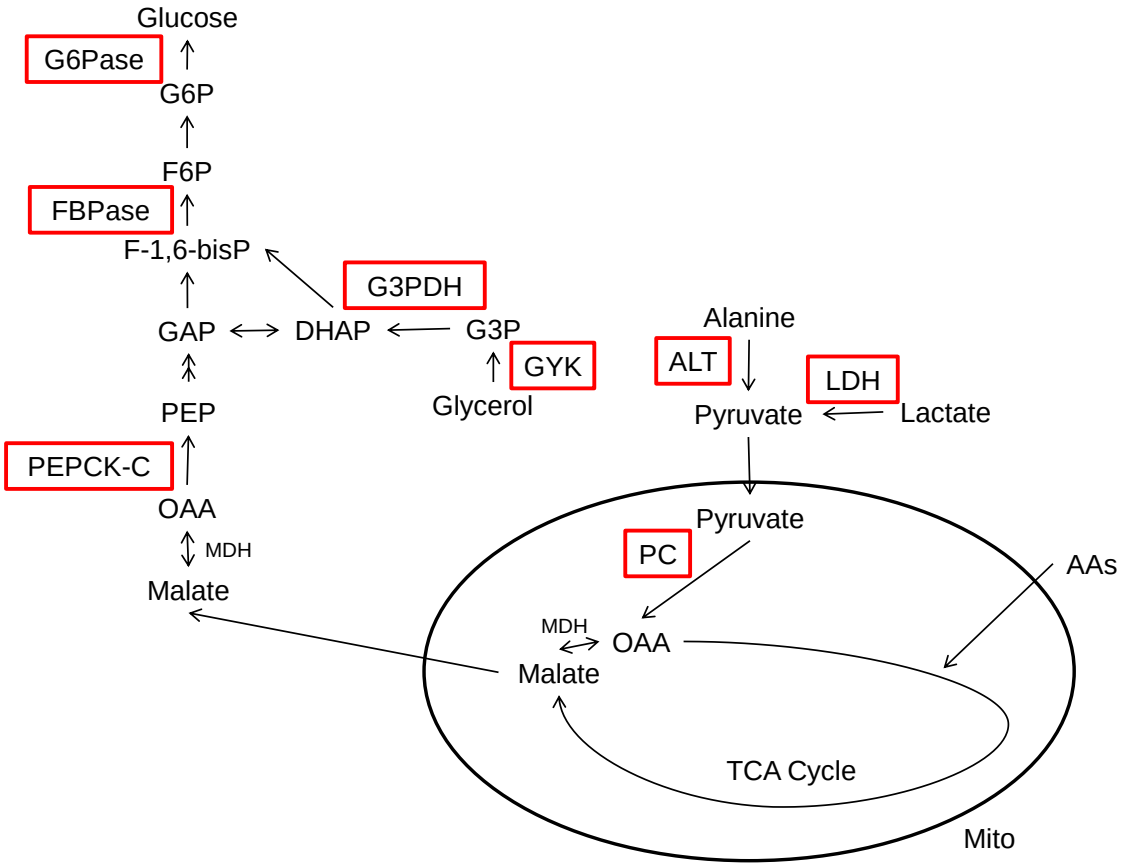

Figure 2-11: Schematic of the gluconeogenic pathway in the liver. In the liver, glucose is generated from glucoeneogenic precursors such as pyruvate, alanine, lactate and glycerol. Glycerol enters the gluconeogenic pathway after first being phosphorylated to G3P and converted to DHAP. Alanine and lactate can be directly converted to pyruvate, reactions catalyzed by ALT and LDH, respectively. Other amino acids can also act as gluconeogenic precursors, being first converted into substrates in the TCA cycle. The first step in the gluconeogenic pathway is the conversion of pyruvate into OAA by PC in the mitochondria (Mito). Once pyruvate has been converted into OAA, it is shuttled into the cytoplasm via the OAA- malate shuttle. OAA is then converted into PEP by PEPCK-C. This is a key step in the gluconeogenic pathway. PEP is then converted into fructose-1,6-bisphosphate through the reversal of steps in the glycolytic pathway. Fructose-1,6-bisphosphate is then converted into fructose-6-phosphate by FBPase and is then converted into G6P by an isomerase. Lastly, G6P is converted to glucose by G6Pase.

and activating PKA. PKA can then phosphorylate the transcription factor CREB at Ser-133, activating it (143). Phosphorylated CREB recruits CBP/p300 (an acetyltransferase) and associates with CREB-regulated transcriptional coactivators (CRTCs) in the promoter of PEPCK-C and G6Pase to increase expression of these proteins (143). CREB has also been shown to increase the expression of *Pgc-1α*, a transcription factor and regulator of gluconeogenesis (141). The importance of CREB and CRTC2 (the liver isoform of CRTC) in gluconeogenesis has been shown as knockdown of either led to reduced glucose production and a decrease in the expression of gluconeogenic enzymes (143).

Forkhead box O 1 (FoxO1) and PGC-1α are two important transcription factors involved in the regulation of gluconeogenesis in the liver. Both work to increase gluconeogenesis by upregulating the expression of *Pepck-c* and *G6pase* (143). Importantly, the effects of PGC-1α appear to be dependent on the nuclear receptor hepatocyte nuclear factor (HNF)-4α as induction of PEPCK-C and G6Pase is significantly impaired in hepatocytes from mice with liver-specific knock out of HNF-4α (148). While fasting induces an increase in FoxO1 and PGC-1α, the activities of both transcription factors can be enhanced through deacetylation by SIRT1 (an enzyme activated by the low-energy status of fasting) (143). In contrast, FoxO1 activity is decreased upon insulin–induced AKT phosphorylation which leads to nuclear exclusion of FoxO1 and its inactivation (149).

2.4.2. Fatty acid metabolism in the liver

In the fasted state, liver β-oxidation is increased in order to provide energy for gluconeogenesis and also to produce ketone bodies such as β-hydroxybutyrate,

acetoacetate and acetone that can be used as additional energy sources for extrahepatic tissues during fasting (141). The rate of liver β-oxidation is mediated by CPT-1a, the liver isoform of the CPT-1 protein, that facilitates the transport of LCFAs into the mitochondria (141). CPT-1 is inhibited by malonyl-CoA, an intermediate substrate in fatty acid synthesis that is synthesized by ACC.

β-oxidation in the liver is regulated by PPARα, a transcription factor that is activated by LCFAs (141). PGC-1α, a PPARα cofactor, also promotes β-oxidation in the liver by increasing the expression of oxidative genes (141). Recently, FGF21 has been identified as a hormone that regulates hepatic β-oxidation. FGF21 is induced in the liver with a ketogenic diet or fasting and its induction is largely dependent on PPARα, since PPARα-null mice displayed a reduced ability to increase hepatic FGF21 expression under these conditions (102). The role of FGF21 in mediating β-oxidation was confirmed via global knockdown of the *Fgf21* gene. Knock down of FGF21 resulted in increased serum TAG levels, as well as reductions in the ketogenic diet-induced expression of genes involved in β-oxidation (102). Acute treatment of mice with FGF21 increases liver PGC-1α content (150), demonstrating that FGF21 interacts with both PPARα and PGC-1α to enhance fatty acid oxidation in this tissue.

2.4.3. Liver adaptation to cold

Increases in epinephrine and glucagon during cold exposure activate glycogen phosphorylase to break down glycogen and release glucose (glycogenolysis). Indeed, it has been shown that liver glycogen content is reduced by approximate 50% after one week of cold exposure (151, 152). Cold exposure also increases the expression of *Pepck* and *G6pase* (132) and the activities of PEPCK, G6Pase, FBPase and ALT (151,

153) demonstrating that hepatic gluconeogenesis is also activated with cold to provide glucose. Interestingly, it has been reported that cold exposure does not alter expression of *Pgc-1α* and actually decreases the expression of *Hnf-4α* (154), which seems to be at odds with previous work the showed that PGC-1α-induced expression of gluconeogenic genes was dependent on HNF-4α (148). It is possible that other transcription factors such as FoxO1 may be mediating the cold-induced increase in gluconeogenic genes. In agreement with the increase in gluconeogenesis, liver expression of *Cpt-1a* is increased with cold exposure (132) showing that fatty acid β-oxidation is activated in the cold to provide the energy (ATP) to generate glucose. Lastly, the expression of *Srebp-1c* and *Fas* is reduced with cold exposure (132) as is the rate of acetate-I-C^{14} incorporation into LCFAs (155, 156), demonstrating that hepatic lipogenesis is reduced with cold exposure. Altogether, these findings provide evidence that even though food intake is significantly increased with cold exposure, the liver also undergoes major adaptive changes in its metabolism not only to cope with the high energy demand of thermogenesis, but also to maintain whole-body glucose homeostasis.

2.5. Obesity and T2D: Pathophysiology and Treatment

2.5.1. Alterations in Energy Metabolism with Obesity and T2D

Obesity and its related comorbidity T2D are characterized by an increase in circulating fatty acids and fasting blood glucose, hyperinsulinemia, insulin resistance and lipid deposition in peripheral non-adipose tissues. These changes are the result of alterations in energy metabolism in the WAT, liver and skeletal muscle described in the following section.

Given the large mass of skeletal muscle and its ability to take up glucose from the circulation, this tissue plays a significant role in whole-body glucose metabolism, and impairments in insulin signaling in this tissue have profound effects. Genetic models of obesity as well as diet-induced obese rodents show impaired glucose tolerance and glucose uptake into skeletal muscles (131, 157, 158), providing evidence for a link between obesity and the development of insulin resistance. One of the theories linking the two is lipotoxicity. Obesity leads to the ectopic storage of lipids in the skeletal muscle as the adipose tissue is no longer able to accommodate the excess lipids (159, 160). Lipid derivatives such as diacylglycerol (DAG) and ceramides are increased in obesity and have been shown to impair the insulin signaling pathway. DAG activates protein kinase C (PKC) which can phosphorylate IRS1 at Ser/Thr sites (159), inhibiting the insulin-stimulated signaling pathway. PKC has also been shown to phosphorylate inhibitor kappa B (IκB)-α, removing its inhibitory effects on NF-κB (159), allowing it to translocate to the nucleus and increase expression of pro-inflammatory cytokines such as TNF-α. TNF-α derived from the muscle or secreted from the inflamed adipose tissue can inhibit the insulin signaling pathway by promoting serine phosphorylation of IRS1 (161). Ceramides inhibit the insulin signaling cascade by impairing AKT phosphorylation (160). The large amount of evidence showing that lipid accumulation contributes to impairments in insulin signaling and insulin resistance suggests that new potential therapies for this obesity and T2D should address lipid overload and aim to reduce ectopic lipid deposition.

Obese WAT is characterized by increases in the size of adipocytes as the adipose tissue attempts to store all of the excess fat in this condition. Furthermore, a

state of chronic low-grade inflammation develops where there is an elevated production of cytokines and infiltration of macrophages into the WAT, which also becomes insulin resistant. In terms of metabolism, several studies have shown that obesity increases basal rates of lipolysis but decreases rates of stimulated lipolysis (39, 162). Impaired sensitivity to the antilipolytic effects of insulin may contribute to increased basal lipolysis rates (163), although elevated level of TNF-α secretion from enlarged adipocytes and infiltrated macrophages may also be responsible for increased basal lipolysis in the obese WAT (45). Treatment of 3T3-L1 adipocytes with TNF-α has been shown to increase basal lipolysis rates, primarily by decreasing content of the ATGL inhibitory protein G0S2 (164). TNF-α has also been shown to reduce the expression of *Plin* (164). In agreement with this data, obese individuals and rodents were shown to have reduced expression of *Plin* (15, 165). Obese individuals also have a lower content, phosphorylation, and activity of HSL (15, 39, 162, 165), which explains the reduction in stimulated lipolysis. There may also be impairments in the lipolytic signaling cascade at the adrenergic receptor level. Stimulated rates of lipolysis were reduced in isolated adipocytes from diet-induced obese mice treated with epinephrine, whereas treatment with forskolin (an AC activator that bypasses the β-Adr) led to rates of lipolysis similar to or higher than controls (15). Increased basal rates of lipolysis contribute to the increase in circulating NEFAs observed in obesity, which can negatively affect other peripheral tissues.

The excess adipose tissue-derived NEFAs contribute to the accumulation of excess fat in the liver, a condition known as hepatic steatosis (144). Liver lipogenesis is also increased in obesity, mediated in part through SREBP-1c (166). Expression of

Srebp-1c is increased in obesity and treating diet-induced obese mice with xanthohumol, a flavonoid that prevents the processing of SREBP-1c to its mature form, was shown to reduce hepatic lipid accumulation (166). The liver also becomes insulin-resistant in the obese state; however, it appears to be a selective insulin resistance as both lipogenesis and gluconeogenesis are increased in obesity when insulin should have opposing effects on these processes. This selective insulin resistance could be mediated downstream of AKT at the level of mTORC1, a protein that is required for the induction of SREBP-1c, but not PEPCK-C (167), however the exact mechanism is yet to be determined.

The inability to suppress hepatic gluconeogenesis is a contributing factor to the increased fasting plasma glucose that is observed in obesity and T2D (148, 168). FoxO1, a transcription factor that mediates the effects of insulin on gluconeogenic gene expression, has been shown to be involved in this dysregulation. Targeted disruption of FoxO1 reduced hepatic expression of *Pepck* and *G6pase* in control and HF-fed mice and led to a significant reduction in endogenous glucose production during a hyperinsulinemic-euglycemic clamp (168). PGC-1α, another transcriptional regulator of gluconeogenesis has also been shown to contribute to the dysregulation of this process through the PPARα-dependent activation of tribbles homolog TRB-3, a protein that inhibits AKT (169). The popular antidiabetic drug metformin functions to reduce circulating glucose by reducing the expression of gluconeogenic enzymes *Pepck* and *G6pase* (170, 171). However metformin has been shown to alter expression through an increase in the phosphorylation of AMPK by LKB1 (171). Activated AMPK in turn phosphorylates CRTC2, preventing its translocation to the nucleus where it would

normally increase the expression of *Pgc-1α* and its target genes *Pepck* and *G6pase* (171). Recent data has also shown that metformin can exert its effects in an AMPK-independent manner through alterations in the AMP:ATP ratio of the cell, which alters flux through the gluconeogenic pathway rather than enzyme expression (171).

Similarly to the adipose tissue, the liver is capable of synthesizing inflammatory markers and may also be exposed to a state of chronic low-grade inflammation following the development of steatosis (172). Indeed, HF-fed mice show an increased activity of nuclear factor-kappaB (NF-κB), the transcription factor that upregulates the expression of pro-inflammatory cytokines (172). Expression of inflammatory cytokines IL-1β, IL-6, and TNF-α was also increased in the liver by HF diet (172). Moreover, liver-specific inflammation resulted in reduced glucose tolerance and insulin sensitivity as measured by a hyperinsulinemic-euglycemic clamp and GTT (172), demonstrating that liver-derived inflammation can affect whole-body glucose metabolism.

2.5.2. The Therapeutic Potential of BAT

The significant increase in uptake of glucose and fatty acids from the circulation that occurs with BAT activation would appear to make BAT a target for the development of new therapies to combat obesity, T2D and dyslipidemia. However, up until 2009 BAT was thought to be exclusively present in human newborn infants and hibernating animals (63). It was not until advances in PET/CT scan technology using ^{18}F-fluorodeoxyglucose found active BAT in adult humans that interest was generated and BAT was explored as a potential new therapeutic tool (64, 65).

Recently, cold-induced activation of BAT has been shown to improve triglyceride-rich lipoprotein clearance in diet-induced obese mice and *Apoa5*$^{-/-}$ mice who display

severe hyperlipidemia (81). Furthermore, activation of BAT through treatment with CL 316,243, a β3-Adr agonist, reduced plasma VLDL-TG and plasma total cholesterol (specifically the low density lipoprotein fraction) while also decreasing the size of atherosclerotic lesions in the aortas of mice genetically engineered to develop hyperlipidemia and atherosclerosis (173). These effects were lost in mice with hyperlipidemia who also displayed a dysfunction in clearance of remnant lipoproteins by the liver (173), showing the importance of the liver in lipid homeostasis. BAT activation has also been shown to improve glucose sensitivity in control mice subjected to intermittent cold exposure (4°C, 2 hours/day, 5 days/week for 14 weeks) (174) as well as in HF- fed mice exposed to 12°C for 4 weeks (132) and HF-fed rats exposed to 4°C for 10 weeks (175). In HF-fed mice, the improvements in insulin sensitivity were associated with increased expression and content of GLUT4 in iBAT and skeletal muscles (132). Similar effects have also been found in human subjects. Glucose infusion rate increased in T2D subjects that were acclimated to the cold for 10 days (80). Though there was no effect of the cold on the phosphorylation of AKT in the human vastus lateralis muscle, GLUT4 translocation to the sarcolemma was significantly increased (80), which would have facilitated glucose transport into the muscle.

In addition to providing heat through NST when a mammal is exposed to the cold, the BAT also contributes to maintaining energy homeostasis in a state of obesity through DIT (63, 91). In obesity BAT is recruited through activation of the SNS and the content of UCP1 is increased in order to utilize the excess calories that have accumulated. This has been seen as mechanism by which the organism would attempt

to return the individual to a non-obese state (63). The adipokine leptin, which circulates in proportion to the amount of adipose tissue, has been shown to be involved in the activation of the BAT in obesity. iBAT temperature and *Ucp1* expression were increased following central leptin administration in mice (176, 177) and this response was lost in mice lacking dopamine β-hydroxylase, the enzyme that synthesizes NE showing that NE is critical to the signaling effects of leptin (176). Importantly, it has been shown that leptin signaling remains intact in the dorsomedial hypothalamus of diet-induced obese mice, despite the development of leptin resistance in the arcuate nucleus of hypothalamus (177), verifying that a portion of central leptin signaling remains intact to activate BAT in obesity.

As stated earlier, browning of the WAT can be induced through cold exposure or the use of β-adrenergic agonists. Research has begun to explore the benefits of activation of this tissue as a novel therapy for obesity and related disorders such as T2D. Specific attention has been placed on endocrine regulators of browning as recognized methods of activation such as cold exposure are uncomfortable and unlikely to be adhered to and non-specific SNS stimulators can have adverse effects on the cardiovascular system (178).

Researchers have explored the effects of irisin, the polypeptide shown to induce browning of the Sc Ing fat, in a model of obesity. Treating HF-fed mice with FNDC5-expressing adenovirus led to an increased expression of *Ucp1* that was similar to an increase observed in lean mice (90). Treatment also resulted in an increase in oxygen consumption, a reduction in body weight and an improved glucose tolerance in the HF-fed mice compared to control mice (90). This data suggests that inducing browning can

increase energy expenditure and alleviate the negative consequences of diet-induced obesity. Research has also explored the effects of the browning hormone FGF21. HF-fed mice with a transgenic overexpression of FGF21 gain less weight than control mice (107). Furthermore, overexpression of FGF21 resulted in a reduced percent body fat, reduced liver TAGs and an improved glucose tolerance compared to control mice (179). Monkeys given a human monoclonal antibody named mimAb1 that acts as a β-klotho and FGFR1c agonist displayed a reduction in body weight and fasting and fed plasma insulin and TAG levels (180). Importantly, FGF21 and irisin have been shown to induce UCP1 content and heat production in human neck adipocytes (181); however, the effects of FGF21 and/or irisin on the activation of brown/beige adipocytes *in vivo* in humans and subsequent effects on energy expenditure remain to be elucidated.

2.5.3. Pharmacological inhibition of β-oxidation as a therapy for obesity and T2D

While activation of the BAT and its increased uptake of circulating FAs and glucose is one potential therapeutic strategy for the treatment of obesity and T2D, pharmacological inhibition of FA oxidation could be another therapeutic approach. Rates of β-oxidation are increased in the liver in obesity and T2D, providing ATP and reducing equivalents that promote gluconeogenesis, a process that is already enhanced in an insulin-resistant state. Furthermore, increased FAs released from the adipose tissue in obesity and T2D promote FA oxidation in the skeletal muscle and a reduced reliance on glucose as fuel (182, 183), which could contribute to the elevated circulating glucose levels present in obesity and T2D. Pharmacological inhibition of β-oxidation could thus reduce gluconeogenesis in the liver and promote the use of glucose as fuel in the skeletal muscle that could subsequently reduce circulating glucose levels.

CPT-1, located on the outer mitochondrial membrane, is the rate-controlling enzyme for mitochondrial β-oxidation (182). In order for β-oxidation to proceed, FAs in the cytosol are first converted into their active form, fatty acyl-CoA, by fatty acyl-CoA synthetase (116) (Figure 2-12). CPT-1 then catalyzes the reaction between fatty acyl-CoAs and carnitine to form acylcarnitine (182). There is evidence to show that CD36 is involved in the transport of acylcarnitine from the outer to the inner mitochondrial membrane (184). Acylcarnitine is then shuttled across the inner mitochondrial membrane into the matrix by the carnitine acylcarnitine translocase in a 1:1 exchange with free carnitine (185). In the mitochondria, acylcarnitine is converted back into fatty acyl-CoA in a reaction catalyzed by CPT-2, and the fatty acyl-CoA is released to undergo β-oxidation (182) (Figure 2-12). CPT-1 is inhibited by malonyl-CoA. As described earlier, carboxylation of acetyl-CoA by ACC forms malonyl-CoA, an intermediate substrate in the fatty acid synthesis pathway. Malonyl-CoA can interact with and inhibit CPT-1, preventing LCFA transport into the mitochondria and thus reducing β-oxidation rates (186).

All tissues express the same isoform of CPT-2, whereas CPT-1 is expressed in a tissue-specific manner. Experiments to determine the CPT-1 isoform expression profile were completed using etomoxir, a non-specific inhibitor of CPT-1 (187). Etomoxir is classified as an oxirane carboxylic acid that irreversibly inhibits CPT-1 by competitively binding to the same site on the enzyme as malonyl-CoA (182). Dinitrophenol (DNP)-etomoxir, an analog of etomoxir that is a specific inhibitor of CPT-1a, has also been used to investigate the expression profile of CPT-1 (188). CPT-1a is the liver-specific isoform of CPT-1. It is ~88 kDa in size and is characterized by a Km for carnitine of 30 μM and an I_{50} for malonyl-CoA of 2.7 μM (the concentration of malonyl-CoA required

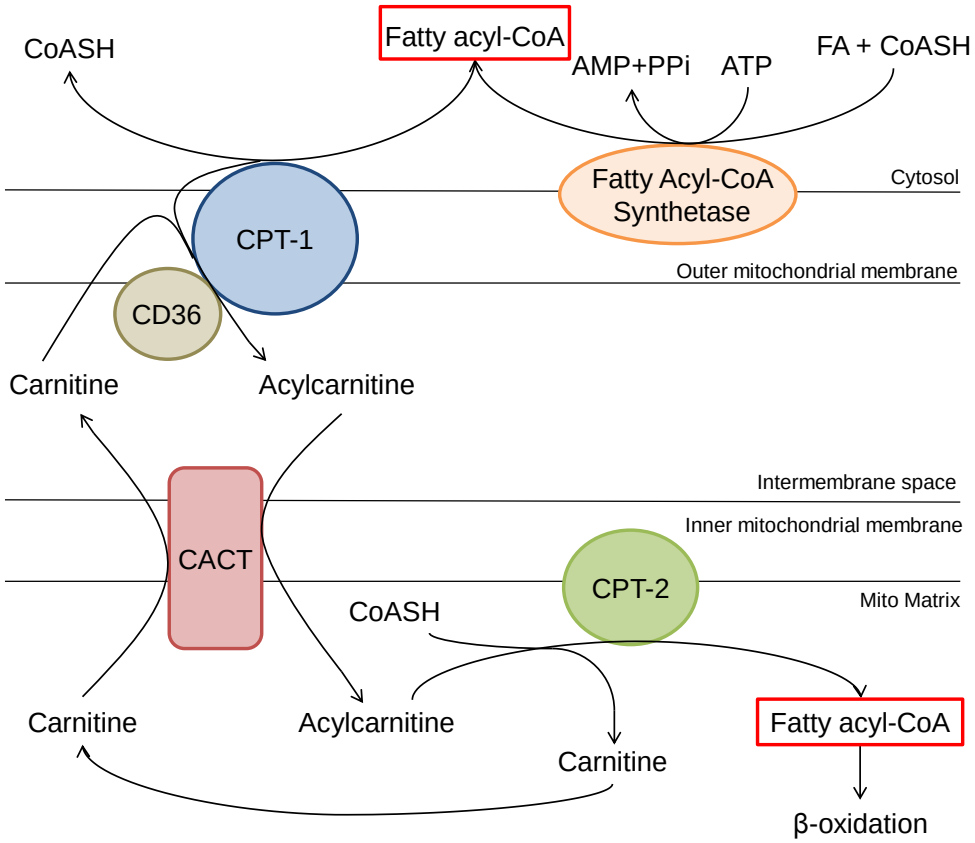

Figure 2-12: Import of LCFA into the mitochondria for β-oxidation. In the cytosol, FAs are first converted into their active form, fatty acyl-CoA, by fatty acyl-CoA synthetase. CPT-1 then catalyzes the reaction between fatty acyl-CoAs and carnitine to form acylcarnitine. There is evidence to show that CD36 is involved in the transport of acylcarnitine from the outer to the inner mitochondrial membrane. Acylcarnitine is then shuttled across the inner mitochondrial membrane into the matrix by the carnitine acylcarnitine translocase (CACT) in an exchange with free carnitine. In the mitochondria, acylcarnitine is converted back into fatty acyl-CoA in a reaction catalyzed by CPT-2, and the fatty acyl-CoA is released to undergo β-oxidation.

to inhibit enzyme activity by 50%) (188). The muscle-specific isoform (CPT-1b) in contrast, is slightly smaller in size at ~82 kDa and is characterized by a higher Km (lower affinity) for carnitine (500 μM) and a lower I_{50} for malonyl-CoA of 0.03 μM (188), showing that malonyl-CoA is a strong inhibitor of this CPT-1 isoform. Interestingly, CPT-1 in the heart displayed characteristics intermediate of the liver and muscle isoforms (a

Km for carnitine of 200 μM and an I_{50} for malonyl-CoA of 0.1 μM) (188). Experiments using dinitrophenol (DNP)-etomoxir demonstrated that the heart contained both CPT-1a and b isoforms, however the CPT-1a isoform only accounted for approximately 2% of total heart CPT-1 activity (188).

The adipose tissue also expresses CPT-1. Using [^{3}H]etomoxir labelling of isolated mitochondria, researchers demonstrated that the heart, skeletal muscle and BAT expressed the CPT-1b isoform, whereas the WAT expressed the CPT-1a isoform (187). As the WAT contains a variety of cell types, it was possible that CPT-1 isoform expression differed amongst the various cells. Indeed, when the WAT adipocytes were isolated and their isolated mitochondria treated with [^{3}H]etomoxir, they were shown to express the CPT-1b isoform (187). CPT-1 is also expressed in the brain (CPT-1a and c), kidney (CPT-1a), pancreas (CPT-1a), lung (CPT-1a), intestine (CPT-1a), ovaries (CPT-1a) and testes (CPT-1b) (182).

CPT-1 is a possible pharmacological target for reducing β-oxidation. As described earlier, β-oxidation is enhanced in the liver in obesity and T2D and promotes gluconeogenesis by generating ATP and reducing equivalents. Thus inhibiting CPT-1 and β-oxidation in this tissue could help reduce rates of gluconeogenesis. Furthermore, inhibiting β-oxidation in the skeletal muscle could increase the reliance of this tissue on glucose as fuel, which could help reduce circulating glucose levels that are elevated in obesity and T2D. The non-specific CPT-1 inhibitor etomoxir has been studied in rodents and humans with metabolic syndrome and T2D. One week of etomoxir treatment significantly reduced fasting blood glucose levels in streptozotocin (STZ) diabetic rats (189). Furthermore, etomoxir treatment increased glucose oxidation in isolated

adipocytes of STZ diabetic rats (190). In healthy, lean humans fed a HF diet, five days of etomoxir treatment increased 24 h respiratory quotients, indicating a reduction in fatty acid oxidation (191). In another study, etomoxir treatment for three days significantly increased glucose oxidation and reduced hepatic glucose production in diabetic patients (192). In fact, a single dose of etomoxir has been shown to enhance glucose metabolic clearance rate during a hyperinsulinemic-euglycemic clamp in T2D patients (193). However, etomoxir has been shown to negatively impact liver mitochondria. Treatment of human and rat liver strips with etomoxir led to significant alterations in mitochondrial morphology and an increase in expression of genes involved in oxidative stress and apoptosis (194). Furthermore a clinical trial investigating etomoxir as a therapy for heart failure patients was terminated in part due to abnormal increases in liver ALT levels (182).

An alternative to the non-specific pharmacological inhibitor etomoxir is oxfenicine (*S*-2-(4-hydroxyphenyl)glycine), which is specific for the CPT-1b isoform present in skeletal muscles and adipose tissue. Oxfenicine could potentially ameliorate glucose utilization in obesity and T2D without the negative consequences that a non-specific inhibitor could have on other tissues (*e.g*. liver). In order to exert its effects, oxfenicine must first be transaminated to its active form, 4-hydroxyphenylglyoxylate (4-HPG), which is competitive with carnitine, preventing the formation of acylcarnitines (195). The tissue-specific inhibition of β-oxidation by oxfenicine is the result of two mechanisms. First, tissues that express CPT-1b have the greatest aminotransferase enzyme activity that is required to transaminate oxfenicine into its active form 4-HPG (195). Second, CPT-1b has an I_{50} for 4-HPG of 11 μM, whereas CPT-1a has an I_{50} for 4-HPG of 510

μM meaning that CPT-1b is more sensitive to the inhibitory effects of 4-HPG (195). Thus, treatment with oxfenicine would specifically target tissues such as the heart, skeletal muscle and WAT that express the CPT-1b isoform. Oxfenicine treatment was originally used to protect the heart from the effects of myocardial ischemia (182), but recent research has focused on the effects of oxfenicine in skeletal muscles. Randle was the first to propose that inhibiting β-oxidation would lead to an increase in glucose uptake and oxidation in the skeletal muscle (196). His theory was based on the fact that increases in mitochondrial acetyl-CoA and the NADH:NAD+ ratio that occur as a result of increased fatty acid oxidation inhibit PDH through activation of pyruvate dehydrogenase kinase, inhibiting glucose oxidation (196). Glucose metabolism could also be inhibited at the level of PFK by citrate and at the level of hexokinase by G6P or long-chain acyl-CoA derivatives (186, 196). Interestingly, recent research has found positive metabolic outcomes in the skeletal muscle of mice treated with oxfenicine. HF-fed mice given daily oxfenicine injections for 14 days had a reduced area under the curve for glycemia following a GTT compared to HF-fed control animals, indicating an improvement in whole-body insulin sensitivity (157). Further analysis of the gastrocnemius muscle revealed an increased phosphorylated AKT to total AKT ratio, as well as an increase in GLUT4 content (157). Muscle-specific inhibition of β-oxidation has also been studied using a muscle-specific deletion of CPT-1b ($Cpt1b^{m-/-}$ mice) (197). These mice had a lower body weight and fat mass than their wild-type controls and also had an increased RER, demonstrating an increase in whole-body glucose oxidation (197). Furthermore, despite an accumulation of ceramide and DAG in the skeletal muscle, the mice had reduced fasting blood glucose and insulin and an

improved glucose tolerance demonstrated during a GTT (197). Notably, in both models of β-oxidation inhibition, plasma NEFAs and TAGs were elevated as a result of the inhibition (157, 197). It is likely that the adipose tissue compensated for this elevation in plasma NEFAs and TAGs through a decrease in lipolysis to prevent additional release of FAs and/or through an increase in lipogenesis to promote storage of the excess lipids. The adipose tissue may also be directly affected by CPT-1b inhibition, since it also expresses this isoform. This requires further research as recent studies lacked any examination of the effect of oxfenicine on the adipose tissue.

CHAPTER 3: Objectives and Hypotheses

This dissertation presents two possible approaches to enhancing glucose utilization, improving insulin sensitivity and reducing fat mass that could be applied in the treatment of obesity and T2D. The mechanisms of action of these approaches are very different. The first is a pharmacological inhibition of mitochondrial LCFA import that limits the oxidation of FAs and increases the reliance on glucose as a fuel. The second approach is cold-induced thermogenesis. Cold activates the BAT and NST, a very energy-consuming process that significantly increases uptake and oxidation of FAs and glucose in this tissue. While both approaches have been studied for their beneficial effects on glucose homeostasis, the effects of these therapeutic approaches on the interactive response of several peripheral tissues remain to be investigated. Specifically, information is lacking on the effects that inhibition of mitochondrial LCFA import would have on the WAT, a tissue that is the main storage depot for fat that could compensate for the reduced fatty acid oxidation. Furthermore, numerous studies have examined the adaptations of the BAT to cold exposure, however information is lacking on the mechanisms involved in the adaptations that occur in the WAT compared to the BAT under cold conditions. In addition, a thorough examination of the mechanisms involved in the adaptations of skeletal muscle, of varying fiber type composition, and liver to cold exposure have not been completed. The 5 studies in this dissertation aim to address these gaps in the literature and enhance our current understanding of these two therapeutic approaches. The specific objectives and hypotheses of each study are outlined below.

OBJECTIVE for STUDY 1 (Chapter 4): A consequence of inhibiting mitochondrial LCFA import is an increase in circulating NEFAs that must find an alternate metabolic fate. The objectives of this study were to investigate and characterize the metabolic adaptations that occur in the Epid and Sc Ing WAT depots following three weeks of treatment with the CPT-1b inhibitor oxfenicine that could compensate for and accommodate this increase in circulating NEFAs.

Hypotheses:

1. Three weeks of oxfenicine treatment will result in a reduction in lipolysis from the Epid and Sc Ing WAT to prevent further release of NEFAs as inhibition of their utilization would promote an accumulation of this substrate in the circulation. Therefore, I hypothesized that lipolysis would be inhibited as a compensatory response.
2. Conversely, lipogenesis in the Epid and Sc Ing WAT would be increased in order to promote the storage of excess NEFAs as TAGs in the WAT.

OBJECTIVE for STUDY 2 (Chapter 5): It has been previously reported that cold exposure activates the BAT and induces browning of Sc Ing WAT, but not the Epid WAT. In this context, the objectives of this study were to characterize the physiological adaptations that occur in the Sc Ing WAT compared to the BAT and Epid WAT and investigate whether cold-induced browning of the Sc Ing WAT depot reduced adiposity through enhancement of UCP1-mediated thermogenesis.

Hypotheses:

1. Cold-induced activation of the iBAT and aBAT would result in increased oxidation of glucose and FAs that would maintain circulating glucose and FA levels similar to that of animals kept at room temperature, despite increases in food intake and WAT lipolysis.

2. Expression of FA transporters would be increased to facilitate increased FA uptake into the iBAT and aBAT.

3. Cold exposure would increase UCP1 content (browning) in the Sc Ing WAT, enhance oxidation of FAs, promote energy dissipation, and reduce the exportation of FAs from this depot.

4. Cold acclimation would increase lipolysis in the Epid WAT in order to provide substrate to fuel thermogenesis in BAT. It would also increase ATGL content, HSL phosphorylation, and facilitate adiposity reduction.

OBJECTIVE for STUDY 3 (Chapter 6): FGF21 is a protein that is induced with cold exposure and that has been shown to activate BAT and induce browning of the Sc Ing WAT. The objectives of this study were to investigate the source of cold-induced FGF21 and examine the FGF21 signaling pathway in two depots of BAT and two depots of WAT.

Hypotheses:

1. Cold exposure would increase circulating FGF21 as well as the expression of *Fgf21*, the FGF receptor *Fgfr1,* and the receptor co-factor *β-klotho* in the BAT and Sc Ing WAT.

2. Downstream signaling of FGF21 would be increased in BAT and Sc Ing WAT, the WAT depot that is known to undergo browning, but not the Epid WAT, a depot that does not undergo browning.

OBJECTIVE for STUDY 4 (Chapter 7): Glycogen synthesis in the skeletal muscle is a main contributor to whole-body glucose and energy homeostasis. However, muscles with different fiber type composition display distinct metabolic characteristics with respect to glucose and lipid metabolism. Thus, metabolic adaptation to cold exposure

may also be fiber type-specific. The objectives of this study were to investigate the adaptations to seven days of cold exposure of skeletal muscles with different fiber type composition and to determine the contribution of this organ to glucose and fat disposal under cold acclimating conditions.

Hypotheses:

1. Cold exposure would enhance downstream insulin signaling in all muscles regardless of fiber type composition.

2. Cold exposure would increase FA oxidation specifically in muscles that contain predominantly type I fibers, an effect that would be mediated by an increase in the phosphorylation of AMPK and the expression of *Pgc-1α,* and fat transporters in these muscles.

3. Cold-induced upregulation of SLN would occur in a fiber type-dependent manner.

OBJECTIVE for STUDY 5 (Chapter 8): The liver plays a critical role in maintaining whole-body energy homeostasis, both in terms of glucose and lipid metabolism. Under conditions of cold exposure the liver is expected to undergo significant metabolic adaptation in order to maintain glucose homeostasis and provide addition substrate to thermogenic tissues. This is because cold acclimated rats display hyperphagia and enhanced substrate utilization in BAT and other peripheral tissues. Thus, the objectives of this study were to examine the changes in hepatic gluconeogenesis, lipogenesis and glucose and FA oxidation in order to characterize the role of the liver in maintaining energy homeostasis during cold adaptation. I also aimed to unravel the molecular mechanisms controlling these adaptations.

Hypotheses:

1. Circulating insulin would be reduced and circulating glucagon increased in order to promote hepatic gluconeogenesis under cold acclimating conditions. Furthermore, the expression of *FoxO1*, *Crtc2*, *G6pase* and *Fbp1*, and protein content of PEPCK and PGC-1α, which are major factors involved in the regulation of hepatic gluconeogenesis, would be increased with cold exposure.

2. Glucose and FA oxidation would be enhanced with cold exposure in order to fuel the increased energy requirements of this tissue under cold stress. FA oxidation would also provide ATP and reducing equivalents for gluconeogenesis. The expression of *Cpt-1a, Acot2,* and *Cox6c* would be increased, whereas the expression of *Pdk4* would be decreased to facilitate upregulation of oxidation.

3. Enhanced gluconeogenesis and glucose oxidation would result in a reduction in glycogen content in the liver.

CHAPTER 4: Antilipolytic and antilipogenic effects of the CPT-1b inhibitor oxfenicine in the white adipose tissue of rats

Diane M. Sepa-Kishi, Michelle V. Wu, Abinas Uthayakumar, Arta Mohasses, Rolando B. Ceddia.

School of Kinesiology and Health Science, York University, Toronto, Ontario, Canada

Keywords: Fatty acid/Oxidation; Subcutaneous and visceral fat; Insulin resistance; Lipolysis and fatty acid metabolism; CPT-1b inhibition

(**Diane M. Sepa-Kishi**, Michelle V. Wu, Abinas Uthayakumar, Arta Mohasses, Rolando B. Ceddia. Antilipolytic and antilipogenic effects of the CPT-1b inhibitor oxfenicine in the white adipose tissue of rats. *Am J Physiol Regul Integr Comp Physiol* 311: R779-R787, 2016.)

Statement of Labour

The majority of the experiments conducted in this study were carried out by Diane M. Sepa-Kishi. DMSK's contributions included administration of the high fat diet, daily oxfenicine injections, performing the glucose tolerance test (GTT), collection of blood samples, extraction of tissues, isolation of adipocytes, and conducting the oxidation, lipolysis and glucose incorporation into lipids assays. DMSK was also responsible for conducting and collecting all western blot data, analyzing and interpreting the results, preparing figures, and writing and revising the manuscript. DMSK was supported by a NSERC Alexander Graham Bell Canada Graduate Scholarship and an Elia Scholarship. Due to the logistics of this study, MVW, AU, and AM assisted with administration of the HF diet, daily oxfenicine injections, performing the GTT, collection of blood samples and extraction of tissues. MVW also assisted with the isolation of adipocytes, conducting the assays, and analyzing the results. MVW, AU, and AM revised the manuscript.

Dr. Rolando Ceddia is the primary investigator and supervisor of this project and this research was funded by a Discovery Grant from NSERC and by infrastructure grants from the Canada Foundation for Innovation and the Ontario Research Fund.

4.1. Abstract

Oxfenicine is a carnitine-palmitoyl transferase 1b (CPT-1b)-specific inhibitor that has been shown to improve whole-body insulin sensitivity while suppressing fatty acid (FA) oxidation and increasing circulating FA. Because the white adipose tissue (WAT) is an organ that stores and releases FAs, this study investigated whether oxfenicine-induced inhibition of FA oxidation affected adiposity and WAT metabolism in rats fed either low (LF) or high-fat (HF) diets. Following 8 weeks of dietary intervention, male Sprague-Dawley rats were given a daily i.p. injection of oxfenicine (150 mg/kg body weight) or vehicle (PBS) for 3 weeks. Oxfenicine treatment reduced whole-body fat oxidation, body weight, and adiposity and improved insulin sensitivity in HF-fed rats. All these effects occurred without alterations in food intake, energy expenditure, and ambulatory activity. *In vivo* oxfenicine treatment reduced FA oxidation and lipolysis in subcutaneous inguinal (Sc Ing) adipocytes, whereas glucose incorporation into lipids (lipogenesis) was significantly reduced in both Sc Ing and epididymal (Epid) adipocytes. In summary, our results show that oxfenicine-induced inhibition of CPT-1b markedly affects WAT metabolism, leading to reduced adiposity through a mechanism that involves reduced lipogenesis in the Sc Ing and Epid fat depots of rats.

4.2. Introduction

Obesity is a prevalent metabolic disorder and major risk factor for type 2 diabetes (T2D). In this context, strategies to prevent the development of insulin resistance and progression to T2D are of great therapeutic interest. Many theories exist attempting to mechanistically link obesity and T2D and identify appropriate targets for intervention, one of which is the Randle cycle of substrate interaction (196). The Randle cycle proposed that the increases in mitochondrial acetyl-CoA, NADH:NAD^+ ratio and citrate that occur with increased fatty acid uptake and oxidation are responsible for inhibiting key enzymes and transporters involved in glucose oxidation and uptake (196). On the basis of this theory, it was hypothesized that inhibiting fatty acid oxidation would result in an increase in glucose uptake and oxidation. While it may seem counterintuitive to decrease rates of fatty acid oxidation in a state of obesity in which fat is abundant, studies have attributed the development of insulin resistance to an overload of fatty acid oxidation and have shown that decreasing it through genetic manipulation prevents the declines seen in insulin sensitivity (198). The concern was that inhibition of β-oxidation would lead to an accumulation of lipid derivatives such as diacylglycerol (DAG) and ceramides in skeletal muscle, which have been previously shown to contribute to the development of insulin resistance (159, 199). However, beneficial effects of reduced β-oxidation have been reported, despite intracellular accumulation of DAG and ceramides (197, 200).

Reductions in fatty acid oxidation have been achieved through the inhibition of carnitine-palmitoyl transferase-1 (CPT-1). CPT-1 is the rate-controlling enzyme for mitochondrial β-oxidation, facilitating the import of long-chain (>12C) fatty acids

(LCFAs) into the mitochondria (182). Located on the outer mitochondrial membrane, CPT-1 catalyzes the reaction between long-chain acyl-CoAs and carnitine to form acylcarnitine, which is then shuttled via the carnitine acylcarnitine translocase into the mitochondria, converted back into acyl-CoA (by CPT-2) and then released to undergo β-oxidation (182). Three isoforms of CPT-1 exist: liver (CPT-1a), heart and skeletal muscle (CPT-1b), and brain (CPT-1c) (182, 201).

Oxfenicine [*S*-2-(4-hydroxyphenyl)glycine] is considered a CPT-1b-specific inhibitor. It must be transaminated to its active form, 4-hydroxyphenylglyoxylate (4-HPG), which is competitive with carnitine, preventing the formation of acylcarnitines (195). Because CPT-1b shows the highest sensitivity to 4-HPG (195), inhibition of fatty acid oxidation by oxfenicine takes place selectively in those tissues that express this CPT isoform (182). Skeletal muscle, heart, white and brown adipose tissues are the ones with the highest content of CPT-1b in the body (182). Therefore, these tissues are expected to be the ones most responsive to oxfenicine-induced inhibition of LCFA oxidation. The effects of oxfenicine in skeletal muscle have been studied and show positive metabolic outcomes. High fat (HF)-fed mice given daily oxfenicine injections for 14 days had a reduced area under the curve for glycemia following a glucose tolerance test compared to HF-fed control animals, indicating an improvement in whole-body insulin sensitivity (157). Further analysis of the gastrocnemius muscle revealed an increased phosphorylated AKT to total AKT ratio, as well as an increase in GLUT4 content (157).

An additional metabolic outcome of inhibiting fatty acid β-oxidation is an increase in circulating non-esterified fatty acids (NEFAs), which must find an alternate metabolic

fate to oxidation. In this context, we hypothesized that the adipose tissue would undergo metabolic changes to accommodate and adjust for these excess non-oxidized fatty acids. It could do so by reducing its rates of lipolysis to prevent the further release of NEFAs, and/or by increasing rates of lipogenesis to promote the storage of excess fatty acids as triacylglycerols (TAGs). These, however, have never been previously investigated. Additionally, since the adipose tissue itself also expresses CPT-1b (182), pharmacological inhibition could also have direct effects on lipid metabolism in this tissue. Importantly, metabolic differences clearly exist between the visceral (*e.g.* epididymal, Epid) and the subcutaneous (Sc) (*e.g.* Sc inguinal, Sc Ing) fat depots. The Sc depot is considered to be metabolically protective (16) and more likely to change its metabolic function under various physiological conditions (202). However, it is currently unknown whether visceral and Sc fat depots elicit distinct metabolic responses upon CPT-1b inhibition. Importantly, it has also been shown that oxidative capacity differs between the two depots (19, 203), which could significantly affect the response to inhibition of β-oxidation. Our study is the first to examine the *in vivo* and *in vitro* effects of oxfenicine-induced CPT-1b inhibition on adipocyte metabolism. We provide novel evidence that CPT-1b inhibition causes fat depot-specific adaptive metabolic responses that affect lipolysis, lipogenesis, and adiposity in rats.

4.3. Materials and methods

Reagents – Type II collagenase, isoproterenol, FA-free bovine serum albumin (BSA), palmitic acid, oxfenicine (4-hydroxy-L-phenylglycine), and free glycerol determination kit were obtained from Sigma (St. Louis, MO, USA). [1-^{14}C] palmitic acid was from American Radiolabeled Chemicals (St. Louis, MO, USA) and D-[U-^{14}C] glucose was

from GE Healthcare Radiochemicals (Quebec City, QC, Canada). Protease (Complete Ultra Tablets) and phosphatase (PhosStop) inhibitors were from Roche Diagnostics GmbH (Mannheim, Germany). The non-esterified fatty acid (NEFA) kit was from Wako Chemicals (NEFA-HR kit, Richmond, VA, USA).

Animals – Male albino rats (Sprague Dawley strain) age 50-55 days and weighing ~250 g (upon commencement of the diet) were housed individually at 22 °C on a 12:12-hr light/dark cycle and fed for 11 wk *ad libitum* either a low fat (LF) (Control, 27%, 13%, and 60% of calories provided by protein, fat, and carbohydrates, respectively, energy density 3.43 kcal/g) or a high fat (HF) diet (20%, 60%, and 20% of calories provided by protein [casein], fat [lard, soybean oil], and carbohydrates [amylodextrin/sucrose], respectively, energy density 5.24 kcal/g). The LF control diet (standard chow catalog #5012) was purchased from LabDiet (St. Louis, MO, USA) and the HF diet (catalog # D12492) was purchased from Research Diets Inc™ (New Brunswick, NJ, USA). Food intake and body weight were measured for 2 wk prior to and every day during the oxfenicine treatment. At the end of treatment, animals were placed in the Comprehensive Laboratory Animal Monitoring System (CLAMS) from Columbus Instruments for 24 h for the measurement of *in vivo* metabolic parameters. The animals were allowed to acclimatize for 1 h prior to collection of data as previously described (204). The protocol containing all animal procedures described in this study was specifically approved by the Committee on the Ethics of Animal Experiments of York University (York University Animal Care Committee, YUACC, permit number 2012-03) and performed strictly in accordance with the YUACC guidelines. All surgery was

performed under ketamine/xylazine anesthesia, and all efforts were made to minimize suffering.

In vivo *treatment with oxfenicine* – Following 8 wk of either LF or HF diets, rats were given a daily intraperitoneal injection of oxfenicine (150 mg/kg body weight) suspended in 1X PBS, or just PBS (control) for 3 consecutive weeks.

Determination of fasting plasma NEFAs and insulin, and procedure for the glucose tolerance test – Following treatment with oxfenicine (week 11), the animals were fasted overnight and blood was collected by saphenous vein bleeding. The animals were then intraperitoneally injected with a 20% glucose solution (2 g/kg body weight) and saphenous blood samples were taken at 15, 30, 60 and 120 minutes post injection. Glucose was measured by the glucose oxidase method using a OneTouch Ultra Mini® monitor. Aliquots of blood were centrifuged for 10 min at 4 °C and plasma was stored at -80 °C for subsequent analysis of NEFAs and insulin.

Adipocyte isolation – Animals were anesthetized (0.4 mg ketamine and 8 mg xylazine per 100 g body weight) in the fed state. Subcutaneous inguinal (Sc Ing) and epididymal (Epid) fat pads were extracted and weighed. A sample of each fat pad was immediately frozen in liquid nitrogen and stored at -80 °C for subsequent Western blot analysis. The remaining tissue was used for adipocyte isolation as described previously (19). Briefly, the adipose tissue was finely minced in Krebs-Ringer Buffer (0.154 M NaCl, 0.154 M KCl, 0.11 M $CaCl_2$, 0.154 M $MgSO_4$, 0.154 M KH_2PO_4, 0.154 M $NaHCO_3$, pH 7.4) with 5.5 mM glucose and 30 mM HEPES (KRBH) supplemented with type II collagenase (1 mg/ml). The finely minced tissues were then incubated at 37 °C with gentle agitation

(120 orbital strokes/min) for ~30-45 min. Digested tissue was strained using a nylon mesh and cells were transferred to 50-mL tubes, carefully washed three times and resuspended in KRBH containing 3.5% BSA (KRBH-3.5% BSA). To distribute an equal number of adipocytes in each treatment condition, cell diameters and numbers were measured as described by DiGirolamo and Fine (205).

Determination of adipocyte lipolysis – Lipolysis was measured by incubating adipocytes (5×10^5 cells) either in the absence or presence of isoproterenol (100 nM). Triplicates for each condition were used and the isolated adipocytes were incubated for 75 min at 37 °C with gentle agitation (50 orbital strokes/min). Isoproterenol was used to stimulate lipolysis by acting as a non-specific β-adrenergic agonist (206). After incubation, a 200 µl aliquot of media was taken for the determination of glycerol concentration.

Measurement of palmitate oxidation in adipocytes – Adipocyte oxidative capacity was assessed as previously described by measuring the production of $^{14}CO_2$ (19). Briefly, 2.5×10^5 cells were incubated in KRBH-3.5% BSA containing 0.2 µCi/ml of [1-^{14}C] palmitic acid and 200 µM non-labelled palmitate for 1 h. The vials used for incubation had a centered well containing a loosely folded piece of filter paper. After the 1-h incubation period, the filter paper was moistened with 0.2 ml of 2-phenylethylamine/methanol (1:1, vol:vol) and the media was acidified with 0.2 ml of H_2SO_4 (5N). The flasks were maintained sealed at 37°C for an additional 1 h for the collection of CO_2 released from the cells and the media. At the end of the incubation, the filter paper was removed and transferred to a scintillation vial for radioactivity counting (15, 49).

Western blotting analysis of content and phosphorylation of proteins – Adipose tissue collected from the Epid and Sc Ing depots was homogenized in a buffer containing 25 mM Tris-HCl, 25 mM NaCl (pH 7.4), 1 mM $MgCl_2$, 2.7 mM KCl, 1% Triton-X and protease and phosphatase inhibitors (Roche Diagnostics GmbH, Mannheim, Germany). Homogenates were centrifuged, the infranatant collected, and an aliquot was used to measure protein by the Bradford method. Samples were diluted 1:1 (vol/vol) with 2X Laemmli sample buffer, heated to 95 °C for 5 min, subjected to SDS-PAGE and transferred to PVDF membrane. Membranes were subsequently probed with primary antibodies (1:1,000 dilution), followed by horseradish peroxidase-conjugated anti-rabbit secondary antibody (dilution of 1:2,000). β-actin was used as a loading control. Blots were visualized using chemiluminescence (Luminata forte, Millipore, Billerica, MA) and scanned directly into an image quantification program.

In vitro *treatment of isolated adipocytes with oxfenicine* – Sc Ing and Epid adipocytes were isolated as previously described from LF-fed rats weighting ~250 g. Following isolation, cells were incubated in various concentrations of oxfenicine for 2 h at 37 °C with gentle agitation. Assays for lipolysis, palmitate oxidation, and glucose incorporation into lipids were then performed as described in these methods.

Measurement of glucose incorporation into lipids in adipocytes – Following treatment with oxfenicine, glucose incorporation into lipids in adipocytes was assessed as previously described (61). Briefly, 1 x 10^6 cells were incubated in KRBH-3.5% BSA (containing 5 mM glucose) with 0.5 µCi/ml of D-[U-^{14}C] glucose under basal or insulin-stimulated (100 nM) conditions for 1 h at 37°C. The cells were then lysed by the addition

of H_2SO_4 (5N) and 5 mL of Dole's reagent (40:10:1 of isopropanol, heptane and 1 M H_2SO_4, vol/vol/vol) was subsequently added to the vial to extract total lipids. Radioactivity of the total lipid fraction was counted and corresponds to glucose conversion to TAG (207).

Statistical analyses – Normality was evaluated using the Kolmogorov-Smirnov normality test. For data that passed normality, statistical analyses were assessed by one-way and two-way ANOVAs with Bonferroni post hoc test. For data that did not pass normality, statistical analyses were assessed by Kruskal-Wallis test with the Dunn multiple-comparison test or Mann Whitney *U*-test, as indicated in the figure legends. Statistical significance was set at $P < 0.05$.

4.4. Results

Oxygen consumption, ambulatory activity, respiratory exchange ratio, and fasting plasma NEFAs – To examine the *in vivo* effects of the oxfenicine treatment, animals were placed in the CLAMS for 24 h following oxfenicine treatment and their VO_2, ambulatory activity, and respiratory exchange ratio (RER) were measured. Oxfenicine had no effect on VO_2 (Fig. 4-1A) or ambulatory activity (Fig. 4-1B) during the light or dark cycles. Treatment with oxfenicine also had no effect on the RER of animals fed the LF diet, whereas those fed a HF diet had significantly higher RER values, particularly during the dark cycle (Fig. 4-1C and D). This is indicative of the effectiveness of oxfenicine at inhibiting fatty acid β-oxidation, resulting in an increased reliance on carbohydrate oxidation. This was more pronounced during the dark cycle (1900 to 700), when the animals were the most active and ate the most food

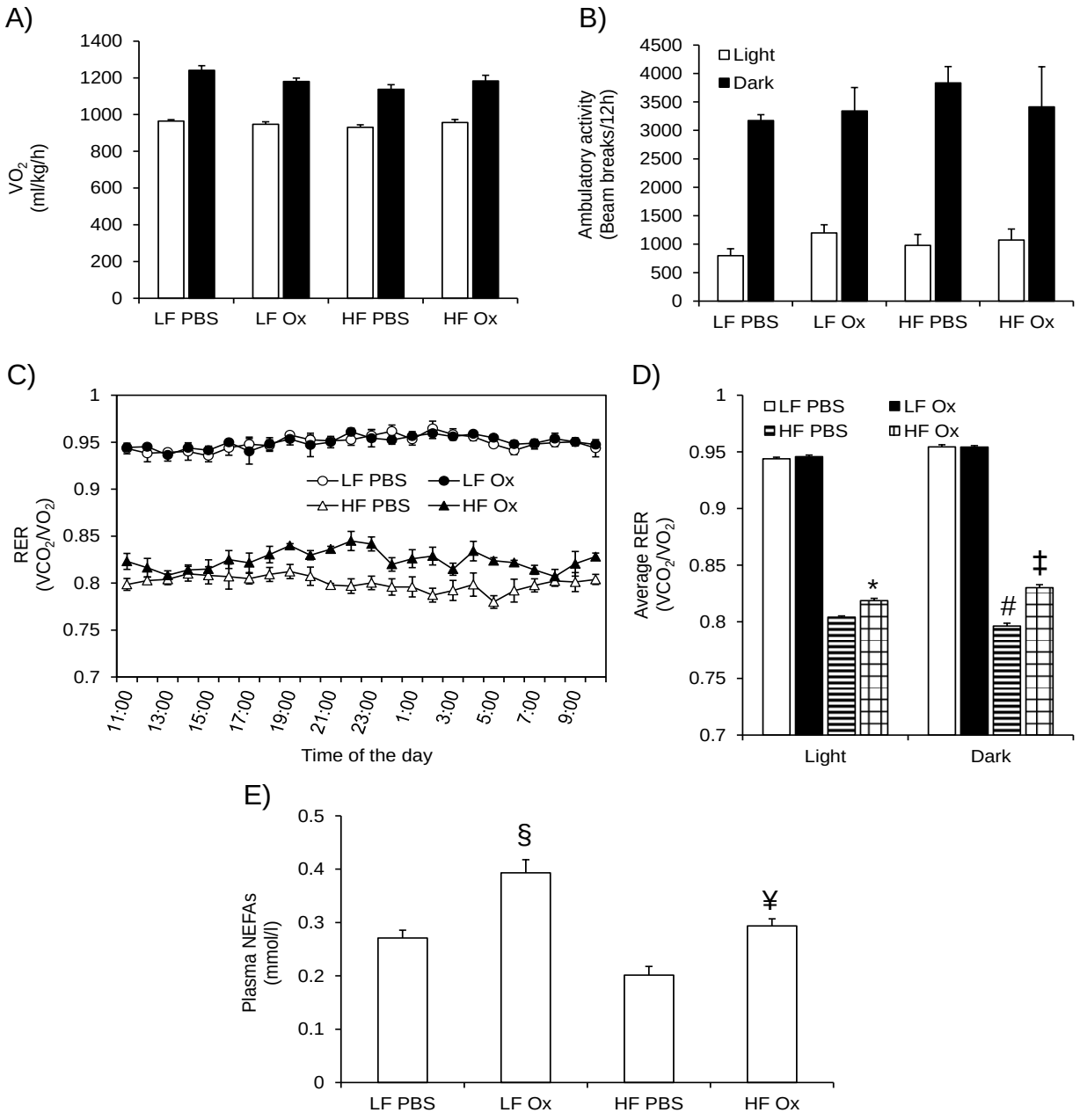

Figure 4-1: Oxfenicine does not affect VO_2 or ambulatory activity, but reduces whole-body fat oxidation and increases circulating non-esterified fatty acids (NEFAs). The animals were fed high fat (HF) or low fat (LF) diets for 8 wk and then daily injected for 3 wk with either PBS (control) or oxfenicine (Ox, 150 mg/kg of BW). At the end of the oxfenicine treatment, rats were placed in the Comprehensive Laboratory Animal Monitoring System (CLAMS) for the determination of VO2 (A), ambulatory activity (B), and respiratory exchange ratio (RER) during a 24h-period (C and D). Subsequently, the animals were overnight-fasted and blood was collected for the determination of non-esterified fatty acids (NEFAs) in the plasma (E). Kruskal-Wallis test, $n = 5$ for ambulatory activity. Mann-Whitney *U*-test, $n = 5$ for NEFAs. All other data were obtained by two-way analysis of variance (ANOVAs), $n = 5$. *$P < 0.05$ vs. HF PBS in the light cycle; #$P < 0.05$ vs. HF PBS light cycle; ‡$P < 0.05$ vs. HF Ox light cycle and HF PBS dark cycle; §$P < 0.05$ vs. LF PBS; ¥$P < 0.01$ vs. HF PBS.

(0.830 ± 0.00271 VCO_2/VO_2 vs. 0.796 ± 0.00244, VCO_2/VO_2, Fig. 4-1C and D). Fasting plasma NEFAs were also 1.45- and 1.46-fold higher in the LF- and HF-fed animals, respectively, following 3 wk of oxfenicine treatment (Fig. 4-1E). An increase in circulating fatty acids provides further evidence of the effectiveness of the oxfenicine treatment in reducing fatty acid oxidation.

Fasting plasma insulin and glucose tolerance test – As expected, HF-fed animals had a 1.6-fold increase in fasting plasma insulin compared to controls, indicating that these animals were insulin resistant (Fig. 4-2A). Further analysis of the area under the curve (AUC) of the glucose tolerance test (GTT) showed that plasma glucose remained 1.3-fold higher in the HF-fed animals compared to the LF-fed controls, confirming the development of insulin resistance in HF-fed animals (Fig. 4-2B and C). Oxfenicine treatment reversed the effects of the HF diet, returning fasting insulin and plasma glucose AUC levels to those seen in the control animals (Fig. 4-2). Oxfenicine treatment did not affect the glycemic response of low-fat-fed rats during the GTT.

Body weight and food intake – Energy intake during the oxfenicine treatment did not differ in the animals fed the LF (101.56 ± 5.68 kcal/rat/day vs. 94.45 ± 2.41 $kcal \cdot rat^{-1} \cdot day^{-1}$, Fig. 4-3B) or HF diet (100.40 ± 3.68 kcal/rat/day vs. 98.46 ± 4.44 $kcal \cdot rat^{-1} \cdot day^{-1}$, Fig. 3B). Body weight of LF-fed oxfenicine-treated rats was ~8% lower than the LF-fed PBS-treated rats (519.31 ± 9.64 g vs. 566.62 ± 24.05 g, respectively, Fig. 3A), although this did not reach statistical significance. However, there was a 10% significant reduction in final body weight in HF-fed animals treated with oxfenicine (Fig. 4-3A). Furthermore, oxfenicine treatment reduced Epid fat mass by 29% in the HF-fed animals (Fig. 4-3C).

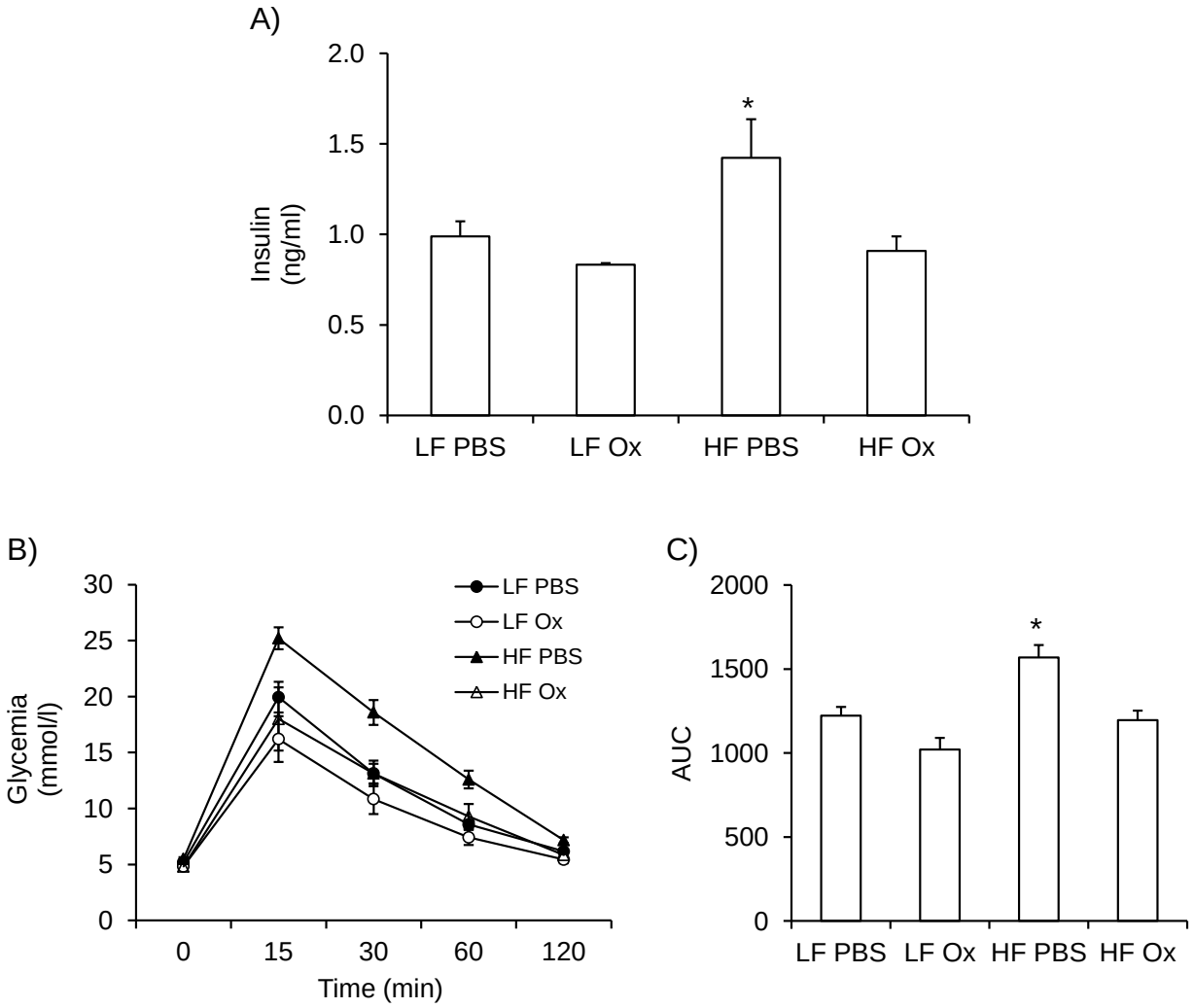

Figure 4-2: Oxfenicine normalizes fasting insulin and improves insulin sensitivity. The animals were fed HF or LF diets for 8 wk and then daily injected for 3 wk with either PBS (control) or oxfenicine (Ox, 150 mg/kg of BW). A: at the end of the oxfenicine treatment, rats were fasted overnight and blood was collected for the determination of insulin in the plasma. B and C: overnight-fasted rats then underwent an intraperitoneal glucose tolerance test. AUC, area under the curve. Mann-Whitney *U*-test, $n = 5$. *$P < 0.05$ vs. LF PBS and HF Ox.

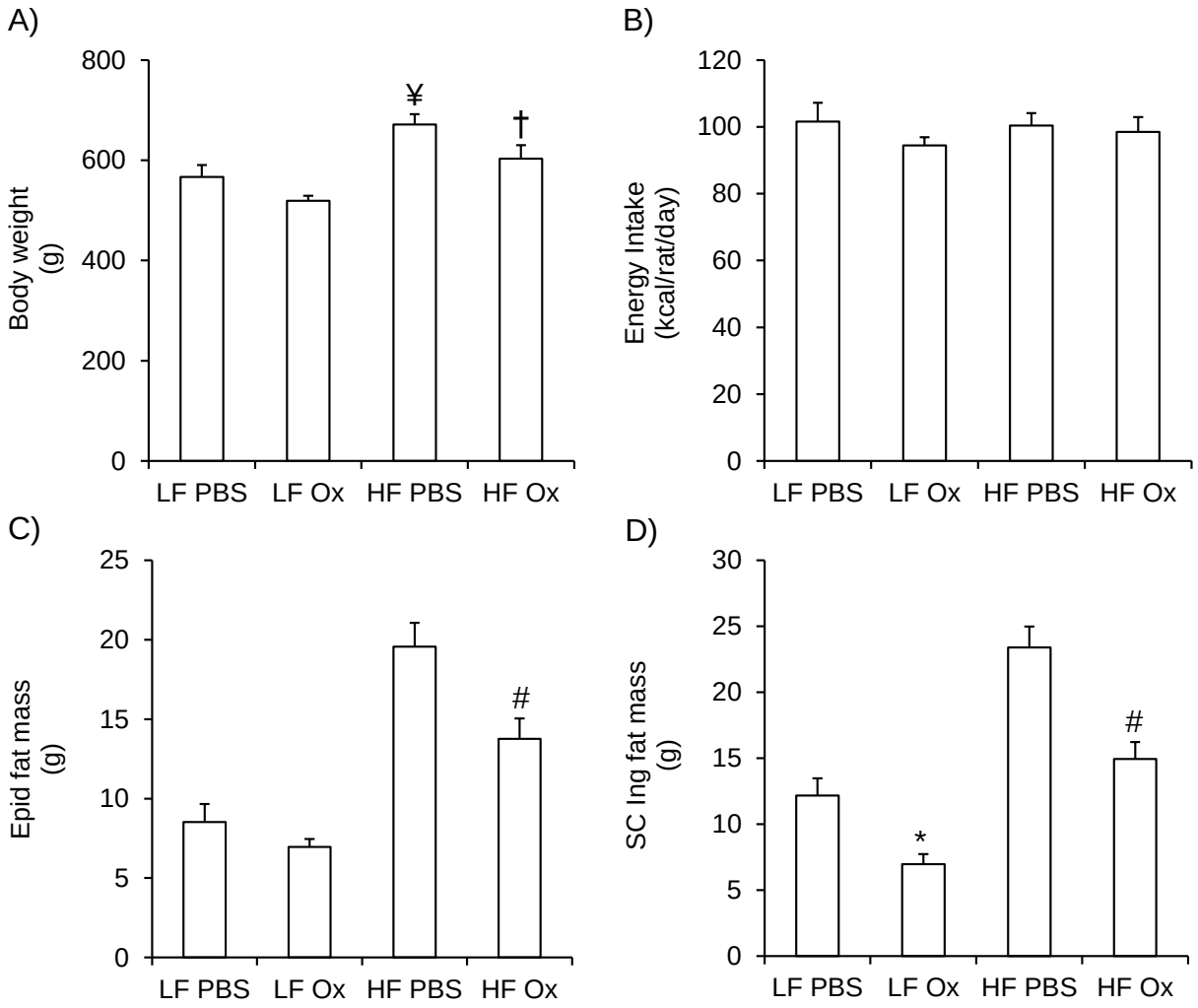

Figure 4-3: Oxfenicine does not affect energy intake (B), but reduces body weight (A) and Epid (C) and Sc Ing (D) fat pad mass. Rats were fed a LF or HF diet for 8 wk and treated with either PBS or oxfenicine (Ox, 150mg/kg BW) for 3 wk. Kruskal-Wallis test, $n = 5$ for energy intake. All other data, two-way ANOVAs, $n = 5$. ¥$P < 0.01$ vs. LF PBS, †$P < 0.05$ vs. HF PBS and LF Ox, *$P < 0.05$ vs. LF PBS, #$P < 0.01$ vs. HF PBS.

This effect was more pronounced in the Sc Ing fat depot where oxfenicine treatment reduced fat mass by 43% and 37% in the LF- and HF-fed animals, respectively (Fig. 4-3D).

Palmitate oxidation – In adipocytes isolated from the Epid fat depot, palmitate oxidation was reduced in the LF-fed (0.965 ± 0.102 *vs.* 0.711 ± 0.056 nmol/h/2.5x10^5 cells, Fig. 4-4A) and HF-fed (1.092 ± 0.11 *vs.* 0.952 ± 0.101 nmol/h/2.5x10^5 cells, Fig. 4-4A) animals, although these effects were not statistically significant. This effect of oxfenicine on palmitate oxidation was more pronounced in adipocytes isolated from the Sc Ing depot. In fact, palmitate oxidation in SC In adipocytes was decreased by 40% in the LF-fed animals and by 63% in the HF-fed animals (Fig. 4-4B).

Lipolysis – As expected, basal and isoproterenol-stimulated lipolysis differed in adipocytes isolated from the Sc Ing and Epid fat depots (Fig. 4-5A and B). In Epid adipocytes, there was no effect of diet or oxfenicine treatment on basal or isoproterenol-stimulated rates of lipolysis (Fig. 4-5A). However, in Sc Ing adipocytes, oxfenicine treatment decreased stimulated lipolysis by 42% in the LF-fed animals (Fig. 4-5B). There was no effect of oxfenicine treatment on stimulated lipolysis in the HF-fed animals, however the diet itself resulted in a 74% and 73% reduction in stimulated lipolysis in the HF PBS and HF Ox groups, respectively, compared to the LF-fed PBS animals (Fig. 4-5B).

Palmitate oxidation, lipolysis, and glucose incorporation into lipids in isolated adipocytes – In isolated adipocytes from both the Epid and Sc Ing fat depots treated with 1 mM oxfenicine,

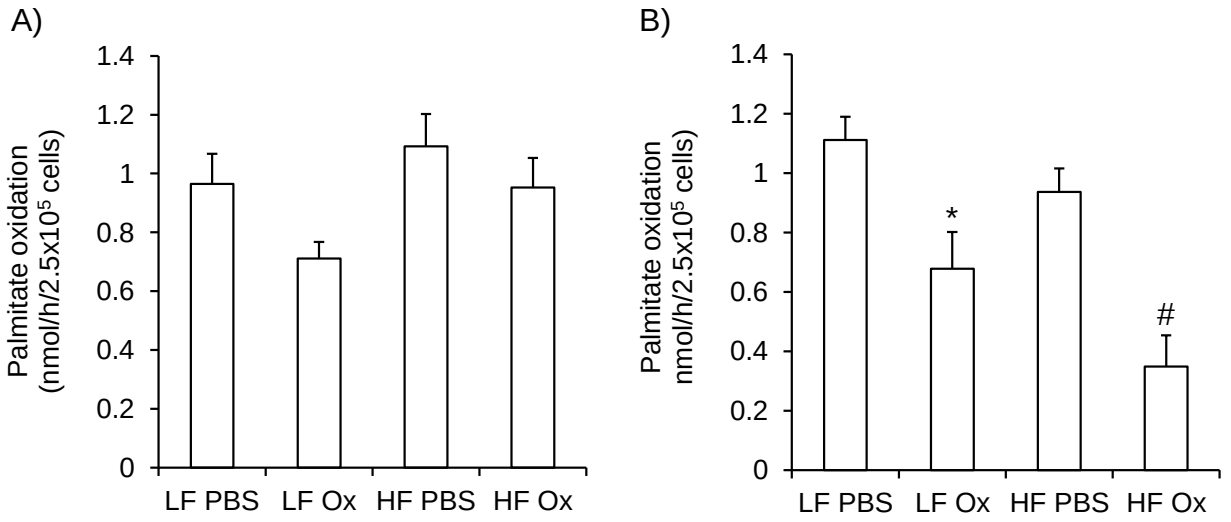

Figure 4-4: Administration of oxfenicine reduces palmitate oxidation in epididymal (A) and subcutaneous inguinal (B) adipocytes. Rats were fed LF or HF diets for 8 wk and then either injected with PBS or oxfenicine (Ox, 150 mg/kg of BW) for 3 wk. Two-way ANOVAs, n = 5. *P < 0.05 vs. LF PBS; #P < 0.01 vs. HF PBS.

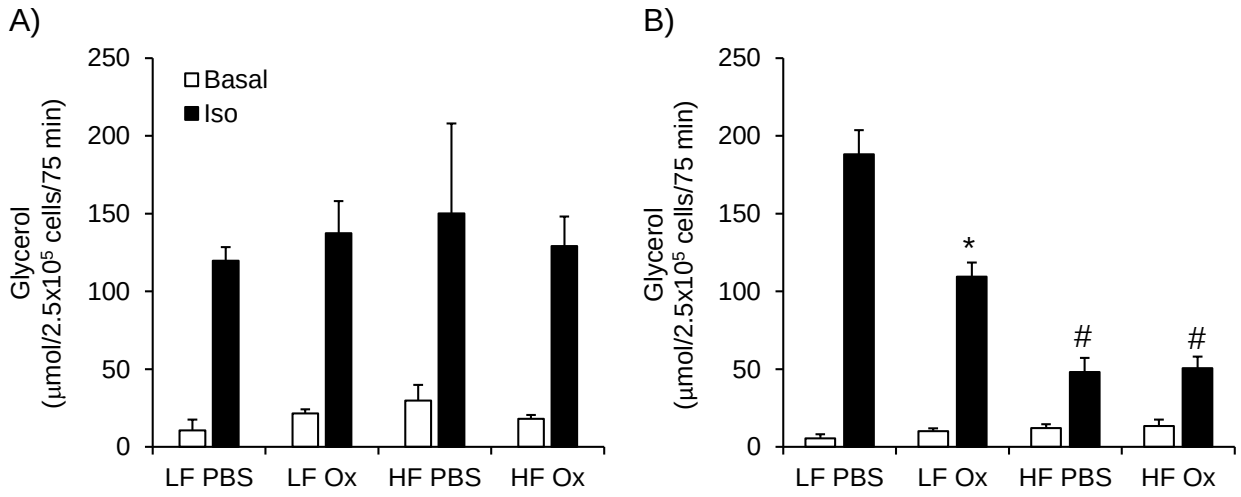

Figure 4-5: Glycerol release is reduced in subcutaneous inguinal (B) but not in epididymal (A) adipocytes from LF- or HF-fed rats either injected with PBS or oxfenicine (Ox, 150 mg/kg of BW). Two-way ANOVAs, n = 5. *P < 0.001 vs. LF PBS, HF PBS and HF Ox. $^{\#}P$ < 0.001 vs. LF PBS and LF Ox.

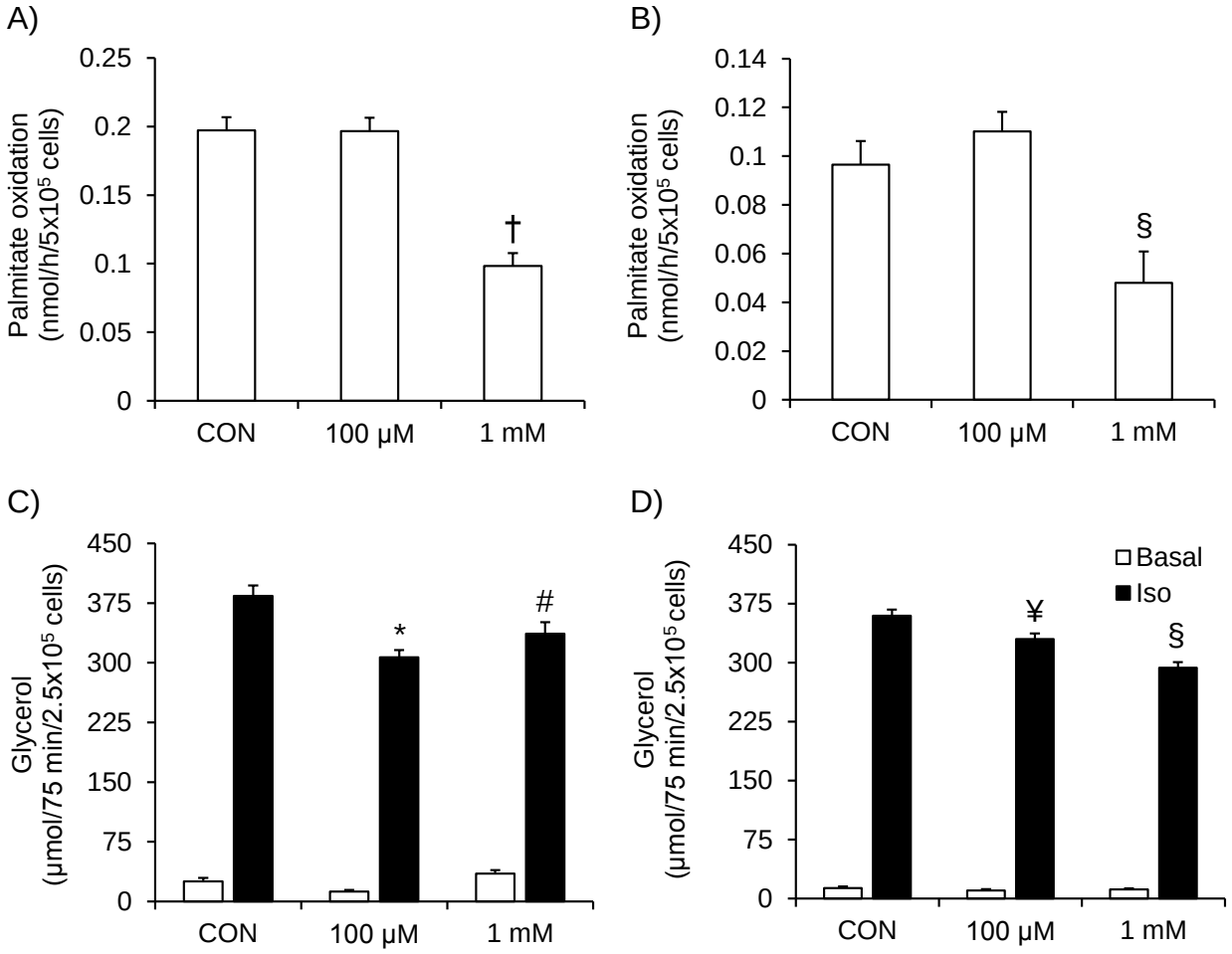

Figure 4-6: The direct effect of oxfenicine on palmitate oxidation and lipolysis in white adipocytes. Treatment with 1 mM oxfenicine reduces palmitate oxidation and isoproterenol (ISO)-stimulated lipolysis in epididymal (A and C) and subcutaneous inguinal (B and D) adipocytes. Adipocytes were extracted from lean rats and exposed to Ox (100 µM or 1 mM) in vitro for 2 h and then assayed for glycerol and palmitate oxidation. Two-way and one-way ANOVAs, $n = 5$. §$P < 0.01$ vs. CON and 100 µM. $^{\dagger}P < 0.0001$ vs. CON and 100 µM. $^{*}P < 0.001$ vs. CON. $^{\#}P < 0.01$ vs. CON. $^{¥}P < 0.05$ vs. CON.

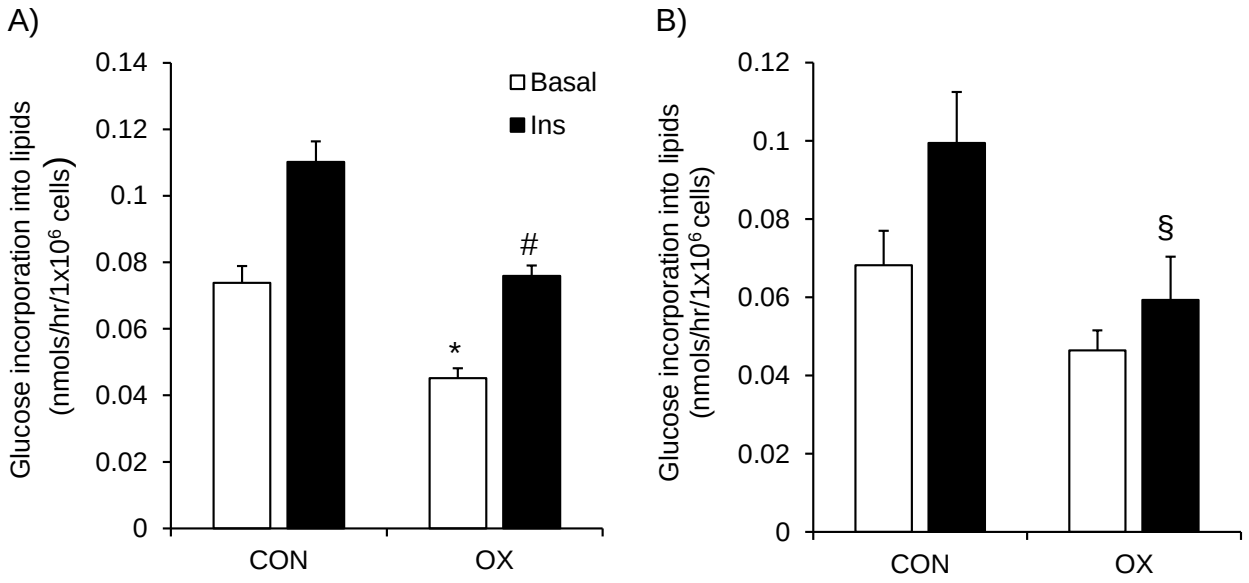

Figure 4-7: Oxfenicine reduces glucose incorporation into lipids in epididymal (A) and subcutaneous inguinal (B) adipocytes. Adipocytes were extracted from lean rats and exposed to Ox (1 mM) in vitro for 2 h and then assayed for glucose incorporation into lipids. Two-way ANOVAs, $n = 5$. $^{*}P < 0.001$ vs. Con Bas. $^{\#}P < 0.001$ vs. Con Ins. $^{\S}P < 0.05$ vs. Con Ins.

palmitate oxidation was significantly reduced by 50% when compared to control cells (Fig. 4-6A and B). Isoproterenol-stimulated lipolysis was significantly decreased by 20% and 12% in Epid adipocytes following treatment with 100 μM and 1 mM oxfenicine, respectively (Fig. 4-6C). Similarly, in Sc Ing adipocytes treatment with 100 μM and 1 mM of oxfenicine decreased stimulated lipolysis by 8% and 18%, respectively (Fig. 4-6D). There was no effect of oxfenicine on basal rates of lipolysis in Epid and Sc Ing adipocytes (Fig. 4-6C and D). Basal and insulin-stimulated glucose incorporation into lipids, the measure for lipogenesis, was reduced by 39% and 31%, respectively, in Epid adipocytes following treatment with 1 mM oxfenicine (Fig. 4-7A). In adipocytes from the Sc Ing fat depot, the incorporation of glucose into lipids was also reduced by 41% under insulin-stimulated conditions, following 1 mM oxfenicine treatment (Fig. 4-7B).

ATGL content and HSL content and phosphorylation – Oxfenicine treatment significantly reduced ATGL content in the Epid adipose tissue in rats fed a LF diet (Fig. 4-8A). In the HF-fed animals, there was no effect of oxfenicine; however, the diet itself resulted in a significant decrease in ATGL content in this fat depot (Fig. 4-8A). In contrast, ATGL content in the Sc Ing adipose tissue was significantly increased with a HF diet in the PBS control animals, with no effect of oxfenicine treatment evident in rats fed either the LF or HF diet (Fig. 4-8B). There was no difference in phosphorylation of hormone sensitive lipase $(HSL)_{660}$ in either fat depot with diet or oxfenicine treatment (Fig. 4-8C and D).

4.5. Discussion

Here, we report the novel findings of depot-specific alterations in adipose tissue and adipocyte metabolism following pharmacological selective inhibition of CPT-1b. The effects were characterized by a reduction in isoproterenol-stimulated lipolysis in adipocytes from the Sc Ing fat depot following 3 wk of daily oxfenicine injection, indicating an increased sensitivity to oxfenicine in this fat depot. *In vitro* incubation of adipocytes from both fat depots with oxfenicine also resulted in a reduction in stimulated rates of lipolysis. This suggests that fat cells adjusted their metabolism to compensate for the increased circulating NEFAs seen with inhibition of β-oxidation. We also expected glucose incorporation into lipids to be increased with oxfenicine treatment to promote storage of the excess lipids resulting from CPT-1b inhibition. Contrary to our original hypothesis, basal and insulin-stimulated glucose incorporation into lipids was significantly reduced in Epid and Sc Ing adipocytes directly treated with oxfenicine. This reduction likely contributed to sustain elevated levels of circulating NEFAs seen in

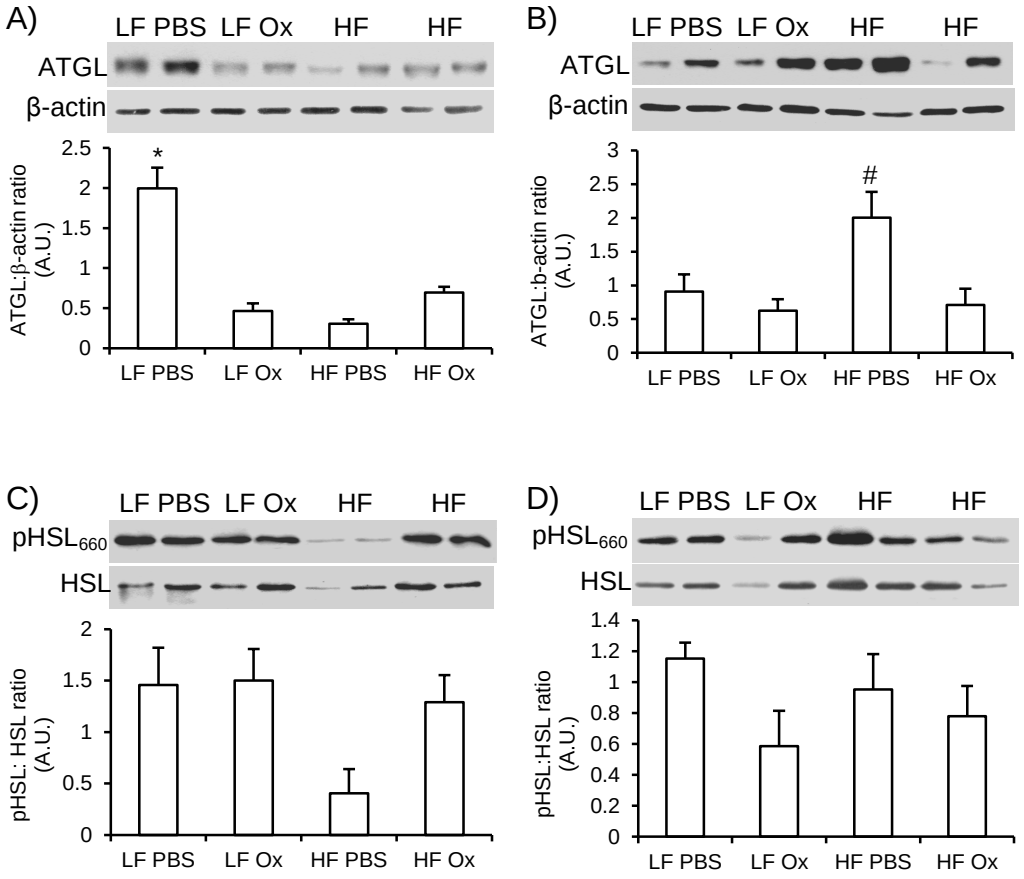

Figure 4-8: Effects of oxfenicine on content of ATGL and content and phosphorylation of hormone sensitive lipase (HSL) in the WAT. Analyses were performed in the epididymal (A and C) and subcutaneous inguinal (B and D) adipose tissue. Animals were fed either a LF or HF diet for 8 wk, followed by 3 wk of treatment with PBS or Ox (150 mg/kg BW). Mann-Whitney *U*-test; $n = 3$. *$P < 0.05$ vs. LF Ox and HF PBS. #$P < 0.05$ vs. all other groups.

oxfenicine-treated rats. It also, at least partially, explains the decrease in Epid and Sc Ing fat mass observed in oxfenicine-treated animals, as no alterations in food intake or ambulatory activity were observed with the treatment. This suggests that reduced adiposity in oxfenicine-treated rats was mainly driven by alterations in substrate partitioning, preventing the storage of fat in the adipose tissue. This could be attributed to lower levels of the lipogenic hormone insulin in the plasma of HF-fed oxfenicine-treated rats, which is compatible with higher levels of circulating NEFAs in the oxfenicine-treated rats.

Body weight of LF Ox was slightly lower (~8%) than that of LF PBS rats; however, this was not statistically different and did not characterize that rats lost weight independent of the diet following oxfenicine treatment. This could be due to the fact that in LF-fed rats treated with oxfenicine only the Sc Ing fat pad was significantly reduced (43%) in its mass (Fig. 4-3C), whereas in HF-fed rats oxfenicine treatment caused a marked reduction in both Epid (29%) and Sc Ing fat (37%) masses. Combining the effect of oxfenicine on Epid and Sc Ing fat depots adds up to a 66% reduction in adiposity as opposed to 43% in Sc Ing only in LF-fed rats. The impact of these fat depot-specific responses to oxfenicine could be the determining factor for reaching statistical significance with regard to the differences of body weight. On the basis of our findings, it appears that the effect of oxfenicine on adiposity and body weight is more evident when the organism is challenged by a HF diet, an intervention that promotes and exacerbates the accumulation of fat in the adipose tissue. Importantly, the density of adipose tissue is lower than other tissues, so a marked reduction in its content is normally required for it to exert a robust impact on total body weight. Under such

conditions, the rat-reducing effect of oxfenicine seems to have caused a more pronounced effect on total body weight in HF-fed rats, and likely allowed statistical significance to be reached in this group.

The effectiveness of our pharmacological inhibition on CPT-1b was evaluated by placing the animals in the CLAMS for 24 h and measuring RER as an indication of substrate oxidation. There was a significant increase in RER in HF-fed, oxfenicine-treated animals during both the light and dark cycles, indicating a shift towards carbohydrate metabolism. Similarly to previous work (157, 197), the effect was more pronounced during the dark cycle as this was when the animals were eating the most food and were the most active, requiring an increase in energy metabolism. Interestingly, there was no change in RER in animals fed the LF diet and treated with oxfenicine in either the light or dark cycles. Oxfenicine still seems to be exerting its inhibitory effects on β-oxidation in these animals as plasma NEFAs are increased following treatment, to a similar extent as that seen in the HF-fed animals. It is possible that any changes in RER are masked in the LF-fed animals as they are consuming a diet relatively low in fat that provides 60% of its energy content from carbohydrates. Under such conditions carbohydrate is the main substrate for oxidation, so inhibition of fat oxidation does not affect RER in these animals. VO_2 and ambulatory activity were also measured *in vivo* in the CLAMS and was not different between any of the groups, suggesting that these variables did not have an effect on the RER and adiposity data.

Previous studies examining the effects of CPT-1b inhibition have focused mainly on the metabolic improvements in skeletal muscle in animals fed a HF diet. Keung et al. (157) treated HF-fed mice with daily injections of oxfenicine for 4 wk, which resulted in

an increase in the phosphorylated AKT: total AKT ratio, as well as an increase in GLUT4 content in the gastrocnemius muscle. This was accompanied by a reduction in AUC for glycemia following a glucose tolerance test (157). Treatment of HF-fed mice with daily injections of etomoxir, a broad CPT-1 inhibitor, for 8 days has also been reported to improve whole-body glucose tolerance, an effect that was accompanied by increases in phosphorylated AKT and in GLUT4 content in the tibialis anterior muscle of mice (200). Similar to this work, we also observed a reduction in glucose AUC following a GTT in our HF-fed, oxfenicine-treated animals. This was accompanied by a reduction in fasting insulin levels, indicating an overall improvement in whole-body insulin sensitivity. The effects of fatty acid inhibition on the insulin signaling pathway and whole-body insulin sensitivity are likely secondary to increases in skeletal muscle glucose oxidation, as has been observed in numerous studies (196, 208, 209). In addition to the beneficial effects on glucose metabolism, we also found that oxfenicine treatment reduced body weight and adiposity in HF-fed animals. This is in line with data from Wicks et al. (197) in which a reduction in body weight and adiposity was reported in mice with muscle-specific deletion of CPT1b ($Cpt1b^{m-/-}$). Unlike our study, reduction in body weight in $Cpt1b^{m-/-}$ mice could be partially explained by a reduction in food intake (197); however the reduction in food intake began 3-4 wk after the initial decrease in body weight and adiposity occurred, suggesting that another variable could have contributed to the decrease in weight. Our study provides evidence that a reduction in lipogenesis in the fat depots could be this alternate variable, which could at least partially explain the reduction in adiposity induced by the suppression of CPT-1b activity.

A further effect of oxfenicine treatment was the reduction in stimulated lipolysis in adipocytes isolated from the Sc Ing fat depot of LF- and HF-fed animals. Stimulated lipolysis was also reduced in adipocytes that were directly treated with 1 mM oxfenicine. We expected to find a reduction in lipolysis as an adjustment made by the adipose tissue to compensate for the increased circulating NEFAs seen with CPT-1b inhibition in both LF- and HF-fed animals. The compensation makes sense physiologically as it would prevent the further release of NEFAs into the circulation where there is already an abundance. These NEFAs are not able to be metabolized in oxidative tissues, such as the skeletal muscle due to the CPT-1b inhibition. Despite the decrease in lipolysis, circulating NEFAs were still elevated in the oxfenicine-treated animals. This could be due to the fact that lipogenesis was also markedly inhibited in oxfenicine-treated adipocytes, which likely contributed to maintain circulating NEFAs elevated. Importantly, chronically elevated NEFAs could result in an accumulation of lipid species in tissues such as the skeletal muscle, a condition that has been demonstrated to negatively impact insulin signaling in this tissue (210). Previous studies have indeed shown an increase in intramyocellular lipid and DAG contents in the skeletal muscle of the $Cpt1b^{m-/-}$ mice (197) and in animals treated with etomoxir (200). However, in both studies there was no detrimental effect on insulin signaling. In fact, oxfenicine treatment led to an improvement in whole-body glucose tolerance (197, 200). Our data is also in line with these observations, since oxfenicine treatment reduced glycemia and insulinemia in HF-fed animals to values similar to those of LF-fed controls.

Our novel results emphasize the metabolic differences between fat depots. The Sc Ing fat depot has previously been shown to be metabolically protective as it is able to

store excess lipid while remaining insulin sensitive (16). We (15, 211) and others (16, 212, 213) have demonstrated depot-specific differences in the regulation of lipolysis; however, the mechanisms underlying these differences remain poorly understood. Differences in HSL expression and activity between the Sc Ing and Epid fat depots may be one possible explanation (212, 213). We were particularly interested in the regulation of ATGL, the main TAG lipase, and HSL, the main DAG lipase, in the different fat depots. The ATGL content in the Epid fat depot was significantly lower in LF-oxfenicine and HF-PBS rats when compared to LF-PBS controls. However, none of these effects were accompanied by altered lipolysis in Epid adipocytes from animals either treated or non-treated with oxfenicine. In the Sc Ing fat depot the content of ATGL was increased only in the HF-fed, PBS-treated animals compared with all other groups, whereas no difference in HSL phosphorylation at serine 660 was found between any groups. ATGL is regulated by an activator, comparative gene identification 58 (35) and the full activation of both ATGL and HSL has been shown to require the phosphorylation of perilipin A (33, 214). Therefore it is possible that lipolysis is being regulated at other proteins besides ATGL and HSL and additional studies are required to test these possibilities.

Perspectives and Significance

Chronic CPT-1b inhibition has been shown to significantly improve whole body and skeletal muscle insulin sensitivity, making it a potential obesity and T2D therapy. In our study, we present novel findings showing that oxfenicine treatment also altered lipid metabolism in adipose tissue, resulting in a reduction in fat mass in animals fed a HF diet. A daily dose of oxfenicine for 3 wk was sufficient to increase RER and circulating

NEFAs. It was also accompanied by the inhibition of fatty acid oxidation in adipocytes isolated from both the Epid and Sc Ing depots and reduced lipolysis in Sc Ing adipocytes. In addition, directly treating adipocytes with oxfenicine reduced lipid storage, which must have contributed to the reduction of adiposity. To the best of our knowledge, this is the first study to examine the adaptive changes in adipose tissue metabolism that occur as a result of suppressing fatty acid oxidation through CPT-1b inhibition *in vivo* and provides novel additional information regarding this potential obesity and T2D therapy.

GRANT SUPPORT

This study was funded by a Discovery Grant from the Natural Sciences and Engineering Research Council of Canada (NSERC) and by infrastructure grants from the Canada Foundation for Innovation (CFI) and the Ontario Research Fund (ORF) awarded to RBC. DMSK was supported by the Elia Scholarship and the NSERC Alexander Graham Bell Canada Graduate Scholarship.

CHAPTER 5: Activation of a futile cycle rather than mitochondria uncoupling promotes energy dissipation in cold-induced browning of the subcutaneous inguinal white adipose tissue in rats

Diane M. Sepa-Kishi and Rolando B. Ceddia.

Muscle Health Research Centre, School of Kinesiology and Health Science, York University, Toronto, Ontario, Canada

Keywords: Brown adipose tissue, lipolysis, UCP1, adipose tissue metabolism, subcutaneous fat, visceral fat, oligomycin

Statement of Labour

The majority of the experiments conducted in this study were carried out by Diane M. Sepa-Kishi. DMSK's contributions included extraction of tissues, isolation of adipocytes, and conducting the oxidation, lipolysis and glycerol incorporation into lipids assays. DMSK was also responsible for conducting and collecting all western blot and real-time PCR data, analyzing and interpreting all of the results, preparing the figures, and revising the manuscript. DMSK was supported by a NSERC Alexander Graham Bell Canada Graduate Scholarship and an Elia Scholarship. Due to the logistics of this study, RBC assisted with the extraction of tissues and the isolation of adipocytes.

Dr. Rolando Ceddia is the primary investigator and supervisor of this project and this research was funded by a Discovery Grant from NSERC and by infrastructure grants from the Canada Foundation for Innovation and the Ontario Research Fund.

5.1. Abstract

The objective of this study was to investigate whether cold-induced browning of the white adipose tissue (WAT) reduces adiposity by increasing fat oxidation through uncoupling protein 1 (UCP1)-mediated thermogenesis in primary adipocytes. Male Wistar rats were exposed to cold (4^{o}C) for 7 days and then the subcutaneous (Sc) inguinal (Ing) and epididymal (Epid) fat depots were extracted for the assessment of UCP1 content, palmitate and glucose oxidation, glycerol incorporation into lipids, lipolysis, as well as gene expression and content and phosphorylation of proteins involved in the regulation of these pathways. Cold increased mass and UCP1 levels of brown adipose tissue (BAT) and reduced WAT mass. In the Sc Ing fat depot, cold increased UCP1 levels 3.2-fold, although this represented only ~5% of the UCP1 content in BAT of cold rats. Glycerol kinase expression increased 10-fold, lipolysis 2-fold, and glycerol incorporation into lipids 2.5-fold in cold Sc Ing WAT. Cold enhanced glucose and palmitate oxidation in BAT, but not in Epid and Sc Ing adipocytes, whereas oligomycin did not affect palmitate oxidation in BAT from control and cold-acclimated rats, but drastically inhibited it in Epid and Sc Ing adipocytes. Surprisingly, cold Sc Ing adipocytes treated with oligomycin exhibited 44% lower rates of palmitate oxidation than control cells. This indicates that even though UCP1 levels increased, cold acclimation actually reduced mitochondria uncoupling-mediated fat oxidation in Sc Ing adipocytes. Therefore, instead of UCP1-mediated thermogenesis, cold-induced browning promoted energy dissipation within Sc Ing adipocytes essentially through the activation of a futile triacylglycerol breakdown/resynthesis cycle.

5.2. Introduction

The white adipose tissue (WAT) is specialized to store and release fat under conditions of surplus and deficit of energy, respectively, whereas BAT is well known for its ability to consume substrate and dissipate energy in the form of heat (63). Classical BAT is rich in mitochondria containing UCP1 that uncouples oxidative phosphorylation from ATP synthesis, so the potential energy from the mitochondrial proton gradient is used to produce heat instead of ATP. This process is also known as non-shivering thermogenesis (63). Cold is a potent physiological stimulus to induce the activation of UCP1 in classical BAT (63), but it has also been shown to induce a brown-like phenotype ("browning effect") in the WAT of rodents (215). WAT that underwent browning is characterized by the presence of fat cells containing multiple small lipid droplets (multilocular adipocytes) that display increased expression and content of UCP1 (215). These cells are also known as beige or "brite" (brown in white) adipocytes (216). It has been suggested that the induction of browning could lead to a shift in WAT from an essentially fat storage compartment to a tissue that burns fat and dissipates energy within itself. Such metabolic shift could reduce adiposity and be of great therapeutic value for obesity and its related metabolic disorders. However, there appears to be differences in the capacities of various WAT depots to undergo browning. In fact, it has been reported that in rodents the Sc Ing fat depot is more prone to browning than other visceral fat depots (84, 90, 91). Thus, it appears that only specific compartments of WAT could actually be recruited for thermogenesis. Most data supporting a thermogenic function in brite/beige adipocytes originate from morphological analysis (presence of multilocular lipid droplets and mitochondrial

remodeling) and molecular characteristics (expression of genes involved in mitochondrial biogenesis and UCP1 mRNA expression). Whether these morphological and molecular changes ultimately cause an increase in substrate consumption at the WAT level to significantly affect adiposity remains debatable (217, 218).

Previous studies in which browning of the Sc Ing WAT in rats was induced by chronic endurance training provided evidence that this fat pad indeed increased its fatty acid oxidative capacity, and this coincided with reduced adiposity and increased whole-body energy expenditure (91). It has also been demonstrated that UCP1 protein content in mitochondria isolated from the Sc Ing WAT of cold-acclimated mice almost reached the levels found in the interscapular BAT (iBAT), and these mitochondria exhibited UCP1-dependent thermogenesis (88). However, UCP1-dependent oxygen consumption per gram of Sc Ing WAT was maximally one-fifth of that of iBAT (88). Lastly, transgenic mice overexpressing UCP1 in the WAT at levels corresponding to only 2-10% of the level normally detected in BAT displayed a reduction in Sc fat. When the transgene was expressed in A^{vy} genetically obese mice reductions in total body weight and Sc fat stores were also observed (219). These findings suggest that, compared to brown fat, relatively low amounts of UCP1 are required to elicit a fat-reducing effect in white adipocytes, providing support to the notion that WAT can become an energy dissipating compartment and be effective for fat reduction. However, it still remains to be unequivocally demonstrated in intact fully-differentiated and freshly isolated beige/brite adipocytes that reduced mass of the WAT that underwent browning is due to UCP1-mediated uncoupling and increased fat utilization within the tissue. This is important because lipolysis and alternative thermogenic energy-consuming pathways (*e.g.*

triacylglycerol (TAG) hydrolysis/lipogenesis futile cycle; activation of Na^+-K^+-ATPase, etc.) could also be activated under conditions of WAT browning (217, 220, 221), and actually lead to reduced adiposity independently of UCP1-mediated non-shivering thermogenesis.

Cold-induced activation of UCP1 in classical BAT is triggered by lipolysis mainly through β3-adrenergic signaling leading to the release of non-esterified fatty acids (NEFAs). It is generally accepted that it is the rise of NEFAs in the cell after lipolysis that causes activation of UCP1. In fact, NEFAs released by lipolysis have been proposed to serve both as activators of UCP1 and fuel for thermogenesis in BAT (63). Therefore, if the regulation of UCP1 activity is similar in classical brown and beige/brite adipocytes, then induction of lipolysis should be followed by increased respiration and fatty acid oxidation in both types of cells. Indeed, there are reports that both cultured brite/beige and brown adipocytes differentiated from mice stromal vascular cells (SVC) extracted from the Sc Ing fat depot and iBAT, respectively, increased respiration upon treatment with isoproterenol (217, 222). This effect was drastically reduced in cells originating from mice lacking adipose triglyceride lipase (ATGL) and hormone sensitive lipase (HSL), providing evidence that lipolysis is crucial to induce a respiratory response in these cells (222). However, lipolysis-induced respiration can be independent of UCP1-mediated mitochondrial uncoupling, since it can be detected in brown and beige adipocytes from UCP1 knock out mice (222), as well as in mouse (217) and human (223) primary white adipocytes. This has been attributed to elevated intracellular levels of fatty acids that promote mitochondrial uncoupling on their own and leak respiration (222, 223). Therefore, caution has to be taken when interpreting respiration data from

adipocytes undergoing lipolysis with respect to distinguishing UCP1- from fatty acid-mediated uncoupling. Additionally, differentiation of SVC extracted from iBAT and Sc Ing fat depots into adipocytes may not provide a true representation of the metabolic differences and physiological responses of classical brown and beige/brite adipocytes. Cultured SVC are devoid of the regulatory mechanisms that drive cell differentiation and metabolic adaptive responses within the tissue. This is particularly relevant under conditions in which the organism is exposed to thermogenic challenges that promote adaptive metabolic responses in both BAT and WAT. In this context, the present study was designed to assess whether cold-induced browning of the WAT actually leads to enhanced fat consumption through mitochondrial uncoupling. We used an approach in which WAT browning was induced *in vivo.* To accomplish that, rats were acclimated to cold (4^{o}C) for 7 days to activate classical BAT and to promote browning of the WAT. After that, iBAT, aortic brown adipose tissue (aBAT), and Sc Ing and Epid fat depots were extracted and used for direct assessment of UCP1 content, as well as glucose and fatty acid oxidation, glycerol incorporation into lipids, lipolysis, and the molecular mechanisms regulating these pathways either in tissue samples or isolated primary adipocytes. Here, we provide a detailed analysis of the contribution of cold-induced UCP1-dependent and independent energy-consuming pathways to substrate consumption in classical brown and beige/brite adipose tissues.

5.3 Materials and Methods

Reagents – Type II collagenase, isoproterenol, CL 316,243, dobutamine, FA-free bovine serum albumin (BSA), palmitic acid, and free glycerol determination kit were obtained from Sigma (St. Louis, MO, USA). Oligomycin was purchased from Cayman

Chemical (Ann Arbor, MI, USA). [1-^{14}C] palmitic acid and [^{14}C(U)] glycerol were from American Radiolabeled Chemicals (St. Louis, MO, USA), and D-[U-^{14}C] glucose was from GE Healthcare (Little Chalfont, UK). Protease (cOmplete Ultra Tablets) and phosphatase (PhosSTOP) inhibitors were from Roche Diagnostics GmbH (Mannheim, Germany). The NEFA kit was from Wako (Mountain View, CA, USA). All antibodies were purchased from Cell Signaling (Danvers, MA, USA), except for the β3-AdR which was purchased from Santa Cruz Biotechnology (Dallas, TX, USA) and UCP1 which was purchased from Abcam (Toronto, ON, Canada).

Animals – Male albino rats (Wistar strain) were housed at 22°C on a 12/12-h light/dark cycle and fed standard laboratory chow (Lab Diet Cat #5012) *ad libitum*. The same animals used for this study were also used in the subsequent studies that make up Chapters 6, 7 and 8 of this dissertation. The protocol containing all animal procedures described in this study was specifically approved by the Committee on the Ethics of Animal Experiments of York University (York University Animal Care Committee, YUACC, permit number 2016-5) and performed strictly in accordance with the YUACC guidelines. All surgery was performed under ketamine/ xylazine anesthesia, and all efforts were made to minimize suffering.

Cold exposure – The rats were age- and weight-matched (~400 g) and randomly allocated to either the control or cold-exposed group. Animals in the cold exposed group were housed at 4°C for 7 days on a 12/12-h light/dark cycle, while control animals were maintained at 22°C. Food intake and body weight were measured on a daily basis for 5 days prior to (baseline) and for the entire duration of the cold exposure. Blood samples were collected daily in the fed state, centrifuged for 10 min at 4°C, and the plasma was

collected and stored at -80°C for subsequent analysis. Upon completion of the protocol, animals were anesthetized (0.4 mg ketamine and 8 mg xylazine per 100 g body weight) in the fed state and the iBAT, aBAT, Epid), and Sc Ing fat pads were extracted and weighed. A sample of each was flash frozen in liquid nitrogen for subsequent analysis.

Adipocyte isolation – Adipocyte isolation from the Epid and Sc Ing fat pads was performed as previously described (19). Briefly, the adipose tissue was minced in Krebs-Ringer Buffer (0.154 M NaCl, 0.154 M KCl, 0.11 M $CaCl_2$, 0.154 M $MgSO_4$, 0.154 M KH_2PO_4, 0.154 M $NaHCO_3$, pH 7.4) with 5.5 mM glucose and 30 mM HEPES (KRBH) supplemented with type II collagenase (0.5 mg/ml). Minced tissues were incubated at 37°C with gentle agitation (120 orbital strokes/ min) for approximately 25-30 min. The digested tissue was then strained using a nylon mesh and cells were transferred to 50 ml tubes, washed 3 times, and resuspended in KRBH containing 3.5% FA free BSA (KRBH-3.5% BSA). In order to distribute an equal number of adipocytes in each treatment condition, cell diameters were measured and total cell numbers determined (224).

Measurement of glucose and palmitate oxidation – Glucose and palmitate oxidation as measures of oxidative capacity were assessed by production of $^{14}CO_2$ in Epid and Sc Ing isolated adipocytes (5 x 10^5 cells) and in finely minced iBAT and aBAT tissue (~20 mg) as previously described (19). Briefly, cells and tissues were incubated in KRBH-3.5% BSA containing either 0.2 µCi/ml of [1-^{14}C] palmitic acid and 200 µM non-labelled palmitate, or 0.2 µCi/ml of D-[U-^{14}C] glucose and 5.5 mM non-labeled D-glucose for 1 h. To examine the effects of increased lipolysis on fatty acid oxidation, isolated adipocytes were stimulated with the β-adrenergic receptor agonist isoproterenol. To distinguish

substrate utilization used for ATP synthesis (coupled respiration) from proton leak (uncoupled respiration), 15 min prior to the addition of isoproterenol, adipocytes were treated with the ATP synthase inhibitor oligomycin. Following 1 h incubation either in the absence or in the continuous presence of isoproterenol (100 nM) and oligomycin (100 μM), the media were then acidified with 0.2 ml of H_2SO_4 (5 N), and the vials were maintained sealed at 37°C for an additional 1 h for the collection of $^{14}CO_2$ released from the cells/tissue and the media. The vials used for incubation had a centered isolated well containing a loosely folded piece of filter paper that was moistened with 0.2 ml of 2-phenylethylamine/ methanol (1:1, vol:vol) for the capture of $^{14}CO_2$. At the end of the incubation, the filter paper was removed and transferred to a scintillation vial for radioactivity counting (49, 15).

Measurement of glycerol incorporation into lipids – Glycerol incorporation into lipids was measured in isolated adipocytes (5 x 10^5 cells) from the Epid and Sc Ing fat depots as previously described (49). Briefly, cells were incubated in KRBH-3.5% BSA (with and without 5.5 mM glucose) containing 0.2 μCi/ml of [^{14}C(U)] glycerol for 1 h. Lipids were then extracted according to the method of Dole and Meinertz (225) and assessed for radioactivity (49).

Determination of lipolysis – Lipolysis was measured in isolated Epid and Sc Ing adipocytes (5 x 10^5 cells). In order to stimulate lipolysis, adipocytes were incubated in the presence of one of the following β-adrenergic agonists: isoproterenol (β-non-specific) (206), CL 316,243 (β3-specific), and dobutamine (β1-specific). Each condition was assayed in triplicates and the samples were incubated for 75 min at 37°C with

gentle agitation (50 orbital strokes/min). After incubation, a 200 µl aliquot of medium was taken from each vial for the determination of glycerol concentration.

RNA isolation and quantitative PCR – Primers were designed using the software PrimerQuest (IDT) based on probe sequences available at the Affymetrix database (NetAffx™ Analysis Centre, http://www.affymetrix.com/ analysis) for each given gene. RNA was isolated from adipose tissue using the RNeasy Lipid Tissue Kit (Germantown, MD, USA) and complimentary DNA (cDNA) was made from 1 µg of extracted RNA using the iScript Select cDNA Synthesis Kit (Bio-Rad, Mississauga, ON, Canada), according to the manufacturer's instructions. Samples were run in duplicate on 96-well plates, and each 20 µl reaction contained 5 µl cDNA, 0.4 µl primer solution, 10 µl SsoFast EvaGreen Supermix (Bio-Rad, Mississauga, ON, Canada), and 4.6 µl of RNase free water. Real-time PCR analysis was performed using a Bio-Rad CFX96 Real Time PCR Detection System (Bio-Rad, Mississauga, ON, Canada) using the following amplification conditions: 95°C (30 s); 40 cycles of 95°C (10 s), 55°C (10 s). All genes were normalized to the control gene GAPDH, and relative differences in gene expression between treatment groups were determined using the ΔΔCt method (226). Values are presented as fold increases relative to the Con group.

Western blotting analysis of content and phosphorylation of proteins – Adipose tissue samples collected from the Epid, Sc Ing, iBAT and aBAT depots were homogenized in a buffer containing 25 mM Tris-HCl, 25 mM NaCl (pH 7.4), 1 mM $MgCl_2$, 2.7 mM KCl, 1% Triton-X and protease and phosphatase inhibitors (Roche Diagnostics GmbH, Mannheim, Germany). Adipose tissue homogenates were centrifuged, the infranatant collected, and an aliquot was used to measure protein by the Bradford method.

Samples were diluted 1:1 (vol:vol) with 2x Laemmli sample buffer and heated to 95°C for 5 min. Samples were then subjected to SDS-PAGE, transferred to PVDF membrane, and probed for the proteins of interest. All primary antibodies were used at a dilution of 1:1,000 and β-actin was used as a loading control. All densitometry analyses were performed using the Scion Image program.

Statistical analyses – Statistical analyses were performed by either unpaired two-tailed t-tests or two-way analysis of variance (ANOVA) with Bonferroni post-hoc tests using the GraphPad Prism statistical software program. Statistical significance was set at $p<0.05$.

5.4. Results

Effects of cold exposure on body weight, energy intake, and fat mass – There was no difference in body weight between the control (395.12 ± 6.05 g) and cold-exposed animals (412.12 ± 5.15 g) at baseline or following cold exposure (411.61 ± 6.40 g vs. 408.64 ± 4.07 g). This occurred despite an average 46% increase in energy intake in cold-exposed animals (Fig. 5-1A). Cold exposure also caused 1.6- and 1.5-fold increases in iBAT and aBAT masses, respectively (Fig. 5-1B), indicating expansion and activation of these tissues by cold. In contrast, Epid and Sc Ing fat masses decreased by 25% and 20%, respectively, in cold-acclimated rats (Fig. 5-1C).

The effects of cold exposure on UCP1 content, Pgc-1α, Lpl, and Cd36 gene expression, and palmitate and glucose oxidation in iBAT, aBAT, Sc Ing, and Epid fat depots – As expected, cold exposure led to a significant increase in UCP1 content in iBAT (3.6-fold) (Fig. 5-1D), aBAT (4-fold) (Fig. 5-1E), and Sc Ing (3.2-fold) (Fig. 5-1F), but not in the

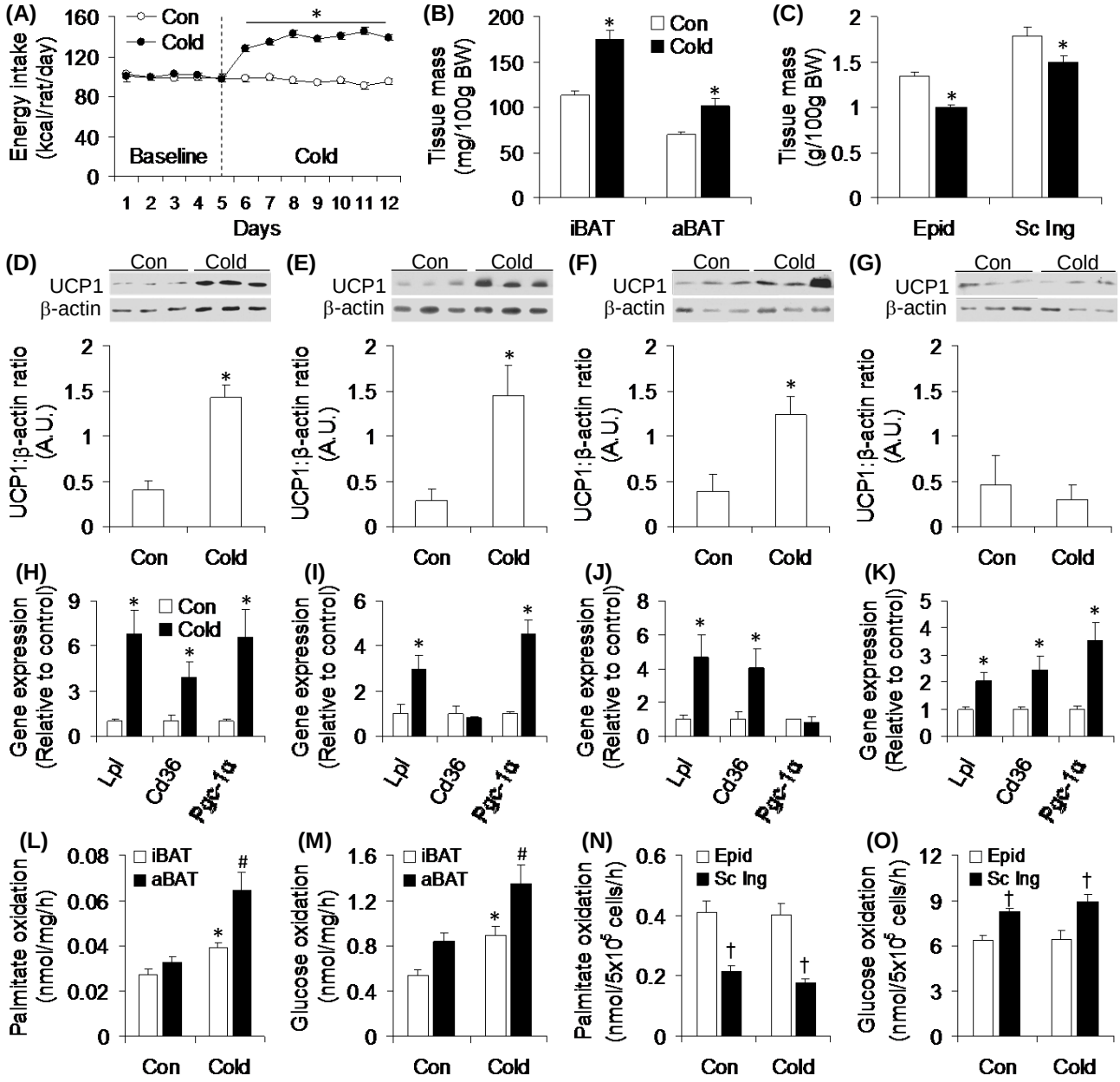

Figure 5-1: The effects of cold acclimation on energy intake, tissue mass, UCP1 content, gene expression of *Lpl, Cd36* and *Pgc-1α,* and substrate oxidation. Cold acclimation caused hyperphagia (A), increased interscapular and aortic brown adipose tissue (iBAT and aBAT, respectively) masses (B), and reduced epididymal (Epid) and subcutaneous (Sc) inguinal (Ing) adiposity (C). UCP1 content in iBAT (D), aBAT (E), and Sc Ing (F), and Epid (G) fat depots. *Lpl*, *Cd36*, and *Pgc-1α* gene expressions in iBAT (H), aBAT (I), Epid (J), and Sc Ing (K) fat depots. Glucose and palmitate oxidation in iBAT and aBAT (L and M) and in Epid and Sc Ing fat (N and O) depots. *p<0.05 vs. control (Con); $^{\#}$p<0.05 vs. Con and iBAT Cold; †p<0.05 vs. Epid. Two-way ANOVA was used to compare groups/conditions, except for UCP1 content and gene expression that t-test was used.

Epid fat depot (Fig. 5-1G). *Pgc-1α* expression was elevated by 6.6-fold in the iBAT (Fig. 5-1H), by 4.5-fold in the aBAT (Fig. 5-1I), and by 3.6-fold in the Sc Ing fat depot (Fig. 5-1K). No alteration in *Pgc-1α* expression was observed in the Epid fat pad (Fig. 5-1J) under cold conditions. *Lpl and Cd36* gene expressions were also elevated in iBAT by 6.82-fold and 3.9-fold, respectively (Fig. 5-1H). In aBAT, the expression of *Lpl* increased by 3-fold and no alteration was observed for *Cd36* expression in this tissue (Fig. 5-1I). In the Epid fat depot (Fig. 5-1J), the expressions of *Lpl* and *Cd36* were both increased by 4.6-fold and 4.1-fold, respectively. Cold exposure also increased *Lpl and Cd36* gene expressions by 2.1-fold and 2.5-fold, respectively, in the Sc Ing fat depot (Fig. 5-1K). The rates of palmitate (Fig. 5-1L) and glucose (Fig. 5-1M) oxidation increased in both iBAT (1.45-fold and 1.65-fold) and aBAT (2.2-fold and 1.6-fold). Furthermore, under cold acclimating conditions, the oxidation rates of palmitate (Fig. 5-1L) and glucose (Fig. 5-1M) were 1.7- and 1.52-fold greater in aBAT than iBAT, respectively. Differences in glucose oxidation rates between aBAT and iBAT were also detected in control animals, with the former being 1.6-fold higher than the latter (Fig. 5-1M). Cold acclimation had no effect on palmitate or glucose oxidation in adipocytes isolated from either the Epid or Sc Ing fat depots (Fig. 5-1N and O). However, palmitate oxidation was 2-fold greater in the Epid compared to the Sc Ing depot (Fig. 5-1N), whereas glucose oxidation was 1.4-fold greater in Sc Ing than Epid adipocytes (Fig. 5-1O) both in control and cold-acclimated rats.

Effects of isoproterenol and oligomycin on palmitate oxidation in Epid and Sc Ing adipocytes – No significant differences were found for palmitate oxidation between control and cold Epid adipocytes either in the absence or presence of isoproterenol or

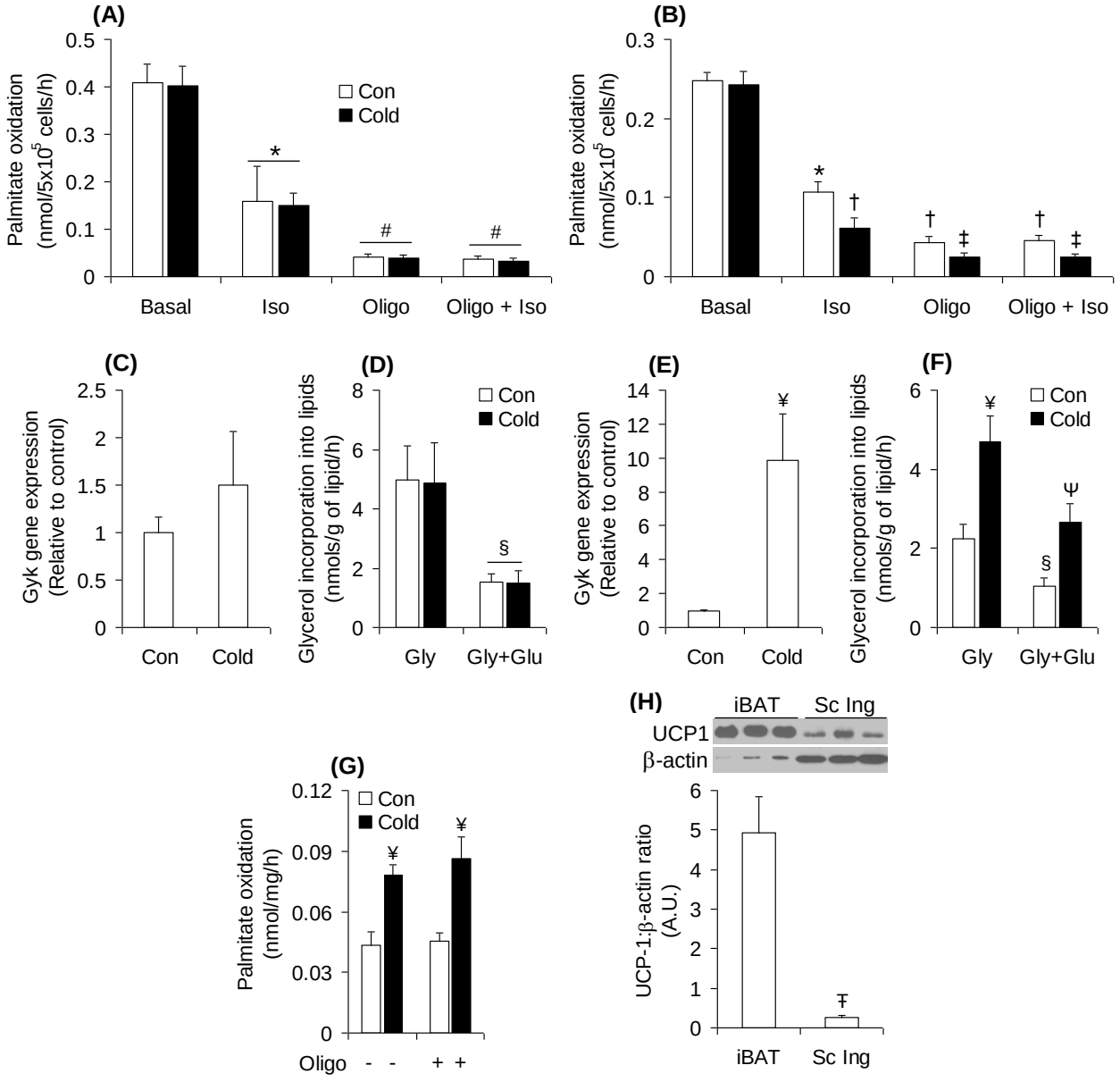

Figure 5-2: Basal and oligomycin-inhibited palmitate oxidation, *Gyk* expression and glycerol incorporation into lipids. Isoproterenol (Iso) and oligomycin (Oligo) inhibited palmitate oxidation in adipocytes from the epididymal (Epid) (A) and subcutaneous (Sc) inguinal (Ing) (B) fat pads of both control (Con) and cold-acclimated rats. Glycerol kinase (*Gyk*) gene expression (C) and incorporation of glycerol (Gly) into lipids in Epid (D) and Sc Ing (E and F) fat depots either in the absence or presence of glucose (Glu). Effect of Oligo on palmitate oxidation in aBAT (G) from Con or cold-acclimated rats. Comparison of UCP1 content between iBAT and Sc Ing fat depots of cold-acclimated rats (H). *p<0.05 *vs*. Basal; ¥p<0.05 *vs*. Con; #p<0.05 *vs*. Iso; †p<0.05 *vs*. Con Iso; ‡p<0.05 *vs*. Con Oligo and Con Oligo+Iso; §p<0.05 *vs*. Con Gly and Cold Gly; Ψp<0.05 *vs*. Cold Gly; ∓p<0.05 *vs*. iBAT. Two-way ANOVA was used to compare groups/conditions, except for *Gyk* gene expression and UCP1 content that t-tests were used.

oligomycin (Fig. 5-2A). However, isoproterenol and and oligomycin reduced palmitate oxidation by ~61% and 90%, respectively, in both control and cold Epid adipocytes, and the combination of isoproterenol and oligomycin did not cause any additional effect when compared to oligomycin alone (Fig. 5-2A). Similarly to what was observed in Epid adipocytes, palmitate oxidation did not differ between control and cold under basal conditions in Sc Ing adipocytes (Fig. 5-2B). However, the rates of palmitate oxidation in Sc Ing adipocytes were significantly different between control and cold conditions either in the presence of isoproterenol or oligomycin. In fact, isoproterenol reduced palmitate oxidation by 56% in control and by 74% in cold cells in comparison to basal conditions (Fig. 5-2B). Thus, a significantly lower (~44%) rate of palmitate oxidation was found for cold adipocytes when compared to control cells when exposed to isoproterenol (Fig. 5-2B). Oligomycin exerted an even more pronounced inhibitory effect, and reduced palmitate oxidation by 83% and 90% in control and cold Sc Ing adipocytes, respectively, when compared to basal conditions (Fig. 5-2B). Again, cold Sc Ing adipocytes displayed a significant lower rate (42%) of palmitate oxidation in comparison to control cells when exposed to oligomycin. The combination of isoproterenol and oligomycin did not cause any additive inhibitory effect in palmitate oxidation when compared to oligomycin alone, and the lower (46%) rates exhibited by cold in comparison to control adipocytes remained essentially unaltered (Fig. 5-2B).

Effects of cold acclimation on glycerol kinase (Gyk) expression and the incorporation of glycerol into lipids in Epid and Sc Ing adipocytes – *Gyk* expression did not differ between control and cold conditions in the Epid fat depot (Fig. 5-2C). Furthermore, no differences were found between control and cold Epid adipocytes with respect to

glycerol incorporation into lipids either in the absence or presence of glucose (Fig. 5-2D), although both control and cold adipocytes displayed a 60% reduction in glycerol incorporation into lipids when glucose was added to the incubation buffer (Fig. 5-2D). In Sc Ing WAT, cold acclimation increased *Gyk* expression ~10-fold (Fig. 5-2E), and this was accompanied by 2-fold increase in glycerol incorporation into lipids in the absence of glucose (Fig. 5-2F). Even though the addition of glucose to the incubation medium reduced glycerol incorporation into lipids by 53% in control cells and by 43% in cold cells, a much higher rate (2.53-fold) was displayed by cold than control Sc Ing adipocytes (Fig. 5-2F).

Effect of oligomycin on palmitate oxidation in aBAT and comparative analysis of UCP1 content in iBAT and Sc Ing fat depots – Even though oligomycin exerted a very potent inhibitory effect on palmitate oxidation in Epid and Sc Ing adipocytes (Fig. 5-2A and B), in aBAT this drug did not affect the rates of palmitate oxidation either in tissues from control or cold-acclimated rats (Fig. 5-2G). In fact, besides exhibiting enhanced rates of palmitate oxidation upon cold exposure (Fig. 5-1L and Fig. 5-2G), iBAT (data not shown) and aBAT (Fig. 5-2G) were insensitive to oligomycin, indicating that mitochondrial uncoupling accounted for essentially the entire consumption of fatty acids in these tissues. Comparative analysis of UCP1 content in Sc Ing and iBAT revealed that after cold acclimation UCP1 levels in the former tissue was equivalent to only ~5% of the levels of this protein in the latter tissue (Fig. 5-2H). Thus, the impact of UCP1-mediated uncoupling on substrate consumption in the Sc Ing fat depot under conditions of cold acclimation is limited.

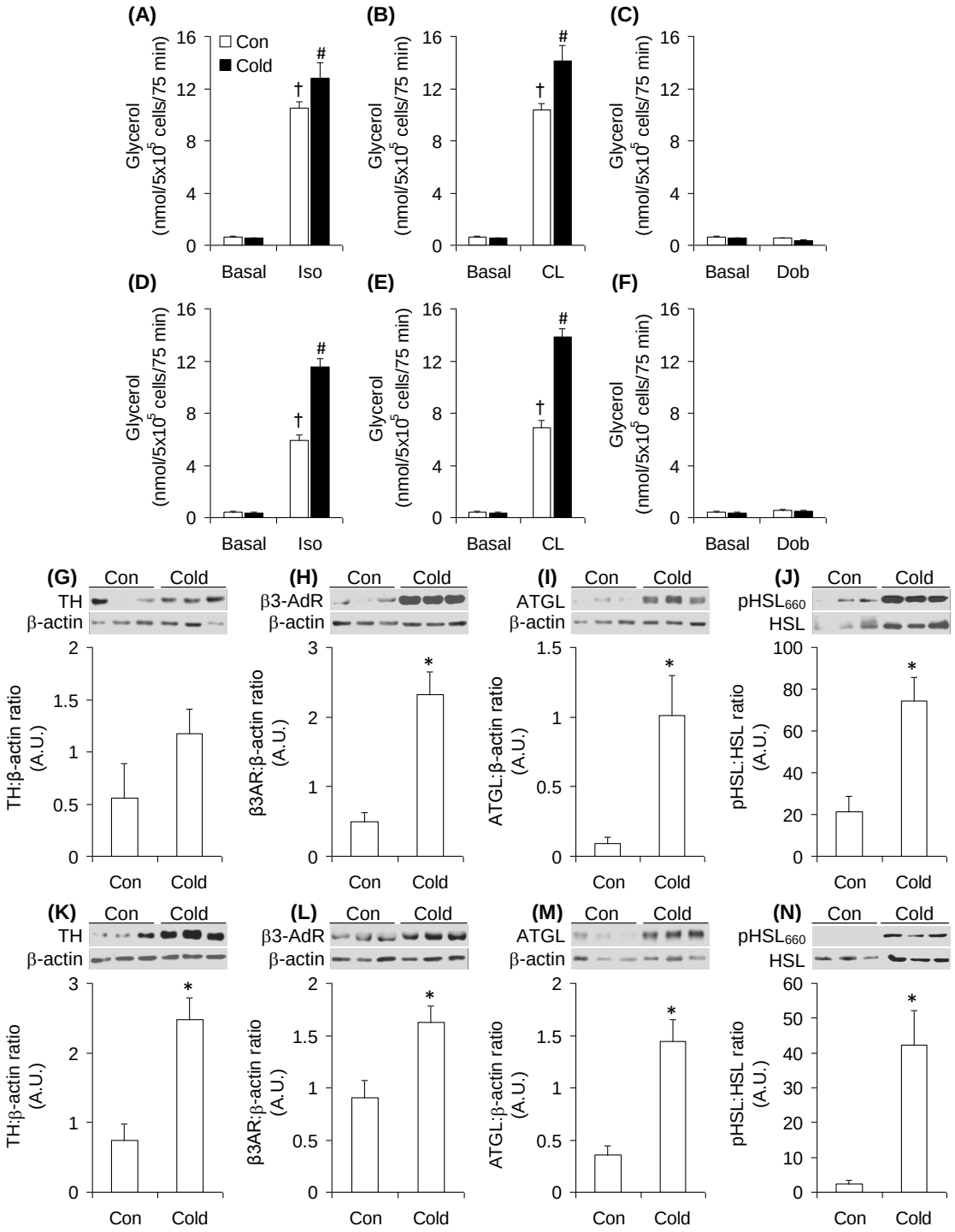

Figure 5-3: The effects of cold acclimation on lipolysis and the lipolytic cascade in the WAT. Cold acclimation enhanced isoproterenol (Iso)- and CL 316,243 (CL)-, but not dobutamine (Dob)-stimulated lipolysis in epididymal (Epid) (A-C) and subcutaneous (Sc) inguinal (Ing) (D-F) fat depots. Tyrosine hydroxylase (TH), β3-adrenergic receptor (β3-AdR), and adipose triglyceride lipase (ATGL) contents, and hormone sensitive lipase (HSL) phosphorylation in Epid (G-J) and Sc Ing (K-N) fat depots of cold-acclimated rats. $^{\dagger}p<0.05$ vs. Basal Con and Cold; $^{\#}p<0.05$ vs. Con Iso; *$p<0.05$ vs. Con. Two-way ANOVA was used to compare groups/conditions, except for western blot data that t-tests were used.

Effects of cold acclimation on lipolysis, contents of TH, β3-AdR, ATGL, and HSL phosphorylation – As expected, in adipocytes isolated from the Epid and Sc Ing fat depots, β-adrenergic agonists caused marked increases in lipolysis (Fig. 5-3A-F). In fact, isoproterenol stimulated lipolysis above basal levels by 17-fold and 14-fold in Epid (Fig. 5-3A) and Sc Ing (Fig. 5-3D) adipocytes, respectively. In the presence of CL 316,243, lipolysis was stimulated by 17-fold in Epid (Fig. 5-3B) and by 16-fold in Sc Ing adipocytes (Fig. 5-3E), whereas dobutamine exerted no stimulatory effect in adipocytes from either tissue (Fig. 5-3C and F). Cold exposure significantly increased rates of lipolysis in adipocytes isolated from both WAT depots (Fig. 5-3A-F). In Epid adipocytes, cold exposure led to 1.2- and 1.36-fold increases in isoproterenol- and CL 316,243-stimulated lipolysis, respectively (Fig. 5-3A and B). These effects were even more pronounced in adipocytes isolated from the Sc Ing depot, where both isoproterenol and CL 316,243 increased glycerol release by ~2-fold when compared to adipocytes from control rats (Fig. 5-3D and E). Overall, adipocytes from both fat depots elicited very potent lipolytic responses to β-adrenergic receptor agonists, and cold exposure even exacerbated the lipolytic response to these agents. Even though TH content did not differ between control and cold in the Epid fat depot (Fig. 5-3G), β3-AdR and ATGL contents, and HSL_{660} phosphorylation increased by 4.7-fold (Fig. 5-3H), 7-fold (Fig. 5-3I), and 3.5-fold (Fig. 5-3J), respectively, upon cold acclimation in this fat depot. In the Sc Ing fat depot, TH, β3-AdR, and ATGL contents, as well as HSL_{660} phosphorylation increased by 3.3-fold (Fig. 5-3K), 1.8-fold (Fig. 5-3L), 4-fold (Fig. 5-3M), and 18-fold (Fig. 5-3N), respectively, by cold acclimation.

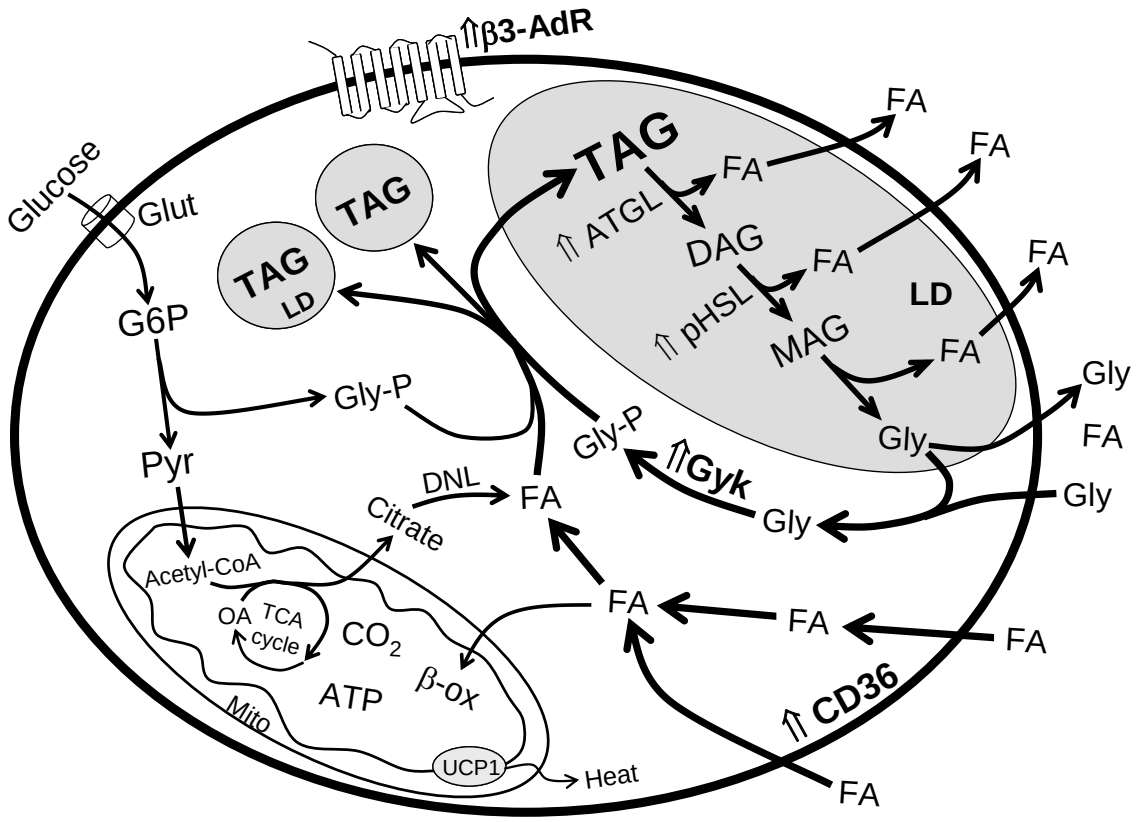

Figure 5-4: Diagram depicting the proposed metabolic and morphological alterations that characterize cold-induced browning and the appearance of beige adipocytes in the subcutaneous WAT. Chronic β3-AdR stimulation leads to enhanced activation of ATGL and HSL and to a marked increase in adipocyte lipolysis. This culminates in a massive release of FAs that can be exported to the extracellular medium, undergo β-oxidation (β-ox), or be re-esterified into TAG. The latter pathway creates a thermogenic energy-consuming futile cycle of TAG hydrolysis and re-synthesis that is greatly facilitated by increased expression of Gyk and fatty acid transporters (*e.g.* CD36). Beige adipocytes also increase their UCP1 content; however, UCP1-mediated mitochondrial uncoupling has only a minor thermogenic contribution in these cells. In fact, a greater flow of FAs is diverted toward the TAG breakdown/re-synthesis futile cycle, which also facilitates the formation of multiple smaller lipid droplets (LD) and changes the appearance of the adipocyte from unilocular to multilocular. Beige adipocytes use glucose and FAs in the tricarboxylic acid (TCA) cycle for the production of energy to fuel multiple futile cycles, although glucose also contributes metabolic intermediates that are essential for FA re-esterification and *de novo* lipid synthesis (DNL) in beige adipocytes. β-ox = β-oxidation; DAG = diacylglycerol; MAG = monoacylglycerol; G6P = glucose-6-phosphate; Gly = glycerol; Gly-P = glycerol phosphate; Glut = glucose transporter; LD = lipid droplet; Mito = mitochondria; OA = oxaloacetate; Pyr = pyruvate. ⇑ denotes increase and thick arrows indicate higher flow through the pathway.

5.5. Discussion

Here, we provide novel evidence that cold-induced increases in UCP1 content in the Sc Ing fat depot did not lead to an increase in the capacity of adipocytes residing in this tissue to oxidize fat or glucose. Furthermore, oligomycin suppressed 90% of the palmitate oxidation response of Sc Ing adipocytes, providing evidence that cold-induced WAT browning did not promote a significant thermogenic response mediated by mitochondrial uncoupling within the tissue. In fact, the inhibitory effect of oligomycin on palmitate oxidation was more pronounced in cold Sc Ing adipocytes than controls, which indicates that rates of UCP1-mediated uncoupled respiration in this tissue were actually reduced, despite a 3.2-fold increase in UCP1 levels in comparison to control cells. Importantly, the UCP1 content in the Sc Ing fat of cold-acclimated rats was equivalent to only ~5% of what was found in the classical BAT of these animals. Therefore, it may not have been sufficient to cause a significant impact on mitochondrial uncoupling and substrate utilization after cold-induced browning took place in the Sc Ing fat depot. Additionally, in comparison to BAT, mitochondria in WAT are less numerous, thinner and more elongated, contain fewer and randomly oriented cristae (215), and display low levels of CPT1 activity (227). These features of WAT mitochondria may have limited the capacity of white adipocytes to increase their fat-oxidative capacity, despite increased UCP1 levels upon cold acclimation. Lastly, we cannot rule out the possibility that 7 days of cold exposure might not have been sufficient for the entire oxidative machinery of the white adipocyte to be fully developed, and for mitochondrial uncoupling to actually translate into higher rates of substrate oxidation, particularly in a tissue with naturally low oxidative capacity such as WAT. In fact, the dynamics of mitochondrial turnover

have been reported to differ between iBAT and SC Ing WAT, with the latter tissue displaying higher variability under conditions of varying temperatures (228). Thus, a longer period of cold exposure might have been required for all components of the oxidative machinery to be fully assembled and stabilized in order for increased oxidative capacity to be detected as a consequence of UCP1 upregulation in SC Ing adipocytes. In classical BAT that contain a large number of mitochondria packed with transverse cristae and great abundance of UCP1 (215) this was not the case because iBAT and aBAT displayed significant increases in both glucose and palmitate oxidation upon cold acclimation. Interestingly, the rates of cold-induced palmitate and glucose oxidation were 67% and 61% higher, respectively, in aBAT than in iBAT. This is likely due to the fact that aBAT displayed a higher increase (5-fold) than iBAT (3.6-fold) in UCP1 levels upon cold exposure. We are unaware of any other study that has reported such metabolic differences between two classical brown adipose tissues with respect to their capabilities to oxidize glucose and fat under control and cold acclimating conditions. From a functional perspective, the higher oxidative response of aBAT to cold may be related to the fact that this tissue is closer to the heart, which could more quickly dissipate heat to other regions of the body than iBAT.

It was also surprising to find that isoproterenol reduced palmitate oxidation in Sc Ing adipocytes, and again more so in cold than control cells. We had originally hypothesized that isoproterenol would increase palmitate oxidation in cold Sc Ing adipocytes. This would be caused by the stimulation of lipolysis and fatty acid-induced activation of UCP1 (63). Indeed, cold markedly enhanced isoproterenol- and CL 316,243-induced lipolysis in Sc Ing adipocytes, but this was followed by a reduction instead of an

increase in fatty acid oxidation in comparison to control cells. Thus, the fact that β-adrenergic-induced lipolysis elevates respiration in adipocytes (217, 222, 223) does not necessarily mean that fatty acid consumption through oxidation is also increased in these cells. From the lipolysis data obtained from isolated adipocytes exposed to isoproterenol and CL 316,243 it was clear that cold acclimation markedly increased the ability of the WAT to export fatty acids. In fact, the main components of the molecular machinery that drive lipolysis were robustly upregulated in both Epid and Sc In fat depots, including the contents of TH, β3-AdR, and ATGL, as well as HSL phosphorylation. However, we also observed that the gene expressions of *Lpl* and *Cd36* were significantly elevated. This indicates that besides exportation, cold also increased the ability of WAT and BAT to uptake fatty acids, which is compatible with hyperphagia in cold-acclimated rats. What then would be the fate of these incoming fatty acids, if not diverted to oxidation within the WAT? To answer this question we measured the expression of Gyk and glycerol incorporation into lipids to test whether fatty acids entering white adipocytes were actually being diverted toward re-esterification instead. This would create a futile cycle that could allow the cell to deal with an abundance of incoming fatty acids in an environment of accelerated lipolysis (229). Indeed, in the Sc Ing fat depot Gyk expression increased ~10-fold, whereas in the Epid fat depot it was unaltered by cold acclimation. We next assessed glycerol incorporation into lipids either in the absence or presence of glucose because adipocytes use this sugar for glycerol production and fatty acid esterification. When incubated in medium devoid of glucose, Sc Ing adipocytes from cold-acclimated rats displayed a 2-fold increase in glycerol incorporation into lipids. The addition of glucose (5.5 mM) reduced glycerol

incorporation into lipids in both control and cold adipocytes, but it still remained 2.5-fold higher in cold than control Sc Ing adipocytes. This demonstrates that, even in the presence of glucose, cold Sc Ing adipocytes used lipolysis-derived glycerol to recycle TAG. These data are consistent with the activation of a futile cycle that actually diverts incoming fatty acids toward esterification (229), and provide an explanation for the lower rates of fatty acid oxidation in cold Sc Ing adipocytes than control cells when exposed to oligomycin and isoproterenol.

In mice, the browning effect of cold exposure on WAT has been proposed to derive from extensive structural remodeling of the lipid droplet through a dynamic process that involves continuous break down and re-synthesis of TAG in this tissue (87). Such remodeling process appears to be required for the formation of multilocular adipocytes with enlarged surface area. This facilitates the access of lipases to the lipid droplet and ultimately translates into a higher capability for the adipocyte to break down TAG and export fatty acids (87). Our findings demonstrate that cells from Sc Ing WAT indeed enhanced their biochemical machinery to export and recycle TAG, which is in line with the remodeling of the lipid droplet that is typical of cold-induced browning (87) (Fig. 4). However, this did not seem to be the case with the Epid fat pad that displayed an increase in content and phosphorylation of proteins involved in the lipolytic cascade, but did not elicit any changes in Gyk expression and glycerol incorporation into lipids upon cold exposure. Besides the induction of browning, Epid and Sc Ing adipocytes also differed in the preference for substrate oxidation either under control or cold-stimulated conditions. In fact, palmitate oxidation was ~2-fold higher in Epid than Sc Ing adipocytes, whereas glucose oxidation was 1.4-fold higher in Sc Ing than Epid

adipocytes. The higher rate of glucose oxidation in Sc adipocytes could facilitate glucose disposal and favourably contribute to whole-body glycemic control.

In summary, our findings provide novel evidence that even though cold-induced browning of the Sc Ing fat depot significantly increases UCP1 content in this tissue, adipocytes from this fat depot do not enhance glucose or fat consumption through UCP1 mediated mitochondrial uncoupling. In fact, fat oxidation is even lower in beige/brite than in white adipocytes after coupled respiration is inhibited in both cells. Thus, our findings are contrary to the idea that beige/brite adipocytes can burn significant amounts of fat for thermogenesis and ultimately reduce adiposity. Rather, under conditions of cold-induced browning, the Sc WAT enhances its ability to export fat to other thermogenic tissues in the body and simultaneously activates an energy-consuming futile cycle of TAG breakdown and re-synthesis (lipolysis/lipogenesis). Such futile cycle seems to constitute the main thermogenic response of the Sc Ing WAT under cold acclimating conditions and allows the cell to handle a high rate of TAG turnover in a condition of accelerated lipolysis and enhanced fatty acid uptake (Fig. 4). It may also lead to the formation of multiple small lipid droplets that change the appearance of white adipocytes from unilocular to multilocular resembling classical brown adipocytes (Fig. 5-4). However, these beige/brown cells do not seem to shift their metabolism from an essentially fat storage/release compartment to a tissue that burns fat and dissipates energy within itself like classical BAT.

CHAPTER 6: Cold-induced autocrine/paracrine effects of fibroblast growth factor 21: Implications for depot-specific white adipose tissue browning in rats

Diane M. Sepa-Kishi and Rolando B. Ceddia.

Muscle Health Research Centre, School of Kinesiology and Health Science, York University, Toronto, Ontario, Canada

Keywords: FGF21, ERK1/2, UCP1, β-klotho, FGFR, thermogenesis, liver, adipose tissue

Statement of Labour

The experiments conducted in this study were carried out by Diane M. Sepa-Kishi. DMSK's contributions included collection of blood samples, extraction of tissues, isolation of adipocytes, collection of conditioned media and analysis of FGF21. DMSK was also responsible for conducting and collecting the western blot and qPCR data, analyzing and interpreting all of the results, preparing the figures, and writing and revising the manuscript. DMSK was supported by a NSERC Alexander Graham Bell Canada Graduate Scholarship and an Elia Scholarship. Due to the logistics of this study, RBC assisted with the collection of blood samples and the extraction of tissues.

Dr. Rolando Ceddia is the primary investigator and supervisor of this project and this research was funded by a Discovery Grant from NSERC and by infrastructure grants from the Canada Foundation for Innovation and the Ontario Research Fund.

6.1. Abstract

Fibroblast growth factor 21 (FGF21) is a hormone induced by cold in brown and white adipose tissues (BAT and WAT) that upregulates the expression of uncoupling protein 1 (UCP1) and promotes browning of the subcutaneous (Sc) inguinal (Ing) WAT. Thus, the objective of this study was to investigate the source of cold-induced FGF21 and assess the activation of its downstream signaling pathway in classical BAT and WAT depots. Male Wistar rats were acclimatized to cold (4°C) for 7 days and blood samples were taken daily. Subsequently, liver, interscapular and aortic BAT (iBAT and aBAT), and the Sc Ing and epididymal (Epid) WAT were extracted. Circulating FGF21 and its liver expression were reduced by 31% and 73%, respectively under cold-acclimating conditions. Conversely, expression and content of FGF21 were increased in iBAT, aBAT and Sc Ing fat depots, and so were the expressions of the *Fgf21* receptor (*Fgfr1)* and the receptor co-factor *β-klotho* in iBAT, Sc Ing, and Epid fat depots. FGF21 secretion from Sc Ing adipocytes was also increased, although phosphorylation of ERK1/2, a downstream FGF21 signaling target, was only enhanced in iBAT and Sc Ing fat depots following cold acclimation. These findings provide novel evidence that FGF21 acts in an autocrine/paracrine manner in iBAT and Sc Ing fat depots to drive depot-specific thermogenic adaptive responses under cold-acclimating conditions.

6.2. Introduction

Fibroblast growth factor-21 (FGF21) is a hormone that belongs to a large family of small generally secreted proteins that are involved in diverse actions such as cell growth, cell differentiation, embryonic development (230), and metabolic regulation (231). FGF21 is expressed in several organs, including the liver, brown and white adipose tissues (BAT and WAT, respectively), pancreatic β-cells, and thymus (101). It was initially described as a protein that enhanced glucose uptake in 3T3-L1 and human primary adipocytes by increasing *Glut1* mRNA and protein (107). However, it is now well recognized that FGF21 exerts multiple metabolic effects and increases energy expenditure in response to specific stimuli such as cold exposure, high-fat and ketogenic diets, and fasting/refeeding (231). Under conditions of cold-induced thermogenesis, FGF21 up-regulates *Ucp1* expression in classical BAT and also in the subcutaneous (Sc) inguinal (Ing) white adipose tissue (WAT). The latter effect characterizes the ability of FGF21 to induce browning of the Sc Ing WAT, which is actually impaired in mice deficient in FGF21 (108). In fact, in mice lacking FGF21 the ability of the WAT to undergo cold-induced browning and acquire multilocular, *Ucp1*-expressing adipocytes known as beige or brite ("brown-in-white") adipocytes is markedly impaired (108). Therefore, compelling evidence exists that FGF21 is crucial for the induction of thermogenic adaptive responses in both classical brown and WAT adipocytes upon cold exposure.

In order for FGF21 to signal, it requires the presence of the single-pass transmembrane protein β-klotho and the FGF receptor (FGFR) (103, 104). FGF21 binds β-klotho at the C terminus and interacts with FGFR through its N terminus (104, 232).

Thus, activation of the FGFR requires that both termini of FGF21 are intact (233, 234). Importantly, β-klotho expression is essential for FGF21 signaling and is the primary determinant of tissue specificity because it limits the action of the hormone to those tissues that express both the receptor and β-klotho, as is the case for BAT and WAT (103, 104). Binding of FGF21 to its receptor and the formation of the FGF21/FGFR/β-klotho complex results in autophosphorylation of tyrosine residues on the receptor (105), which subsequently leads to the phosphorylation and activation of MAPK/ERK kinase (MEK)1/2 (106). MEK1/2 phosphorylate tyrosine and threonine in extracellular signal-regulated kinase (ERK)1/2, a kinase that has multiple downstream targets (106). There is evidence that FGF21 signals in the brain to activate the sympathetic nervous system (SNS) and induce adipose tissue thermogenesis and that an intact adrenergic system is necessary for FGF21 action (235). However, more recently it has been reported that even in the absence of β3-adrenergic receptor cold-induced thermogenic gene expression (*Ucp1*, *Pgc1a*, *Dio2*, and *Cidea*) in brown or brite/beige adipose tissues still occurs (236). Furthermore, previous studies have demonstrated that FGF21 can increase thermogenic gene expression (*e.g. Ucp1* and *Cidea*) in isolated primary WAT and BAT adipocytes (108). Therefore, it appears that FGF21 can enhance BAT thermogenesis and induce WAT browning either via SNS activation or through a direct cell-autonomous effect in these tissues.

Based on various rodent studies, it is now well established that the ability of the WAT to undergo browning varies among different fat depots, with the Sc Ing WAT being the most prone to acquiring a brown-like phenotype (87, 91, 215, 237). In this context, it is still unclear whether it is a systemic increase or a tissue-specific autocrine/paracrine

FGF21 effect that can potentially drive cold-induced browning of WAT. In mouse tissues, the highest level of *Fgf21* expression was found in the liver (238), and this organ is considered the main source of circulating FGF21 (239). Interestingly, previous studies have reported a reduction in *Fgf21* expression in the liver of cold-exposed mice, although this was not accompanied by a reduction in circulating FGF21 levels in these animals (108). Because FGF21 is also produced by BAT, WAT and skeletal muscles (240), it could be that a reduction in liver expression and production did not cause a drop in circulating levels of FGF21 due to a compensatory increase in the production of this hormone by these other tissues. However, it still remains to be demonstrated whether or not other sites of production can compensate for a potentially reduced hepatic production and maintain unaltered circulating levels of FG21 under cold-acclimating conditions. Furthermore, there has been no clear comparison between BAT and WAT depots with respect to FGF21 expression and content. Of particular interest are the responses in the Sc Ing and Epid WAT depots and how they compare to each other, and to the classical BAT depots. Because FGF21 treatment induces *Ucp1* in Sc Ing but not in Epid fat, differences in the FGF21 signaling may likely exist between these two depots, and this could help explain depot-specific differences with respect to cold-induced WAT browning. In this context, we designed a study to investigate the source of cold-induced FGF21 and examined WAT and BAT depot-specific content, release, and downstream signaling of the FGF21 pathway. We exposed rats to cold (4°C) for 7 days, after that, we extracted the interscapular and aortic BAT (iBAT and aBAT, respectively) and the Sc Ing and Epid fat depots. These tissues were used for the determination of FGF21 content and expression, *β-klotho* and *Fgfr1* expression, and

phosphorylation of the downstream FGF21 signaling target ERK1/2. Sc Ing and Epid WAT were also used to isolate adipocytes and assess the release of FGF21 by these cells *in vitro*. Blood samples were collected on a daily basis to determine potential time-dependent alterations in circulating FGF21 levels, and the livers were extracted to assess *Fgf21* gene expression in this organ at the end of the study. Here, we provide data regarding the effects of cold acclimation on circulating FGF21 levels, as well as a novel comparative analysis of FGF21 expression, content, release, and activation of its downstream signaling pathway in classical BAT and WAT depots.

6.3. Materials and Methods

Reagents – Type II collagenase was obtained from Sigma (St. Louis, MO, USA). Protease (cOmplete™ Ultra Tablets) and phosphatase (PhosSTOP™) inhibitors were from Roche Diagnostics GmbH (Mannheim, Germany). The HR Series non-esterified fatty acid (NEFA)-HR(2) kit was from Wako Diagnostics (Richmond, VA, USA). The rat FGF21 ELISA was from R&D Systems (Minneapolis, MN, USA). All antibodies were purchased from Cell Signaling (Danvers, MA, USA), except for the FGF21 antibody that was purchased from Abcam (Toronto, ON, Canada).

Animals – Male albino rats (Wistar strain) were housed at 22°C on a 12/12-h light/dark cycle and fed standard laboratory chow (Lab Diet Cat #5012) *ad libitum*. The protocol containing all animal procedures described in this study was specifically approved by the Committee on the Ethics of Animal Experiments of York University (York University Animal Care Committee, YUACC, permit number 2016-5) and performed strictly in accordance with the YUACC guidelines. All surgery was performed under ketamine/xylazine anesthesia, and all efforts were made to minimize suffering.

Cold exposure – The rats were age- and weight-matched (~400 g) and randomly allocated to either the control or cold-exposed group. The rats were housed in individual cages and maintained on a 12/12-h light/dark cycle at 22°C (Con) or 4°C (Cold) for 7 days. Food intake was measured prior to (baseline) and on the final day of the cold exposure period. Blood samples were collected daily in the fed state, centrifuged for 10 min at 4°C and the plasma stored at -80°C for analysis of NEFAs and FGF21. Upon completion of the protocol, animals were anesthetized (0.4 mg ketamine and 8 mg xylazine per 100 g body weight) in the fed state and the iBAT, aBAT, Epid and SC Ing fat pads as well as the liver were extracted and weighed. A sample of each was flash frozen in liquid nitrogen for quantitative PCR and western blot analysis.

Adipocyte isolation and conditioned media – Adipocyte isolation from the Epid and SC Ing fat pads was performed as previously described (19). Briefly, the adipose tissue was minced in Krebs-Ringer Buffer (0.154 M NaCl, 0.154 M KCl, 0.11 M $CaCl_2$, 0.154 M $MgSO_4$, 0.154 M KH_2PO_4, 0.154 M $NaHCO_3$, pH 7.4) with 5.5 mM glucose and 30 mM HEPES (KRBH) supplemented with type II collagenase (0.5 mg/ml). Minced tissues were incubated at 37°C with gentle agitation (120 orbital strokes/ min) for approximately 25-30 min. The digested tissue was then strained using a nylon mesh and cells were transferred to 50 ml tubes, washed, and resuspended in fresh KRBH. The total cell numbers were determined as previously described (224) and an equal number of adipocytes (3.3×10^6/ml) from each depot was incubated in KRBH for a total of 4 h at 37°C. The conditioned media was collected at the end of the incubation period and frozen at -80°C for subsequent analysis of secreted FGF21.

RNA isolation and quantitative PCR – Primers were designed using the software PrimerQuest (IDT) based on probe sequences available at the Affymetrix database (NetAffx™ Analysis Centre, http://www.affymetrix.com/analysis) for each given gene. RNA was extracted from the adipose tissue and liver using TRIzol™ reagent (ThermoFisher Scientific, Mississauga, ON, Canada). Adipose tissue complimentary DNA (cDNA) was made from 5 µg of extracted RNA using the SuperScript II reverse transcriptase (ThermoFisher Scientific, Waltham, MA, USA) and liver cDNA was made from 2 µg of extracted RNA using the ABM EasyScript™ Reverse Transcriptase cDNA synthesis kit (Diamed, Mississauga, ON, Canada), according to the manufacturer's instructions. Samples were run using 10 µl of ABM EvaGreen qPCR Mastermix (Diamed, Mississauga, ON, Canada) using the following amplification conditions: 95°C (10 min); 40 cycles of 95°C (15 s), 60°C (60 s). Adipose tissue genes were normalized to the control gene GAPDH and liver genes were normalized to the control gene β-actin. Relative differences in gene expression between treatment groups were determined using the ΔΔCt method (226). Values are presented as fold increases relative to the Con group.

Western blotting analysis of content and phosphorylation of proteins, and conditioned media – Adipose tissue collected from the iBAT, aBAT, Epid and SC Ing depots was homogenized in a buffer containing 25 mM Tris-HCl, 25 mM NaCl (pH 7.4), 1 mM $MgCl_2$, 2.7 mM KCl, 1% Triton-X and protease and phosphatase inhibitors (Roche Diagnostics GmbH, Mannheim, Germany). Adipose tissue homogenates were centrifuged, the infranatant collected, and an aliquot was used to measure protein by the Bradford method. Samples were diluted 1:1 (vol:vol) with 2x Laemmli sample buffer

and heated to 95°C for 5 min. Samples were then subjected to SDS-PAGE, transferred to PVDF membrane and probed for the proteins of interest. All primary antibodies were used at a dilution of 1:1,000. β-actin was used as a loading control. For the conditioned media, samples were diluted 1:1 (vol:vol) with 2x Laemmli sample buffer, heated to 95°C for 5 min and an equal volume of each sample was subjected to SDS-PAGE. Samples were then transferred to PVDF membrane and subsequently probed for FGF21 (dilution of 1:1,000). Densitometric analyses of western blots were performed using the Scion Image program.

Statistical analyses – Statistical analyses were assessed by unpaired, two-tailed t-test or two-way ANOVA with Bonferroni post-hoc test using the GraphPad Prism statistical software program. Statistical significance was set at $p<0.05$.

6.4. Results

Effects of cold exposure on food intake, plasma NEFA levels, circulating FGF21, and liver Fgf21 expression – At baseline, food intake was similar between the two groups of rats. However, rats that were cold acclimated consumed 47% more food than control animals (Table 6-1). NEFA levels did not differ between the two groups either at baseline or after 7 days of cold exposure (Table 6-1).Time course analysis of plasma FGF21 shows that the circulating levels of this hormone progressively reduced throughout the 7-day period of cold exposure, reaching values ~40% lower than control after 4 days of cold exposure (Fig. 6-1A). Calculation of area under curve throughout the 7-day period revealed a significant reduction of 31% in circulating FGF21 levels in cold animals in comparison to controls (Fig. 6-1A and B). As the liver is the main source of circulating FGF21 (239), we also measured its expression in this tissue. In agreement

Table 6-1: Food intake (g/rat/day) and plasma NEFAs (mmol/l) at baseline and following seven days of cold exposure. Age- and weight-matched animals were either kept at room temperature or cold exposed (4°C) for 7 days.

	Baseline		7 Days Cold Exposure	
	Control	Cold	Control	Cold
Food Intake (g/rat/day)	28.68 ± 1.09	28.44 ± 0.78	27.69 ± 0.87	40.91 ± 0.83*
NEFA (mmol/l)	0.268 ± 0.028	0.215 ± 0.031	0.293 ± 0.022	0.236 ± 0.012

Food intake and plasma NEFAs were measured prior to (baseline) and on the final day of the cold exposure period. Plasma samples were taken in the fed state. Values are mean ± SEM. Two-way ANOVA, n = 7. *p<0.05 vs. Baseline Cold and 7 Days Cold Exposure Control.

with the plasma data, liver *Fgf21* gene expression was markedly reduced (73%) by cold exposure (Fig. 6-1C).

Effects of cold exposure on Fgf21 expression, content, and signaling in iBAT and aBAT – In contrast to the liver, cold exposure significantly increased *Fgf21* expression and its content by 11.2- and 1.8-fold, respectively, in the iBAT (Fig. 6-2A and B). In the aBAT, there was no significant alteration in *Fgf21* expression; however there was a 7-fold increase in FGF21 content in this tissue following cold exposure (Fig. 6-2C and D). In iBAT, cold exposure significantly elevated the expression of *Fgfr1* and *β-klotho* by 2.3- and 2.5-fold, respectively (Fig. 6-3A), and this was accompanied by a 4.2-fold increase in the phosphorylation of the FGF21 downstream signaling target ERK1/2 (Fig. 6-3B). In contrast to the iBAT, no change in the expression of *Fgfr1* was found in aBAT, whereas *β-klotho* expression was reduced by 50% following cold exposure (Fig. 6-3C). Furthermore, phosphorylation of ERK1/2 was also reduced by 78% in the aBAT of cold-exposed rats (Fig. 6-3D).

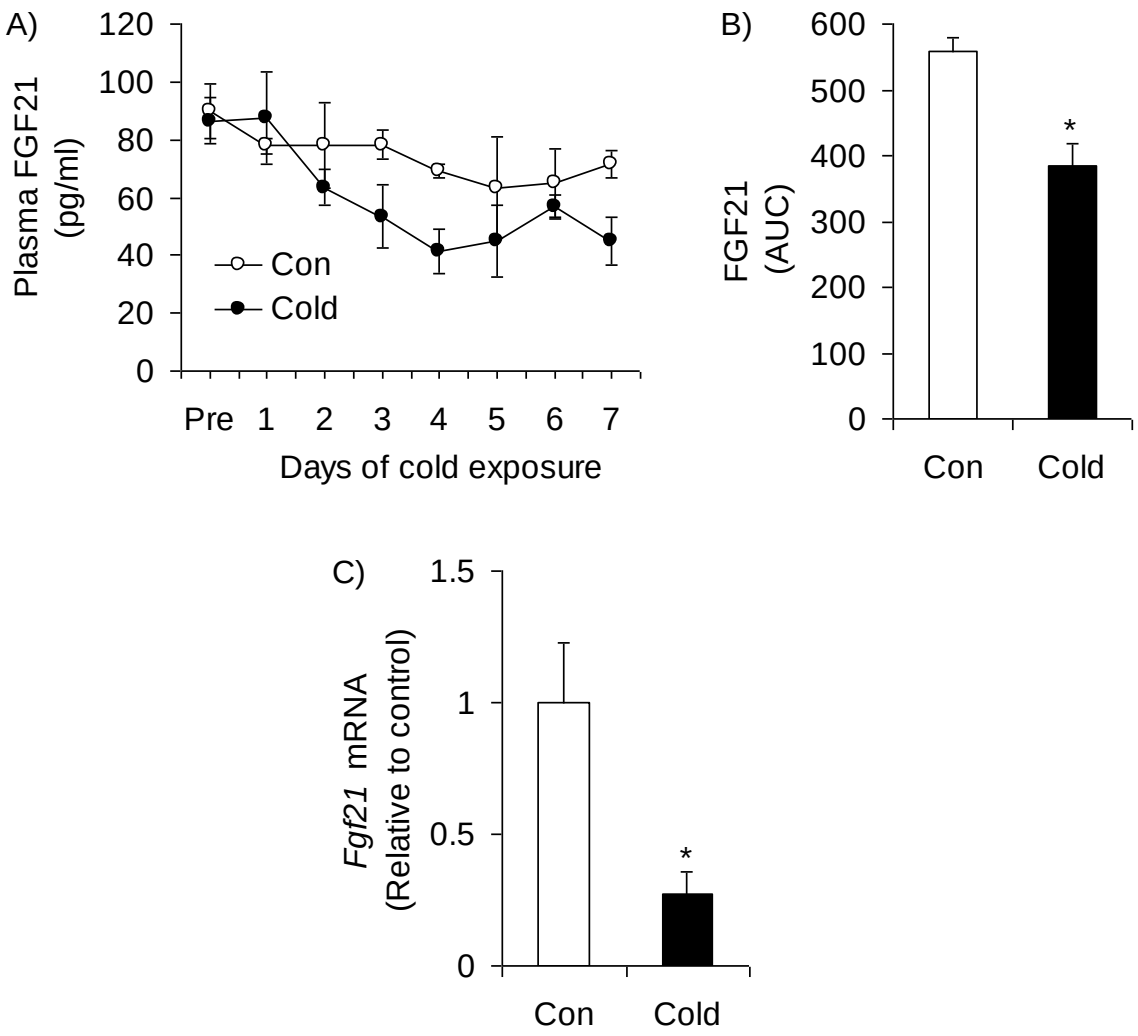

Figure 6-1: Plasma FGF21 and liver *Fgf21* gene expression following cold acclimation. Cold acclimation reduces plasma FGF21 (A and B) and liver gene expression of Fgf21 (C). Age- and weight-matched animals were either kept at room temperature or cold exposed (4°C) for 7 days. Plasma samples were taken daily in the fed state. AUC = area under the curve. *p<0.05 vs. Con. Unpaired, two-tailed t-test, n = 7 for the plasma data and n = 9 for the gene expression data.

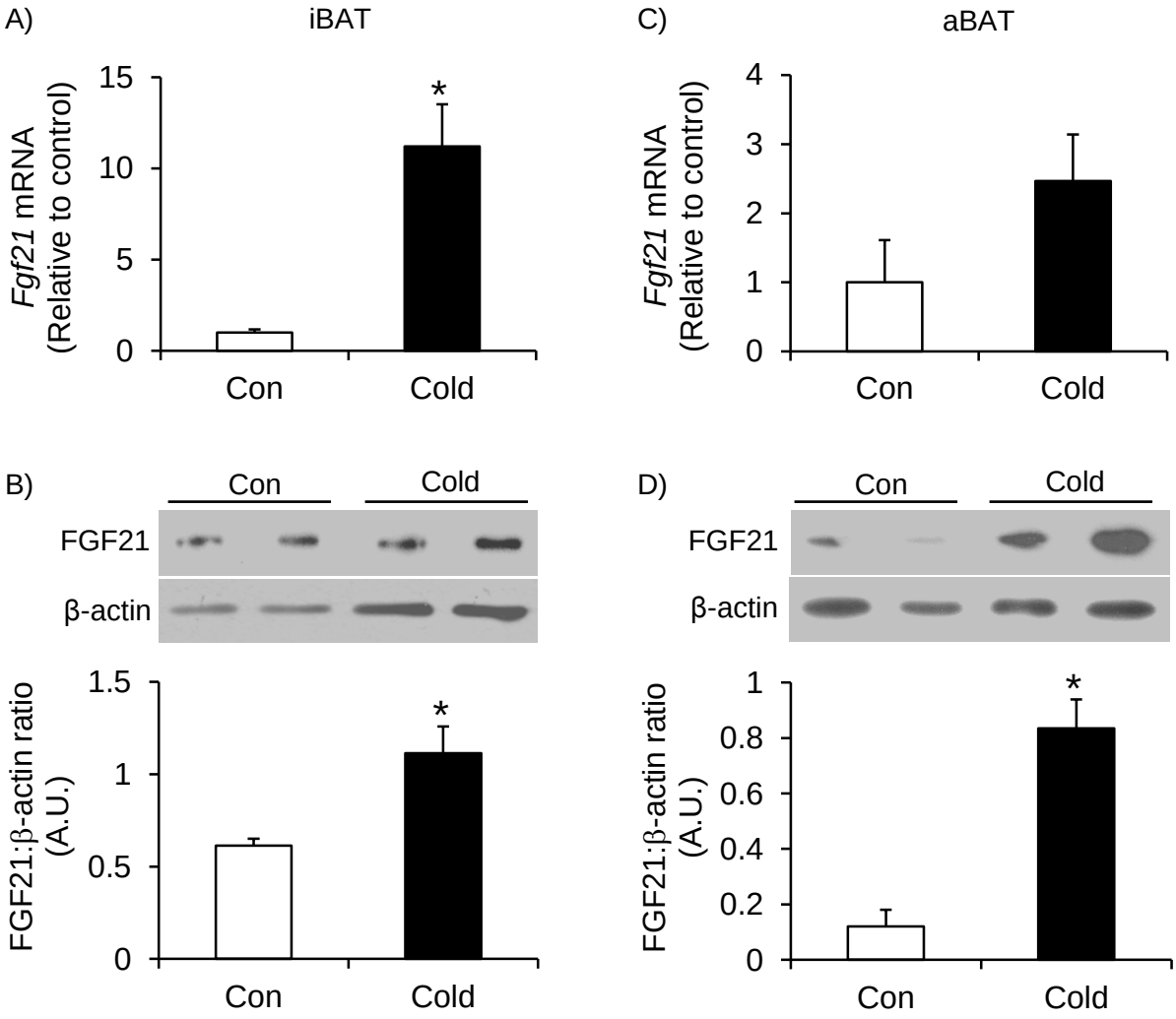

Figure 6-2: Expression and content of FGF21 in the BAT following cold exposure. Cold exposure increases the expression and content of FGF21 and the content of FGF21 in the iBAT (A and B) and aBAT (C and D). Age- and weight-matched animals were either kept at room temperature or cold exposed (4°C) for 7 days. *p<0.05 vs. Con. Unpaired, two-tailed t-test, n = 4-9.

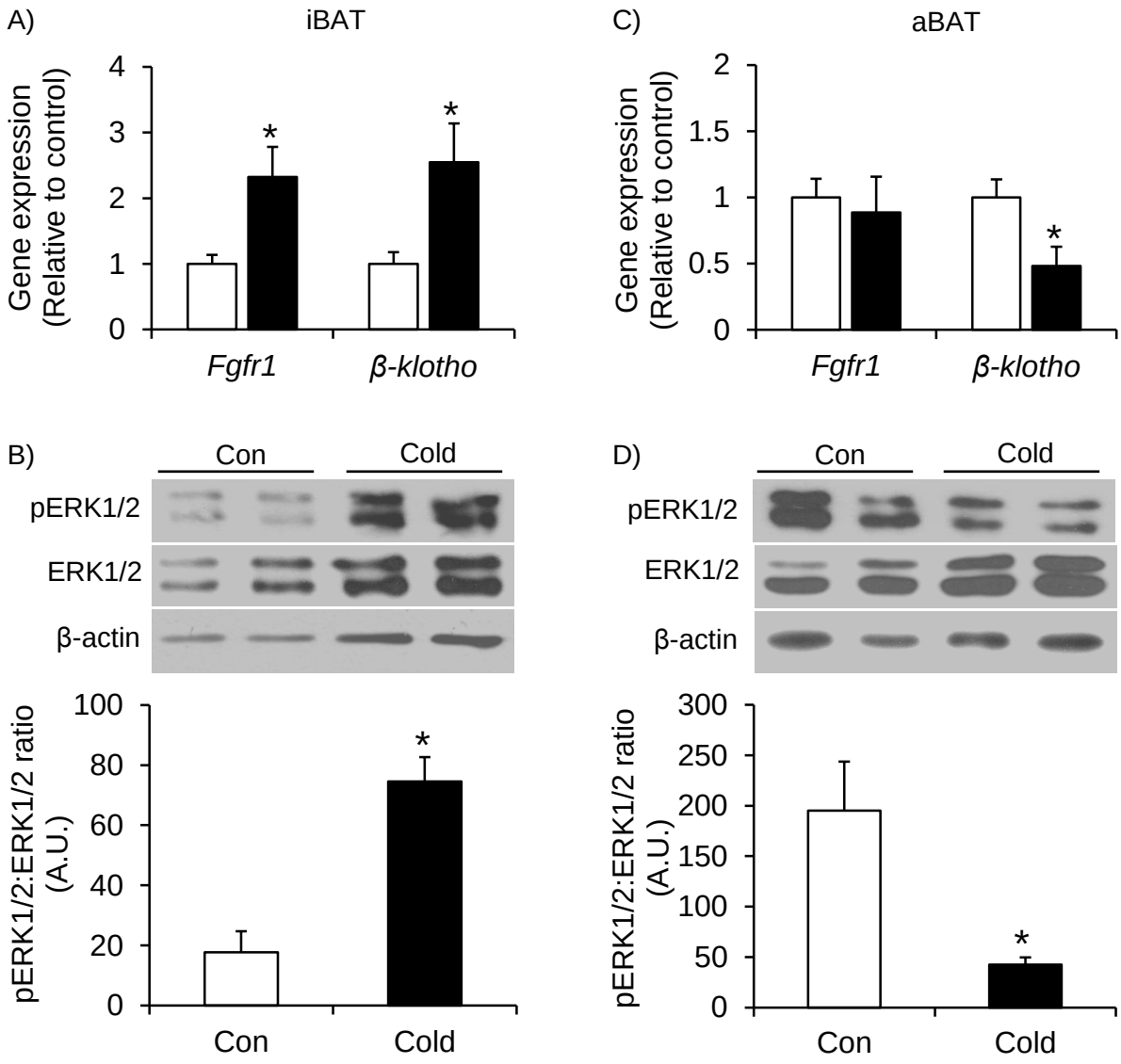

Figure 6-3: The effects of cold exposure on the FGF21 signaling pathway in the BAT.Cold exposure enhances the FGF21 signaling pathway in the iBAT (A and B) but not the aBAT (C and D). Age- and weight-matched animals were either kept at room temperature or cold exposed (4°C) for 7 days. *p<0.05 vs. Con. Unpaired, two-tailed t-test, n = 4-9.

Effects of cold exposure on the expression, content and secretion of FGF21 in the Sc Ing and Epid WAT – There were significant differences in the expression and content of FGF21 between the two WAT depots. Expression and content of FGF21 was 2-fold greater in the Sc Ing fat of cold-exposed rats compared to control rats (Fig. 6-4A and C), whereas in the Epid fat depot these variables did not differ between control and cold acclimating conditions (Fig. 6-4B and C). Additionally, the content of FGF21 in the cold-exposed Sc Ing fat was 4-fold greater than the Epid fat (Fig. 6-4C). In agreement with this data, there was a 5-fold increase in the amount of FGF21 secreted from Sc Ing adipocytes following cold exposure (Fig. 6-4D), whereas no significant differences in secreted FGF21 from the Epid adipocytes were found between control and cold conditions (Fig. 6-4E).

Effects of cold exposure on the FGF21 signaling pathway in the Sc Ing and Epid WAT – In addition to the increases in *Fgf21* expression and content in the Sc Ing WAT, expression of *Fgfr1* and *β-klotho* was also increased 3-fold in this depot following cold exposure (Fig. 6-5A). Phosphorylation of the downstream signaling target ERK1/2 was also increased by 1.6-fold in the Sc Ing WAT upon cold acclimation (Fig. 6-5B). Despite not affecting the expression and content of FGF21 in the Epid fat depot, cold acclimation significantly increased the expression of *Fgfr1* and *β-kotho* by 2.8-fold in this depot (Fig. 6-5C). However, this did not seem to have affected FGF21 signaling because there was no alteration in the phosphorylation of ERK1/2 in the Epid fat following cold exposure (Fig. 6-5D).

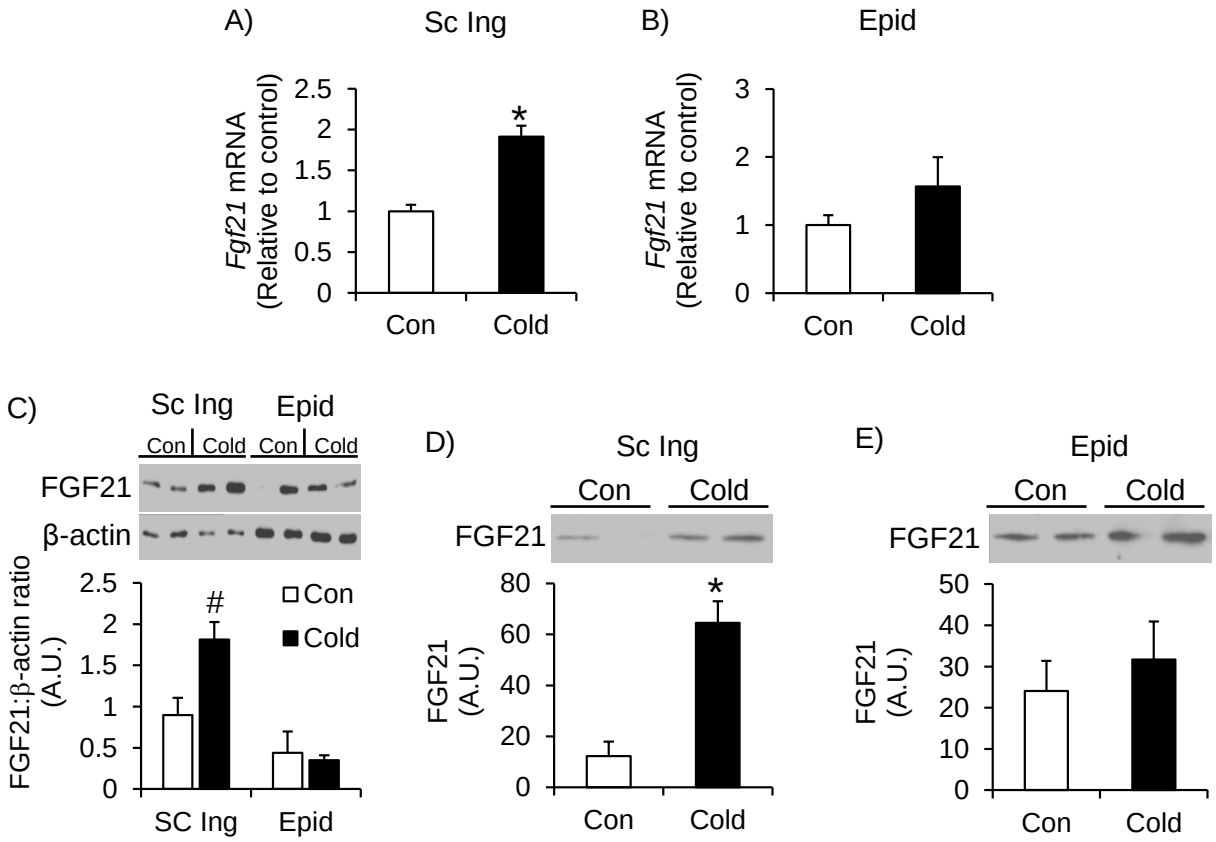

Figure 6-4: The expression, content and secretion of FGF21 from the WAT following cold exposure. Cold exposure increases the expression, content and secretion of FGF21 in the Sc Ing fat (A, C and D) but not the Epid fat (B, C and E). Age- and weight-matched animals were either kept at room temperature or cold exposed (4°C) for 7 days. *p<0.05 vs. Con. Unpaired, two-tailed t-test, n = 4-9. $^{\#}$p<0.05 vs. all other groups. Two-way ANOVA, n = 6.

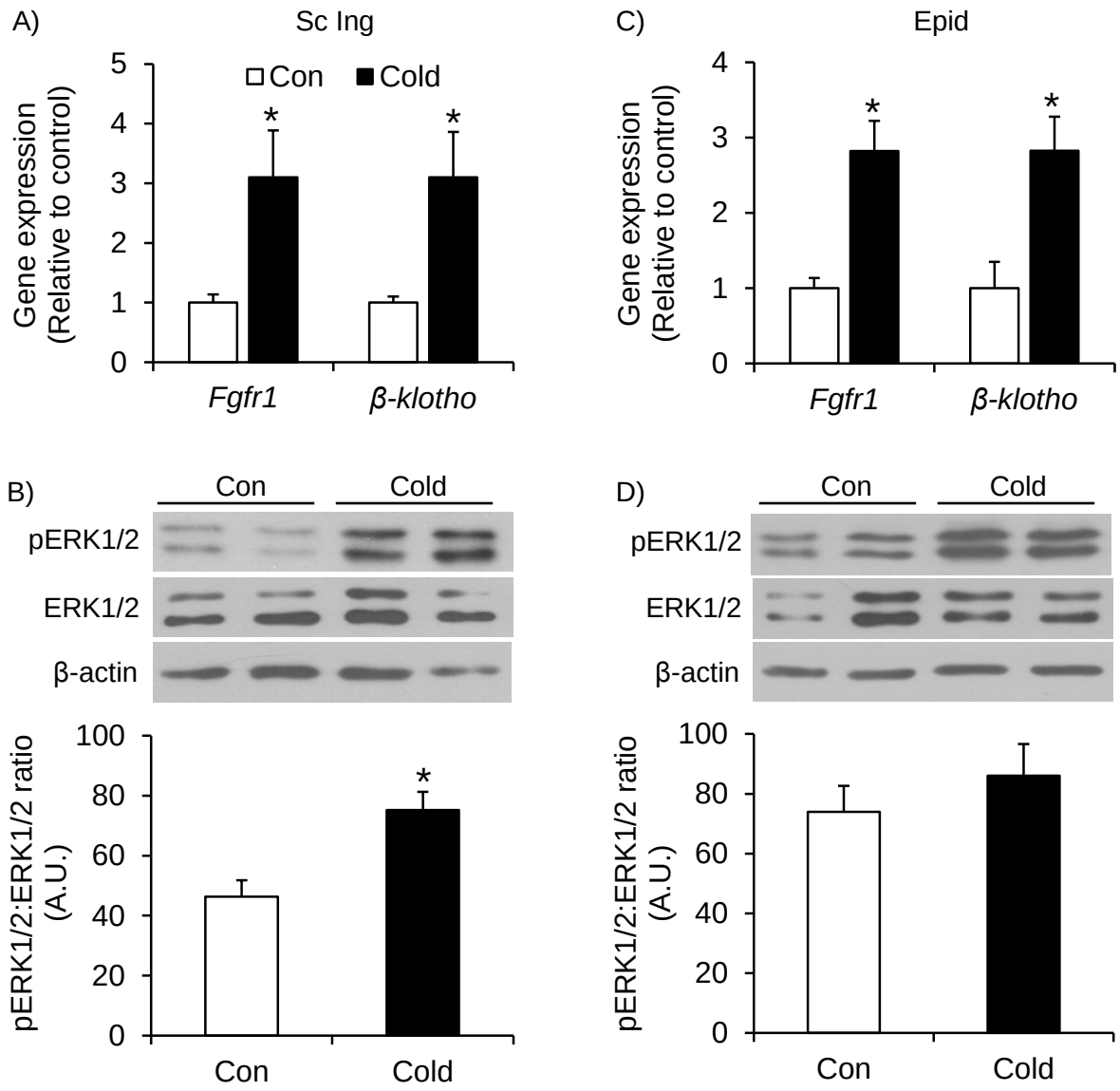

Figure 6-5: The effects of cold exposure on the FGF21 signaling pathway in the WAT. Cold exposure increases the expression of the FGF21 receptor *Fgfr1* and the receptor co-factor *β-klotho* in both the Sc Ing (A) and the Epid (C) fat depots, but only enhances phosphorylation or ERK in the Sc Ing fat (B and D). Age- and weight-matched animals were either kept at room temperature or cold exposed (4°C) for 7 days. *p<0.05 vs. Con. Unpaired, two-tailed t-test, n = 9.

6.5. Discussion

FGF21 is a hormone known to activate the BAT and induce browning of the Sc Ing WAT (108, 109) and we tested whether or not plasma levels would be increased following cold exposure to facilitate this activation and induction of WAT browning. Here, we report that plasma FGF21 was actually significantly reduced with cold acclimation as a result of its marked reduction in expression in the liver, the organ which is the main source of circulating FGF21 (239). In the liver, FGF21 is upregulated by peroxisome proliferator-activated receptor (PPAR)α, a transcription factor that is activated under fasting conditions, in particular by long-chain FAs that are abundant under these conditions (102, 241). Previous work has shown that hepatic *Pparα* expression is reduced following 24 h of cold exposure (8°C) (154), which could explain the reduction in *Fgf21* expression we found in the liver. However, we measured *Ppar*α in the livers from cold-acclimated rats (data not shown), but no significant difference was found when compared to control. Even though *Ppar*α expression was not affected by cold acclimation, we cannot rule out the possibility that its content and activity were actually downregulated. In particular because fatty acids are important for PPARα activation (141), and plasma NEFAs did not differ between control and cold acclimated rats, despite the fact that the latter animals ate 47% more than the former ones. Importantly, NEFAs can be rapidly consumed by BAT (78) and other peripheral tissues (*e.g.* skeletal muscles) (136) to fuel thermogenesis under cold acclimating conditions; therefore, their circulating levels did not increase as a consequence of cold acclimation. Once inside the cells, NEFAs were likely diverted toward oxidation, which must also have limited their availability to participate in other intracellular pathways. Thus, cold acclimation did

not seem to have created a physiological environment that was conducive to PPARα activation or an increase in *Fgf21* expression in the liver.

Because the lack of FGF21 limits the ability of the WAT to undergo browning under conditions of cold exposure (108), it could be that FGF21 was being produced within BAT and WAT, where it could exert an autocrine/paracrine effect and induce a thermogenic adaptive response. This would provide an alternative source of FGF21 that is independent of hepatic production. To test this hypothesis, we first investigated two classical BAT depots and then compared the results to those in two typical WAT depots. We found that iBAT exhibited increased expression and content of FGF21 along with enhancement of its downstream signaling pathway with cold exposure, whereas in aBAT only FGF21 content increased. To our knowledge, this is the first study to show this distinct difference in FGF21 signaling between two classical BAT depots. iBAT and aBAT are very similar with respect to their multilocular appearance and UCP1 content (91, 242); however, we have previously found higher rates of palmitate and glucose oxidation in aBAT compared to iBAT (91), demonstrating that metabolic differences exist between these two depots. Interestingly, it has been reported that adipocytes from aBAT do not originate from the same Myf5^{+} lineage as adipocytes from iBAT (242). Furthermore, aBAT (also known as mediastinal BAT or mBAT) does not express *Zic1,* a gene that is highly expressed in iBAT and frequently used as a marker for classical BAT (82, 243). These data provide evidence of a different developmental origin for aBAT compared to iBAT, which could explain the distinct metabolic differences exhibited by aBAT. The perirenal BAT (prBAT) is another classical BAT depot that does not express *Zic1* (243). Interestingly, both aBAT and prBAT are located more centrally in the rat

suggesting that anatomical location of these BAT depots is an important determinant of their metabolic function. Further work is required to determine if prBAT is similar to aBAT in terms of FGF21 signaling and thus different from other classical BAT depots such as iBAT.

We have also found depot-specific differences in *Fgf21* expression and signaling in two distinct depots of WAT. In Sc Ing WAT, the depot known to undergo browning, the content of FGF21 and the expressions of *Fgf21, Fgfr1* and *β-klotho* were increased, similarly to iBAT. In contrast, only the expressions of *Fgfr1* and *β-klotho* were increased in Epid WAT, a depot that does not undergo browning. Secretion of FGF21 was also only enhanced in Sc Ing adipocytes following cold exposure. Finally, phosphorylation of ERK1/2 was found in Sc Ing, but not in Epid WAT, despite the fact that in the latter tissue the expressions of both *Fgfr1* and *β-klotho* were enhanced with cold exposure. It is possible that there was not a high enough local concentration of FGF21 to stimulate a response in the Epid WAT, since cold exposure did not increase the expression or secretion of FGF21 in this fat depot. This suggests that a potent stimulation might be required for the Epid fat to elicit a downstream response. Indeed, treatment of mice with FGF21 or bFKB1, a recombinant monoclonal antibody that selectively binds the FGFR1-β-klotho complex, resulted in increased expression of *Erg-1* (a downstream target of ERK1/2) and increased phosphorylation of ERK1/2, respectively, in the Epid fat (179, 244). However, despite eliciting a signaling response, FGF21 or bFKB1 treatment did not increase glucose uptake in the Epid depot, whereas in the Sc Ing depot it elicited both a downstream signaling response and an increase in glucose uptake (179, 244). Additionally, it has been shown that in transgenic mice overexpressing *Fgf21, Ucp1*

expression (an indication of browning) increased in the Sc Ing, but not in the Epid fat depot (179). Collectively these data suggest that a potent stimulation of the Epid fat could elicit a downstream response of the FGF21 signaling pathway, but would likely not result in further metabolic alterations or browning of this tissue. It is possible that depot-specific alterations further downstream in the signaling pathway could explain these differences between fat depots. It has been reported that phosphorylation/activation of p90 ribosomal S6 kinase (p90RSK), a target of ERK1/2, is enhanced in primary mouse brown adipocytes with FGF21 treatment (245). p90RSK can subsequently phosphorylate and activate CREB, which in turn enhances the transcription of *Pgc1α* and *Ucp1* (245). This is one possible molecular mechanism linking FGF21 with an increase in UCP1 that could be distinctly regulated in the Sc Ing compared to the Epid fat depot and determine depot-specific propensity to browning; however, further research is warranted to test this possibility.

In summary, we provide evidence that circulating FGF21 is reduced during cold acclimation as a consequence of a marked suppression of its gene expression in the liver. However, this does not prevent FGF21 from acting on iBAT and Sc Ing WAT under cold-acclimating conditions. This is possible because expression and release of FGF21 are increased within iBAT and Sc Ing WAT, allowing for an autocrine/paracrine effect of this hormone that can promote a robust thermogenic response in iBAT and induce browning of the Sc Ing WAT. Conversely, the lack of an increase in *Fgf21* expression and release by Epid adipocytes may limit the ability of the Epid fat depot to undergo browning under cold-acclimating conditions. These findings provide a potential

explanation for the depot-specific browning response that is observed following cold acclimation.

CHAPTER 7: Cold acclimation causes fiber type-specific responses in glucose and fat metabolism in rat skeletal muscles

Diane M. Sepa-Kishi, Yass Sotoudeh-Nia, Ayesha Iqbal, George Bikopoulos, Rolando B. Ceddia.

Muscle Health Research Centre, School of Kinesiology and Health Science, York University, Toronto, Ontario, Canada

Keywords: glycogen, palmitate oxidation, GSK3, GLUT4, PGC-1α, CD36, LPL

Statement of Labour

The majority of the experiments conducted in this study were carried out by Diane M. Sepa-Kishi. DMSK's contributions included extraction of tissues, and incubation of muscle strips for the measurement of glucose and fatty acid oxidation, as well as glycogen synthesis and glycogen content. DMSK was also responsible for conducting and collecting all western blot data, some real-time PCR data, analyzing and interpreting all of the results, preparing the figures, and writing and revising the manuscript. DMSK was supported by a NSERC Alexander Graham Bell Canada Graduate Scholarship and an Elia Scholarship. Due to the logistics of this study, YSN, AI and GB assisted with the extraction of tissues and the incubation of skeletal muscle strips. YSN and AI performed the majority of the real-time PCR work and YSN, AI and GB all revised the manuscript.

Dr. Rolando Ceddia is the primary investigator and supervisor of this project and this research was funded by a Discovery Grant from NSERC and by infrastructure grants from the Canada Foundation for Innovation and the Ontario Research Fund.

7.1. Abstract

This study investigated fiber type-specific metabolic responses and the molecular mechanisms that regulate glucose and fat metabolism in oxidative and glycolytic muscles upon cold acclimation. Male Wistar rats were exposed to cold (4^{o}C) for 7 days, and then glycogen synthesis and content, glucose and palmitate oxidation, and the molecular mechanisms underlying these metabolic pathways were assessed in soleus (Sol), extensor digitorum longus (EDL), and epitrochlearis (Epit) muscles. Cold acclimation increased glycogen synthesis, glycogen content, glucose oxidation, and reduced glycogen synthase (GS) phosphorylation only in Sol muscles. Protein kinase B (AKT), glycogen synthase kinase 3 (GSK3), and AMP-activated protein kinase (AMPK) phosphorylation increased in all three muscles upon cold acclimation. Cold acclimation increased palmitate oxidation, gene expression of the transcriptional co-activator *Pgc-1α,* lipoprotein lipase (*Lpl*), fatty acid transporter (*Cd36)*, and Sarco/endoplasmic reticulum Ca^{2+}-ATPase (*Serca*) in Sol, EDL, and Epit muscles. Sarcolipin was only detected and had its content increased in Sol muscles. In conclusion, cold-induced thermogenes activated similar signaling pathways in oxidative and glycolytic muscles, but the metabolic fate of glucose differed in skeletal muscles with distinct fiber type composition. Furthermore, only muscles rich in type I fibers appeared to have the capacity for sarcolipin-mediated SERCA uncoupling.

7.2. Introduction

Acute cold exposure and cold acclimation in rodents have been reported to markedly increase whole-body energy expenditure (246), which is accompanied by profound metabolic changes including hyperphagia, reduced insulinemia, enhanced hepatic glucose production, and increased glucose and fat utilization by peripheral tissues (78, 152, 246–249). The brown adipose tissue (BAT) is the main site of non-shivering thermogenesis (250–252) and greatly contributes to the metabolic changes induced by cold exposure (246). However, skeletal muscles also have the capacity for both shivering and non-shivering thermogenesis (135, 249), and have been demonstrated to significantly increase substrate utilization under acute cold exposure (247) and cold acclimating conditions (249). Skeletal muscles make up a large proportion of total body mass (~40% and 30% in men and women, respectively) (110) and, therefore, can play an important role in determining the metabolic adaptive responses to cold-induced thermogenesis. From a metabolic perspective, fatty acids are considered the principal fuel oxidized during cold-induced thermogenesis (78); however, fatty acids cannot entirely substitute for glucose as a fuel for cold-induced thermogenesis. In fact, glucose appears to play an important regulatory role by generating essential glycolytic metabolites or by replenishing citric acid cycle intermediates to sustain an elevated rate of fatty acid oxidation (FAO) under conditions of cold exposure (253, 254). This could be particularly relevant in highly oxidative muscles that consume large amounts of fatty acids to fuel cold-induced thermogenesis.

Because cold exposure leads to insulinopenia (131, 249, 253), it has been suggested that the cold-induced increase in glucose uptake in skeletal muscles is

primarily diverted to fuel the oxidative pathway that is upregulated in an insulin-independent manner (253). This can be attributed to cold-induced shivering (contractile activity) (131, 255, 256), since it resembles the effects of exercise on glucose uptake in this tissue (131, 257). However, shivering progressively stops and non-shivering thermogenesis takes over as cold acclimation takes place (258, 259). Despite the cessation of shivering, glucose and fat metabolism remain elevated in skeletal muscles of cold acclimated rats (246, 249), suggesting that mechanisms independent of contractile activity operate to maintain elevated rates of substrate utilization in skeletal muscles in these animals. In this context, it has been hypothesized that prolonged cold exposure increases glucose uptake and its metabolism in skeletal muscles by: (a) increasing tissue sensitivity to insulin, and (b) stimulating glucose uptake via insulin-independent pathways (131, 249). These effects have been attributed to elevated release of norepinephrine from sympathetic nerve endings as a consequence of sympathetic nervous system (SNS) activation by cold (249). However, the molecular mechanisms by which cold-induced thermogenesis influences the activity of the glucose transport protein and glucose and fat metabolism in skeletal muscles remain largely undetermined.

More recently, it has been demonstrated that elevated sarco/endoplasmic reticulum Ca^{2+}-ATPase (SERCA) activity plays an important role in non-shivering thermogenesis in skeletal muscles (135). As an ATP-driven pump, SERCA efficiently couples the hydrolysis of ATP to the transport of Ca^{2+} across the membrane, and it does so in a way that two Ca^{2+} ions are transported for each ATP molecule hydrolysed (134, 136). The mechanism by which cold increases SERCA-mediated non-shivering thermogenesis

has been attributed to the presence of sarcolipin (SLN), a protein that uncouples hydrolysis of ATP from the transport of Ca^{2+} by SERCA (135, 136, 260). However, the different SERCA isoforms and SLN do not seem to be equally expressed in oxidative and glycolytic muscles (135, 261, 262), which suggests that heterogeneity exists with respect to the contribution of SLN-mediated SERCA uncoupling to cold-induced enhancement of glucose and fat metabolism among muscles of different fiber type composition. Another potential mechanism by which skeletal muscles could enhance substrate utilization in an insulin-independent manner is through the activation of the cellular energy sensor AMP-activated protein kinase (AMPK). Activation of AMPK could be initially triggered by muscle contractions (shivering) and ATP consumption and remain activated as non-shivering thermogenesis takes over due to SERCA uncoupling or even increased activity of the Na^{+}-K^{+} ATPase under the influence of SNS activity and norepinephrine release. In its activated state, AMPK is well known for promoting insulin-independent glucose uptake and enhancement of FAO (263) in skeletal muscle cells. Besides responding to alterations in the intracellular AMP:ATP ratio, AMPK can also be covalently activated by calcium/calmodulin dependent kinase kinase 2 (CAMKK2) in response to alterations in intracellular Ca^{2+} flux (263). Therefore, AMPK activity could be induced by SERCA uncoupling in skeletal muscle under conditions of cold acclimation. However, the expression of the α catalytic and β regulatory subunits of AMPK differs between oxidative and glycolytic muscle fibers (264–266), suggesting that the potential role of AMPK in the regulation of glucose and fatty acid metabolism under cold acclimation and non-shivering thermogenesis is also fibre type-specific. Because the molecular mechanisms that regulate energy metabolism in skeletal muscles operate

in a fiber-type dependent manner, we hypothesized that substrate partitioning in skeletal muscles would be distinctly regulated in oxidative and glycolytic muscles under conditions of cold-induced thermogenesis. In order to test this hypothesis, we exposed rats to a cold acclimation protocol and then assessed glucose and fatty acid metabolism in skeletal muscles with distinct fiber type distribution. We also investigated the insulin-dependent and independent signaling pathways that drive substrate partitioning and assessed the molecular mechanisms underlying the adaptive metabolic responses of oxidative and glycolytic muscles to cold acclimation.

7.3. Materials and Methods

Reagents – Fatty acid-free bovine serum albumin (FA-free BSA), palmitic acid, triethanolamine hydrochloride (TRA), amyloglucosidase and hexokinase/glucose-6-phosphate dehydrogenase were obtained from Sigma (St. Louis, MO, USA). [1-^{14}C] palmitic acid was from Perkin Elmer (Woodbridge, ON, Canada). D-[U-^{14}C] glucose was from GE Healthcare (Mississauga, ON, Canada). Protease (cOmplete Ultra Tablets) and phosphatase (PhosSTOP) inhibitors were from Roche Diagnostics GmbH (Mannheim, Germany). Glucose was measured by the glucose oxidase method using a OneTouch Ultra Mini Monitor. The NEFA kit was from Wako (Mountain View, CA, USA) and the rat insulin ELISA kit was from Alpco (Salem, NH, USA). All antibodies were purchased from Cell Signaling (Danvers, MA, USA) except for SLN which was purchased from Millipore (Billerica, MA, USA).

Animals and cold exposure – Male albino rats (Wistar strain) were age- and weight-matched (~400 g) and allocated to either the control or cold-exposed group. All animals were housed individually on a 12/12 h light/dark cycle and fed standard laboratory chow

(Lab Diet Cat #5012) *ad libitum* throughout the 7-day protocol. The control animals were housed at 22°C, while those exposed to cold were kept at 4°C. Food intake and body weight measurements were taken for 5 days prior to (baseline) and every day during the cold acclimation period. A blood sample was collected in the fed state each morning at 09:00 am, centrifuged, and the plasma frozen at -80°C until subsequent analysis. Upon completion of the protocol the animals were anesthetized at approximately 09:00 am using ketamine/xylazine (0.2 ml per 100 g body weight) and the muscles immediately extracted for subsequent analysis. All efforts were made to minimize suffering. The protocol containing all animal procedures described in this study was specifically approved by the Committee on the Ethics of Animal Experiments of York University (York University Animal Care Committee, YUACC, permit number 2016-5) and performed strictly in accordance with the YUACC guidelines.

Measurement of glycogen synthesis and palmitate and glucose oxidation – Sol, EDL, and Epit muscles were chosen because of their distinct fiber-type distributions, which clearly characterizes them as mainly oxidative or glycolytic. The percentages of type I, type IIa, type IIb and type IIx in Sol, EDL, and Epit muscles are 88/12/0/0, 2/12/57/29, and 8/13/51/28 (267), respectively. Thin strips of each muscle (~20 mg) were mounted onto stainless steel wire clips in order to maintain a relaxed resting length and incubated as previously described (268). Muscle strips were then incubated in plastic scintillation vials at 37 °C for 1 h in 2 ml of gassed (45 min with O_2:CO_2 - 95:5% vol:vol) Krebs Ringer buffer (0.154 M NaCl, 0.154 M KCl, 0.11 M $CaCl_2$, 0.154 M $MgSO_4$, 0.154 M KH_2PO_4, 0.154 M $NaHCO_3$, pH 7.4, with 5.5 mM glucose and 30 mM HEPES (KRBH)) supplemented with 3.5% FA-free BSA. For glycogen synthesis and glucose oxidation

muscle strips were incubated in 2 ml of KRBH-3% FA-free BSA with 0.2 µCi/ml of D-[U-^{14}C] glucose, either in the absence or presence of insulin (100 nM) (268). Subsequently, muscle strips were digested in 0.5 ml of KOH (1M) and an aliquot (400 µl) was used to detect the amount of radiolabeled glucose incorporated into glycogen as previously described (268). For palmitate oxidation muscle strips were incubated in 2 ml of KRBH-3%BSA with 0.2 µCi/ml of [1-^{14}C] palmitic acid and 200 µM non-labelled palmitate. Oxidation was measured by the production of $^{14}CO_2$ either from glucose or palmitate as previously described (49, 15).

Measurement of glycogen content – Muscle strips were incubated in 2 ml of KRBH-3% FA-free BSA with 0.2 µCi/ml of D-[U-^{14}C] glucose, either in the absence or presence of insulin (100 nM) (268). At the end of the incubation, the muscles were digested in 1 M KOH and 100 µl of the digested solution was used for the assessment of glycogen content. The pH of the muscle digest was titrated to 4.8 and 500 µl of acetate buffer (pH 4.8) containing 0.5 mg/ml amyloglucosidase was added. Hydrolyzation of the muscle glycogen was allowed to proceed overnight at room temperature. The solution was neutralized prior to adding 1 ml of TRA buffer (TRA 0.3 M, $MgSO_4$ 4.05 mM, KOH 1 N, pH 7.5, with hexokinase/glucose-6-phosphate dehydrogenase 250 U/ml, ATP 1 mM and NADP 0.9 mM) for the enzymatic analysis of glucose. The samples were then incubated at room temperature for 30 min and absorbance was read at 340 nm wavelength in a spectrophotometer (Ultraspec 2100 pro; Biochrom Ltd., Cambridge, UK) (268).

RNA isolation and quantitative PCR – A portion of each skeletal muscle that did not undergo incubation was flash frozen in liquid nitrogen and stored at -80°C until RNA isolation. RNA was isolated from skeletal muscle tissue using TRIzol™ (ThermoFisher

Scientific, Waltham, MA, USA) and complimentary DNA (cDNA) was made from 2 µg of extracted RNA using the ABM EasyScript™ Reverse Transcriptase cDNA synthesis kit (Diamed, Mississauga, ON, Canada), according to the manufacturer's instructions. Primers were designed using the software PrimerQuest (IDT) based on probe sequences available at the Affymetrix database (NetAffx™ Analysis Centre, http://www.affymetrix.com/analysis) for each given gene. Real-time PCR analysis was performed using a Bio-Rad CFX96 Real Time PCR Detection System (Bio-Rad, Mississauga, ON, Canada) using the following amplification conditions: 95°C (10 min); 40 cycles of 95°C (15 s), 60°C (60 s). All genes were normalized to the control gene TBP, and relative differences in gene expression between treatment groups were determined using the ΔΔCt method (226). Values are presented as fold increases relative to the Con group. The primers used in this study are as follows: Glut4 (5'- CAT TCT CGG ACG GTT CCT CAT - 3' (Forward), 5' - CCA AGG CAC CCC GAA GAT - 3' (Reverse)), Glut1 (5'- AAT GAG CTA GGA GGC TTT ACC GCA - 3' (Forward), 5' – TGG AAG AGA CAG GAA TGG GCG AAT - 3' (Reverse)), Lpl (5'- TTG AGA AAG GGC TCT GCC TGA GTT - 3' (Forward), 5' – TGC TTC TCT TGG CTC TGA CCT TGT - 3' (Reverse)), Cd36 (5'- ACG ACT GCA GGT CAA CAT ACT GGT - 3' (Forward), 5' – TGG TCC CAG TCT CAT TTA GCC ACA - 3' (Reverse)), Pgc-1α (5'- ACC GTA AAT CTG CGG GAT GAT GGA - 3' (Forward), 5' - ATT CTC AAG AGC AGC GAA AGC GTC- 3' (Reverse)), Serca1 (5'- TTC ATT GCT CGG AAC TAT CTG G - 3' (Forward), 5' - GGG CTG GTT ACT TCC TTC TTT - 3' (Reverse)), Serca2 (5'- CTG TAG GTC TGA TGG TTC TGT TTA - 3' (Forward), 5' – CTA GGC GAA GGG ACA GAA AC - 3' (Reverse)).

Western blotting analysis of content and phosphorylation of proteins – A portion of each skeletal muscle that did not undergo incubation was flash frozen in liquid nitrogen and stored at -80°C until western blotting analysis. Muscle tissues from the Sol, EDL and Epit were homogenized in a buffer containing 25 mM Tris-HCl, 25 mM NaCl (pH 7.4), 1 mM $MgCl_2$, 2.7 mM KCl, 1% Triton-X and protease and phosphatase inhibitors (Roche Diagnostics GmbH, Mannheim, Germany). Samples were diluted 1:1 vol:vol with 2x Laemmli sample buffer, heated to 95°C for 5 min and subjected to SDS-PAGE. The following primary antibodies were used at a dilution of 1:1,000: P-AKT (Ser 473, 60 kDa, Cell Signaling Cat# 9271); AKT (60 kDa, Cell Signaling Cat# 9272); P-GSK3α (Ser 21, 51 kDa, Cell Signaling Cat# 9327); GSK3α (51 kDa, Cell Signaling Cat# 5676); P-GS (Ser 641, 85-90 kDa, Cell Signaling Cat# 3891); GS (84 kDa, Cell Signaling Cat# 3886); P-AMPK (Thr 172, 62 kDa, Cell Signaling Cat# 2535); AMPK (62 kDa, Cell Signaling Cat# 2532); SLN (6 kDa, Millipore Cat# ABT13). β-actin (45 kDa, Cell Signaling Cat# 4967) was used as a loading control. Phospho and total blots were run simultaneously on two separate membranes loaded with the same samples, the same amount of protein and in the same order. Blots for the housekeeping proteins were taken from either the phospho or the total membranes.

Statistical analyses – Statistical analyses were assessed by unpaired, two-tailed t-test and two-way ANOVA with Bonferroni post-hoc test. Statistical significance was set at $p<0.05$.

7.4. Results

Effects of cold exposure on food intake and body weight, and circulating glucose, insulin and non-esterified fatty acids (NEFAs) – Food intake was 45% higher in cold-acclimated

rats compared to controls. Despite hyperphagia, no significant differences were found in body weight, glycemia, and NEFAs at the end of the cold exposure protocol between control and cold-acclimated rats (Table 8-1 and Fig. 8-8). In contrast, circulating insulin levels were reduced by ~35% after 1 day of cold exposure (control 1.73 ± 0.20 ng/ml vs. cold 1.13 ± 0.08 ng/ml) and remained significantly lower throughout the entire 7-day cold acclimation period.

Effects of cold exposure on basal and insulin-stimulated skeletal muscle glycogen synthesis and glucose oxidation – Under basal conditions, the rates of glycogen synthesis were not significantly altered by cold exposure in all three muscles (Fig. 7-1A-C), although a trend of increase was found for the Sol muscle (Fig. 7-1A). As expected, Sol, EDL, and Epit muscles from control rats elicited 4.7-fold (Fig. 7-1A), 2.9-fold (Fig. 7-1B), and 3.4-fold (Fig. 7-1C) increases in insulin-stimulated glycogen synthesis, respectively. Similarly, in muscles from cold-exposed rats, insulin significantly increased glycogen synthesis by 2.3-fold in the Sol (Fig. 7-1A), 2.4-fold in the EDL (Fig. 7-1B), and 3.6-fold in the Epit muscle (Fig. 7-1C). However, in the Sol muscles we found that cold exposure had an additive effect, which enhanced insulin-stimulated glycogen synthesis by 80% when compared to control rats (Fig. 7-1A). Glucose oxidation in Sol, EDL, and Epit muscles from control rats also increased by ~2.2-fold (Fig. 7-1D), 2.1-fold (Fig. 7-1E), and 2.25-fold (Fig. 7-1F), respectively, when stimulated by insulin. Similarly to glycogen synthesis, all three muscles increased their rates of glucose oxidation when stimulated by insulin (Fig. 7-1D-F). However, an additive effect (~76%) in glucose oxidation was only observed in the Sol muscle (Fig. 7-1D) when compared to controls.

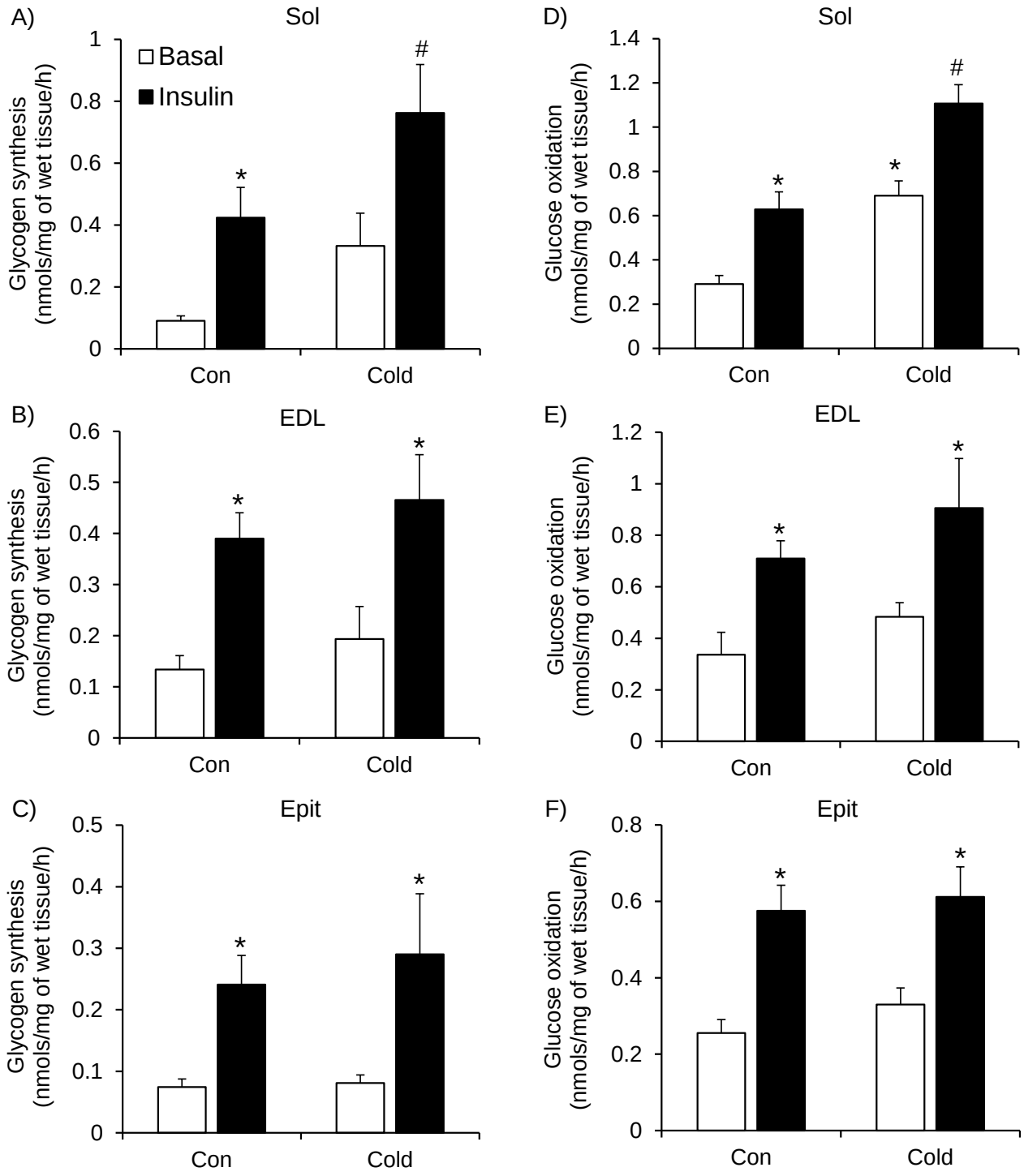

Figure 7-1: Cold-induced alterations in glycogen synthesis and glucose oxidation in the Sol, EDL and Epit. Cold exposure increases insulin-stimulated glycogen synthesis (A) and basal and insulin-stimulated glucose oxidation (D) in the Sol, but does not alter glycogen synthesis or glucose oxidation in the EDL (B and E) or the Epit (C and F). Two-way ANOVA, n = 11. *$p<0.05$ vs. Basal. $^{\#}p<0.05$ vs. all other conditions.

Effects of cold exposure on skeletal muscle glycogen content under basal and insulin-stimulated conditions – Sol, EDL, and Epit muscles from control rats had similar contents of glycogen (Fig. 7-2A-C), and upon stimulation with insulin it increased by 39% (Fig. 7-2A), 32% (Fig. 7-2B), and 34% (Fig. 7-2C), respectively. In muscles from cold-exposed rats, insulin stimulation increased glycogen content by 22% in the Sol, by 41% in the EDL, and by 26% in the Epit muscles. However, only the Sol muscle displayed an additive effect of ~50% and 30% under basal and insulin-stimulated conditions (Fig. 7-2A), respectively, when compared to control. This additive effect of cold exposure on glycogen content is consistent with similar increases in glycogen synthesis observed only in the Sol muscle.

Effects of cold exposure on the phosphorylation of AKT, GSK3, and GS, and on Glut4 and Glut1 gene expression in skeletal muscles – Cold exposure significantly increased the phosphorylation of AKT by 2.9-fold (Fig. 7-3A), 1.73-fold (Fig. 7-3B), and 2-fold (Fig. 7-3C) in Sol, EDL, and Epit muscles, respectively. A similar effect was observed for GSK3α phosphorylation that significantly increased by ~2.3-fold in the Sol (Fig. 7-3D), by 1.9-fold in the EDL (Fig. 7-3E), and by 2.25-fold (Fig. 7-3F) in the Epit muscles. GS phosphorylation was significantly reduced (~60%) only in the Sol of cold-exposed rats (Fig. 7-3G-I). *Glut4* gene expression was significantly increased by ~8-fold in the Sol (Fig. 7-4A) of cold-exposed rats, whereas in the EDL (Fig. 7-4B) and Epit (Fig. 7-4C) muscles this variable did not differ between control and cold-exposed rats. No significant differences were observed for *Glut1* expression in any of the muscles from cold-exposed rats (Fig. 7-4A-C). These findings are in line with increased rates of

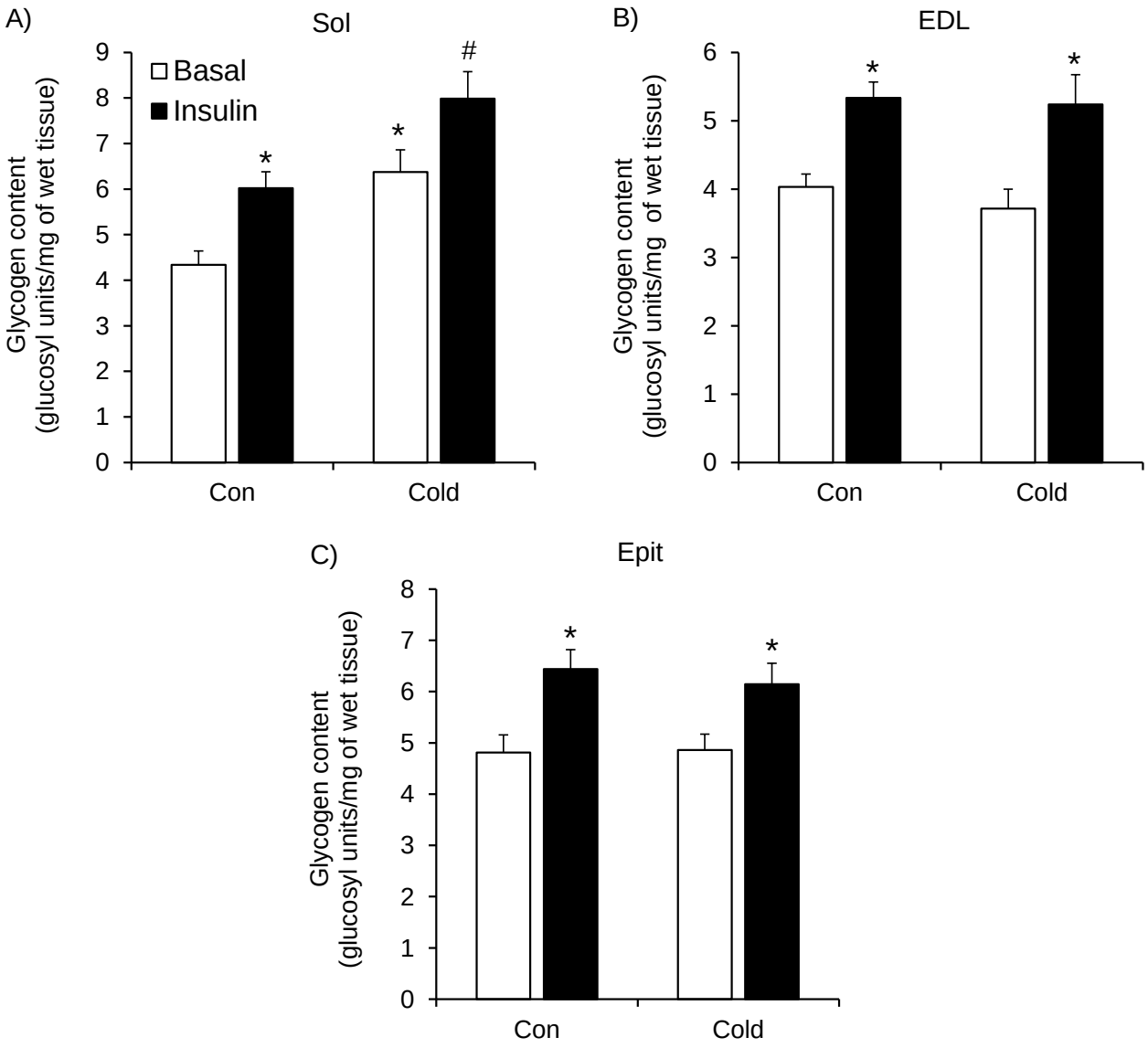

Figure 7-2: Basal and insulin-stimulated glycogen content under control and cold conditions in the Sol, EDL, and Epit. Cold exposure increases basal and insulin-stimulated glycogen content in the Sol (A), but not in the EDL (B) or Epit (C). Two-way ANOVA, n = 12. *p<0.05 vs. Basal. #p<0.05 vs. all other conditions.

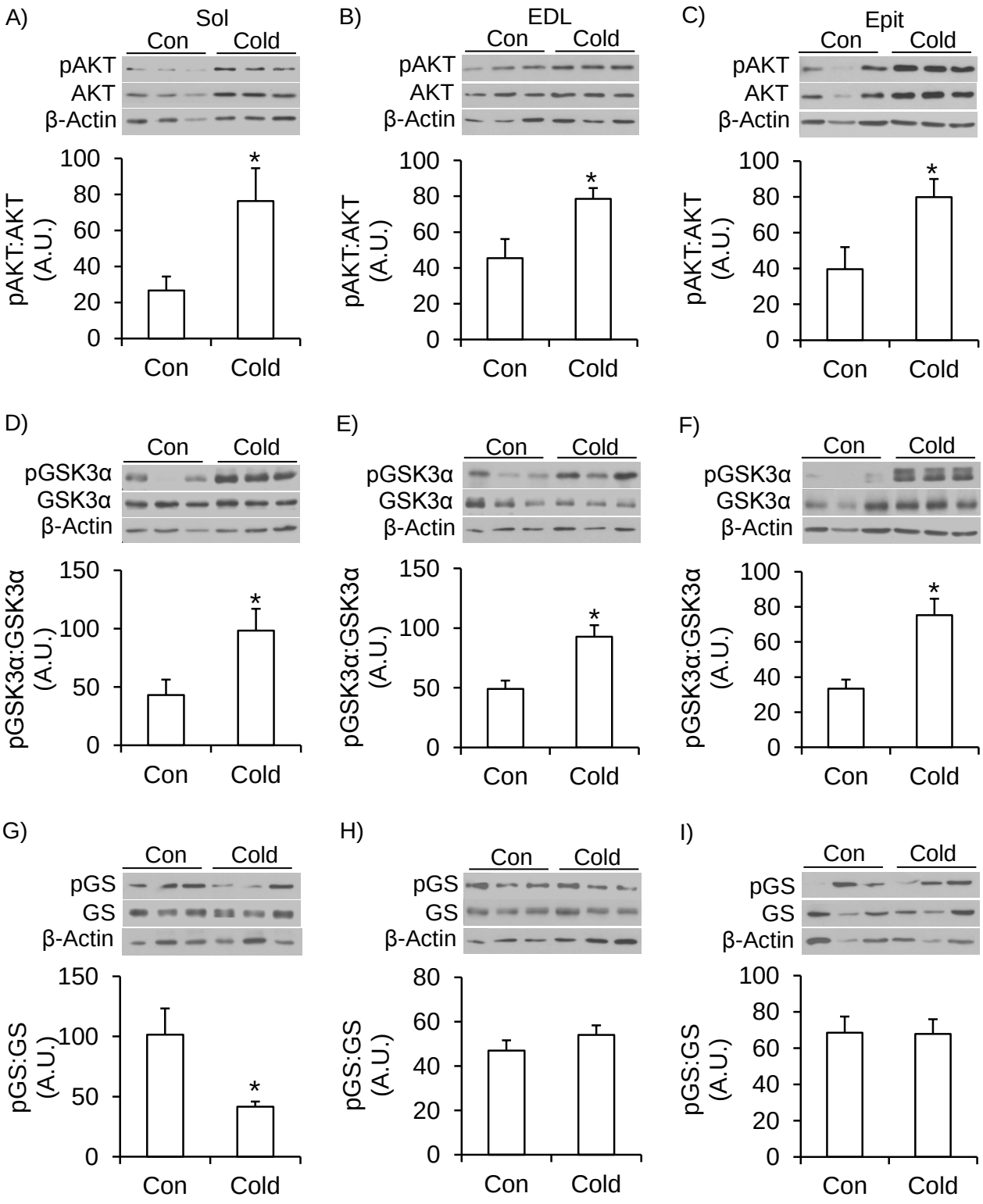

Figure 7-3: Cold-induced alterations in content and phosphorylation of AKT, GSK3α, and GS in the Sol, EDL, and Epit. Cold acclimation increases AKT (A to C) and GSK3 (D to F) phosphorylation in Sol, EDL and Epit muscles, but it only decreases GS phosphorylation (G to I) in the Sol muscle. Student's t-test, n = 6-12. *p<0.05 vs. Control (Con).

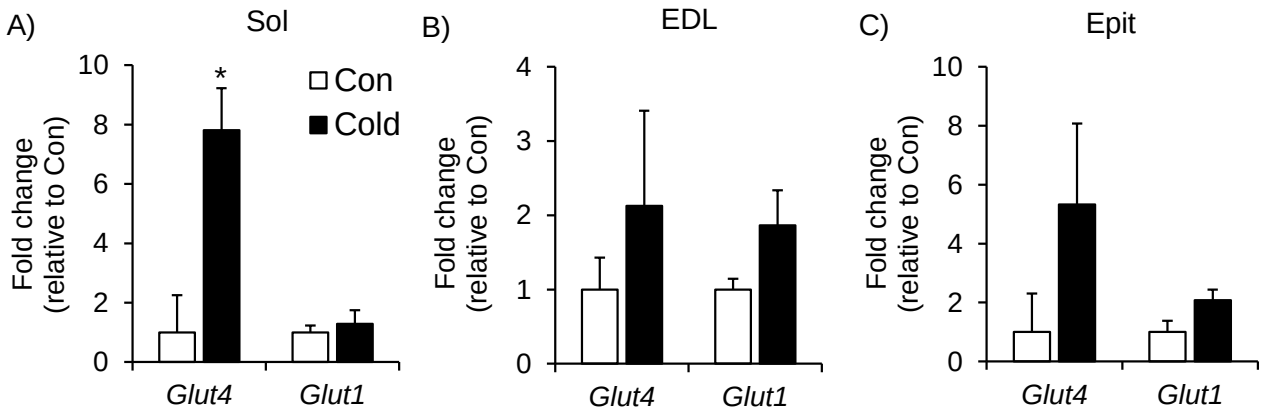

Figure 7-4: Cold-induced alterations in the expression of *Glut4* and *Glut1* in the Sol, EDL, and Epit. Cold exposure increases *Glut4* expression in Sol muscles (A), but does not significantly change the gene expression of *Glut1* in Sol, nor of *Glut1* and *Glut4* in EDL (B) and Epit (C). Student's t-test, n = 6-9. *p<0.05 vs. Control (Con).

glycogen synthesis and glycogen content that were only observed in the Sol muscles of cold-exposed rats.

Effects of cold exposure on palmitate oxidation, gene expression of Lpl, Cd36, and Pgc-1α, and AMPK phosphorylation in skeletal muscles – Sol muscles exhibited the highest rate of palmitate oxidation (Fig. 7-5A), but all three muscles significantly increased (~2-fold) (Fig. 7-5A) their capacity to oxidize palmitate upon cold acclimation. These adaptive responses in FAO were accompanied by significant increases in *Lpl, Cd36* and *Pgc-1α* expression in Sol (~11-fold, 5-fold, and 10-fold, respectively) (Fig. 7-5B) and EDL (~2.6-fold, 2.8-fold, and 8.5-fold, respectively) (Fig. 7-5C). In the Epit muscle only *Pgc-1α* gene expression was significantly increased (~6.5-fold) by cold exposure, whereas *Lpl and Cd36* did not change (Fig. 7-5D). All alterations in the expression of genes involved in the breakdown and uptake of circulating fatty acids and mitochondria biogenesis were more pronounced in the Sol than EDL and Epit muscles, which is compatible with the higher rates of palmitate oxidation found in Sol than EDL and Epit

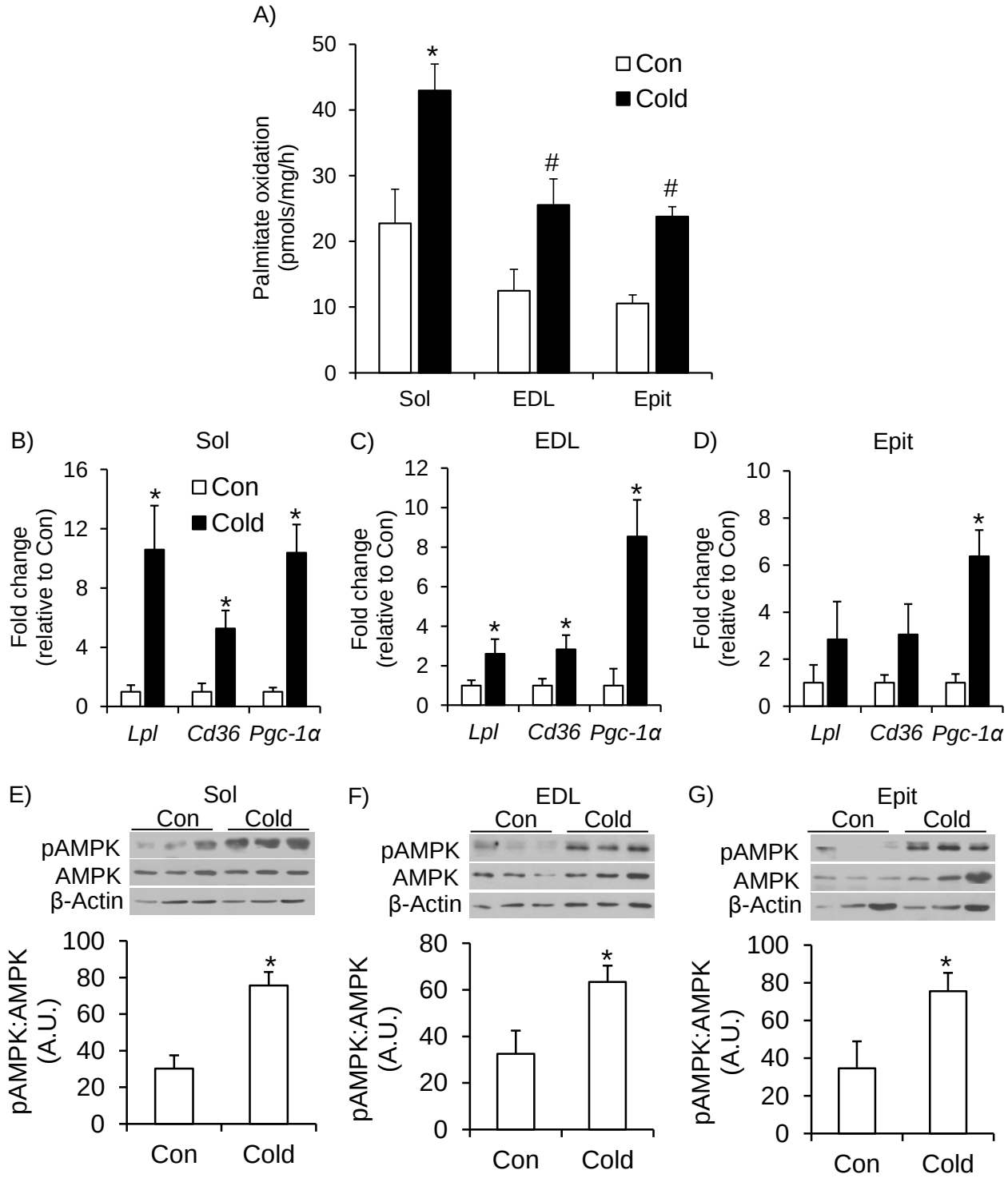

Figure 7-5: Palmitate oxidation, gene expression of *Lpl, Cd36* and *Pgc-1α*, and content and phosphorylation of AMPK following cold acclimation in the Sol, EDL, and Epit. Cold acclimation increases palmitate oxidation (A), the expression of genes involved in fatty acid transport and oxidation (B-D), and the content and phosphorylation of AMPK (E-G) in the Sol, EDL and Epit muscles. For A, two-way ANOVA, n = 12. *p<0.05 vs. all other conditions. #p<0.05 vs. respective control (Con). For B-G, student's t-test n = 6-9. *p<0.05 vs. respective control (Con).

muscles from cold-exposed rats. AMPK phosphorylation also increased by 2.5-fold in the Sol (Fig. 7-5E), by 1.95-fold in the EDL (Fig. 7-5F), and by 2.2-fold in the Epit (Fig. 7-5G) muscles upon cold acclimation.

Effects of cold exposure on gene expression of Serca1 and Serca2 and SLN protein content in skeletal muscles – Cold increased *Serca1* and *Serca2* gene expressions in the Sol by ~21-fold and 25-fold, respectively (Fig. 7-6A). In the EDL muscle, cold increased *Serca1* gene expression by ~12-fold, but did not affect the expression of *Serca2* (Fig. 7-6B). In the Epit muscle, cold increased *Serca1* gene expression by 23.4-fold and *Serca2* by 7-fold (Fig. 7-6C). SLN was only consistently detected by western blotting in the Sol muscle (Fig. 7-6D), and upon cold exposure the content of this protein was significantly increased by ~2.4-fold in this muscle (Fig. 7-6D).

7.5. Discussion

The results of this study provide novel evidence that substrate partitioning is distinctly regulated in oxidative and glycolytic muscles under conditions of cold acclimation. This is supported by our findings that the Sol muscle (rich in type I fibers (267)) increased its rates of glucose oxidation and glycogen synthesis, whereas in the EDL and Epit (rich in type IIb fibers (267)) these variables were not significantly affected either under basal or insulin-stimulated conditions after 7 days of cold exposure. In fact, despite enhancing their ability to utilize glucose to fuel its energy metabolism, Sol muscles increased by ~80% their ability to synthesize glycogen in response to insulin, which was also accompanied by 50% and 30% increases in glycogen content under basal and insulin-stimulated conditions, respectively. Importantly, cold-acclimated rats were hyperphagic, but exhibited reduced insulinemia

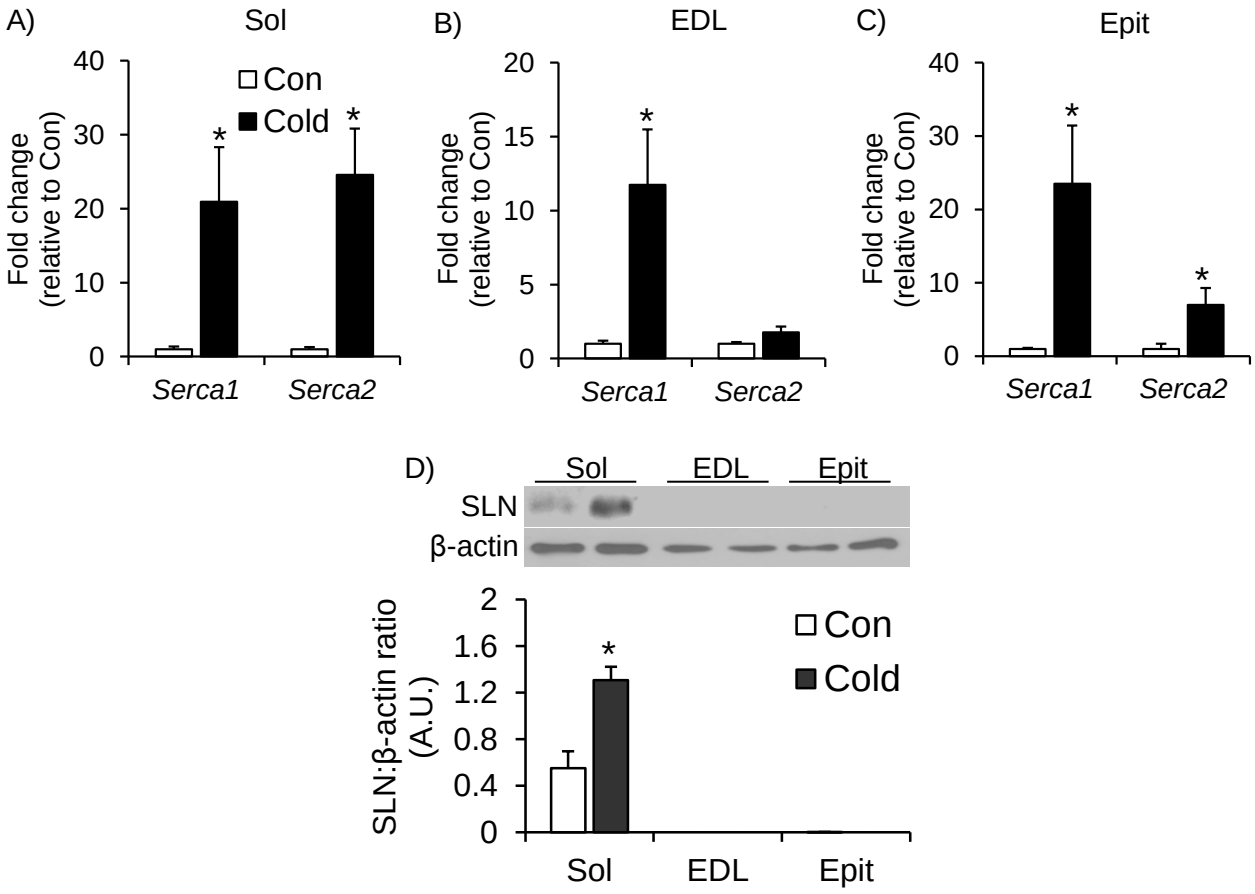

Figure 7-6: Expression of *Serca1* and *2* and content of SLN in the Sol, EDL, and Epit following cold acclimation. Cold exposure increases the expression of *Serca* in the Sol (A), EDL (B) and Epit (C) muscles but increases the content of SLN only in the Sol (D). Student's t-test, n = 6-9. *p<0.05 vs. Control (Con).

in comparison to controls. This indicates that cold-induced accumulation of glycogen in Sol muscles *in vivo* was not driven by elevated circulating insulin levels. Heterogeneity in insulin sensitivity and responsiveness among muscles of different fiber compositions has previously been reported (269) and our findings demonstrate that under conditions of cold-induced thermogenesis such metabolic heterogeneity actually dictates the magnitude of substrate utilization and the intracellular fate of glucose. It is important to note that our results were collected from control animals that were housed at 22°C,

which is below thermoneutrality for a rat (28°C) (270). Thus, these control animals were also exposed to some degree of cold stress, which may have attenuated the magnitude of the differences in metabolic responses and regulatory mechanisms we observed following cold acclimation.

Despite eliciting clear fiber type differences with respect to glucose metabolism, all three muscles displayed increased AKT and GSK3 phosphorylation after acclimating to cold. This is consistent with previous reports that cold exposure increases glucose uptake in oxidative and glycolytic muscles (249, 253). However, analysis of GS phosphorylation revealed that insulin-stimulated dephosphorylation/ activation of GS only took place in the Sol muscle, which is compatible with our observations that insulin-stimulated glycogen synthesis was only enhanced in this muscle. Thus, our findings indicate that the regulation of GS phosphorylation and its activity is also fiber-type specific, and that AKT-induced phosphorylation/deactivation of GSK3 does not suffice for cold exposure to enhance glycogen synthesis in glycolytic muscles. Because glucose metabolism in skeletal muscle is largely dependent on its ability to uptake this substrate, we also assessed the expression of *Glut1* and *Glut4* in all three muscles. Sol muscles elicited a robust increase (~8-fold) in *Glut4* expression, whereas EDL and Epit muscles were quite variable and did not display any significant increases in the expression of either glucose transporter after 7 days of cold exposure. Again, this is consistent with much higher rates of glucose metabolism in Sol than in EDL and Epit muscles. However, it is important to consider that, regardless of gene expression, GLUT4 protein abundance and/or translocation could still be enhanced by cold exposure and facilitate glucose uptake in all muscles. In fact, it has recently been

demonstrated that cold acclimation in humans is accompanied by increased GLUT4 localization at the sarcolemma (80, 271), which supports cold-induced enhancement of skeletal muscle capacity to uptake glucose, although in these studies no data was provided with respect to potential fiber type differences. In our studies, GLUT4 translocation could also have been triggered by AMPK activation that actually significantly increased in all three muscles upon cold acclimation. Therefore, based on our findings, at least two signaling pathways could be simultaneously engaged to promote GLUT4 translocation in skeletal muscles under cold acclimating conditions: one mediated by AKT and another by AMPK. Importantly, rat skeletal muscles rich in type I muscle fibers have been reported to contain a higher abundance of GLUT4 protein (272) compared to muscles rich in type II fibers. Furthermore, human type I muscle fibers have been reported to contain a higher abundance of proteins that phosphorylate glucose (Hexokinase II), and synthesize glycogen (GS) (119) than type II fibers. Additionally, we have found that *Glut4* expression was markedly increased in the Sol muscle, whereas in EDL and Epit muscles only a trend was observed upon cold acclimation. In this context, cold-induced simultaneous activation of the AKT and AMPK could at least partially explain why a much more pronounced effect on glucose metabolism was observed in Sol than in EDL and Epit muscles.

We have also found that palmitate oxidation was significantly increased in all three muscles after cold acclimation. Interestingly, the relative increase in FAO was similar (2- to 2.25-fold) among all three muscles, indicating that, besides glucose, myocytes also enhanced their capacity to utilize fatty acids to fuel cold-induced thermogenesis. This was consistent with significant increases in *Pgc-1*α expression and AMPK

phosphorylation in oxidative and glycolytic muscles upon cold acclimation. We have also found significantly elevated expression of *Lpl* and *Cd36* in Sol and EDL muscles, which are crucial for lipolysis of triglycerides from lipoproteins and fatty acid uptake, respectively. The Sol displayed by far the most robust increase in Lpl (~10-fold) and *Cd36* (~5-fold) expression followed by the EDL (2.6- and 2.9-fold, respectively), whereas in the Epit muscle only a trend towards an increase in the expression of these proteins was observed after cold acclimation. Though gene expression data is not indicative of functional capacity, the mRNA data in this study complement and are compatible with the FAO data we obtained from freshly extracted muscle. As expected, the absolute value of FAO for the Sol muscle was much higher (almost double) than the values obtained for the EDL and Epit in control and cold-acclimated rats. It is remarkable that the Sol muscle sustained such high rates of both fatty acid and glucose oxidation under cold acclimating conditions, and yet increased its glycogen content. This could be attributed to the insulin sensitizing effect of cold acclimation that enhanced glucose uptake and promoted allosteric activation of GS. This has been demonstrated to occur through an increased in intracellular glucose-6-phosphate (G6P) levels (122). In fact, evidence has been provided that allosteric activation of GS is the primary mechanism by which insulin promotes muscle glycogen accumulation *in vivo* (122). This is consistent with our observations that Sol muscles from cold-acclimated rats had increased rates of insulin-stimulated glycogen synthesis. Because EDL and Epit muscles did not elicit any significant enhancement in glucose metabolism, it is likely that the G6P availability was not high enough to activate GS and promote glycogen synthesis under cold-acclimating conditions in these muscles.

We had originally hypothesized that SLN-induced SERCA uncoupling could contribute to non-shivering thermogenesis in skeletal muscles. It would do so by increasing ATP turnover and leading to acceleration of the citric acid cycle, glycolysis, and β-oxidation, ultimately resulting in an enhancement of glucose and fat oxidation under conditions of cold acclimation. Gene expression analysis revealed that *Serca1* expression was markedly increased in all three muscles, whereas *Serca2* expression was upregulated in Sol and Epit, but not in the EDL of cold-acclimated rats. We also tried to assess SERCA protein levels in all three muscles using a commercially available antibody to further validate our mRNA data, but we could not acquire a clear signal that allowed us to determine whether protein levels were affected by cold acclimation. Thus, despite fiber type differences, our findings suggest that in all muscles SERCA-mediated hydrolysis of ATP to transport of Ca^{2+} across the membrane was enhanced to some extent, with potential to contribute to cold-induced thermogenesis in these tissues. However, it has been previously reported that SERCA1a and SERCA2a protein contents are reduced and increased, respectively, in cold-acclimated mice (139). This indicates that it is the latter isoform of SERCA that seems to play an important role in non-shivering thermogenesis is skeletal muscles. With respect to SLN, we could only detect this protein in the Sol muscle, and its content was indeed significantly increased upon cold acclimation in this muscle. This is in line with other reports of muscle fiber-type specific expression of SLN (135, 261, 262), and provides evidence that SLN-mediated SERCA uncoupling following cold acclimation may increase the energy requirements of muscles with high content of type I fibers. It is possible that these increased energy demands could be met in the Sol muscles, which showed the highest

absolute rates of fatty acid and glucose oxidation following cold acclimation when compared to the EDL and Epit. Of note, it has been previously demonstrated that SLN protein content is increased by cold acclimation in the red portion of gastrocnemius (139), which is consistent with our observations that muscles rich in type I fibers have the capacity for SLN-mediated SERCA uncoupling.

In summary, here we show that fiber type composition plays a major role in determining the metabolic fate of glucose and fatty acids in skeletal muscles under conditions of cold-induced thermogenesis. The molecular mechanisms that drive these metabolic adaptive responses to cold in oxidative and glycolytic muscles overlap to some extent and involve the activation of AKT and AMPK. However, only in the highly oxidative Sol muscle GS activity seems to be induced and ultimately leads to glycogen accumulation. The molecular machinery involved in mitochondrial biogenesis and FAO was also upregulated in all muscles and characterized by increased expression of *Pgc-1*α, *Lpl*, and *Cd36*, although the absolute rate of FAO was much higher in oxidative than glycolytic muscles upon cold acclimation. We have also found that the expression of SERCA isoforms is fiber type-specific and that the capacity for SLN-mediated SERCA uncoupling seems to be present only in muscles rich in type I fibers. Despite these major fiber type-specific metabolic differences, cold acclimation promoted an insulin-sensitizing effect and enhanced the disposal of glucose and fatty acids in skeletal muscles. These metabolic adaptive responses to cold acclimation may be of great importance for diseases characterized by hyperglycemia and dyslipidemia such as obesity and type II diabetes.

CHAPTER 8: Cold acclimation reduces hepatic protein kinase B and AMP-activated protein kinase phosphorylation and increases gluconeogenesis in rats

Diane M. Sepa-Kishi*, George Bikopoulos*, Glen Katsnelson, Ayesha Iqbal, and Rolando B. Ceddia.

Muscle Health Research Centre, School of Kinesiology and Health Science, York University, Toronto, Ontario, M3J 1P3, Canada

*Contributed equally to this study.

Keywords: Liver, AMPK, HNF4α, fatty acid oxidation, glycogen

Statement of Labour

The experiments conducted in this study were carried out equally by Diane M. Sepa-Kishi and George Bikopoulos. DMSK's contributions included collection of blood samples, extraction of tissues, and incubation of liver strips for the measurement of glucose and fatty acid oxidation, as well as glycogen content. DMSK was also responsible for the insulin and glucagon assay, analyzing and interpreting the results, preparing the figures, and revising the manuscript. DMSK was supported by a NSERC Alexander Graham Bell Canada Graduate Scholarship and an Elia Scholarship. GB's contributions included collection of blood samples, the extraction of tissues, the running of western blots, conducting the real-time PCR analysis, analyzing and interpreting the results, preparing the figures and revising the manuscript. GK ran the majority of the western blots and assisted in the preparation of figures. AI ran the majority of the real-time PCR and assisted with the preparation of figures. GK and AI both reviewed the final manuscript.

Dr. Rolando Ceddia is the primary investigator and supervisor of this project and this research was funded by a Discovery Grant from NSERC and by infrastructure grants from the Canada Foundation for Innovation and the Ontario Research Fund.

8.1. Abstract

This study investigated the molecular and metabolic responses of the liver to cold-induced thermogenesis. To accomplish that, male Wistar rats were exposed to cold ($4^{o}C$) for 7 days. Livers were then extracted and used for the determination of glucose and fatty acid oxidation, glycogen content, the expression and content of proteins involved in insulin signaling, as well as in the regulation of gluconeogenesis and *de novo* lipid synthesis. Despite being hyperphagic, cold-acclimated rats displayed normoglycemia with reduced insulinemia, which suggests improved whole-body insulin sensitivity. However, liver protein kinase B (AKT) and glycogen synthase kinase 3 (GSK3) phosphorylations were markedly reduced along with the expressions of the insulin receptor (IR) and its substrates IRS1 and IRS2, whereas glycogen synthase (GS) phosphorylation increased. Thus, major signaling steps of the glycogen synthesis pathway in the liver were inhibited. Furthermore, glucagonemia and hepatic glucose and fatty acid oxidation were increased, whereas liver glycogen content was reduced by cold acclimation. This was accompanied by significantly elevated expressions of the gluconeogenic transcription regulators CRTC2, PGC-1α, and FoxO1, as well as of major gluconeogenic enzymes (G6Pase, FBP1, and PEPCK). Conversely, phosphorylation and contents of AMP-activate protein kinase (AMPK) and acetyl-CoA carboxylase (ACC) and fatty acid synthase (FAS) content were markedly downregulated in livers of cold-acclimated rats. In conclusion, cold acclimation suppressed hepatic glycogen synthesis and promoted profound metabolic changes in the liver so the organ could sustain its ability to regulate whole-body glucose and lipid metabolism under conditions of high energy demand in thermogenic tissues.

8.2. Introduction

Cold acclimation has been reported to cause profound systemic metabolic changes in order to allow the organism to adapt to the thermoregulatory challenge of this condition (273). The brown adipose tissue (BAT) is the main organ for non-shivering thermogenesis and burns fuel to generate significant amounts of heat through uncoupling of its mitochondria (63). In fact, in its activated state, BAT is estimated to burn up to 50% and 75% of ingested triglycerides (TG) and glucose, respectively, to support thermoregulation (274). This is consistent with reports that cold-induced BAT activation accelerates the clearance of TG-rich lipoproteins from the blood and reverses hyperlipidemia and glucose intolerance in mice (81, 173). These BAT-mediated thermogenic effects are also accompanied by significant increases in food intake and enhanced mobilization of TG from the white adipose tissue (WAT) (274). In this context, the liver, an organ that plays a major role in regulating systemic fuel availability, is also expected to undergo profound metabolic changes under conditions of cold stress. This is crucial for the maintenance of proper glycemic control in the face of hyperphagia and accelerated mobilization of substrates to fuel thermogenesis in BAT (63, 274) and other peripheral tissues such as skeletal muscles (246, 249).

Previous studies (220) have reported that despite hyperphagia (~50% increase in food intake), cold ($4^{o}C$) acclimated mice have liver TG and glycogen contents reduced by 22% and 49%, respectively, when compared to mice maintained at $28^{o}C$. These findings suggest that fat and glucose oxidation could be enhanced within the liver to support its increased energy requirements under conditions of cold stress, leading to a reduction in hepatic content of these substrates. Increased fatty acid oxidation (FAO)

could generate the ATP necessary for the liver to provide the body with glucose via gluconeogenesis. Additionally, enhanced exportation of lipids and glucose to fuel non-shivering (63) and shivering thermogenesis (220, 275), as well as to maintain proper glycemic control (274), could account for the cold-induced reduction in TG and glycogen contents of the liver (220). Indeed, gluconeogenic rates have been reported to increase after 5 (276) and 7 days (277) of cold exposure in rats, which supports the notion that glucose is largely exported by the liver under conditions of cold stress. Additionally, serum β-hydroxybutyrate increased 2.4-fold in cold acclimated mice (220), indicating that elevated rates of FAO lead to increased ketone production by the liver. The latter can provide an important alternative fuel source to glucose, especially for the central nervous system under conditions of prolonged cold stress. These adaptive metabolic responses seem intuitive; however, there is still limited and conflicting information regarding substrate partitioning and the molecular mechanisms underlying the adaptive metabolic responses that take place in the liver under cold stress.

It has been demonstrated that hepatic peroxisome proliferator-activated receptor gamma co-activator 1α (PGC-1α) promotes constitutive activation of gluconeogenesis and FAO through its association with hepatocyte nuclear factor 4α (HNF4α) and peroxisome proliferator activated receptor α (PPARα) (148, 169). Thus, the expression of these transcription factors would be expected to be upregulated under cold stress. However, transcriptomic analysis of liver from mice subjected for 24 h to cold (8^{o}C) exposure reported accentuated down regulation of *Hnf4α* and *Pparα* mRNA expression in the liver (154). Furthermore, no significant alterations have been found in genes involved in glucose metabolism (phosphoenolpyruvate carboxykinase, *Pepck*, and

glucose-6-phosphatase, *G6pase*), fatty acid synthesis (sterol regulatory element-binding protein-1c, *Srebp-1c*; fatty acid synthase, *Fas*; acetyl-CoA carboxylase, *Acc*; and stearoyl-Coenzyme A desaturase 1, *Scd1*), and mitochondrial biogenesis/FAO (*Pgc-1α*; carnitine palmitoyl transferase 1, *Cpt1*; nuclear respiratory factor 1, *Nrf1*; and the mitochondrial transcription factor A, *Tfam*) in livers of mice exposed to cold for 24h (154). These findings are at odds with previous reports that hepatic glucose and fat metabolism are profoundly affected under cold stress (220, 277). This is particularly relevant to the full transcriptional activation of the PEPCK promoter and enhancement of gluconeogenesis that requires co-activation by PGC-1α of the liver-enriched transcription factor HNF4α (278). In fact, in hepatocytes from mice lacking liver HNF4α, the ability of PGC-1α to activate key genes of gluconeogenesis (*Pepck* and *G6pase*) was lost, although the activation of genes involved in FAO and ketogenesis by PGC-1α did not seem to be affected by the lack of HNF4α (148). Thus, a reduction in *Hnf4α* gene expression (154) is apparently in conflict with enhanced liver gluconeogenesis previously described in rats under cold stress (246, 277). In order to determine the alterations that occur in glucose and fatty acid metabolism in the liver, as well as to elucidate discrepancies regarding the molecular mechanisms underlying the adaptive metabolic responses of the liver to cold stress, we subjected rats to a 7-day cold (4^{o}C) acclimation protocol. We then assessed glucose and FAO, glycogen content, protein kinase B (AKT), glycogen synthase kinase 3 (GSK3), glycogen synthase (GS), AMP-activated protein kinase (AMPK), and ACC contents and phosphorylation, as well as PGC-1α and PEPCK protein contents and the expression of transcription factors involved in FAO, lipid synthesis, and gluconeogenesis in the liver. Here, we report novel

findings that cold acclimation created a unique set of conditions in which the liver increased its capacity to oxidize glucose and fatty acids and caused a significant reduction in hepatic glycogen content. These findings provide evidence that the liver undergoes profound metabolic changes in order to maintain glucose homeostasis and also to support whole-body energy needs of cold-induced thermogenesis.

8.3. Materials and Methods

Reagents – Fatty acid-free bovine serum albumin (BSA) and palmitic acid were obtained from Sigma (St. Louis, MO, USA). Glycogen, amyloglucosidase, hexokinase, and glucose-6-phosphate dehydrogenase were obtained from Sigma (St. Louis, MO). [1-^{14}C] palmitic acid was from American Radiolabeled Chemicals (St. Louis, MO, USA) and D-[U-^{14}C] glucose was from GE Healthcare (Little Chalfont, UK). Protease (cOmplete Ultra Tablets) and phosphatase (PhosStop) inhibitors were from Roche Diagnostics GmbH (Mannheim, Germany). The non-esterified fatty acids (NEFAs) kit was from Wako (Mountain View, CA, USA) and the TG quantification colorimetric kit was from BioVision (Milpitas, CA, USA). Glucose was measured by the glucose oxidase method using a OneTouch Ultra Mini Monitor. The rat glucagon and insulin ELISA kits were from R&D Systems (Minneapolis, MN, USA) and Alpco (Salem, NH, USA), respectively. All antibodies were purchased from Cell Signaling (Danvers, MA, USA), except for P-ACC and PGC-1α which were purchased from Millipore (Billerica, MA, USA), and the PEPCK antibody that was purchased from Abcam (Cambridge, MA, USA).

Animals – Male albino rats (Wistar strain) were housed at 22 °C on a 12/12 h light/dark cycle and fed standard laboratory chow (Lab Diet Cat #5012) *ad libitum*. The protocol containing all animal procedures described in this study was specifically approved by the Committee on the Ethics of Animal Experiments of York University (York University Animal Care Committee, YUACC, permit number 2016-05) and performed strictly in accordance with the YUACC guidelines. All surgery was performed under Ketamine/Xylazine anesthesia, and all efforts were made to minimize suffering.

Cold exposure – The rats were age- and weight-matched (~12 weeks old and ~400 g) and randomly allocated to either the control or cold-exposed groups. The animals were housed in individual cages and the cold-exposed group was maintained at 4 °C for 7 days on a 12/12 h light/dark cycle, while control animals were maintained at 22 °C with *ad libitum* food and water. Food intake and body weight were measured on a daily basis for five days prior to (baseline) and for the entire duration of the cold exposure. Blood samples were collected in the fed state, centrifuged for 10 minutes at 4°C and the plasma was stored at -80°C for subsequent analysis. Upon completion of the protocol, animals were anesthetized (0.4 mg Ketamine and 8 mg Xylazine per 100 g body weight) in the fed state and the livers were extracted and weighed. Liver samples were quickly collected and frozen in liquid nitrogen for subsequent analysis.

Measurement of glucose and palmitate oxidation in liver slices – Glucose and palmitate oxidation as measures of oxidative capacity were assessed by production of $^{14}CO_2$ as previously described (19). Briefly, immediately after extraction, thin liver slices (~30 mg) were placed in plastic scintillation vials containing 2 ml of continuously gassed (O_2:CO_2-95:5% vol/vol) Krebs Ringer Buffer with HEPES (KRBH) plus 3.5% fatty acid-free

bovine serum albumin (KRBH-3.5% BSA) and 5.5 mM glucose in the presence of either 0.2 µCi/ml of [1-^{14}C] palmitic acid and 200 µM non-labelled palmitate, or 0.2 µCi/ml of D-[U-^{14}C] glucose for 1 h. The media was then acidified with 0.2 ml of H_2SO_4 (5 N), and the vials were maintained sealed at 37°C for an additional 1 h for the collection of CO_2 released by the tissue slices. The vials used for incubation had a centered isolated well containing a loosely folded piece of filter paper that was moistened with 0.2 ml of 2-phenylethylamine/methanol (1:1, vol/vol) for the capture of all CO_2. At the end of the incubation, the filter paper was removed and transferred to a scintillation vial for radioactivity counting (19).

Measurement of liver glycogen content – The content of glycogen in liver samples was determined as previously described (268). Briefly, liver samples were first digested in 0.5 ml of 1 M KOH, and then the pH of the liver digest was titrated to 4.8 before the addition of acetate buffer (pH 4.8) and 0.5 mg/ml amyloglucosidase. Subsequently glycogen was hydrolyzed at 40^{o} C for 2 h and glucose was analyzed enzymatically and the absorbance read in a spectrophotometer (Ultraspec 2100 pro; Biochrom Ltd., Cambridge, UK) at 340 nm wavelength (268).

RNA isolation and quantitative PCR – Primers were designed using the software PrimerQuest (IDT) based on probe sequences available at the Affymetrix database (NetAffx™ Analysis Centre, http://www.affymetrix.com/analysis) for each given gene. RNA was isolated from liver using TRIzol® reagent (ThermoFisher Scientific,Waltham, MA, USA) and cDNA was made from 2 µg of extracted RNA using the EasyScript cDNA synthesis kit from Applied Biological Materials (ABM) Inc. (Richmond, BC, Canada), according to the manufacturer's instructions. Samples were run using the following

amplification conditions: 95°C (10 min); 40 cycles of 95°C (15 s), 60°C (60 s). All genes were normalized to the control genes TBP and β-actin, and relative differences in gene expression between treatment groups were determined using the ΔΔCt method (226). Values are presented as alterations relative to the control group.

Western blotting analysis of content and phosphorylation of proteins – Liver samples were collected and homogenized in a buffer containing 25 mM Tris-HCl, 25 mM NaCl (pH 7.4), 1 mM $MgCl_2$, 2.7 mM KCl, 1% Triton-X and protease and phosphatase inhibitors (Roche Diagnostics GmbH, Mannheim, Germany). Liver homogenates were centrifuged, the supernatant was collected, and an aliquot was used to measure protein by the Bradford method. Samples were diluted 1:1 (vol/vol) with 2x Laemmli sample buffer and heated to 95°C for 5 min. Samples were then subjected to SDS-PAGE, transferred to a PVDF membrane and probed for the proteins of interest. The following primary antibodies were used at a dilution of 1:1,000: PEPCK (69 kDa, Cat# ab28455); PGC-1α (100 kDa, Cat# AB3242); P-AMPK (62 kDa, Cat# 2535); AMPK (62 kDa, Cat# 2532); P-ACC (257 kDa, Cat# 07-303); ACC (280 kDa, Cat# 3662); P-AKT (60 kDa, Cat# 9271); AKT (60 kDa, Cat# 9272); P-GSK3α (51 kDa, Cat# 9327); GSK3α/β (51 and 46 kDa, Cat# 5676); P-GS (85-90 kDa, Cat# 3891); GS (84 kDa, Cat# 3886); FAS (273 kDa, Cat# 3180). β-actin (45 kDa, Cat# 4967) was used as a loading control.

Statistical analyses – Statistical analyses were assessed by unpaired two-tailed t-test. Statistical significance was set at $p<0.05$.

8.4. Results

Food intake (FI), body weight, liver mass, and NEFA – Rats exposed to cold were hyperphagic and by day 7 the average FI was 45% higher in the cold-exposed than the control group (Table 8-1). Body weight and liver masses did not differ between control and cold-acclimated rats. Control and cold-acclimated rats also displayed similar circulating NEFA values (Table 8-1).

Table 8-1: Food intake (FI), body weigth, liver mass, and circulating non-esterified fatty acids (NEFAs) in control (Con) and cold-acclimated rats.

	Con	Cold
FI (g/day/rat)	30.0	43.5*
Body weight (g)	409.71 ± 6.51	406.49 ± 4.21
Liver mass (g)	14.89 ± 0.59	14.9 ± 0.60
NEFAs (mmol/l)	0.29 ± 0.02	0.24 ± 0.01

Values measured after 7 days of cold exposure. n = 6-8. *p<0.05, t-test.

Palmitate and glucose oxidation, and glycogen content – The rates of palmitate and glucose oxidation were 1.6-fold (Fig. 8-1A) and 1.47-fold (Fig. 8-1B) higher, respectively, in cold-exposed than control rats. Analysis of glycogen content also revealed that this variable was reduced by 46% (Fig. 8-1C) in cold-exposed rats when compared to controls.

Contents of PEPCK and PGC-1α and phosphorylation and content of AMPK and ACC – The content of the gluconeogenic enzyme PEPCK was 1.78-fold higher (Fig. 8-2A) in livers of cold-acclimated than control rats. This was also accompanied by a 2-fold increase in PGC-1α content (Fig. 8-2B), whereas the hepatic phosphorylation rates and

the contents of AMPK and ACC were significantly reduced in cold-acclimated rats (Fig. 8-2C and D). In fact, AMPK and ACC phosphorylation were reduced by 66% and 46%, respectively, in the liver of cold-acclimated rats in comparison to control animals.

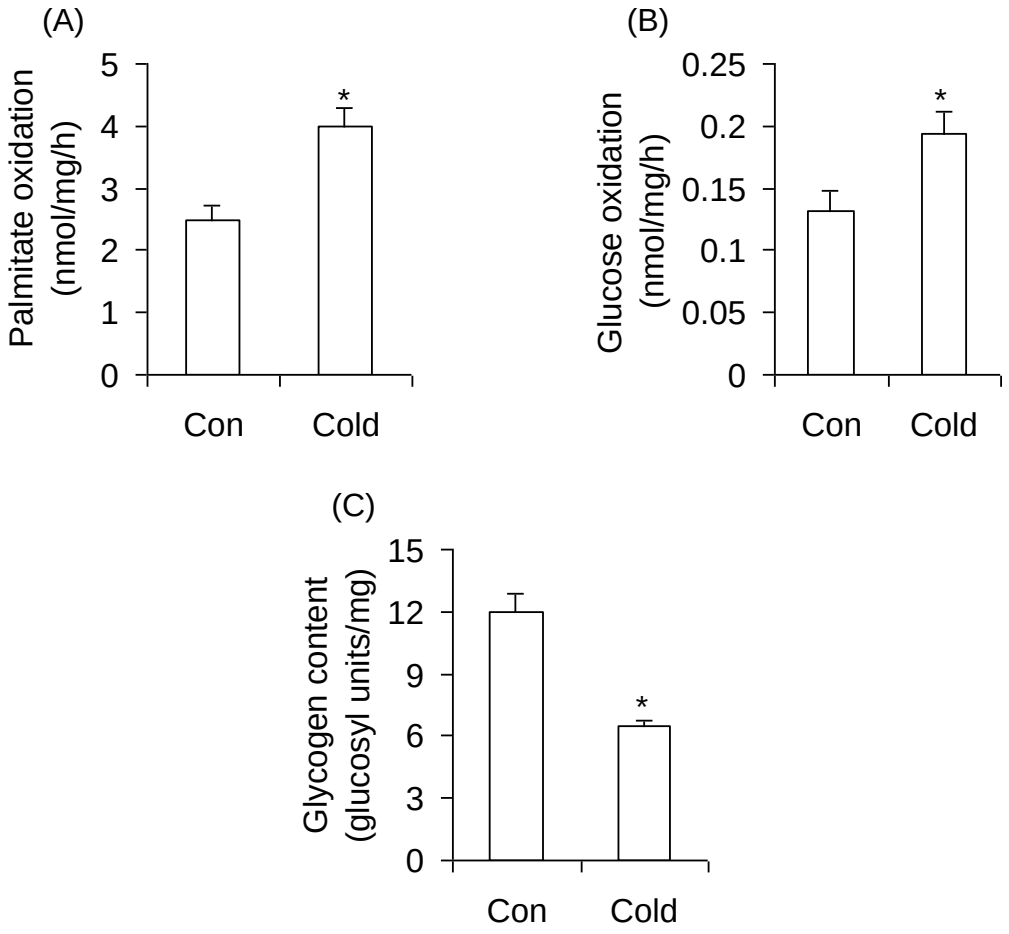

Figure 8-1: Cold-induced alterations in palmitate and glucose oxidation, and glycogen content in the liver. Cold acclimation increases palmitate (A) and glucose (B) oxidation and reduces glycogen content (C) in rat livers. Con = control, n=18 rats per condition. *p<0.05, t-test.

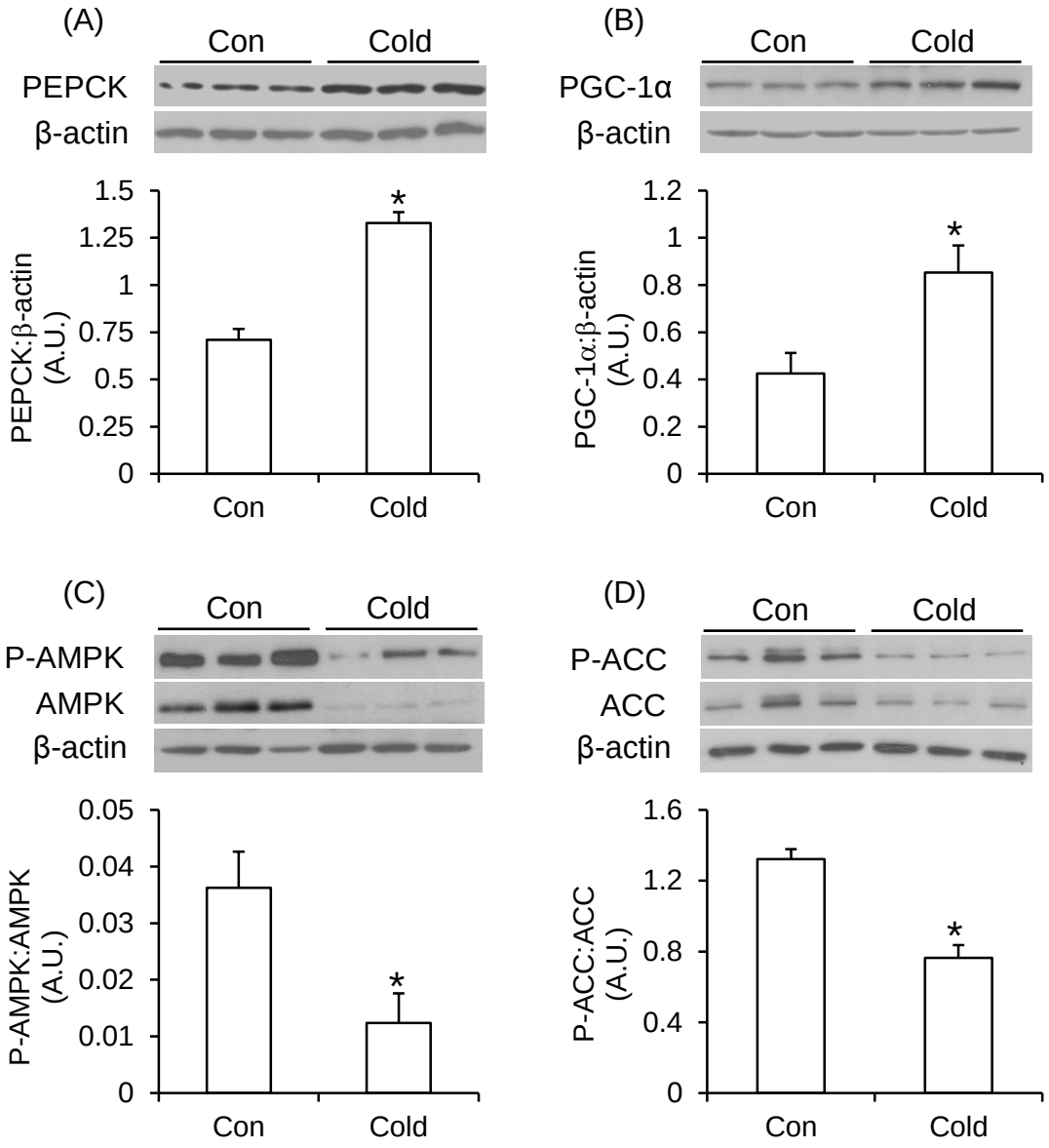

Figure 8-2: Content of PEPCK and PGC-1α, and content and phosphorylation of AMPK and ACC in the liver of cold acclimated rats. Cold acclimation increases PEPCK (A) and PGC-1α (B) contents and reduces the phosphorylation and contents of AMPK (C) and ACC (D) in rat livers. Con = control, n=6 rats per condition. *p<0.05, t-test.

Protein content and phosphorylation of *AKT (protein kinase B), glycogen synthase kinase 3 α/β (GSK3α/β), and glycogen synthase (GS)* – Assessment of proteins involved in insulin signaling revealed that AKT phosphorylation was significantly reduced (76%) in livers of cold-acclimated rats (Fig. 8-3A). The content of AKT was also markedly reduced in these rats (Fig. 8-3A). Phosphorylation of the downstream target of AKT, GSK3α/β, reduced by 61% (Fig. 8-3B), whereas GS phosphorylation significantly increased by 2.57-fold (Fig. 8-3C) in livers of cold-acclimated rats when compared to those of control animals.

mRNA expression of genes involved in insulin signaling and glucose metabolism – The mRNA levels of *the insulin receptor* (*Ir*), insulin receptor substrate 1 (*Irs1*), and insulin receptor substrate 2 (*Irs2*) were significantly reduced by 79% (Fig. 8-4A), 62% (Fig. 8-4B), and 49% (Fig. 8-4C), respectively, whereas *G6pase* and fructose bisphosphate 1 (*Fbp1*) mRNA levels were significantly increased by 10.5–fold (Fig. 8-4D) and 2.2–fold (Fig. 8-4E), respectively, in livers of cold-acclimated rats. Conversely, the mRNA levels of glucokinase (*Gk*) reduced by 77% (Fig. 8-4F) and of pyruvate dehydrogenase kinase 4 (*Pdk4*) by 69% (Fig. 8-4G) in cold-acclimated rats.

mRNA expression of transcriptional regulators of hepatic gluconeogenesis – The mRNA levels of CREB regulated transcription coactivator 2 (*Crtc2/Torc2*), *Pgc-1α*, and forkhead box O1 (*FoxO1*) increased by 1.61-fold, 3.43-fold, and 1.72-fold, respectively, after 7 days of cold exposure (Fig. 8-5A-C). No significant changes were found in the mRNA expression of *Pparα, Pparγ, Hnf3β*, and *Hnf4α*, in livers of cold-acclimated rats (Fig. 8-5D-G).

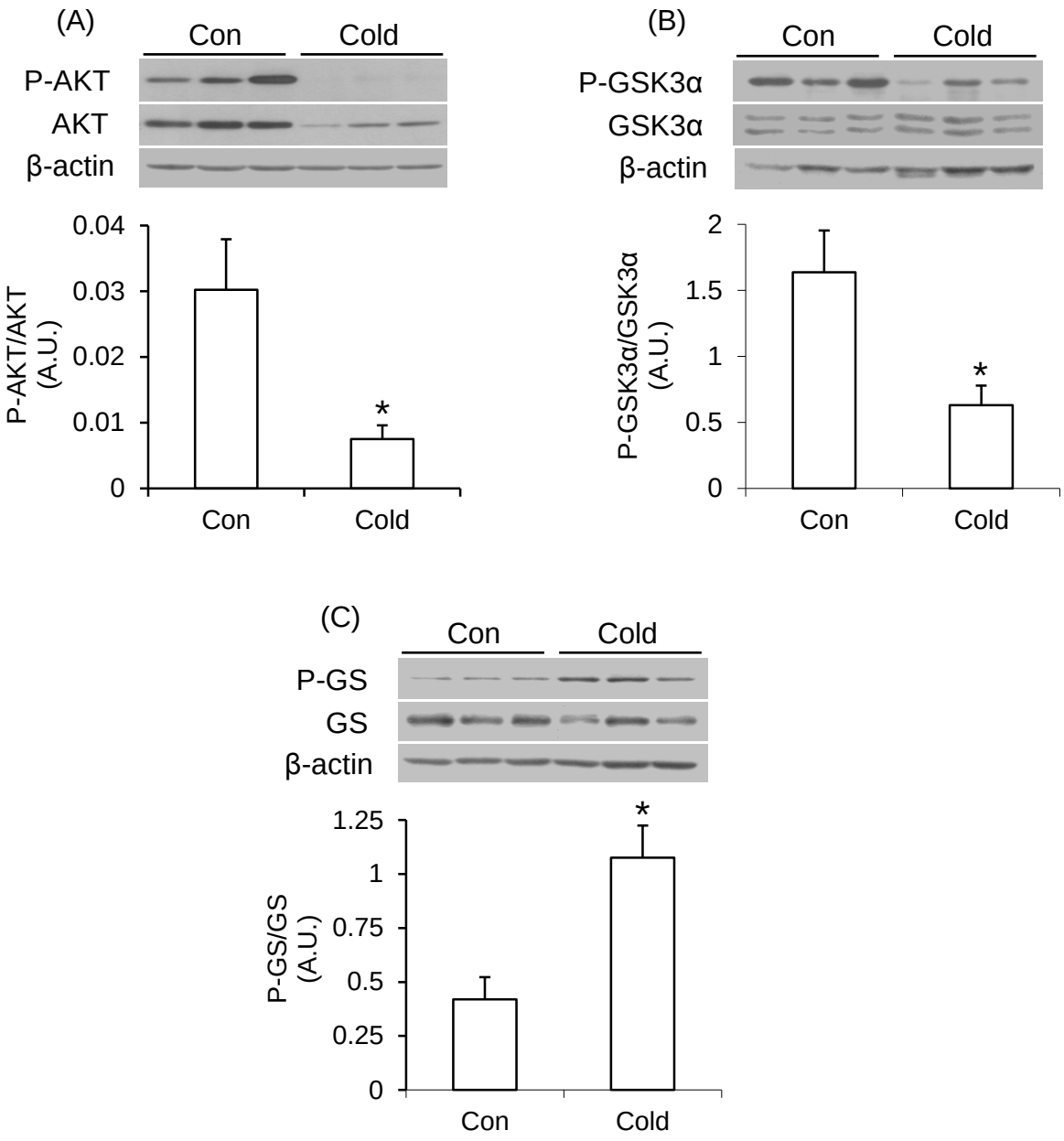

Figure 8-3: Content and phosphorylation of AKT, GSK3α, and GS in the liver of cold-acclimated rats. Cold acclimation reduces the phosphorylation of AKT (A) and GSK3α (B) and increases the phosphorylation of GS (C) in rat livers. Con = control, n=6 rats per condition. *p<0.05, t-test.

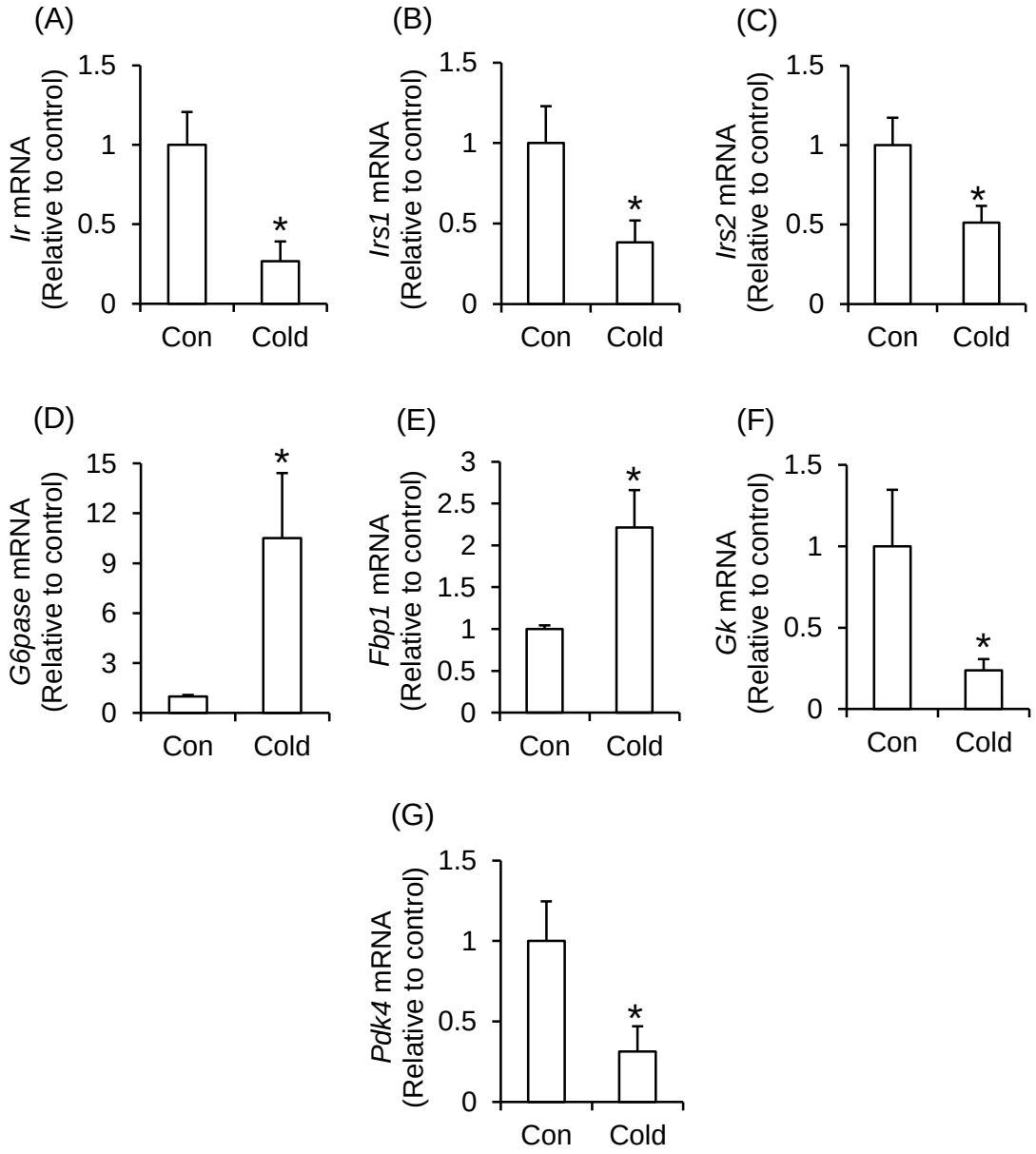

Figure 8-4: Gene expression of proteins involved in insulin signaling and the gluconeogenic pathway in the livers of cold-acclimated rats. Cold acclimation reduces the mRNA expression of proteins involved in insulin signaling (*Ir* (A), *Irs1* (B) and *Irs2* (C)), increases the mRNA expression of proteins in the gluconeogenic pathway (*G6pase* (D), and *Fbp1* (E)), and also markedly reduces *Gk* (F) and *Pdk4* (G) in rat livers. Con = control, n=6-8 rats per condition. *p<0.05, t-test.

FAS protein content and mRNA expression of genes involved in lipid synthesis – Cold exposure significantly reduced the content of FAS by 64% (Fig. 8-6A) and the mRNA levels of this enzyme by 77% (Fig. 8-6B) when compared to controls. The mRNA levels of *Acc*, *Srebp-1c*, and elongation of very long chain fatty acids protein 3 (*Elovl3*) were also significantly reduced by 79% (Fig. 8-6C), 68% (Fig. 8-6D), and 77% (Fig. 8-6E), respectively, in livers of cold-acclimated rats.

mRNA expression of genes involved in fat oxidation – *Cpt1*, Acyl-CoA thioesterase (*Acot2*), and cytochrome c oxidase subunit 6c (*Cox6c*) mRNA levels increased by 3-fold (Fig. 8-7A), 2.8-fold (Fig. 8-7B), and 5.8-fold (Fig. 8-7C) in livers of cold-acclimated rats when compared to controls.

Time-course of glucose, insulin, and plasma glucagon – Glycemia did not differ between control and cold-acclimated rats either prior to or during the cold acclimation period (Fig. 8-8A and B). However, even though circulating insulin was similar in both groups prior to cold exposure, insulinemia significantly reduced (35%) after day 1 of cold exposure and remained as such throughout the entire cold acclimation period (Fig. 8-8C). In fact, area under the curve (AUC) reveals a 28% reduction in insulinemia in cold-acclimated rats in comparison to controls (Fig. 8-8D). Rats in the control and cold-exposed groups had similar plasma glucagon levels prior to the beginning of the study (107.6 $\pm$ 11.9 and 87.8 $\pm$ 11.4 pg/ml, respectively) (Fig. 8-8E). However, plasma glucagon levels increased by 62% after day 1 and remained consistently elevated throughout the 7-day period of cold acclimation (Fig. 8-8E). In fact, the AUC reflecting plasma glucagon levels during the study was 1.41-fold higher in cold-acclimated than control rats (Fig. 8-8F).

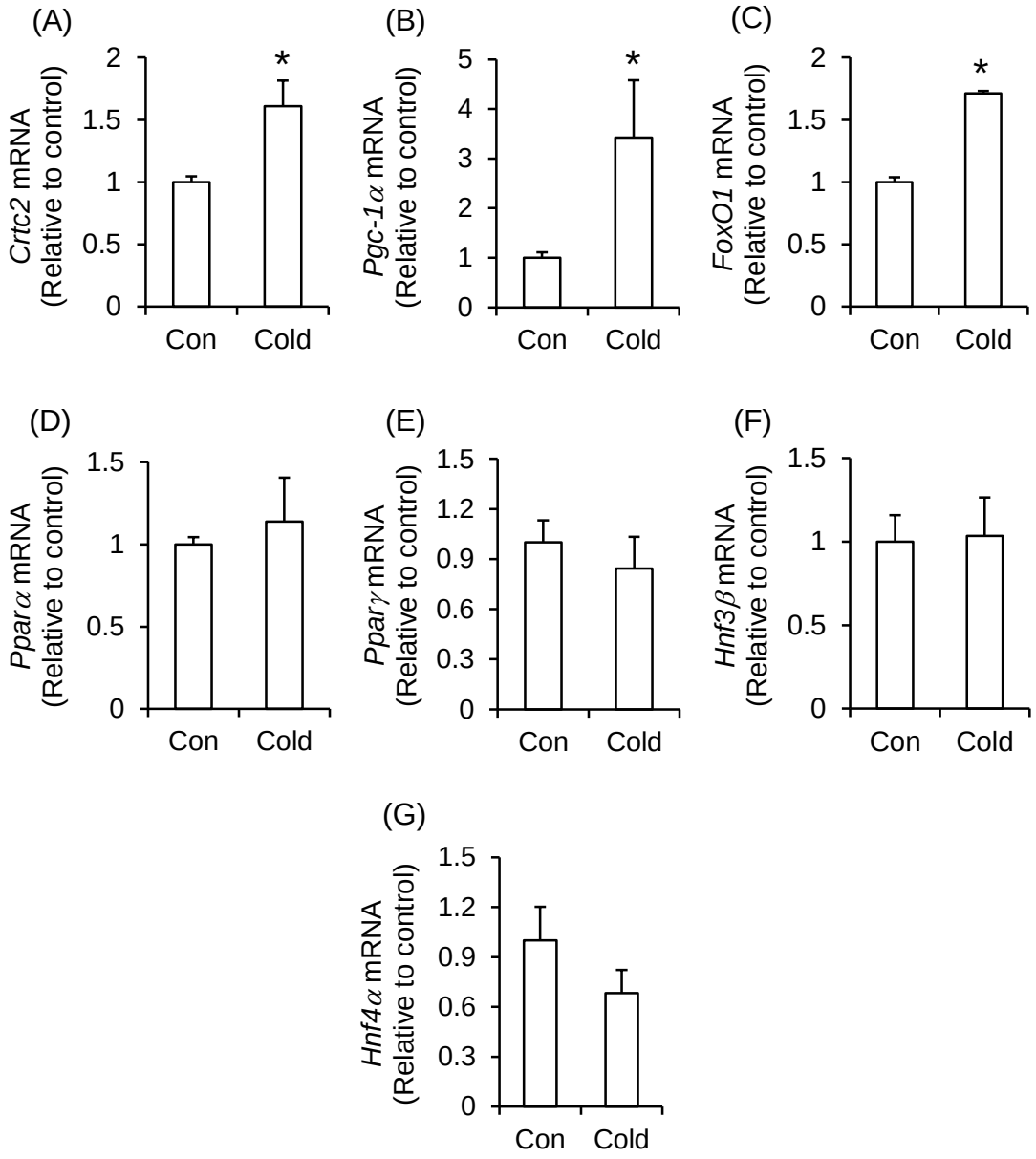

Figure 8-5: The effects of cold acclimation on the expression of transcriptional regulators of hepatic gluconeogenesis. Cold acclimation increases the mRNA expression of *Crtc2* (A), *Pgc-1α* (B), and *FoxO1* (C), but it does not alter the mRNA expression of *Pparα*, *Pparγ*, *Hnf3β*, and *Hnf4α* in rat livers. Con = control, n=6-8 rats per condition. *p<0.05, t-test.

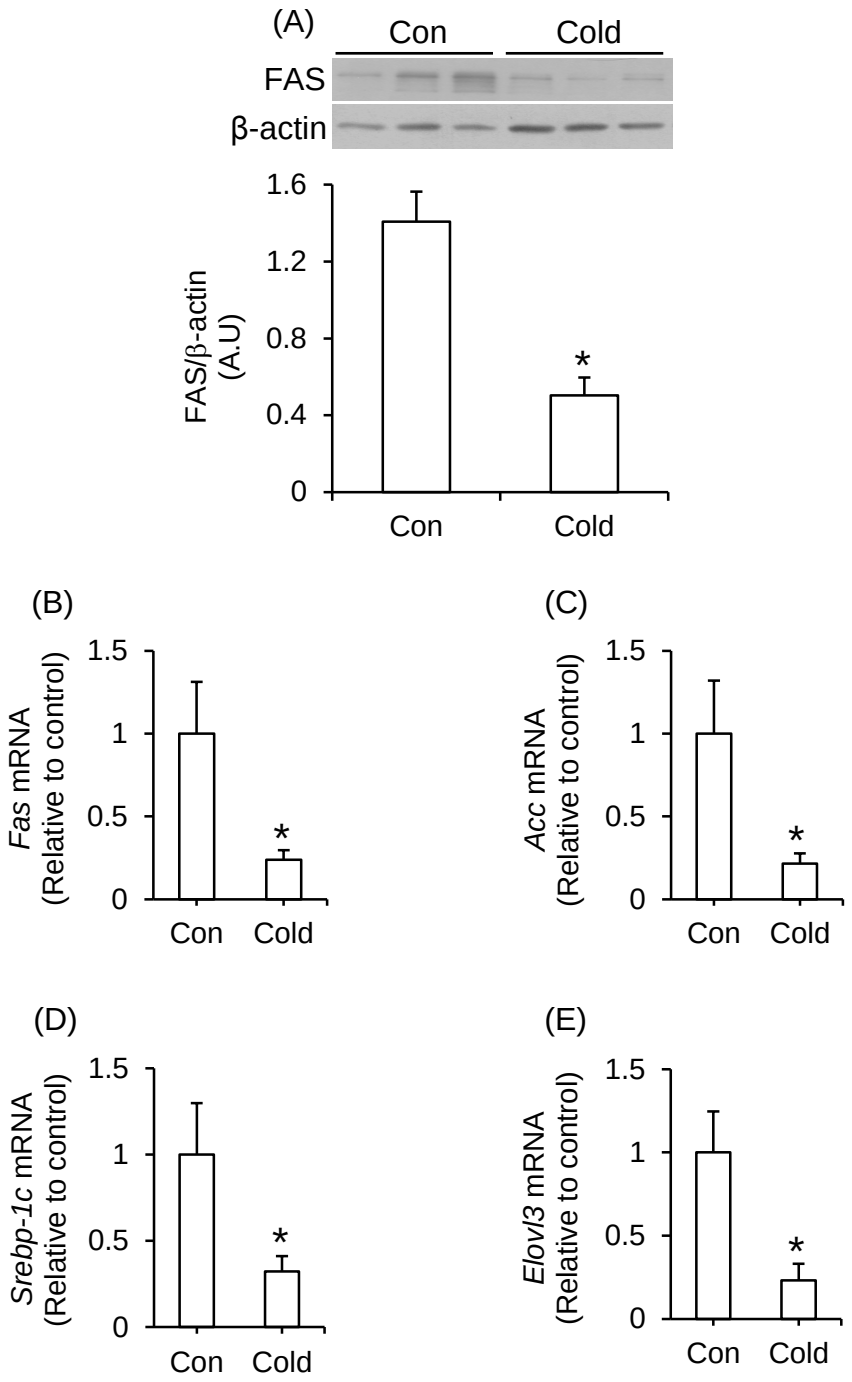

Figure 8-6: The effects of cold acclimation on the content and expression of proteins involved in lipid synthesis. Cold exposure reduces the content and expression of FAS (A and B), as well as the expression of *Acc* (C), *Srebp-1c* (D), and *Elovl3* (E) in rat livers. Con = control, n=6-8 rats per condition. *p<0.05, t-test.

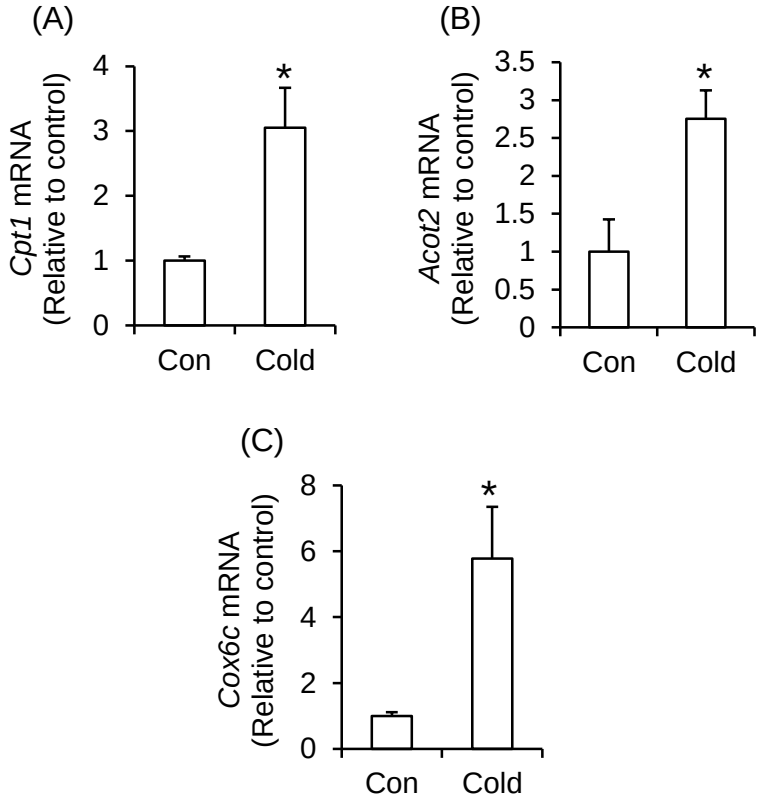

Figure 8-7: The effects of cold acclimation on the expression of genes involved in fat oxidation. Cold exposure increases mRNA expression of *Cpt1* (A), *Acot2* (B), and *Cox6c* (C) in rat livers. Con = control. n=6 rats per condition. *p<0.05, t-test.

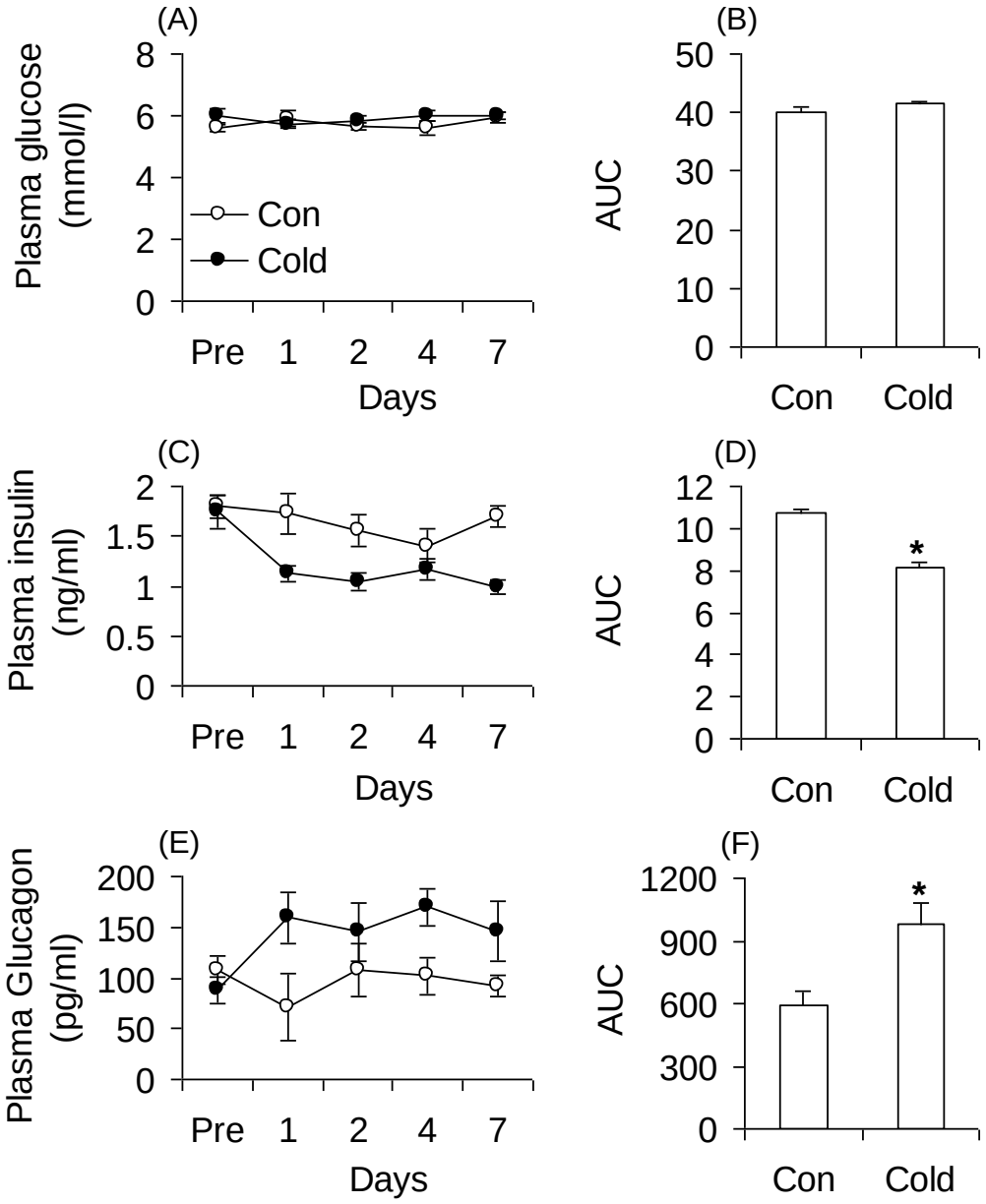

Figure 8-8: Time-course analysis of circulating glucose, insulin and glucagon in control (Con) and cold-exposed (Cold) rats. Cold exposure did not increase glycemia (A and B), but it reduced insulinemia (C and D) and increased plasma glucagon (E and F) in rats. Area under the curve (AUC). n=6 rats per condition. *p<0.05, t-test.

8.5. Discussion

Here, we provide a comprehensive analysis of the molecular and metabolic changes that take place in the liver under conditions of cold acclimation. As we originally hypothesized, in order to meet the increased energy demands of cold-induced thermogenesis, several metabolic adaptive changes have to occur in the liver, since this organ plays a major role in the maintenance of whole-body energy and glucose homeostasis (141). The increased demand for fuel in major thermogenic organs such as BAT and skeletal muscles was met to some extent by hyperphagia in cold exposed rats. However, the extra intake of food did not seem to be sufficient to fuel thermogenesis because the liver enhanced its molecular machinery that drives hepatic gluconeogenesis. This must have been important to provide additional substrate for thermogenic organs, as well as for the maintenance of whole-body glucose homeostasis. This is supported by our findings that even though the capacity of the liver to oxidize fatty acids and glucose was significantly increased, hepatic glycogen content was reduced by ~50% in cold-acclimated rats. Furthermore, analysis of AKT and GSK3 content and phosphorylation revealed that these were markedly reduced, which must have led to increased GS phosphorylation and reduced hepatic glycogen synthesis in the livers of cold acclimated rats. This is because GS is activated by dephosphorylation that occurs when its upstream kinase GSK3 is phosphorylated and deactivated by AKT (279, 280). We have also assessed the expression of genes involved in signaling steps upstream of AKT that are also crucial for insulin-mediated regulation of glucose metabolism in the liver. We found that the expressions of the *Ir*, *Irs1*, and *Irs2* in the liver were markedly downregulated by cold exposure, which is in line with reduced AKT and

GSK3 phosphorylation in this organ. Conversely, the content of PEPCK and the expressions of *G6pase* and *Fbp1*, crucial enzymes of the gluconeogenic pathway (279), were upregulated in livers of cold-acclimated rats.

We have also found that *Gk* and *Pdk4* expressions were markedly suppressed in cold-acclimated rats. GK catalyzes the first reaction of glucose as this sugar enters the hepatocyte through GLUT2, resulting in the formation of glucose-6-phosphate (G6P) (280). G6P activates GS by allosteric stimulation of the inactive phosphorylated form and also induces a conformation change that renders the enzyme a better substrate for dephosphorylation/activation to occur (280). Thus, a reduction in the expression of *Gk* indicates a lower capacity of hepatocytes to promote synthesis and storage of glycogen under conditions of cold acclimation. PDK4 phosphorylates and deactivates the pyruvate dehydrogenase complex (PDC) and potentially limits the flux of glucose into the Krebs cycle (281, 282). In this context, reduced expression of *Pdk4* is compatible with our observations that glucose oxidation was enhanced in the livers of cold-acclimated rats, particularly under hyperphagic conditions in which the flux of glucose to the liver was increased. However, from the perspective of hepatic glucose output, a rather increase in *Pdk4* expression would be expected in order for glucose to be spared for exportation. This apparent paradox can be reconciled by the fact that the oxidation of both glucose and fatty acids were similarly enhanced (50 to 60%) in livers of cold-acclimated rats. Therefore, despite a marked reduction in *Pdk4* expression and elevated rates of glucose oxidation, hepatocytes relied on a mixture of substrates to supply their own energy needs. This way the liver could still spare some glucose and maintain its capacity to export this substrate to peripheral tissues under conditions of cold-induced

thermogenesis. Thus, our findings indicate that the liver adapted its molecular machinery to simultaneously oxidize and release glucose instead of storing it, and they also provide a mechanistic explanation for why liver glycogen content in cold-acclimated rats was much lower than in control animals.

Importantly, glycemia remained constant throughout the cold-exposure period, despite hyperphagia and a significant reduction in insulinemia (~28%). These findings are in agreement with previous observations that glucose is an important fuel for thermogenesis (78, 152), and that insulinemia is reduced (131), whereas peripheral insulin sensitivity is improved in cold-acclimated rats (249, 283). Indeed, our findings of reduced insulinemia with normal glycemia and hyperphagia in cold-acclimated rats are indicative of improved whole-body insulin sensitivity. We have also found that blood glucagon levels were consistently elevated (~40%) throughout the 7-day cold acclimation-period. Glucagon is a major stimulator of gluconeogenesis and also promotes glycogen breakdown (glycogenolysis) in the liver (279). Through signaling in hepatocytes, glucagon regulates and coordinates the expression of various transcription factors that drive hepatic gluconeogenesis. In fact, *Crtc2*, *Pgc-1*α, and *FoxO1* gene expressions were all significantly increased in livers of cold-acclimated rats. Additionally, western blotting analysis revealed that PGC-1α protein content was robustly increased in the livers of these animals. These are all compatible with glucagon signaling and activation of protein kinase A (PKA) in hepatocytes, a crucial early step in a cascade of events that leads to increased transcriptional activity and enhancement of the machinery that promotes hepatic glucose output (279). Reduced AKT and AMPK phosphorylation in the livers of cold-acclimated rats must also have favoured

gluconeogenesis. This is because reduced AKT activity prevents the phosphorylation and nuclear exclusion of FoxO1 and subsequent suppression of gluconeogenic genes (279, 284). Similarly, marked reductions in AMPK content and phosphorylation in livers of cold-acclimated rats also contributed to enhance gluconeogenesis, since in its phosphorylated and activated state, AMPK phosphorylates CRTC2 leading to its retention in the cytoplasm and suppression of gluconeogenic genes (285–287). Of note, AMPK activation is also known for increasing fatty acid oxidation (288); therefore, a reduction in AMPK phosphorylation seems contrary to our findings of cold-induced enhancement in palmitate oxidation. However, ACC phosphorylation and content were downregulated under cold acclimating conditions and we also found that FAS content was drastically reduced. Therefore, even if reduced ACC phosphorylation indicated elevated enzyme activity, markedly reduced ACC content likely limited the activity of this enzyme. So, in a condition of hyperphagia and significantly elevated *Cpt1* expression, the import of long chain fatty acids into the mitochondria must have been facilitated and enhanced their oxidation, which is consistent with our findings of elevated palmitate oxidation upon cold acclimation.

Even though PPARα, PPARγ, HNF3β, and HNF4α have been demonstrated to play important roles in the regulation of hepatic gluconeogenesis (148, 169), we found that the gene expression for these transcriptional factors did not differ between control and cold-acclimated rats. However, it has been proposed that the expression of transcriptional co-activators involved in the stimulation of hepatic gluconeogenesis is regulated in a temporal manner (289). In this context, it could be that PPARα, PPARγ, HNF3β, and HNF4α had their expressions affected in a time-dependent manner and

then returned to basal values after 7 days of cold exposure when liver mRNA was actually extracted. A time-dependent analysis of the expression of these transcription factors might be required to test this possibility. It could also be that the presence of a basal amount of PPARα and HNF4α suffices for the adaptive hepatic metabolic responses to take place when gluconeogenesis needs to be up-regulated. In fact, the requirement of PPARα and HNF4α for a hepatic gluconeogenic response to fasting was identified in mice that had these transcription factors genetically deleted (148, 169). Our findings suggest that there was no need for the hepatic expression of these transcription factors to be increased in order for the liver to enhance its gluconeogenic molecular machinery during cold-acclimation.

Besides promoting hepatic glucose output, our findings also indicate that cold acclimation down-regulated the *de novo* lipid synthesis pathway in the liver. This was supported by potently reduced *Fas*, *Acc*, *Srebp-1c* and *Elovl3* gene expressions in livers of cold-acclimated rats, which is further corroborated by a much lower FAS protein content in livers of cold-acclimated than control rats. Conversely, *Cpt1*, *Acot2*, and *Cox6c* mRNA expressions were increased, which is in line with our findings of a cold-induced enhanced hepatic FAO response. Thus, lipid metabolism was shifted towards oxidation in livers of cold-acclimated rats. These observations are compatible with previous reports that BAT activation through either cold exposure or β3-adrenergic stimulation leads to a marked reduction in circulating TG and increases hepatic VLDL remnant clearance (173). In fact, the metabolic changes that take place in the liver under conditions of cold-induced thermogenesis have the potential to significantly

ameliorate dyslipidemia and protect against atherogenic cardiovascular diseases (81, 173).

In conclusion, our data provide novel evidence that cold-induced metabolic adaptive responses in the liver were mediated by suppression of AKT and AMPK phosphorylation/activation, reduced insulinemia, increased glucagonemia, and elevated expression of *Pgc-1*α, *Crtc2*, and *FoxO1*, which are major components of the molecular machinery that drives hepatic gluconeogenesis. We also demonstrate that cold acclimation enhanced the capacity to oxidize glucose, depleted glycogen stores, and markedly downregulated the expression of enzymes involved in the *de novo* lipid synthesis pathway in the liver. Altogether, these metabolic changes allowed the liver to sustain its ability to regulate whole-body glucose and lipid metabolism under conditions of high energy demand in thermogenic tissues.

CHAPTER 9: Integrated Summary

This dissertation examined two therapeutic approaches to enhancing glucose utilization, improving insulin sensitivity and reducing fat mass that could be potential alternative therapies for obesity and T2D. These approaches exerted their effects through two distinct mechanisms: a) enhanced glucose and fatty acid oxidation through cold-induced thermogenesis and b) suppression of mitochondrial long-chain fatty acid transport through CPT1b inhibition.

Cold-induced thermogenesis promotes the activation of BAT, a process that significantly increased energy expenditure through NST. BAT activation increased its substrate metabolism and caused significant adaptive responses in other peripheral tissues in order to sustain NST and core body temperature. I conducted 4 studies to examine the metabolic adaptive responses of BAT, WAT, skeletal muscles, and liver to cold acclimation in order to provide a comprehensive understanding of each organ's physiological role under these conditions (Fig. 9-1).

To fuel the increased energy demands of NST, FA and glucose uptake were enhanced in BAT, clearing these substrates at increased rates from the circulation. This meant that BAT required a constant supply of substrate that originated from a number of sources. First, food intake was increased by ~46% in rats that were acclimated to cold, providing an extra supply of glucose and fat. The increase in food intake was apparent immediately after initial exposure to cold reaching a plateau at day 3. Cold-induced SNS activation also stimulated lipolysis in the Epid and Sc Ing WAT depots, providing an additional source of NEFAs. Upregulation in the contents of β3-AdR, TH and ATGL, as well as phosphorylation of HSL facilitated the lipolytic response of these WAT. One

consequence of this enhanced lipolysis was a reduction in both Epid and Sc Ing fat masses, which would be of great therapeutic value to counteract the excessive accumulation of fat that characterizes obesity. The liver was another organ that provided substrate to fuel NST. Glycogen content was significantly reduced in the liver following cold exposure, showing that glycogenolysis was activated in this tissue in order to maintain glucose homeostasis. Furthermore, PEPCK and PGC-1α contents and the expression of *G6pase, Pgc-1α, Crtc2* and *FoxO1* were all increased. These responses are consistent with enhanced gluconeogenesis in the liver following cold exposure. Furthermore, both FA and glucose oxidation increased, which must have been crucial to provide ATP for the gluconeogenic process in the liver.

Despite increases in food intake, WAT lipolysis, and hepatic gluconeogenesis, there were no significant alterations in plasma NEFAs or glucose following cold acclimation, and plasma insulin was reduced by 28%. Plasma TAGs drastically dropped following cold exposure (see Supplementary Data). This was consistent with increased expression of *Lpl* and *Cd36* in iBAT, which provides evidence that lipolysis of TAGs from lipoproteins was enhanced and that FAs were being taken up by the BAT to fuel NST. A similar increase in *Lpl* and *Cd36* expression was also found in Sol and EDL muscles, suggesting that the same process was occurring in skeletal muscles with the FAs being used mainly to fuel shivering and NST in this tissue. In line with this data, FA oxidation was enhanced in oxidative and glycolytic muscles. Importantly, SLN was only detected in the Sol muscle and its content increased upon cold acclimation in this muscle. These findings indicate that the contribution of SLN to NST in skeletal muscles in fiber type-dependent. In this context, SLN-mediated SERCA uncoupling must have

contributed to accelerate glucose disposal in Sol muscles and probably also in other highly oxidative muscles. Consistent with this idea was the fact that *Glut4* expression was enhanced in the Sol following cold acclimation, suggesting that glucose transport was indeed enhanced in this muscle. Furthermore, we observed a significant increase in the glycogen synthesis rate and glycogen content in Sol muscles following cold acclimation. This was facilitated by an increase in phosphorylation of AKT and GSK3α and a reduction in the phosphorylation of GS. Glycogen synthesis is a major pathway for glucose disposal and maintenance of glucose homeostasis *in vivo* (124). Interestingly, only Sol muscles displayed increased ability to store glycogen under cold acclimating conditions. This was likely due to the fact that the Sol muscle can also rely on FAs for energy production, so some glucose can be diverted toward glycogen synthesis in this muscle.

The significant clearance of substrate from the circulation following BAT activation, specifically under hypoinsulinemic conditions, demonstrates that insulin sensitivity was enhanced under these conditions and highlights the potential effectiveness that this approach could have on the treatment of conditions where circulating plasma glucose and NEFAs are significantly elevated as is the case for obesity and T2D.

In addition to activation of BAT, cold acclimation increased UCP1 content in the Sc Ing WAT. We hypothesized that this increase in UCP1 content would promote mitochondrial uncoupling and increase FA and glucose oxidation in this fat depot, similarly to what is observed in BAT. However, contrary to our hypothesis, no increases in substrate oxidation in the Sc Ing fat were found following cold acclimation.

Furthermore, oligomycin, an ATP synthase inhibitor, inhibited palmitate oxidation in Sc Ing fat adipocytes isolated from both control and cold-acclimated rats. Surprisingly, in Sc Ing adipocytes from cold-acclimated rats the inhibitory effect of oligomycin on FA oxidation was more pronounced that in control cells. These finding indicate that very little uncoupled respiration existed in the Sc Ing fat depot, and that cold-induced browning of this tissue even reduced substrate utilization through UCP1-mediated mitochondrial uncoupling. Instead, we found that a futile cycle of lipolysis and lipogenesis was activated in the Sc Ing fat depot. This futile cycle appears to be the main contributor to increases in energy expenditure from the Sc Ing fat during cold exposure. We did not observe any increase in UCP1 content or any evidence of a futile cycle of lipolysis and lipogenesis in the Epid fat.

Because FGF21 has been demonstrated to promote WAT browning under conditions of cold exposure, I conducted another study in order to examine the potential role of FGF21 in determining depot-specific effects with respect to cold-induced browning of the WAT. Even though circulating FGF21 was reduced with cold exposure, I found that FGF21 expression and release was increased in a depot-specific manner. In fact, I obtained evidence that FGF21 acted in an autocrine/paracrine manner in iBAT and Sc Ing WAT depots. This was supported by increases in expression and content of FGF21 in iBAT and Sc Ing WAT, and also by enhanced FGF21 secretion in the latter tissue. Furthermore, downstream FGF21 signaling was enhanced in iBAT and Sc Ing WAT, but not the Epid WAT with cold acclimation, providing a mechanistic explanation for the differences in the induction of browning (increased UCP1 content) observed between the Sc Ing and Epid WAT.

Similarly to BAT activation, administration of oxfenicine is another way of significantly perturbing the system that leads to enhanced insulin sensitivity. The main idea was to force glucose utilization by blocking the ability of tissues that contain CPT1b to oxidize long-chain fatty acids. The effects of oxfenicine on insulin sensitivity were most apparent in HF-fed rats that showed a reduction in AUC for glycemia and reduced plasma insulin levels. Changes in glucose uptake and insulin sensitivity were likely secondary to the fact that these tissues were requiring and oxidizing more glucose because FA oxidation was inhibited. An additional consequence of oxfenicine treatment was an increase in plasma NEFAs. We hypothesized that the WAT would alter its metabolism following oxfenicine treatment in order to accommodate this increase by reducing lipolysis or the release of NEFAs and by increasing lipogenesis or the storage of NEFAs. Our results showed that lipolysis was indeed reduced with oxfenicine treatment, but that lipogenesis was also reduced. However this reduction in lipogenesis likely explains the reduction in fat mass that was also observed with oxfenicine treatment and demonstrates that in addition to improving insulin sensitivity, this pharmacological approach could also reduce fat mass.

In summary, this dissertation provides evidence that both a pharmacological selective inhibition of β-oxidation and activation of BAT could be used as therapeutic approaches for the treatment of obesity and T2D, conditions characterized by insulin resistance and excess fat mass. These novel alternative therapeutic approaches could be of particular importance to individuals who do not tolerate current pharmacological treatment options or who have difficulty maintaining weight loss through traditional methods (e.g. dietary restriction and exercise).

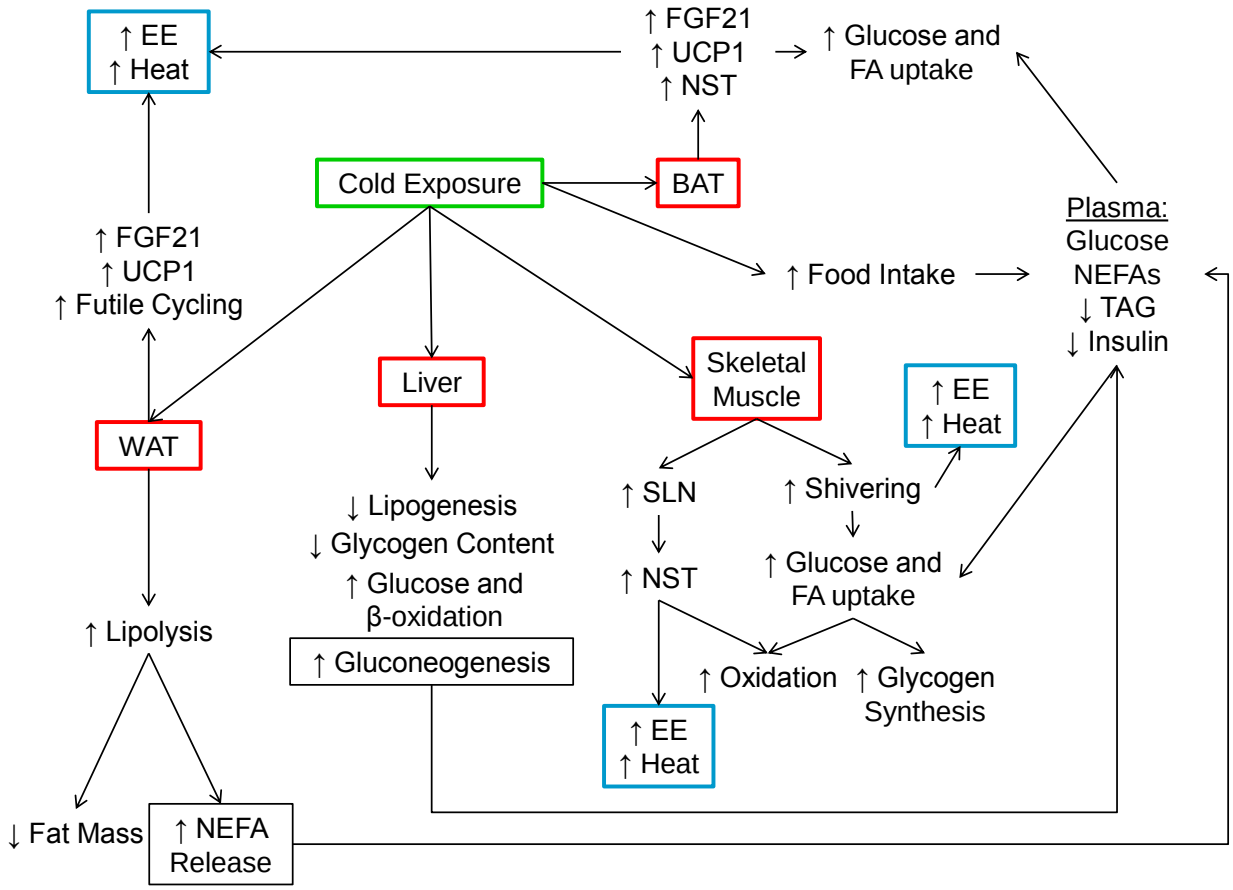

Figure 9-1: BAT, WAT, liver and skeletal muscle adaptations to cold exposure. Cold exposure induces UCP1 in the BAT and enhances NST which increases energy expenditure in this tissue and produces heat. The BAT takes up FA and glucose from the circulation in order to fuel the energy-consuming process of NST. FA and glucose in the circulation are provided through an increase in food intake, an increase in lipolysis from the WAT and an increase in glycogenolysis and gluconeogenesis from the liver. The skeletal muscle also generates heat through both shivering thermogenesis and SLN-mediated NST. Thus, FA and glucose uptake is also enhanced in the skeletal muscle following cold exposure. In addition to increases in substrate oxidation, muscles rich in type I fibers also increase their rate of glycogen synthesis and glycogen content. Glycogen content is significantly reduced in the liver as it undergoes glycogenolysis to release glucose into the circulation. Lipogenesis is also reduced while FA and glucose oxidation are enhanced in this organ in order to provide ATP for the process of gluconeogenesis. While the WAT undergoes lipolysis, there is also depot-specific browning of the Sc Ing WAT that occurs following cold exposure. Though UCP1 content is increased in this depot, substrate oxidation is not enhanced. Instead, a futile cycle of lipolysis and lipogenesis is activated that is the main contributor to increased energy expenditure and heat production from this depot. FGF21 is a hormone that could potentially explain the depot-specific differences in browning between the Sc Ing and Epid WAT.

CHAPTER 10: Study Limitations

Although every effort was made in the design and execution of the studies in this dissertation to control for variables, it must be acknowledged that limitations do exist.

In chapter 4, in order to investigate the direct effects of oxfenicine on WAT metabolism, I used isolated adipocytes from lean, control rats. These adipocytes had not been chronically exposed to oxfenicine nor to the effects of a HF diet and their responsiveness to the drug may have differed with longer-term exposure to either of these factors. This may explain some of the discrepancies between my *in vivo* and *ex vivo* data in this study. Furthermore, while this study used oxfenicine, a specific inhibitor of CPT-1b, I did not investigate the effects that oxfenicine treatment may have had on other tissues that express the CPT-1b isoform such as the BAT and heart. Alterations in metabolism in these tissues, particularly with regards to the BAT and its role in DIT, could have been involved in mediating some of the whole body alterations seen with oxfenicine treatment.

In chapters 5, 6, 7 and 8 my control animals were housed at 22°C which is below thermalneutrality for a rat (28°C) (270). At 22°C it is likely that the BAT of the rats would have been partially activated and other changes in metabolism in peripheral tissues could have occurred. Thus, the magnitude of the changes I observed could have been blunted by the fact that the thermogenic response was already activated at 22°C prior to our cold exposure. With my measurements I was also not able to determine individual tissue contributions to energy expenditure that were observed following cold adaptation. Given the enhancement in BAT mass, UCP1 content and substrate oxidation, I know that this tissue was activated and generated heat under cold conditions. However I also

observed the activation of a futile cycle of lipolysis and lipogenesis in the Sc Ing WAT that would also have enhanced energy expenditure from this fat, and shivering and NST were also activated in the skeletal muscle following cold exposure. Further experiments in rodents with the iBAT and/or Sc Ing fat pads removed would be required in order to determine individual tissue contributions.

In chapter 6 I showed that FGF21 acted in an autocrine manner in the iBAT and Sc Ing WAT as content was increased in these two fat depots and downstream signaling was activated following cold exposure. However, I would need to run additional experiments in rodents lacking FGF21 specifically in the adipose tissue in order to determine if this hormone is essential for the full activation of BAT and browning of the Sc Ing Wat under cold conditions.

In chapters 5 and 7 I eluded to the fact that both the BAT and skeletal muscle (particularly muscle rich in type I fibers) take up significant amounts of FAs and glucose following cold adaptation; however, I was not able to quantify the exact amount of glucose or FAs that was taken up by the individual tissues and thus could not comment on each tissue's individual contribution to maintaining plasma glucose and FAs levels. Additional experiments using labelled metabolites would be required to determine specific tissue contributions.

Finally in chapter 8, I present data to provide substantial evidence of the activation and enhancement of gluconeogenesis in the liver following cold exposure; however, I do not have any data from an accompanying functional assay to show that the process is increased following cold exposure.

CHAPTER 11: Future Directions

Seven days of cold exposure significantly increased UCP1 content in the Sc Ing WAT, but did not result in any increase in FA oxidation in this depot. However there was evidence of a futile cycle of lipolysis and re-esterification in this depot, suggesting that the major contribution of this depot to increasing energy expenditure during cold exposure was through this futile cycle and not UCP1-derived NST. However the effects of a longer cold adaptation period on NST and futile cycling in the Sc Ing WAT are currently unknown. To investigate this further, male Wistar rats (~400 g) would be exposed to 4°C for a much longer period, probably one month or even longer. Body weight and food intake would be measured on a daily basis and blood samples taken on a daily basis for analysis of glucose, insulin, NEFAs and TAGs. At the end of the cold protocol, animals would be placed in the CLAMS to measure VO_2, RER, energy expenditure and ambulatory activity. Following the cold exposure period, animals will be anesthetized and the Epid and Sc Ing WAT extracted and weighed. Some of the tissue would be frozen at -80°C for western blotting of proteins involved in NST, substrate partitioning and lipolysis (β3-Adr, TH, UCP1, ATGL and total and phosphorylated AMPK and HSL). Gene expression analysis would examine the induction of *Gyk* and FA transporters. The remaining tissue would be used for the isolation of adipocytes for the measurement of basal and stimulated lipolysis, palmitate and glucose oxidation, and glycerol incorporation into lipids. This work will provide insight into the activation of NST and futile cycling following long-term cold exposure in the Sc Ing WAT and provide information as to the contribution of this depot to increasing energy expenditure under these conditions.

It has been shown that treatment with FGF21 leads to increases in the expression of *Ucp1* and other thermogenic genes in both BAT and Sc Ing WAT (108, 109, 290, 291), providing evidence of a role of FGF21 in activating the BAT and inducing browning in the Sc Ing WAT. FGF21 has been shown to be induced by cold exposure and β-adrenergic agonists and thus could provide a mechanistic link between cold exposure and the activation of thermogenesis in the BAT and Sc Ing WAT. The data from this dissertation provide further evidence of this role of FGF21 as content and expression of FGF21 was increased in the iBAT and Sc Ing WAT following cold exposure. In addition, cold exposure increased the expression of *Fgfr1* and *β-klotho* and increased the phosphorylation of ERK1/2 in the iBAT and Sc Ing WAT, providing evidence that FGF21 can be produced and act in an autocrine/paracrine manner on the iBAT and Sc Ing WAT. Interestingly, FGF21 treatment has also been shown to enhance the expression of genes involved in lipolysis and TAG synthesis in the WAT (290) suggesting that it could also be involved in regulating a futile cycle in the WAT. However, the exact contribution of FGF21 in mediating NST and the activation of a futile cycle in the Sc Ing WAT compared to the BAT and Epid WAT following cold exposure has not been previously investigated.

One approach to studying the role of FGF21 is through genetic manipulation in mice. $FGF21^{loxP}$ mice (C57BL/6 background) are commercially available from Jackson Laboratories (Stock# 022361, Bar Harbor, ME, USA). This strain could be bred with the commercially available Adipoq-Cre mouse (mouse carrying a transgene expressing Cre-recombinase under the control of the adiponectin promoter, Jackson Laboratories, C57BL/6 background, Stock# 028020) to specifically target FGF21 in the adipose

tissue. This particular genetic strain could then be used to determine the specific contribution of FGF21 in inducing the expression of thermogenic genes and/or activating a futile cycle in the WAT under cold conditions. These mice would be exposed to cold for seven days and food intake and body weight measurements would be taken on a daily basis. Blood samples would also be collected in the fed state in order to determine plasma concentrations of glucose, insulin, NEFAs, TAGs and FGF21. The animals would be placed in the CLAMS on day 6 of the cold exposure protocol in order to measure VO_2, energy expenditure, RER and ambulatory activity. At the end of the cold exposure protocol, the BAT, Epid and Sc Ing WAT will be extracted. A portion of the tissue will be frozen at -80°C for western blotting of proteins involved in NST, substrate partitioning and lipolysis (β3-Adr, TH, UCP1, ATGL and total and phosphorylated AMPK and HSL). Adipocytes will be isolated from the remaining tissue in order to measure palmitate and glucose oxidation, lipolysis and glycerol incorporation into lipids. We could also repeat the experiment in mice kept in the cold for a month to investigate the importance of FGF21 following a longer acclimation to the cold. This study will provide insight into the role of adipose tissue FGF21 in the activation of NST and futile cycling following cold exposure in the Epid and Sc Ing WAT and the contribution of these processes to increasing energy expenditure under cold conditions.

References

1. Zobel, E. H., Hansen, T. W., Rossing, P., and von Scholten, B. J. (2016) Global Changes in Food Supply and the Obesity Epidemic. *Curr. Obes. Rep.* 10.1007/s13679-016-0233-8

2. Janssen, I. (2013) The Public Health Burden of Obesity in Canada. *Can. J. Diabetes*. **37**, 90–96

3. Keith, S. W., Redden, D. T., Katzmarzyk, P. T., Boggiano, M. M., Hanlon, E. C., Benca, R. M., Ruden, D., Pietrobelli, A., Barger, J. L., Fontaine, K. R., Wang, C., Aronne, L. J., Wright, S. M., Baskin, M., Dhurandhar, N. V, Lijoi, M. C., Grilo, C. M., DeLuca, M., Westfall, A. O., and Allison, D. B. (2006) Putative contributors to the secular increase in obesity: exploring the roads less traveled. *Int. J. Obes. (Lond).* **30**, 1585–1594

4. Weiss, E. C., Galuska, D. A., Kettel Khan, L., Gillespie, C., and Serdula, M. K. (2007) Weight Regain in U.S. Adults Who Experienced Substantial Weight Loss, 1999-2002. *Am. J. Prev. Med.* **33**, 34–40

5. MacLean, P. S., Wing, R. R., Davidson, T., Epstein, L., Goodpaster, B., Hall, K. D., Levin, B. E., Perri, M. G., Rolls, B. J., Rosenbaum, M., Rothman, A. J., and Ryan, D. (2015) NIH working group report: Innovative research to improve maintenance of weight loss. *Obesity (Silver Spring).* **23**, 7–15

6. Ross, R., and Bradshaw, A. J. (2009) The future of obesity reduction: beyond weight loss. *Nat. Rev. Endocrinol.* **5**, 319–326

7. Wadden, T. A., Hollander, P., Klein, S., Niswender, K., Woo, V., Hale, P. M., and Aronne, L. (2015) Weight maintenance and additional weight loss with liraglutide after low-calorie-diet-induced weight loss: The SCALE Maintenance randomized study. *Int. J. Obes.* **39**, 187–187

8. Yanovski, S., Yanovski, and JA (2014) Long-term Drug Treatment for Obesity: A Systematic and Clinical Review. *Jama*. **311**, 74–86

9. Sjostrom, L., Rissanen, A., Andersen, T., Boldrin, M., Golay, A., Koppeschaar-Hans, P. F., and Krempf, M. (1998) Randomised placebo-controlled trial of orlistat for weight loss and prevention of weight regain in obese patients. *Lancet North Am.* **352**, 173

10. Fruhbeck, G. (2008) Overview of Adipose Tissue and Its Role in Obesity and Metabolic Disorders. in *Adipose Tissue Protocols*, 2nd Ed. (Yang, K. ed), pp. 1–22, Humana Press Inc., London, ON

11. Lee, M.-J., Wu, Y., and Fried, S. K. (2013) Adipose tissue heterogeneity: implication of depot differences in adipose tissue for obesity complications. *Mol.*

Aspects Med. **34**, 1–11

12. Seale, P. (2015) Transcriptional regulatory circuits controlling brown fat development and activation. *Diabetes*. **64**, 2369–2375

13. Cinti, S. (2009) Transdifferentiation properties of adipocytes in the adipose organ. *Am. J. Physiol. Endocrinol. Metab.* **297**, E977-86

14. Ibrahim, M. M. (2010) Subcutaneous and visceral adipose tissue: structural and functional differences. *Obes. Rev.* **11**, 11–8

15. Gaidhu, M., Anthony, N., Patel, P., Hawke, T., and Ceddia, R. B. (2010) Dysregulation of lipolysis and lipid metabolism in visceral and subcutaneous adipocytes by high-fat diet: role of ATGL, HSL, and AMPK. *Am. J. Physiol. Cell Physiol.* **298**, C961–C971

16. Tchkonia, T., Thomou, T., Zhu, Y., Karagiannides, I., Pothoulakis, C., Jensen, M. D., and Kirkland, J. L. (2013) Mechanisms and metabolic implications of regional differences among fat depots. *Cell Metab.* **17**, 644–656

17. Rosen, E. D., and Spiegelman, B. M. (2006) Adipocytes as regulators of energy balance and glucose homeostasis. *Nature*. **444**, 847–53

18. Luo, L., and Liu, M. (2016) Adipose tissue in control of metabolism. *J. Endocrinol.* **231**, R77–R99

19. Gaidhu, M. P., Frontini, A., Hung, S., Pistor, K., Cinti, S., and Ceddia, R. B. (2011) Chronic AMP-kinase activation with AICAR reduces adiposity by remodeling adipocyte metabolism and increasing leptin sensitivity. *J. Lipid Res.* **52**, 1702–11

20. Ceddia, R. B., Somwar, R., Maida, a, Fang, X., Bikopoulos, G., and Sweeney, G. (2005) Globular adiponectin increases GLUT4 translocation and glucose uptake but reduces glycogen synthesis in rat skeletal muscle cells. *Diabetologia*. **48**, 132–9

21. Forest, C., Tordjman, J., Glorian, M., Duplus, E., Chauvet, G., Quette, J., Beale, E. G., and Antoine, B. (2003) Fatty acid recycling in adipocytes: a role for glyceroneogenesis and phosphoenolpyruvate carboxykinase. *Biochem. Soc. Trans.* **31**, 1125–1129

22. Millward, C. a, Desantis, D., Hsieh, C.-W., Heaney, J. D., Pisano, S., Olswang, Y., Reshef, L., Beidelschies, M., Puchowicz, M., and Croniger, C. M. (2010) Phosphoenolpyruvate carboxykinase (Pck1) helps regulate the triglyceride/fatty acid cycle and development of insulin resistance in mice. *J. Lipid Res.* **51**, 1452–63

23. Griffin, M. J., and Sul, H. S. (2004) Insulin regulation of fatty acid synthase gene transcription: roles of USF and SREBP-1c. *IUBMB Life*. **56**, 595–600

24. Foufelle, F., Gouhot, B., Perdereau, D., Girard, J., and Ferre, P. (1994) Regulation of lipogenic enzyme and phosphoenolpyruvate carboxykinase gene expression in cultured white adipose tissue: Glucose and insulin effects are antagonized by cAMP. *Eur. J. Biochem.* **223**, 893–900

25. Reshef, L., Olswang, Y., Cassuto, H., Blum, B., Croniger, C. M., Kalhan, S. C., Tilghman, S. M., and Hanson, R. W. (2003) Glyceroneogenesis and the triglyceride/fatty acid cycle. *J. Biol. Chem.* **278**, 30413–30416

26. Leto, D., and Saltiel, A. R. (2012) Regulation of glucose transport by insulin: traffic control of GLUT4. *Nat. Rev. Mol. Cell Biol.* **13**, 383–96

27. Thong, F. S. L., Dugani, C. B., and Klip, A. (2005) Turning signals on and off: GLUT4 traffic in the insulin-signaling highway. *Physiology (Bethesda).* **20**, 271–284

28. Madeira, A., Moura, T. F., and Soveral, G. (2015) Aquaglyceroporins: Implications in adipose biology and obesity. *Cell. Mol. Life Sci.* **72**, 759–771

29. Olswang, Y., Blum, B., Cassuto, H., Cohen, H., Biberman, Y., Hanson, R. W., and Reshef, L. (2003) Glucocorticoids repress transcription of phosphoenolpyruvate carboxykinase (GTP) gene in adipocytes by inhibiting its C/EBP-mediated activation. *J. Biol. Chem.* **278**, 12929–12936

30. Tesmer, J. J., Sunahara, R. K., Gilman, a G., and Sprang, S. R. (1997) Crystal structure of the catalytic domains of adenylyl cyclase in a complex with Gsalpha.GTPgammaS. *Science*. **278**, 1907–1916

31. Zimmermann, R., Strauss, J. G., Haemmerle, G., Schoiswohl, G., Birner-Gruenberger, R., Riederer, M., Lass, A., Neuberger, G., Eisenhaber, F., Hermetter, A., and Zechner, R. (2004) Fat mobilization in adipose tissue is promoted by adipose triglyceride lipase. *Science*. **306**, 1383–1386

32. Miyoshi, H., Souza, S. C., Zhang, H. H., Strissel, K. J., Christoffolete, M. a., Kovsan, J., Rudich, A., Kraemer, F. B., Bianco, A. C., Obin, M. S., and Greenberg, A. S. (2006) Perilipin promotes hormone-sensitive lipase-mediated adipocyte lipolysis via phosphorylation-dependent and -independent mechanisms. *J. Biol. Chem.* **281**, 15837–15844

33. Sztalryd, C., Xu, G., Dorward, H., Tansey, J. T., Contreras, J. a., Kimmel, A. R., and Londos, C. (2003) Perilipin A is essential for the translocation of hormone-sensitive lipase during lipolytic activation. *J. Cell Biol.* **161**, 1093–1103

34. Duncan, R. E., Ahmadian, M., Jaworski, K., Sarkadi-Nagy, E., and Hei, S. S. (2007) Regulation of lipolysis in adipocytes. *Annu. Rev. Nutr.* **27**, 79–101

35. Lass, A., Zimmermann, R., Haemmerle, G., Riederer, M., Schoiswohl, G., Schweiger, M., Kienesberger, P., Strauss, J. G., Gorkiewicz, G., and Zechner, R.

(2006) Adipose triglyceride lipase-mediated lipolysis of cellular fat stores is activated by CGI-58 and defective in Chanarin-Dorfman Syndrome. *Cell Metab.* **3**, 309–319

36. Granneman, J. G., Moore, H. P. H., Krishnamoorthy, R., and Rathod, M. (2009) Perilipin controls lipolysis by regulating the interactions of AB-hydrolase containing 5 (Abhd5) and adipose triglyceride lipase (Atgl). *J. Biol. Chem.* **284**, 34538–34544

37. Subramanian, V., Rotlienberg, A., Gomez, C., Cohen, A. W., Garcia, A., Bhattacharyya, S., Shapiro, L., Dolios, G., Wang, R., Lisanti, M. P., and Brasaemle, D. L. (2004) Perilipin A mediates the reversible binding of CGI-58 to lipid droplets in 3T3-L1 adipocytes. *J. Biol. Chem.* **279**, 42062–42071

38. Yamaguchi, T., Omatsu, N., Matsushita, S., and Osumi, T. (2004) CGI-58 interacts with perilipin and is localized to lipid droplets: Possible involvement of CGI-58 mislocalization in Chanarin-Dorfman syndrome. *J. Biol. Chem.* **279**, 30490–30497

39. Langin, D., Dicker, A., Tavernier, G., Hoffstedt, J., Mairal, A., Rydén, M., Arner, E., Sicard, A., Jenkins, C. M., Viguerie, N., Van Harmelen, V., Gross, R. W., Holm, C., and Arner, P. (2005) Adipocyte lipases and defect of lipolysis in human obesity. *Diabetes*. **54**, 3190–3197

40. Lass, A., Zimmermann, R., Oberer, M., and Zechner, R. (2011) Lipolysis - A highly regulated multi-enzyme complex mediates the catabolism of cellular fat stores. *Prog. Lipid Res.* **50**, 14–27

41. Lafontan, M., and Berlan, M. (1995) Fat cell alpha2-adrenoceptors: The regulation of fat cell function and lipolysis. *Endocr. Rev.* **16**, 716–738

42. Manolopoulos, K. N., Karpe, F., and Frayn, K. N. (2012) Marked resistance of femoral adipose tissue blood flow and lipolysis to adrenaline in vivo. *Diabetologia*. **55**, 3029–3037

43. Londos, C., Honner, R. C., and Dhillon, G. S. (1985) cAMP-dependent protein kinase and lipolysis in rat adipocytes. III. Multiple modes of insulin regulation of lipolysis and regulation of insulin responses by adenylate cyclase regulators. *J. Biol. Chem.* **260**, 15139–15145

44. Ragolia, L., and Begum, N. (1998) Protein phosphatase-1 and insulin action. *Mol. Cell. Biochem.* **182**, 49–58

45. Arner, P., and Langin, D. (2014) Lipolysis in lipid turnover, cancer cachexia, and obesity-induced insulin resistance. *Trends Endocrinol. Metab.* **25**, 255–262

46. Olsson, H., and Belfrage, P. (1987) The regulatory and basal phosphorylation sites of hormone-sensitive lipase are dephosphorylated by protein phosphatase-1,

2A and 2C but not by protein phosphatase-2B. *Eur. J. Biochem.* **168**, 399–405

47. Ceddia, R. B. (2013) The role of AMP-activated protein kinase in regulating white adipose tissue metabolism. *Mol. Cell. Endocrinol.* **366**, 194–203

48. Anthony, N. M., Gaidhu, M. P., and Ceddia, R. B. (2009) Regulation of visceral and subcutaneous adipocyte lipolysis by acute AICAR-induced AMPK activation. *Obesity (Silver Spring).* **17**, 1312–7

49. Gaidhu, M. P., Fediuc, S., Anthony, N. M., So, M., Mirpourian, M., Perry, R. L. S., and Ceddia, R. B. (2009) Prolonged AICAR-induced AMP-kinase activation promotes energy dissipation in white adipocytes: novel mechanisms integrating HSL and ATGL. *J. Lipid Res.* **50**, 704–15

50. Horowitz, J. F., and Klein, S. (2000) Lipid metabolism during endurance exercise. *Am. J. Clin. Nutr.* **72**, 558S–63S

51. Winder, W. W., Hickson, R. C., Hagberg, J. M., Ehsani, A. A., and McLane, J. A. (1979) Training-induced changes in hormonal and metabolic responses to submaximal exercise. *J. Appl. Physiol.* **46**, 766–71

52. Koivisto, V., Hendler, R., Nadel, E., and Felig, P. (1982) Influence of physical training on the fuel-hormone response to prolonged low intensity exercise. *Metabolism.* **31**, 192–7

53. Hurley, B. F., Nemeth, P. M., Martin, W. H., Hagberg, J. M., Dalsky, G. P., and Holloszy, J. O. (1986) Muscle triglyceride utilization during exercise: effect of training. *J. Appl. Physiol.* **60**, 562–7

54. Martin, W. H., Dalsky, G. P., Hurley, B. F., Matthews, D. E., Bier, D. M., Hagberg, J. M., Rogers, M. A., King, D. S., and Holloszy, J. O. (1993) Effect of endurance training on plasma free fatty acid turnover and oxidation during exercise. *Am. J. Physiol.* **265**, E708-14

55. Phillips, S. M., Green, H. J., Tarnopolsky, M. A., Heigenhauser, G. F., Hill, R. E., and Grant, S. M. (1996) Effects of training duration on substrate turnover and oxidation during exercise. *J. Appl. Physiol.* **81**, 2182–91

56. Crampes, F., Riviere, D., Beauville, M., Marceron, M., and Garrigues, M. (1989) Lipolytic response of adipocytes to epinephrine in sedentary and exercise-trained subjects: sex-related differences. *Eur. J. Appl. Physiol. Occup. Physiol.* **59**, 249–55

57. De Glisezinski, I., Crampes, F., Harant, I., Berlan, M., Hejnova, J., Langin, D., Rivière, D., and Stich, V. (1998) Endurance training changes in lipolytic responsiveness of obese adipose tissue. *Am. J. Physiol.* **275**, E951-6

58. Després, J. P., Bouchard, C., Savard, R., Tremblay, A., Marcotte, M., and

Thériault, G. (1984) The effect of a 20-week endurance training program on adipose-tissue morphology and lipolysis in men and women. *Metabolism.* **33**, 235–9

59. Parizkova, J., and Stankova, L. (1964) Influence of physical activity on a treadmill on the metabolism of adipose tissue in rats. *Br. J. Nutr.* **18**, 325–32

60. Ogasawara, J., Sakurai, T., Kizaki, T., Ishibashi, Y., Izawa, T., Sumitani, Y., Ishida, H., Radak, Z., Haga, S., and Ohno, H. (2012) Higher levels of ATGL are associated with exercise-induced enhancement of lipolysis in rat epididymal adipocytes. *PLoS One*. **7**, e40876

61. Pistor, K. E., Sepa-Kishi, D. M., Hung, S., and Ceddia, R. B. (2014) Lipolysis, lipogenesis, and adiposity are reduced while fatty acid oxidation is increased in visceral and subcutaneous adipocytes of endurance-trained rats. *Adipocyte*. **4**, 22–31

62. Yu, J., Zhang, S., Cui, L., Wang, W., Na, H., Zhu, X., Li, L., Xu, G., Yang, F., Christian, M., and Liu, P. (2015) Lipid droplet remodeling and interaction with mitochondria in mouse brown adipose tissue during cold treatment. *Biochim. Biophys. Acta - Mol. Cell Res.* **1853**, 918–928

63. Cannon, B., and Nedergaard, J. (2004) Brown adipose tissue: function and physiological significance. *Physiol. Rev.* **84**, 277–359

64. van Marken Lichtenbelt, W. D., Vanhommerig, J. W., Smulders, N. M., Drossaerts, J. M. A. F. L., Kemerink, G. J., Bouvy, N. D., Schrauwen, P., and Teule, G. J. J. (2009) Cold-activated brown adipose tissue in healthy men. *N. Engl. J. Med.* **360**, 1500–8

65. Virtanen, K. A., Lidell, M. E., Orava, J., Heglind, M., Westergren, R., Niemi, T., Taittonen, M., Laine, J., Savisto, N.-J., Enerbäck, S., and Nuutila, P. (2009) Functional brown adipose tissue in healthy adults. *N. Engl. J. Med.* **360**, 1518–25

66. Tseng, Y.-H., Kokkotou, E., Schulz, T. J., Huang, T. L., Winnay, J., Taniguchi, C. M., Tran, T. T., Suzuki, R., Espinoza, D. O., Yamamoto, Y., Ahrens, M. J., Dudley, A. T., Norris, A. W., Kulkarni, R. N., and Kahn, C. R. (2008) New role of bone morphogenic protein 7 in brown adipogenesis and energy expenditure. *Nature*. **454**, 1000–1006

67. Seale, P., Bjork, B., Yang, W., Kajimura, S., Chin, S., Kuang, S., Scimè, A., Devarakonda, S., Conroe, H. M., Erdjument-Bromage, H., Tempst, P., Rudnicki, M. A., Beier, D. R., and Spiegelman, B. M. (2008) PRDM16 controls a brown fat/skeletal muscle switch. *Nature*

68. Kajimura, S., Seale, P., Tomaru, T., Erdjument-Bromage, H., Cooper, M. P., Ruas, J. L., Chin, S., Tempst, P., Lazar, M. A., and Spiegelman, B. M. (2008) Regulation of the brown and white fat gene programs through a PRDM16/CtBP

transcriptional complex. *Genes Dev.* **22**, 1397–1409

69. Iida, S., Chen, W., Nakadai, T., Ohkuma, Y., and Roeder, R. G. (2015) PRDM16 enhances nuclear receptor-dependent transcription of the brown fat-specific Ucp1 gene through interactions with Mediator subunit MED1. *Genes Dev.* **29**, 308–321

70. Seale, P., Kajimura, S., Yang, W., Chin, S., Rohas, L. M., Uldry, M., Tavernier, G., Langin, D., and Spiegelman, B. M. (2007) Transcriptional control of brown fat determination by PRDM16. *Cell Metab.* **6**, 38–54

71. Hondares, E., Rosell, M., Díaz-Delfín, J., Olmos, Y., Monsalve, M., Iglesias, R., Villarroya, F., and Giralt, M. (2011) Peroxisome proliferator-activated receptor α (PPARα) induces PPARγ coactivator 1α (PGC-1α) gene expression and contributes to thermogenic activation of brown fat: involvement of PRDM16. *J. Biol. Chem.* **286**, 43112–22

72. Puigserver, P., Wu, Z., Park, C. W., Graves, R., Wright, M., and Spiegelman, B. M. (1998) A cold-inducible coactivator of nuclear receptors linked to adaptive thermogenesis. *Cell*. **92**, 829–39

73. Rodgers, J. T., Lerin, C., Haas, W., Gygi, S. P., Spiegelman, B. M., and Puigserver, P. (2005) Nutrient control of glucose homeostasis through a complex of PGC-1a and SIRT1. *Nature*. **434**, 113–118

74. Fu, T., Seok, S., Choi, S., Huang, Z., Suino-Powell, K., Xu, H. E., Kemper, B., and Kemper, J. K. (2014) MicroRNA 34a Inhibits Beige and Brown Fat Formation in Obesity in Part by Suppressing Adipocyte Fibroblast Growth Factor 21 Signaling and SIRT1 Function. *Mol. Cell. Biol.* **34**, 4130–4142

75. Zhang, H., Guan, M., Townsend, K. L., Huang, T. L., An, D., Yan, X., Schulz, T. J., Winnay, J., Mori, M., Hirshman, M. F., Kristiansen, K., Tsang, J. S., White, A. P., Cypess, A. M., Goodyear, L. J., and Tseng, Y. (2015) MicroRNA- 455 regulates brown adipogenesis via a novel HIF 1 an-AMPK-PGC 1 a signaling network. *EMBO Rep.* **16**, 1378–1393

76. Souza, S. C., Christoffolete, M. a, Ribeiro, M. O., Miyoshi, H., Strissel, K. J., Stancheva, Z. S., Rogers, N. H., D'Eon, T. M., Perfield, J. W., Imachi, H., Obin, M. S., Bianco, A. C., and Greenberg, A. S. (2007) Perilipin regulates the thermogenic actions of norepinephrine in brown adipose tissue. *J. Lipid Res.* **48**, 1273–1279

77. De Jesus, L. A., Carvalho, S. D., Ribeiro, M. O., Schneider, M., Kim, S. W., Harney, J. W., Larsen, P. R., and Bianco, A. C. (2001) The type 2 iodothyronine deiodinase is essential for adaptive thermogenesis in brown adipose tissue. *J. Clin. Invest.* **108**, 1379–1385

78. Labbe, S. M., Caron, A., Bakan, I., Laplante, M., Carpentier, a. C., Lecomte, R., and Richard, D. (2015) In vivo measurement of energy substrate contribution to cold-induced brown adipose tissue thermogenesis. *FASEB J.* **29**, 2046–2058

79. Hao, Q., Yadav, R., Basse, a. L., Petersen, S., Sonne, S. B., Rasmussen, S., Zhu, Q., Lu, Z., Wang, J., Audouze, K., Gupta, R., Madsen, L., Kristiansen, K., and Hansen, J. B. (2014) Transcriptome profiling of brown adipose tissue during cold exposure reveals extensive regulation of glucose metabolism. *AJP Endocrinol. Metab.* **308**, 380–392

80. Hanssen, M. J. W., Hoeks, J., Brans, B., van der Lans, A. a J. J., Schaart, G., van den Driessche, J. J., Jörgensen, J. a, Boekschoten, M. V, Hesselink, M. K. C., Havekes, B., Kersten, S., Mottaghy, F. M., van Marken Lichtenbelt, W. D., and Schrauwen, P. (2015) Short-term cold acclimation improves insulin sensitivity in patients with type 2 diabetes mellitus. *Nat. Med.* **21**, 6–10

81. Bartelt, A., Bruns, O. T., Reimer, R., Hohenberg, H., Ittrich, H., Peldschus, K., Kaul, M. G., Tromsdorf, U. I., Weller, H., Waurisch, C., Eychmüller, A., Gordts, P. L. S. M., Rinninger, F., Bruegelmann, K., Freund, B., Nielsen, P., Merkel, M., and Heeren, J. (2011) Brown adipose tissue activity controls triglyceride clearance. *Nat. Med.* **17**, 200–5

82. Walden, T. B., Hansen, I. R., Timmons, J. a., Cannon, B., and Nedergaard, J. (2012) Recruited vs. nonrecruited molecular signatures of brown, “brite,” and white adipose tissues. *AJP Endocrinol. Metab.* **302**, E19–E31

83. Petrovic, N., Walden, T. B., Shabalina, I. G., Timmons, J. a., Cannon, B., and Nedergaard, J. (2010) Chronic peroxisome proliferator-activated receptor y (PPARy) activation of epididymally derived white adipocyte cultures reveals a population of thermogenically competent, UCP1-containing adipocytes molecularly distinct from classic brown adipocytes. *J. Biol. Chem.* **285**, 7153–7164

84. Wu, J., Boström, P., Sparks, L. M., Ye, L., Choi, J. H., Giang, A.-H., Khandekar, M., Virtanen, K. a, Nuutila, P., Schaart, G., Huang, K., Tu, H., van Marken Lichtenbelt, W. D., Hoeks, J., Enerbäck, S., Schrauwen, P., and Spiegelman, B. M. (2012) Beige adipocytes are a distinct type of thermogenic fat cell in mouse and human. *Cell*. **150**, 366–76

85. Cousin, B., Cinti, S., Morroni, M., Raimbault, S., Ricquier, D., Pénicaud, L., and Casteilla, L. (1992) Occurrence of brown adipocytes in rat white adipose tissue: molecular and morphological characterization. *J. Cell Sci.* **103**, 931–942

86. Seale, P., Conroe, H. M., Estall, J., Kajimura, S., Frontini, A., Ishibashi, J., Cohen, P., Cinti, S., and Spiegelman, B. M. (2011) Prdm16 determines the thermogenic program of subcutaneous white adipose tissue in mice. *J. Clin. Invest.* **121**, 96–105

87. Barneda, D., Frontini, A., Cinti, S., and Christian, M. (2013) Dynamic changes in lipid droplet-associated proteins in the “browning” of white adipose tissues. *Biochim. Biophys. Acta - Mol. Cell Biol. Lipids*. **1831**, 924–933

88. Shabalina, I., Petrovic, N., deJong, J. A., Kalinovich, A., Cannon, B., and Nedergaard, J. (2013) UCP1 in Brite/Beige adipose tissue mitochondria is functionally thermogenic. *Cell Rep.* **5**, 1196–1203

89. Himms-Hagen, J., Melnyk, a, Zingaretti, M. C., Ceresi, E., Barbatelli, G., and Cinti, S. (2000) Multilocular fat cells in WAT of CL-316243-treated rats derive directly from white adipocytes. *Am. J. Physiol. Cell Physiol.* **279**, C670–C681

90. Boström, P., Wu, J., Jedrychowski, M. P., Korde, A., Ye, L., Lo, J. C., Rasbach, K. a, Boström, E. A., Choi, J. H., Long, J. Z., Kajimura, S., Zingaretti, M. C., Vind, B. F., Tu, H., Cinti, S., Højlund, K., Gygi, S. P., and Spiegelman, B. M. (2012) A PGC1-α-dependent myokine that drives brown-fat-like development of white fat and thermogenesis. *Nature*. **481**, 463–8

91. Wu, M. V, Bikopoulos, G., Ceddia, R. B., Wu, M. V, Bikopoulos, G., Hung, S., and Ceddia, R. B. (2014) Thermogenic Capacity Is Antagonistically Regulated in Classical Brown and White Subcutaneous Fat Depots by High Fat Diet and Endurance Training in Rats: Impact on whole-body energy expenditure. *J. Biol. Chem.* **289**, 34129–34140

92. Sepa-Kishi, D. M., and Ceddia, R. B. (2016) Exercise-Mediated Effects on White and Brown Adipose Tissue Plasticity and Metabolism. *Exerc. Sport Sci. Rev.* **44**, 37–44

93. Barbatelli, G., Murano, I., Madsen, L., Hao, Q., Jimenez, M., Kristiansen, K., Giacobino, J. P., De Matteis, R., and Cinti, S. (2010) The emergence of cold-induced brown adipocytes in mouse white fat depots is determined predominantly by white to brown adipocyte transdifferentiation. *Am. J. Physiol. Endocrinol. Metab.* **298**, E1244-53

94. Labbé, S. M., Caron, A., Chechi, K., Laplante, M., Lecomte, R., and Richard, D. (2016) Metabolic activity of brown, beige,'' and white adipose in response to chronic adrenergic stimulation in male mice. *Am J Physiol Endocrinol Metab Am. J. Physiol. -Endocrinology Metab.* **311**, 260–268

95. De Matteis, R., Lucertini, F., Guescini, M., Polidori, E., Zeppa, S., Stocchi, V., Cinti, S., and Cuppini, R. (2013) Exercise as a new physiological stimulus for brown adipose tissue activity. *Nutr. Metab. Cardiovasc. Dis.* **23**, 582–90

96. Perakakis, N., Triantafyllou, G. A., Fernández-Real, J. M., Huh, J. Y., Park, K. H., Seufert, J., and Mantzoros, C. S. (2017) Physiology and role of irisin in glucose homeostasis. *Nat. Rev. Endocrinol.* **13**, 324–337

97. Raschke, S., Elsen, M., Gassenhuber, H., Sommerfeld, M., Schwahn, U., Brockmann, B., Jung, R., Wisløff, U., Tjønna, A. E., Raastad, T., Hallén, J., Norheim, F., Drevon, C. A., Romacho, T., Eckardt, K., and Eckel, J. (2013) Evidence against a beneficial effect of irisin in humans. *PLoS One*. **8**, e73680

98. Lowell, B. B., and Bachman, E. S. (2003) Beta-Adrenergic receptors, diet-induced thermogenesis, and obesity. *J. Biol. Chem.* **278**, 29385–8

99. Bachman, E. S., Dhillon, H., Zhang, C.-Y., Cinti, S., Bianco, A. C., Kobilka, B. K., and Lowell, B. B. (2002) betaAR signaling required for diet-induced thermogenesis and obesity resistance. *Science*. **297**, 843–845

100. Lee, P., Werner, C. D., Kebebew, E., and Celi, F. S. (2014) Functional thermogenic beige adipogenesis is inducible in human neck fat. *Int. J. Obes.* **38**, 170–176

101. Beenken, A., and Mohammadi, M. (2009) The FGF family: biology, pathophysiology and therapy. *Nat. Rev. Drug Discov.* **8**, 235–253

102. Badman, M. K., Pissios, P., Kennedy, A. R., Koukos, G., Flier, J. S., and Maratos-Flier, E. (2007) Hepatic Fibroblast Growth Factor 21 Is Regulated by PPARalpha and Is a Key Mediator of Hepatic Lipid Metabolism in Ketotic States. *Cell Metab.* **5**, 426–437

103. Ogawa, Y., Kurosu, H., Yamamoto, M., Nandi, A., Rosenblatt, K. P., Goetz, R., Eliseenkova, A. V, Mohammadi, M., and Kuro-o, M. (2007) betaKlotho is required for metabolic activity of fibroblast growth factor 21. *PNAS*. **104**, 7432–7437

104. Kurosu, H., Choi, M., Ogawa, Y., Dickson, A. S., Goetz, R., Eliseenkova, A. V, Mohammadi, M., Rosenblatt, K. P., Kliewer, S. a, and Kuro-o, M. (2007) Tissue-specific expression of betaKlotho and fibroblast growth factor (FGF) receptor isoforms determines metabolic activity of FGF19 and FGF21. *J. Biol. Chem.* **282**, 26687–95

105. Su, N., Jin, M., and Chen, L. (2014) Role of FGF/FGFR signaling in skeletal development and homeostasis: learning from mouse models. *Bone Res.* **2**, 14003

106. Roskoski, R. (2012) ERK1/2 MAP kinases: Structure, function, and regulation. *Pharmacol. Res.* **66**, 105–143

107. Kharitonenkov, A., Shiyanova, T. L., Koester, A., Ford, A. M., Micanovic, R., Galbreath, E. J., Sandusky, G. E., Hammond, L. J., Moyers, J. S., Owens, R. a, Gromada, J., Brozinick, J. T., Hawkins, E. D., Wroblewski, V. J., Li, D.-S., Mehrbod, F., Jaskunas, S. R., and Shanafelt, A. B. (2005) FGF-21 as a novel metabolic regulator. *J. Clin. Invest.* **115**, 1627–35

108. Fisher, F. M., Kleiner, S., Douris, N., Fox, E. C., Mepani, R. J., Verdeguer, F., Wu, J., Kharitonenkov, A., Flier, J. S., Maratos-Flier, E., and Spiegelman, B. M. (2012) FGF21 regulates PGC-1α and browning of white adipose tissues in adaptive thermogenesis. *Genes Dev.* **26**, 271–81

109. Hondares, E., Iglesias, R., Giralt, A., Gonzalez, F. J., Giralt, M., Mampel, T., and Villarroya, F. (2011) Thermogenic activation induces FGF21 expression and

release in brown adipose tissue. *J. Biol. Chem.* **286**, 12983–90

110. Elia, M. (1992) Organ and tissue contribution to metabolic rate. in *Energy metabolism: tissue determinants and cellular corrollaries* (Kinney, J., and Tucker, H. eds), pp. 61–80, Raven Press, New York, NY

111. Gehlert, S., Bloch, W., and Suhr, F. (2015) Ca2+-dependent regulations and signaling in skeletal muscle: From electro-mechanical coupling to adaptation. *Int. J. Mol. Sci.* **16**, 1066–1095

112. Blaauw, B., Schiaffino, S., and Reggiani, C. (2013) Mechanisms modulating skeletal muscle phenotype. *Compr. Physiol.* **3**, 1645–1687

113. Rebbeck, R. T., Karunasekara, Y., Board, P. G., Beard, N. A., Casarotto, M. G., and Dulhunty, A. F. (2014) Skeletal muscle excitation-contraction coupling: Who are the dancing partners? *Int. J. Biochem. Cell Biol.* **48**, 28–38

114. Tupling, a. R., Bombardier, E., Gupta, S. C., Hussain, D., Vigna, C., Bloemberg, D., Quadrilatero, J., Trivieri, M. G., Babu, G. J., Backx, P. H., Periasamy, M., MacLennan, D. H., and Gramolini, a. O. (2011) Enhanced Ca2+ transport and muscle relaxation in skeletal muscle from sarcolipin-null mice. *AJP Cell Physiol.* **301**, C841–C849

115. Sahlin, K., and Harris, R. C. (2011) The creatine kinase reaction: a simple reaction with functional complexity. *Amino Acids*. **40**, 1363–1367

116. Elliott, W. H., and Elliott, D. C. (2009) *Biochemistry and Molecular Biology*, 4th Ed., Oxford University Press, Toronto

117. Fisher-Wellman, K. H., and Neufer, P. D. (2012) Linking mitochondrial bioenergetics to insulin resistance via redox biology. *Trends Endocrinol. Metab.* **23**, 142–153

118. Rossi, A. C., Mammucari, C., Argentini, C., Reggiani, C., and Schiaffino, S. (2010) Two novel/ancient myosins in mammalian skeletal muscles: MYH14/7b and MYH15 are expressed in extraocular muscles and muscle spindles. *J. Physiol.* **588**, 353–64

119. Albers, P. H., Pedersen, A. J. T., Birk, J. B., Kristensen, D. E., Vind, B. F., Baba, O., Nøhr, J., Højlund, K., and Wojtaszewski, J. F. P. (2015) Human muscle fiber type-specific insulin signaling: Impact of obesity and type 2 diabetes. *Diabetes*. **64**, 485–497

120. Ausoni, S., Gorza, L., Schiaffino, S., Gundersen, K., and Lømo, T. (1990) Expression of myosin heavy chain isoforms in stimulated fast and slow rat muscles. *J. Neurosci.* **10**, 153–160

121. Gouspillou, G., Sgarioto, N., Norris, B., Barbat-Artigas, S., Aubertin-Leheudre, M.,

Morais, J. A., Burelle, Y., Taivassalo, T., and Hepple, R. T. (2014) The relationship between muscle fiber type-specific PGC-1alpha content and mitochondrial content varies between rodent models and humans. *PLoS One*. **9**, 1–14

122. Bouskila, M., Hunter, R. W., Ibrahim, A. F. M., Delattre, L., Peggie, M., Van Diepen, J. A., Voshol, P. J., Jensen, J., and Sakamoto, K. (2010) Allosteric regulation of glycogen synthase controls glycogen synthesis in muscle. *Cell Metab.* **12**, 456–466

123. Jensen, J., and Lai, Y.-C. (2009) Regulation of muscle glycogen synthase phosphorylation and kinetic properties by insulin, exercise, adrenaline and role in insulin resistance. *Arch. Physiol. Biochem.* **115**, 13–21

124. Shulman, G. I., Rothman, D. L., Jue, T., Stein, P., DeFronzo, R. A., and Shulman, R. G. (1990) Quantitation of muscle glycogen synthesis in normal subjects and subjects with non-insulin-dependent diabetes by 13C nuclear magnetic resonance spectroscopy. *NEJM*. **322**, 223–228

125. Lillioja, S., Mott, D. M., Zawadzki, J. K., Young, A. A., Abbott, W. G., and Bogardus, C. (1986) Glucose storage is a major determinant of in vivo “insulin resistance” in subjects with normal glucose tolerance. *J. Clin. Endocrinol. Metab.* **62**, 922–927

126. Manabe, Y., Gollisch, K. S. C., Holton, L., Kim, Y. B., Fujii, N. L., Hirshman, M. F., and Goodyear, L. J. (2014) Increases in Skeletal Muscle Glycogen Content. *FEBS J.* **280**, 916–926

127. Suzuki, J., Gao, M., Ohinata, H., Kuroshima, A., and Koyama, T. (1997) Chronic cold exposure stimulates microvascular remodeling preferentially in oxidative muscles in rats. *Jpn. J. Physiol.* **47**, 513–520

128. Walters, T. J., and Constable, S. H. (1993) Intermittent cold exposure causes a muscle-specific shift in the fiber type composition in rats. *J. Appl. Physiol.* **75**, 264–267

129. Mizunoya, W., Iwamoto, Y., Sato, Y., Tatsumi, R., and Ikeuchi, Y. (2014) Cold exposure increases slow-type myosin heavy chain 1 (MyHC1) composition of soleus muscle in rats. *Anim. Sci. J.* **85**, 293–304

130. Soni, A., and Katoch, S. S. (1997) Structural and metabolic changes in skeletal muscle of cold acclimated rats. *J. Therm. Biol.* **22**, 95–107

131. Bukowiecki, L. J. (1989) Energy balance and diabetes. The effects of cold exposure, exercise training, and diet composition on glucose tolerance and glucose metabolism in rat peripheral tissues. *Can. J. Physiol. Pharmacol.* **67**, 382–93

132. Ziętak, M., Kovatcheva-Datchary, P., Markiewicz, L. H., Ståhlman, M., Kozak, L. P., and Bäckhed, F. (2016) Altered Microbiota Contributes to Reduced Diet-Induced Obesity upon Cold Exposure. *Cell Metab.* **23**, 1216–1223

133. Mall, S., Broadbridge, R., Harrison, S. L., Gore, M. G., Lee, A. G., and East, J. M. (2006) The presence of sarcolipin results in increased heat production by Ca 2+-ATPase. *J. Biol. Chem.* **281**, 36597–36602

134. Smith, W. S., Broadbridge, R., East, J. M., and Lee, A. G. (2002) Sarcolipin uncouples hydrolysis of ATP from accumulation of Ca2+ by the Ca2+-ATPase of skeletal-muscle sarcoplasmic reticulum. *Biochem. J.* **361**, 277–286

135. Bal, N. C., Maurya, S. K., Sopariwala, D. H., Sahoo, S. K., Gupta, S. C., Shaikh, S. A., Pant, M., Rowland, L. A., Bombardier, E., Goonasekera, S. A., Tupling, A. R., Molkentin, J. D., and Periasamy, M. (2012) Sarcolipin is a newly identified regulator of muscle-based thermogenesis in mammals. *Nat. Med.* **18**, 1575–9

136. Gamu, D., Bombardier, E., Smith, I. C., Fajardo, V. A., and Tupling, A. R. (2014) Sarcolipin Provides a Novel Muscle-Based Mechanism for Adaptive Thermogenesis. *Exerc. Sport Sci. Rev.* **42**, 136–142

137. Sahoo, S. K., Shaikh, S. A., Sopariwala, D. H., Bal, N. C., and Periasamy, M. (2013) Sarcolipin protein interaction with Sarco(endo)plasmic reticulum CA 2+ ATPase (SERCA) Is distinct from phospholamban protein,and only sarcolipin can promote uncoupling of the serca pump. *J. Biol. Chem.* **288**, 6881–6889

138. Tupling, A. R., Asahi, M., and MacLennan, D. H. (2002) Sarcolipin overexpression in rat slow twitch muscle inhibits sarcoplasmic reticulum Ca2+ uptake and impairs contractile function. *J. Biol. Chem.* **277**, 44740–44746

139. Bal, N. C., Maurya, S. K., Singh, S., Wehrens, X. H. T., and Periasamy, M. (2016) Increased reliance on muscle based thermogenesis upon acute minimization of brown adipose tissue function. *J. Biol. Chem.* **291**, jbc.M116.728188

140. Bombardier, E., Smith, I. C., Gamu, D., Fajardo, V. A., Vigna, C., Sayer, R. A., Gupta, S. C., Bal, N. C., Periasamy, M., and Tupling, A. R. (2013) Sarcolipin trumps β-adrenergic receptor signaling as the favored mechanism for muscle-based diet-induced thermogenesis. *FASEB J.* **27**, 3871–3878

141. Rui, L. (2014) Energy metabolism in the liver. *Compr. Physiol.* **4**, 177–197

142. Ceddia, R. B. (2017) *Human Nutrition: Science and Application*, Toronto, ON

143. Han, H.-S., Kang, G., Kim, J. S., Choi, B. H., and Koo, S.-H. (2016) Regulation of glucose metabolism from a liver-centric perspective. *Exp. Mol. Med.* **48**, e218

144. Wang, Y., Viscarra, J., Kim, S.-J., and Sul, H. S. (2015) Transcriptional regulation of hepatic lipogenesis. *Nat. Rev. Mol. Cell Biol.* **16**, 678–689

145. Kabashima, T., Kawaguchi, T., Wadzinski, B. E., and Uyeda, K. (2003) Xylulose 5-phosphate mediates glucose-induced lipogenesis by xylulose 5-phosphate-activated protein phosphatase in rat liver. *Proc. Natl. Acad. Sci. U. S. A.* **100**, 5107–5112

146. Kawaguchi, T., Takenoshita, M., Kabashima, T., and Uyeda, K. (2001) Glucose and cAMP regulate the L-type pyruvate kinase gene by phosphorylation/dephosphorylation of the carbohydrate response element binding protein. *Proc. Natl. Acad. Sci. U. S. A.* **98**, 13710–5

147. Yecies, J. L., Zhang, H. H., Menon, S., Liu, S., Yecies, D., Lipovsky, A. I., Gorgun, C., Kwiatkowski, D. J., Hotamisligil, G. S., Lee, C.-H., and Manning, B. D. (2011) Akt stimulates hepatic SREBP1c and lipogenesis through parallel mTORC1-dependent and independent pathways. *Cell Metab.* **14**, 21–32

148. Rhee, J., Inoue, Y., Yoon, J. C., Puigserver, P., Fan, M., Gonzalez, F. J., and Spiegelman, B. M. (2003) Regulation of hepatic fasting response by PPARgamma coactivator-1alpha (PGC-1): Requirement for hepatocyte nuclear factor 4alpha in gluconeogenesis. *Pnas*. **100**, 4012–4017

149. Haeusler, R. A., Kaestner, K. H., and Accili, D. (2010) FoxOs function synergistically to promote glucose production. *J. Biol. Chem.* **285**, 35245–35248

150. Fisher, F. M., Estall, J. L., Adams, A. C., Antonellis, P. J., Bina, H. a., Flier, J. S., Kharitonenkov, A., Spiegelman, B. M., and Maratos-Flier, E. (2011) Integrated regulation of hepatic metabolism by fibroblast growth factor 21 (FGF21) in vivo. *Endocrinology*. **152**, 2996–3004

151. Klain, G. J., and Hannon, J. P. (1969) Gluconeogenesis in cold-exposed rats. *Fed. Proc.* **28**, 965–8

152. Depocas, F., and Masironi, R. (1960) Body glucose as fuel for thermogenesis in the white rat exposed to cold. *Am. J. Physiol.* **199**, 1051–5

153. Nakagawa, H., and Nagai, K. (1971) Cold adaptation I: Effect of cold-exposure on gluconeogenesis. *J. Biochem.* **69**, 923–934

154. Shore, A. M., Karamitri, A., Kemp, P., Speakman, J. R., Graham, N. S., and Lomax, M. A. (2013) Cold-Induced Changes in Gene Expression in Brown Adipose Tissue, White Adipose Tissue and Liver. *PLoS One*. **8**, 1–9

155. Masoro, E. J. (1960) Depressed lipogenesis induced by cold stress. *Am. J. Physiol.* **199**, 449–52

156. Masoro, E. J., Felts, J. M., and Panagos, S. S. (1957) Effect of prolonged cold exposure on hepatic lipogenesis. *Am. J. Physiol.* **189**, 479–482

157. Keung, W., Ussher, J. R., Jaswal, J. S., Raubenheimer, M., Lam, V. H. M., Wagg,

C. S., and Lopaschuk, G. D. (2013) Inhibition of carnitine palmitoyltransferase-1 activity alleviates insulin resistance in diet-induced obese mice. *Diabetes*. **62**, 711–20

158. Cuendet, G. S., Loten, E. G., Jeanrenaud, B., and Renold, A. E. (1976) Decreased basal, noninsulin-stimulated glucose uptake and metabolism by skeletal soleus muscle isolated from obese-hyperglycemic (ob/ob) mice. *J. Clin. Invest.* **58**, 1078–1088

159. Itani, S. I., Ruderman, N. B., Schmieder, F., and Boden, G. (2002) Lipid-induced insulin resistance in human muscle is associated with changes in diacylglycerol, protein kinase C, and IkappaB-alpha. *Diabetes*. **51**, 2005–2011

160. Pickersgill, L., Litherland, G. J., Greenberg, A. S., Walker, M., and Yeaman, S. J. (2007) Key role for ceramides in mediating insulin resistance in human muscle cells. *J. Biol. Chem.* **282**, 12583–12589

161. Zhang, J., Gao, Z., Yin, J., Quon, M. J., and Ye, J. (2008) S6K directly phosphorylates IRS-1 on Ser-270 to promote insulin resistance in response to TNF-α signaling through IKK2. *J. Biol. Chem.* **283**, 35375–35382

162. Large, V., Reynisdottir, S., Langin, D., Fredby, K., Klannemark, M., Holm, C., and Arner, P. (1999) Decreased expression and function of adipocyte hormone-sensitive lipase in subcutaneous fat cells of obese subjects 1. *J. Lipid Res.* **40**, 2059–2066

163. Ahmed, K., Tunaru, S., Tang, C., Müller, M., Gille, A., Sassmann, A., Hanson, J., and Offermanns, S. (2010) An Autocrine Lactate Loop Mediates Insulin-Dependent Inhibition of Lipolysis through GPR81. *Cell Metab.* **11**, 311–319

164. Yang, X., Zhang, X., Heckmann, B. L., Lu, X., and Liu, J. (2011) Relative contribution of adipose triglyceride lipase and hormone-sensitive lipase to tumor necrosis factor-a (TNF-a)-induced lipolysis in adipocytes. *J. Biol. Chem.* **286**, 40477–40485

165. Ray, H., Pinteur, C., Frering, V., Beylot, M., and Large, V. (2009) Depot-specific differences in perilipin and hormone-sensitive lipase expression in lean and obese. *Lipids Health Dis.* **8**, 58

166. Miyata, S., Inoue, J., Shimizu, M., and Sato, R. (2015) Xanthohumol improves diet-induced obesity and fatty liver by suppressing Sterol Regulatory Element-binding Protein (SREBP) activation. *J. Biol. Chem.* **290**, 20565–20579

167. Li, S., Brown, M. S., and Goldstein, J. L. (2010) Bifurcation of insulin signaling pathway in rat liver: mTORC1 required for stimulation of lipogenesis, but not inhibition of gluconeogenesis. *Proc. Natl. Acad. Sci.* **107**, 3441–3446

168. Samuel, V. T., Choi, C. S., Phillips, T. G., Romanelli, A. J., Geisler, J. G., Bhanot,

S., McKay, R., Monia, B., Shutter, J. R., Lindberg, R. A., Shulman, G. I., and Veniant, M. M. (2006) Targeting Foxo1 in mice using antisense oligonucleotide improves hepatic and peripheral insulin action. *Diabetes*. **55**, 2042–2050

169. Koo, S.-H., Satoh, H., Herzig, S., Lee, C.-H., Hedrick, S., Kulkarni, R., Evans, R. M., Olefsky, J., and Montminy, M. (2004) PGC-1 promotes insulin resistance in liver through PPAR-α-dependent induction of TRB-3. *Nat. Med.* **10**, 530–534

170. Jitrapakdee, S. (2012) Transcription factors and coactivators controlling nutrient and hormonal regulation of hepatic gluconeogenesis. *Int. J. Biochem. Cell Biol.* **44**, 33–45

171. Foretz, M., Hebrard, S., Leclerc, J., Zarrinpashneh, E., Soty, M., Mithieux, G., Sakamoto, K., Andreeli, F., and Viollet, B. (2010) Metformin inhibits hepatic gluconeogenesis in mice independently of the LKB1/AMPK pathway via a decrease in hepatic energy state. *J. Clin. Invest.* **120**, 2355–2369

172. Cai, D., Yuan, M., Frantz, D. F., Melendez, P. A., Hansen, L., Lee, J., and Shoelson, S. E. (2005) Local and systemic insulin resistance resulting from hepatic activation of IKK-β and NF-κB. *Nat. Med.* **11**, 183–190

173. Berbée, J. F. P., Boon, M. R., Khedoe, P. P. S. J., Bartelt, A., Schlein, C., Worthmann, A., Kooijman, S., Hoeke, G., Mol, I. M., John, C., Jung, C., Vazirpanah, N., Brouwers, L. P. J., Gordts, P. L. S. M., Esko, J. D., Hiemstra, P. S., Havekes, L. M., Scheja, L., Heeren, J., and Rensen, P. C. N. (2015) Brown fat activation reduces hypercholesterolaemia and protects from atherosclerosis development. *Nat. Commun.* **6**, 6356

174. Wang, T.-Y., Liu, C., Wang, A., and Sun, Q. (2015) Intermittent cold exposure improves glucose homeostasis associated with brown and white adipose tissues in mice. *Life Sci.* **139**, 153–159

175. Vallerand, A. L., Lupien, J., and Bukowiecki, L. J. (1986) Cold exposure reverses the diabetogenic effects of high-fat feeding. *Diabetes*. **35**, 329–334

176. Commins, S. P., Marsh, D. J., Thomas, S. A., Watson, P. M., Padgett, M. A., Palmiter, R., and Gettys, T. W. (1999) Norepinephrine is required for leptin effects on gene expression in brown and white adipose tissue. *Endocrinology*. **140**, 4772–4778

177. Enriori, P. J., Sinnayah, P., Simonds, S. E., Garcia Rudaz, C., and Cowley, M. A. (2011) Leptin Action in the Dorsomedial Hypothalamus Increases Sympathetic Tone to Brown Adipose Tissue in Spite of Systemic Leptin Resistance. *J. Neurosci.* **31**, 12189–12197

178. Cypess, A. M., Weiner, L. S., Roberts-Toler, C., Elia, E. F., Kessler, S. H., Kahn, P. A., English, J., Chatman, K., Trauger, S. A., Doria, A., and Kolodny, G. M. (2015) Activation of human brown adipose tissue by a beta3-adrenergic receptor

agonist. *Cell Metab.* **21**, 33–38

179. Ding, X., Boney-Montoya, J., Owen, B. M., Bookout, A. L., Coate, K. C., Mangelsdorf, D. J., and Kliewer, S. A. (2012) βKlotho Is Required for Fibroblast Growth Factor 21 Effects on Growth and Metabolism. *Cell Metab.* **16**, 387–393

180. Foltz, I. N., Hu, S., King, C., Wu, X., Yang, C., Wang, W., Weiszmann, J., Stevens, J., Chen, J. S., Nuanmanee, N., Gupte, J., Komorowski, R., Sekirov, L., Hager, T., Arora, T., Ge, H., Baribault, H., Wang, F., Sheng, J., Karow, M., Wang, M., Luo, Y., McKeehan, W., Wang, Z., Véniant, M. M., and Li, Y. (2012) Treating diabetes and obesity with an FGF21-mimetic antibody activating the βKlotho/FGFR1c receptor complex. *Sci. Transl. Med.* **4**, 162ra153

181. Lee, P., Linderman, J. D., Smith, S., Brychta, R. J., Wang, J., Idelson, C., Perron, R. M., Werner, C. D., Phan, G. Q., Kammula, U. S., Kebebew, E., Pacak, K., Chen, K. Y., and Celi, F. S. (2014) Irisin and FGF21 are cold-induced endocrine activators of brown fat function in humans. *Cell Metab.* **19**, 302–9

182. Ceccarelli, S. M., Chomienne, O., Gubler, M., and Arduini, A. (2011) Carnitine palmitoyltransferase (CPT) modulators: a medicinal chemistry perspective on 35 years of research. *J. Med. Chem.* **54**, 3109–52

183. Foley JE (1992) Rationale and Application Of Fatty Acid Oxidation Inhibitors in Treatment of Diabetes Mellitus. *Diabetes Care*. **15**, 773–784

184. Bezaire, V., Bruce, C. R., Heigenhauser, G. J. F., Tandon, N. N., Glatz, J. F. C., Luiken, J. J. J. F., Bonen, A., and Spriet, L. L. (2006) Identification of fatty acid translocase on human skeletal muscle mitochondrial membranes : essential role in fatty acid oxidation. *Am. J. Physiol. - Endocrinol. Metab.* **290**, 509–515

185. Bonnefont, J.-P., Djouadi, F., Prip-Buus, C., Gobin, S., Munnich, A., and Bastin, J. (2004) Carnitine palmitoyltransferases 1 and 2: biochemical, molecular and medical aspects. *Mol. Aspects Med.* **25**, 495–520

186. Hue, L., and Taegtmeyer, H. (2009) The Randle cycle revisited: a new head for an old hat. *Am. J. Physiol. Endocrinol. Metab.* **297**, E578-91

187. Esser, V., Brown, N. F., Cowan, A. T., Foster, D. W., and McGarry, J. D. (1996) Expression of a cDNA Isolated from Rat Brown Adipose Tissue and Heart Identifies the Product as the Muscle Isoform of Carnitine Palmitoyltransferase I (M-CPT I). *J. Biol. Chem.* **271**, 6972–6977

188. Weis, B. C., Cowan, A. T., Brown, N., Foster, W., and McGarry, J. D. (1994) Use of a selective inhibitor of liver carnitine palmitoyltransferase I (CPT I) allows quantification of its contribution to total CPT I activity in rat heart. *J. Biol. Chem.* **269**, 26443–26448

189. Barnett, M., Collier, G. R., and O'Dea, K. (1992) The Longitudinal Effect of

Inhibiting Fatty-Acid Oxidation in Diabetic Rats Fed a High-Fat Diet. *Horm. Metab. Res.* **24**, 360–362

190. Collier, G. R., Traianedes, K., Macaulay, S. L., and O'Dea, K. (1993) Effect of fatty acid oxidation inhibition on glucose metabolism in diabetic rats. *Horm. Metab. Res.* **25**, 9–12

191. Hinderling, V. B., Schrauwen, P., Langhans, W., and Westerterp-Plantenga, M. S. (2002) The effect of etomoxir on 24-h substrate oxidation and satiety in humans. *Am. J. Clin. Nutr.* **76**, 141–147

192. Hübinger, A., Knode, O., Susanto, F., Reinauer, H., and Gries, F. (1997) Effects of the Carnitine-acyltransferase Inhibitor Etomoxir on Insulin Sensitivity, Energy Expenditure and Substrate Oxidation in NIDDM. *Horm. Metab. Res.* **29**, 436–439

193. Hübinger, A., Weikert, G., Wolf, H. P., and Gries, F. A. (1992) The effect of etomoxir on insulin sensitivity in type 2 diabetic patients. *Horm. Metab. Res. = Horm. und Stoffwechselforsch. = Horm. métabolisme*. **24**, 115–8

194. Vickers, A. E. M., Bentley, P., and Fisher, R. L. (2006) Consequences of mitochondrial injury induced by pharmaceutical fatty acid oxidation inhibitors is characterized in human and rat liver slices. *Toxicol. Vitr.* **20**, 1173–1182

195. Stephens, T. W., Higgins, a J., Cook, G. a, and Harris, R. a (1985) Two mechanisms produce tissue-specific inhibition of fatty acid oxidation by oxfenicine. *Biochem. J.* **227**, 651–60

196. Randle, P. J., Garland, P. B., Hales, C. N., and Newsholme, E. A. (1963) The glucose fatty-acid cycle- Its role in insulin sensitivity and the metabolic disturbances of diabetes mellitus. *Lancet*. **1(7285)**, 785–789

197. Wicks, S. E., Vandanmagsar, B., Haynie, K. R., Fuller, S. E., Warfel, J. D., Stephens, J. M., Wang, M., Han, X., Zhang, J., Noland, R. C., and Mynatt, R. L. (2015) Impaired mitochondrial fat oxidation induces adaptive remodeling of muscle metabolism. *Proc. Natl. Acad. Sci.* **112**, E3300–E3309

198. Koves, T. R., Ussher, J. R., Noland, R. C., Slentz, D., Mosedale, M., Ilkayeva, O., Bain, J., Stevens, R., Dyck, J. R. B., Newgard, C. B., Lopaschuk, G. D., and Muoio, D. M. (2008) Mitochondrial Overload and Incomplete Fatty Acid Oxidation Contribute to Skeletal Muscle Insulin Resistance. *Cell Metab.* **7**, 45–56

199. Ussher, J. R., Koves, T. R., Cadete, V. J. J., Zhang, L., Jaswal, J. S., Swyrd, S. J., Lopaschuk, D. G., Proctor, S. D., Keung, W., Muoio, D. M., and Lopaschuk, G. D. (2010) Inhibition of de novo ceramide synthesis reverses diet-induced insulin resistance and enhances whole-body oxygen consumption. *Diabetes*. **59**, 2453–2464

200. Timmers, S., Nabben, M., Bosma, M., van Bree, B., Lenaers, E., van Beurden, D.,

Schaart, G., Westerterp-Plantenga, M. S., Langhans, W., Hesselink, M. K. C., Schrauwen-Hinderling, V. B., and Schrauwen, P. (2012) Augmenting muscle diacylglycerol and triacylglycerol content by blocking fatty acid oxidation does not impede insulin sensitivity. *Proc. Natl. Acad. Sci. U. S. A.* **109**, 11711–6

201. Schreurs, M., Kuipers, F., and van der Leij, F. R. (2010) Regulatory enzymes of mitochondrial beta-oxidation as targets for treatment of the metabolic syndrome. *Obes. Rev.* **11**, 380–8

202. Frontini, A., and Cinti, S. (2010) Distribution and Development of Brown Adipocytes in the Murine and Human Adipose Organ. *Cell Metab.* **11**, 253–256

203. Deveaud, C., Beauvoit, B., Salin, B., Schaeffer, J., and Rigoulet, M. (2004) Regional differences in oxidative capacity of rat white adipose tissue are linked to the mitochondrial content of mature adipocytes. *Mol. Cell. Biochem.* **267**, 157–166

204. Araujo, R. L., Andrade, B. M., Padrón, A. S., Gaidhu, M. P., Perry, R. L. S., Carvalho, D. P., and Ceddia, R. B. (2010) High-fat diet increases thyrotropin and oxygen consumption without altering circulating 3,5,3'-triiodothyronine (T3) and thyroxine in rats: the role of iodothyronine deiodinases, reverse T3 production, and whole-body fat oxidation. *Endocrinology*. **151**, 3460–9

205. DiGirolamo, M., and Fine, J. B. (2001) Cellularity measurements. *Methods Mol. Biol.* **155**, 65–75

206. Ahlquist, R. P. (1976) Present state of alpha- and beta-adrenergic drugs I. The adrenergic receptor. *Am. Heart J.* **92**, 661–4

207. DiGirolamo, M. (2001) Measurements of glucose conversion to its metabolites. in *Methods in Molecular Biology. Adipose Tissue Protocols (Vol 155).* (Ailhaud, G. ed), pp. 181–192, Humana Press Inc., Totowa, NJ

208. Lillioja, S., Bogardus, C., Mott, D. M., Kennedy, A. L., Knowler, W. C., and Howard, B. V (1985) Relationship between Insulin-Mediated Glucose Disposal and Lipid-Metabolism in Man. *J. Clin. Invest.* **75**, 1106–1115

209. Li, J., Stillman, J. S., Clore, J. N., and Blackard, W. G. (1993) Skeletal muscle lipids and glycogen mask substrate competition (Randle cycle). *Metabolism*. **42**, 451–456

210. Jornayvaz, F. R., and Shulman, G. I. (2012) Diacylglycerol activation of protein kinase Cε and hepatic insulin resistance. *Cell Metab.* **15**, 574–84

211. Gaidhu, M. P., Bikopoulos, G., and Ceddia, R. B. (2012) Chronic AICAR-induced AMP-kinase activation regulates adipocyte lipolysis in a time-dependent and fat depot-specific manner in rats. *Am. J. Physiol. Cell Physiol.* **303**, C1192-7

212. Sztalryd, C., and Kraemer, F. B. (1994) Differences in hormone-sensitive lipase

expression in white adipose tissue from various anatomic locations of the rat. *Metabolism*. **43**, 241–247

213. Tavernier, G., Galitzky, J., Valet, P., Remaury, a, Bouloumie, a, Lafontan, M., and Langin, D. (1995) Molecular mechanisms underlying regional variations of catecholamine-induced lipolysis in rat adipocytes. *Am. J. Physiol.* **268**, E1135–E1142

214. Miyoshi, H., Perfield, J. W., Souza, S. C., Shen, W. J., Zhang, H. H., Stancheva, Z. S., Kraemer, F. B., Obin, M. S., and Greenberg, A. S. (2007) Control of adipose triglyceride lipase action by serine 517 of perilipin A globally regulates protein kinase a-stimulated lipolysis in adipocytes. *J. Biol. Chem.* **282**, 996–1002

215. Cinti, S. (2009) Reversible physiological transdifferentiation in the adipose organ. *Proc. Nutr. Soc.* **68**, 340

216. Wu, J., Cohen, P., and Spiegelman, B. M. (2013) Adaptive thermogenesis in adipocytes: is beige the new brown? *Genes Dev.* **27**, 234–50

217. Keipert, S., and Jastroch, M. (2014) Brite/beige fat and UCP1 — is it thermogenesis? *Biochim. Biophys. Acta - Bioenerg.* **1837**, 1075–1082

218. Nedergaard, J., and Cannon, B. (2013) UCP1 mRNA does not produce heat. *Biochim. Biophys. Acta - Mol. Cell Biol. Lipids*. **1831**, 943–949

219. Kopecky, J., Clarke, G., Enerbäck, S., Spiegelman, B., and Kozak, L. P. (1995) Expression of the mitochondrial uncoupling protein gene from the aP2 gene promoter prevents genetic obesity. *J. Clin. Invest.* **96**, 2914–2923

220. Ukropec, J., Anunciado, R. P., Ravussin, Y., Hulver, M. W., and Kozak, L. P. (2006) UCP1-independent thermogenesis in white adipose tissue of cold-acclimated Ucp1-/- mice. *J. Biol. Chem.* **281**, 31894–31908

221. Flachs, P., Rossmeisl, M., Kuda, O., and Kopecky, J. (2013) Stimulation of mitochondrial oxidative capacity in white fat independent of UCP1: A key to lean phenotype. *Biochim. Biophys. Acta - Mol. Cell Biol. Lipids*. **1831**, 986–1003

222. Li, Y., Fromme, T., Schweizer, S., Schöttl, T., and Klingenspor, M. (2014) Taking control over intracellular fatty acid levels is essential for the analysis of thermogenic function in cultured primary brown and brite/beige adipocytes. *EMBO Rep.* **15**, 1069–76

223. Yehuda-Shnaidman, E., Buehrer, B., Pi, J., Kumar, N., and Collins, S. (2010) Acute stimulation of white adipocyte respiration by PKA-induced lipolysis. *Diabetes*. **59**, 2474–2483

224. Fine, J. B., and DiGirolamo, M. (1997) A simple method to predict cellular density in adipocyte metabolic incubations. *Int. J. Obes. Relat. Metab. Disord.* **21**, 764–8

225. Dole, V. P., and Meinertz, H. (1960) Microdetermination of long-chain fatty acids in plasma and tissues. *J. Biol. Chem.* **235**, 2595–9

226. Livak, K. J., and Schmittgen, T. D. (2001) Analysis of Relative Gene Expression Data Using Real-Time Quantitative PCR and the 2−ΔΔCT Method. *Methods*. **25**, 402–408

227. Martin, B. R., and Denton, R. M. (1970) The intracellular localization of enzymes in white-adipose-tissue fat-cells and permeability properties of fat-cell mitochondria. Transfer of acetyl units and reducing power between mitochondria and cytoplasm. *Biochem. J.* **117**, 861–77

228. Gospodarska, E., Nowialis, P., and Kozak, L. P. (2015) Mitochondrial turnover: A phenotype distinguishing brown adipocytes from interscapular brown adipose tissue and white adipose tissue. *J. Biol. Chem.* **290**, 8243–8255

229. Guan, H.-P., Li, Y., Jensen, M. V., Newgard, C. B., Steppan, C. M., and Lazar, M. a (2002) A futile metabolic cycle activated in adipocytes by antidiabetic agents. *Nat. Med.* **8**, 1122–1128

230. Oulion, S., Bertrand, S., and Escriva, H. (2012) Evolution of the FGF Gene Family. *Int. J. Evol. Biol.* **2012**, 1–12

231. Fisher, F. M., and Maratos-Flier, E. (2016) Understanding the Physiology of FGF21. *Annu. Rev. Physiol.* **78**, 223–241

232. Yie, J., Wang, W., Deng, L., Tam, L.-T., Stevens, J., Chen, M. M., Li, Y., Xu, J., Lindberg, R., Hecht, R., Véniant, M., Chen, C., and Wang, M. (2012) Understanding the Physical Interactions in the FGF21/FGFR/β-Klotho Complex: Structural Requirements and Implications in FGF21 Signaling. *Chem. Biol. Drug Des.* **79**, 398–410

233. Yie, J., Hecht, R., Patel, J., Stevens, J., Wang, W., Hawkins, N., Steavenson, S., Smith, S., Winters, D., Fisher, S., Cai, L., Belouski, E., Chen, C., Michaels, M. L., Li, Y.-S., Lindberg, R., Wang, M., Véniant, M., and Xu, J. (2009) FGF21 N- and C-termini play different roles in receptor interaction and activation. *FEBS Lett.* **583**, 19–24

234. Micanovic, R., Raches, D. W., Dunbar, J. D., Driver, D. A., Bina, H. A., Dickinson, C. D., and Kharitonenkov, A. (2009) Different roles of N- and C- termini in the functional activity of FGF21. *J. Cell. Physiol.* **219**, 227–234

235. Douris, N., Stevanovic, D. M., Fisher, ffolliott M., Cisu, T. I., Chee, M. J., Nguyen, N. L., Zarebidaki, E., Adams, A. C., Kharitonenkov, A., Flier, J. S., Bartness, T. J., and Maratos-Flier, E. (2015) Central Fibroblast Growth Factor 21 Browns White Fat via Sympathetic Action in Male Mice. *Endocrinology*. **156**, 2470–2481

236. de Jong, J. M. A., Wouters, R. T. F., Boulet, N., Cannon, B., Nedergaard, J., and

Petrovic, N. (2017) The β 3 -adrenergic receptor is dispensable for browning of adipose tissues. *Am. J. Physiol. - Endocrinol. Metab.* **312**, E508–E518

237. Cousin, B., Casteilla, L., Dani, C., Muzzin, P., Revelli, J. P., and Penicaud, L. (1993) Adipose tissues from various anatomical sites are characterized by different patterns of gene expression and regulation. *Biochem. J.* **292**, 873–6

238. Nishimura, T., Nakatake, Y., Konishi, M., and Itoh, N. (2000) Identification of a novel FGF, FGF-21, preferentially expressed in the liver. *Biochim. Biophys. Acta*. **1492**, 203–6

239. Markan, K. ., Naber, M. C., Ameka, M. K., Anderegg, M. D., Mangelsdorf, D. J., Kliewer, S. a, Mohammadi, M., and Potthoff, M. J. (2014) Circulating FGF21 is liver derived and enhances glucose uptake during refeeding and overfeeding. *Diabetes*. **63**, 4057–4063

240. Itoh, N. (2014) FGF21 as a hepatokine, adipokine, and myokine in metabolism and diseases. *Front. Endocrinol. (Lausanne).* **5**, 4–7

241. Inagaki, T., Dutchak, P., Zhao, G., Ding, X., Gautron, L., Parameswara, V., Li, Y., Goetz, R., Mohammadi, M., Esser, V., Elmquist, J. K., Gerard, R. D., Burgess, S. C., Hammer, R. E., Mangelsdorf, D. J., and Kliewer, S. A. (2007) Endocrine Regulation of the Fasting Response by PPARα-Mediated Induction of Fibroblast Growth Factor 21. *Cell Metab.* **5**, 415–425

242. Sanchez-Gurmaches, J., and Guertin, D. a. (2014) Adipocytes arise from multiple lineages that are heterogeneously and dynamically distributed. *Nat. Commun.* **19**, 4099

243. de Jong, J. M. a, Larsson, O., Cannon, B., and Nedergaard, J. (2015) A stringent validation of mouse adipose tissue identity markers. *Am. J. Physiol. Endocrinol. Metab.* **308**, E1085–E1105

244. Kolumam, G., Chen, M. Z., Tong, R., Zavala-Solorio, J., Kates, L., van Bruggen, N., Ross, J., Wyatt, S. K., Gandham, V. D., Carano, R. A. D., Dunshee, D. R., Wu, A. L., Haley, B., Anderson, K., Warming, S., Rairdan, X. Y., Lewin-Koh, N., Zhang, Y., Gutierrez, J., Baruch, A., Gelzleichter, T. R., Stevens, D., Rajan, S., Bainbridge, T. W., Vernes, J. M., Meng, Y. G., Ziai, J., Soriano, R. H., Brauer, M. J., Chen, Y., Stawicki, S., Kim, H. S., Comps-Agrar, L., Luis, E., Spiess, C., Wu, Y., Ernst, J. A., McGuinness, O. P., Peterson, A. S., and Sonoda, J. (2015) Sustained Brown Fat Stimulation and Insulin Sensitization by a Humanized Bispecific Antibody Agonist for Fibroblast Growth Factor Receptor 1/βKlotho Complex. *EBioMedicine*. **2**, 730–743

245. Wu, A.-L., Kolumam, G., Stawicki, S., Chen, Y., Li, J., Zavala-Solorio, J., Phamluong, K., Feng, B., Li, L., Marsters, S., Kates, L., van Bruggen, N., Leabman, M., Wong, A., West, D., Stern, H., Luis, E., Kim, H. S., Yansura, D., Peterson, A. S., Filvaroff, E., Wu, Y., and Sonoda, J. (2011) Amelioration of Type

2 Diabetes by Antibody-Mediated Activation of Fibroblast Growth Factor Receptor 1. *Sci. Transl. Med.* **3**, 113ra126-113ra126

246. Cunningham, J. J., Gulino, M. A., Meara, P. A., and Bode, H. H. (1985) Enhanced hepatic insulin sensitivity and peripheral glucose uptake in cold acclimating rats. *Endocrinology*. **117**, 1585–9

247. Smith, O. L., and Davidson, S. B. (1982) Shivering thermogenesis and glucose uptake by muscles of normal or diabetic rats. *Am J Physiol*. **242**, R109-15

248. Beaton, J. R. (1963) Nitrogen metabolism in cold-exposed rats. *Can. J. Biochem. Physiol.* **41**, 1169–79

249. Vallerand, A. L., Pérusse, F., and Bukowiecki, L. J. (1990) Stimulatory effects of cold exposure and cold acclimation on glucose uptake in rat peripheral tissues. *Am. J. Physiol.* **259**, R1043-9

250. Foster, D. O., and Frydman, M. L. (1979) Tissue distribution of cold-induced thermogenesis in conscious warm- or cold-acclimated rats reevaluated from changes in tissue blood flow: the dominant role of brown adipose tissue in the replacement of shivering by nonshivering thermogenesis. *Can. J. Physiol. Pharmacol.* **57**, 257–270

251. Foster, D. O. (1984) Quantitative contribution of brown adipose tissue thermogenesis to overall metabolism. *Can. J. Biochem. Cell Biol.* **62**, 618–22

252. Foster, D. O., and Frydman, M. L. (1978) Nonshivering thermogenesis in the rat. II. Measurements of blood flow with microspheres point to brown adipose tissue as the dominant site of the calorigenesis induced by noradrenaline. *Can. J. Physiol. Pharmacol.* **56**, 110–22

253. Shibata, H., Pérusse, F., Vallerand, a, and Bukowiecki, L. J. (1989) Cold exposure reverses inhibitory effects of fasting on peripheral glucose uptake in rats. *Am. J. Physiol.* **257**, R96–R101

254. Nedergaard, J., and Lindberg, O. (1982) The brown fat cell. *Int. Rev. Cytol.* **74**, 187–286

255. Holloszy, J. O., Constable, S. H., and Young, D. A. (1986) Activation of glucose transport in muscle by exercise. *Diabetes. Metab. Rev.* **1**, 409–23

256. Horton, E. S. (1986) Exercise and physical training: effects on insulin sensitivity and glucose metabolism. *Diabetes. Metab. Rev.* **2**, 1–17

257. James, D. E., Kraegen, E. W., and Chisholm, D. J. (1985) Effects of exercise training on in vivo insulin action in individual tissues of the rat. *J. Clin. Invest.* **76**, 657–666

258. Sellers, E. A., Scott, J. W., and Thomas, N. (1954) Electrical activity of skeletal muscle of normal and acclimatized rats on exposure to cold. *Am. J. Physiol.* **177**, 372–6

259. Janský, L. (1973) Non-shivering thermogenesis and its thermoregulatory significance. *Biol. Rev. Camb. Philos. Soc.* **48**, 85–132

260. Mall, S., Broadbridge, R., Harrison, S. L., Gore, M. G., Lee, A. G., and East, J. M. (2006) The Presence of Sarcolipin Results in Increased Heat Production by Ca $^{2+}$ -ATPase. *J. Biol. Chem.* **281**, 36597–36602

261. Sopariwala, D. H., Pant, M., Shaikh, S. A., Goonasekera, S. A., Molkentin, J. D., Weisleder, N., Ma, J., Pan, Z., and Periasamy, M. (2015) Sarcolipin overexpression improves muscle energetics and reduces fatigue. *J. Appl. Physiol.* **118**, 1050–1058

262. Fajardo, V. A., Bombardier, E., Vigna, C., Devji, T., Bloemberg, D., Gamu, D., Gramolini, A. O., Quadrilatero, J., and Tupling, A. R. (2013) Co-Expression of SERCA Isoforms, Phospholamban and Sarcolipin in Human Skeletal Muscle Fibers. *PLoS One*. **8**, e84304

263. Garcia, D., and Shaw, R. J. (2017) AMPK: Mechanisms of Cellular Energy Sensing and Restoration of Metabolic Balance. *Mol. Cell*. **66**, 789–800

264. Putman, C. T., Martins, K. J. B., Gallo, M. E., Lopaschuk, G. D., Pearcey, J. A., MacLean, I. M., Saranchuk, R. J., and Pette, D. (2007) -Catalytic subunits of 5’AMP-activated protein kinase display fiber-specific expression and are upregulated by chronic low-frequency stimulation in rat muscle. *AJP Regul. Integr. Comp. Physiol.* **293**, R1325–R1334

265. Murphy, R. M. (2011) Enhanced technique to measure proteins in single segments of human skeletal muscle fibers: fiber-type dependence of AMPK- 1 and - 1. *J. Appl. Physiol.* **110**, 820–825

266. Lee-Young, R. S., Canny, B. J., Myers, D. E., and McConell, G. K. (2009) AMPK activation is fiber type specific in human skeletal muscle: effects of exercise and short-term exercise training. *J. Appl. Physiol.* **107**, 283–289

267. Castorena, C. M., MacKrell, J. G., Bogan, J. S., Kanzaki, M., and Cartee, G. D. (2011) Clustering of GLUT4, TUG, and RUVBL2 protein levels correlate with myosin heavy chain isoform pattern in skeletal muscles, but AS160 and TBC1D1 levels do not. *J. Appl. Physiol.* **111**, 1106–1117

268. Fediuc, S., Gaidhu, M. P., and Ceddia, R. B. (2006) Inhibition of insulin-stimulated glycogen synthesis by 5-aminoimidasole-4-carboxamide-1-beta-d-ribofuranoside-induced adenosine 5’-monophosphate-activated protein kinase activation: interactions with Akt, glycogen synthase kinase 3-3alpha/beta, and glycog. *Endocrinology*. **147**, 5170–5177

269. James, D. E., Jenkins, A. B., and Kraegen, E. W. (1985) Heterogeneity of insulin action in individual muscles in vivo: euglycemic clamp studies in rats. *Am. J. Physiol.* **248**, E567-74

270. Overton, J. M. (2010) Phenotyping small animals as models for the human metabolic syndrome: thermoneutrality matters. *Int. J. Obes. (Lond).* **34 Suppl 2**, S53–S58

271. Hanssen, M. J. W., van der Lans, A. A. J. J., Brans, B., Hoeks, J., Jardon, K. M. C., Schaart, G., Mottaghy, F. M., Schrauwen, P., and van Marken Lichtenbelt, W. D. (2016) Short-term Cold Acclimation Recruits Brown Adipose Tissue in Obese Humans. *Diabetes*. **65**, 1179–1189

272. Henriksen, E. J., Bourey, R. E., Rodnick, K. J., Koranyi, L., Permutt, M. A., and Holloszy, J. O. (1990) Glucose transporter protein content and glucose transport capacity in rat skeletal muscles. *Am. J. Physiol.* **259**, E593-8

273. Brychta, R. J., and Chen, K. Y. (2017) Cold-induced thermogenesis in humans. *Eur. J. Clin. Nutr.* **71**, 345–352

274. Nedergaard, J., Bengtsson, T., and Cannon, B. (2011) New Powers of Brown Fat: Fighting the Metabolic Syndrome. *Cell Metab.* **13**, 238–240

275. Block, B. (1994) Thermogenesis in muscle. *Annu. Rev. Physiol.* **56**, 535–577

276. Shiota, M., Tanaka, T., and Sugano, T. (1985) Effect of norepinephrine on gluconeogenesis in perfused livers of cold-exposed rats. *Am. J. Physiol.* **249**, E281-6

277. Penner, P. E., and Himms-Hagen, J. (1968) Gluconeogenesis in rats during cold acclimation. *Can. J. Biochem.* **46**, 1205–13

278. Yoon, J. C., Puigserver, P., Chen, G., Donovan, J., Wu, Z., Rhee, J., Adelmant, G., Stafford, J., Kahn, C. R., Granner, D. K., Newgard, C. B., and Spiegelman, B. M. (2001) Control of hepatic gluconeogenesis through the transcriptional coactivator PGC-1. *Nature*. **413**, 131–138

279. Sharabi, K., Tavares, C. D. J., Rines, A. K., and Puigserver, P. (2015) Molecular pathophysiology of hepatic glucose production. *Mol. Aspects Med.* **46**, 21–33

280. Agius, L. (2008) Glucokinase and molecular aspects of liver glycogen metabolism. *Biochem. J.* **414**, 1–18

281. Sugden, M. C., Bulmer, K., Gibbons, G. F., and Holness, M. J. (2001) Role of Peroxisome Proliferator-Activated Receptor-alpha in the Mechanism Underlying Changes in Renal Pyruvate Dehydrogenase Kinase Isoform 4 Protein Expression in Starvation and after Refeeding. *Arch. Biochem. Biophys.* **395**, 246–252

282. Holness, M. J., and Sugden, M. C. (2003) Regulation of pyruvate dehydrogenase complex activity by reversible phosphorylation. *Biochem. Soc. Trans.* **31**, 1143–51

283. Vallerand, A. L., Pérusse, F., and Bukowiecki, L. J. (1987) Cold exposure potentiates the effect of insulin on in vivo glucose uptake. *Am. J. Physiol.* **253**, E179-86

284. Dentin, R., Liu, Y., Koo, S.-H., Hedrick, S., Vargas, T., Heredia, J., Yates, J., and Montminy, M. (2007) Insulin modulates gluconeogenesis by inhibition of the coactivator TORC2. *Nature*. **449**, 366–369

285. Koo, S.-H., Flechner, L., Qi, L., Zhang, X., Screaton, R. A., Jeffries, S., Hedrick, S., Xu, W., Boussouar, F., Brindle, P., Takemori, H., and Montminy, M. (2005) The CREB coactivator TORC2 is a key regulator of fasting glucose metabolism. *Nature*. **437**, 1109–11

286. Shaw, R. J., Lamia, K. A., Vasquez, D., Koo, S.-H., Bardeesy, N., Depinho, R. A., Montminy, M., and Cantley, L. C. (2005) The Kinase LKB1 Mediates Glucose Homeostasis in Liver and Therapeutic Effects of Metformin. *Science (80-.).* **310**, 1642–1646

287. He, L., Sabet, A., Djedjos, S., Miller, R., Sun, X., Hussain, M. A., Radovick, S., and Wondisford, F. E. (2009) Metformin and insulin suppress hepatic gluconeogenesis through phosphorylation of CREB binding protein. *Cell*. **137**, 635–46

288. Hardie, D. G., Ross, F. A., and Hawley, S. A. (2012) AMPK: a nutrient and energy sensor that maintains energy homeostasis. *Nat. Rev. Mol. Cell Biol.* **13**, 251–262

289. Dominy, J. E., Lee, Y., Gerhart-Hines, Z., and Puigserver, P. (2010) Nutrient-dependent regulation of PGC-1?'s acetylation state and metabolic function through the enzymatic activities of Sirt1/GCN5. *Biochim. Biophys. Acta - Proteins Proteomics*. **1804**, 1676–1683

290. Coskun, T., Bina, H. A., Schneider, M. A., Dunbar, J. D., Hu, C. C., Chen, Y., Moller, D. E., and Kharitonenkov, A. (2008) Fibroblast growth factor 21 corrects obesity in mice. *Endocrinology*. **149**, 6018–6027

291. Adams, A. C., Yang, C., Coskun, T., Cheng, C. C., Gimeno, R. E., Luo, Y., and Kharitonenkov, A. (2013) The breadth of FGF21's metabolic actions are governed by FGFR1 in adipose tissue. *Mol. Metab.* **2**, 31–37

Appendix A: Supplementary Data

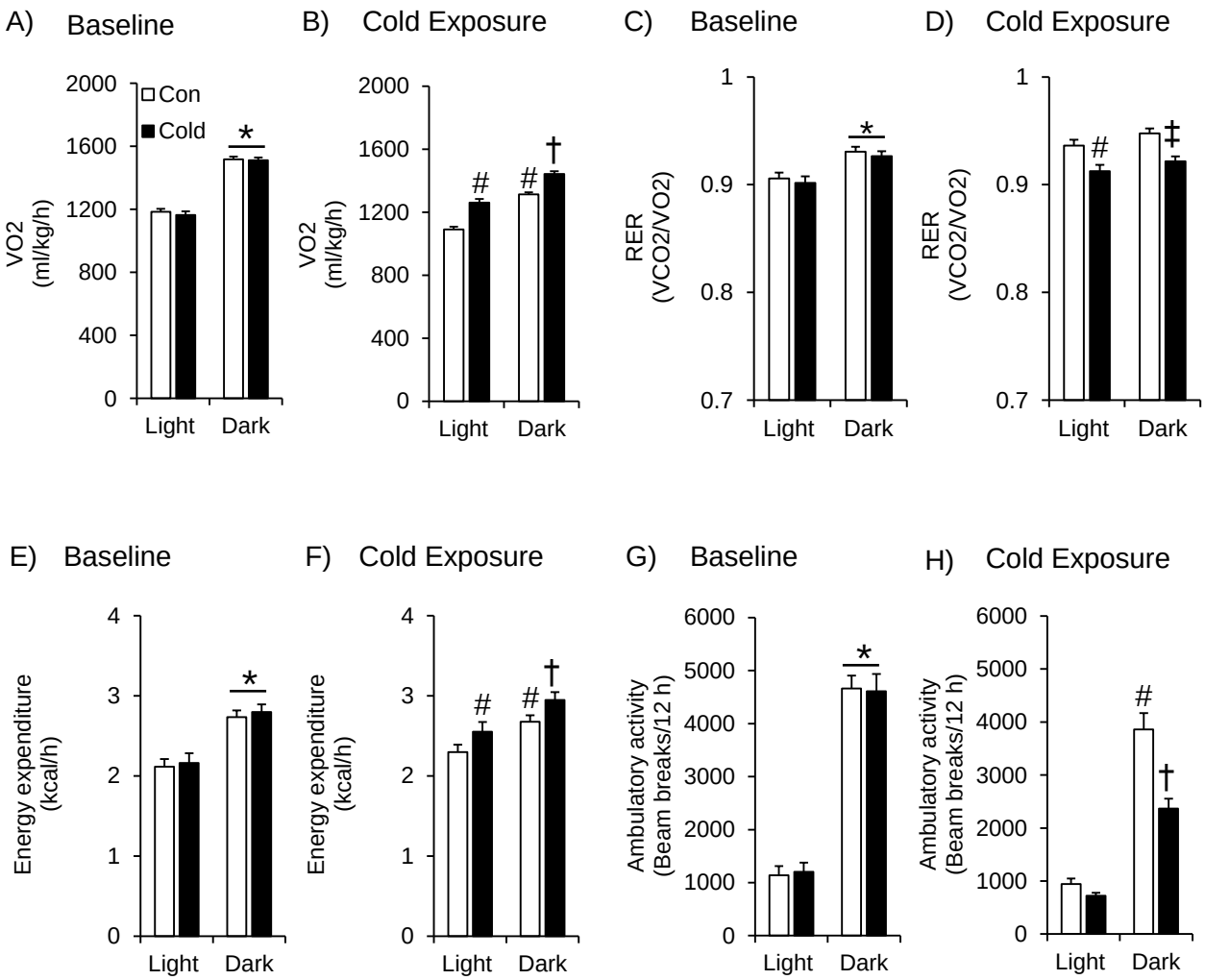

Figure A-0-1: Cold-induced alterations in VO_2, RER, energy expenditure and ambulatory activity. Cold exposure leads to an increase in VO_2 (B), and energy expenditure (F), but leads to a decrease in Epid and SC Ing mass (D), RER (H), and ambulatory activity (L). Age- and weight-matched animals were either kept at room temperature or cold exposed (4°C) for 7 days. At baseline and on day 6 of cold exposure, rats were placed in the CLAMS for the determination of *in vivo* metabolic parameters. *p<0.01 vs. light cycle; #p<0.05 vs. Con in the light cycle; †p<0.05 vs. Cold in the light cycle and Con in the dark cycle; ‡p<0.05 vs. Con in the dark cycle. Two-way ANOVA, n = 11.

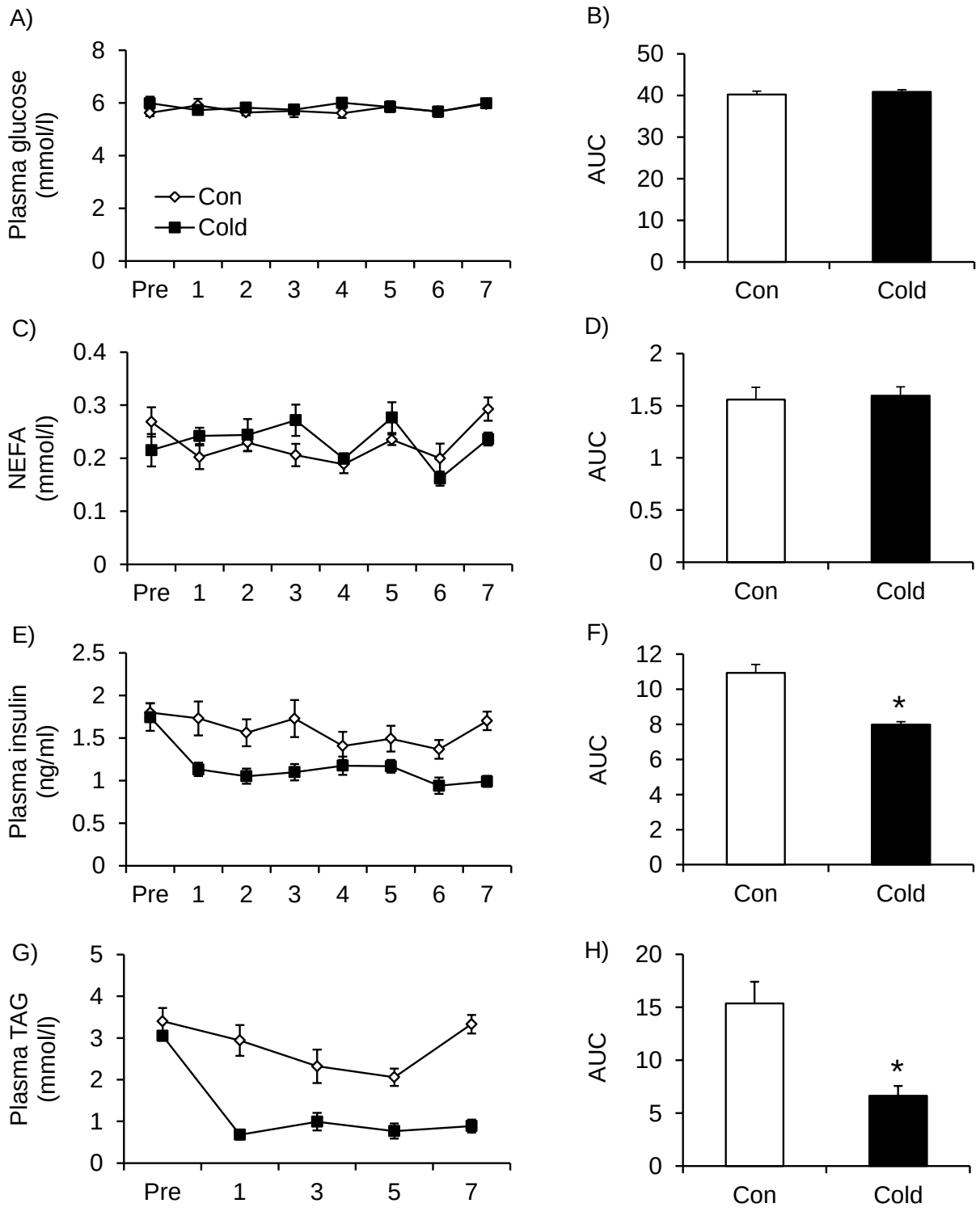

Figure A-0-2: Time course of plasma metabolites throughout 7 days of cold exposure. Cold exposure reduces plasma insulin and triacylglyceride (TAG) in rats, but has no effect on plasma glucose or NEFA. Time-course of plasma glucose (A and B), NEFA (C and D), insulin (E and F) and TAG (G and H) during the 7-day cold exposure. Measurements were taken in the fed state. AUC = area under the curve. *p<0.001 vs. Con. Unp aired, two-tailed t-test, n= 7.

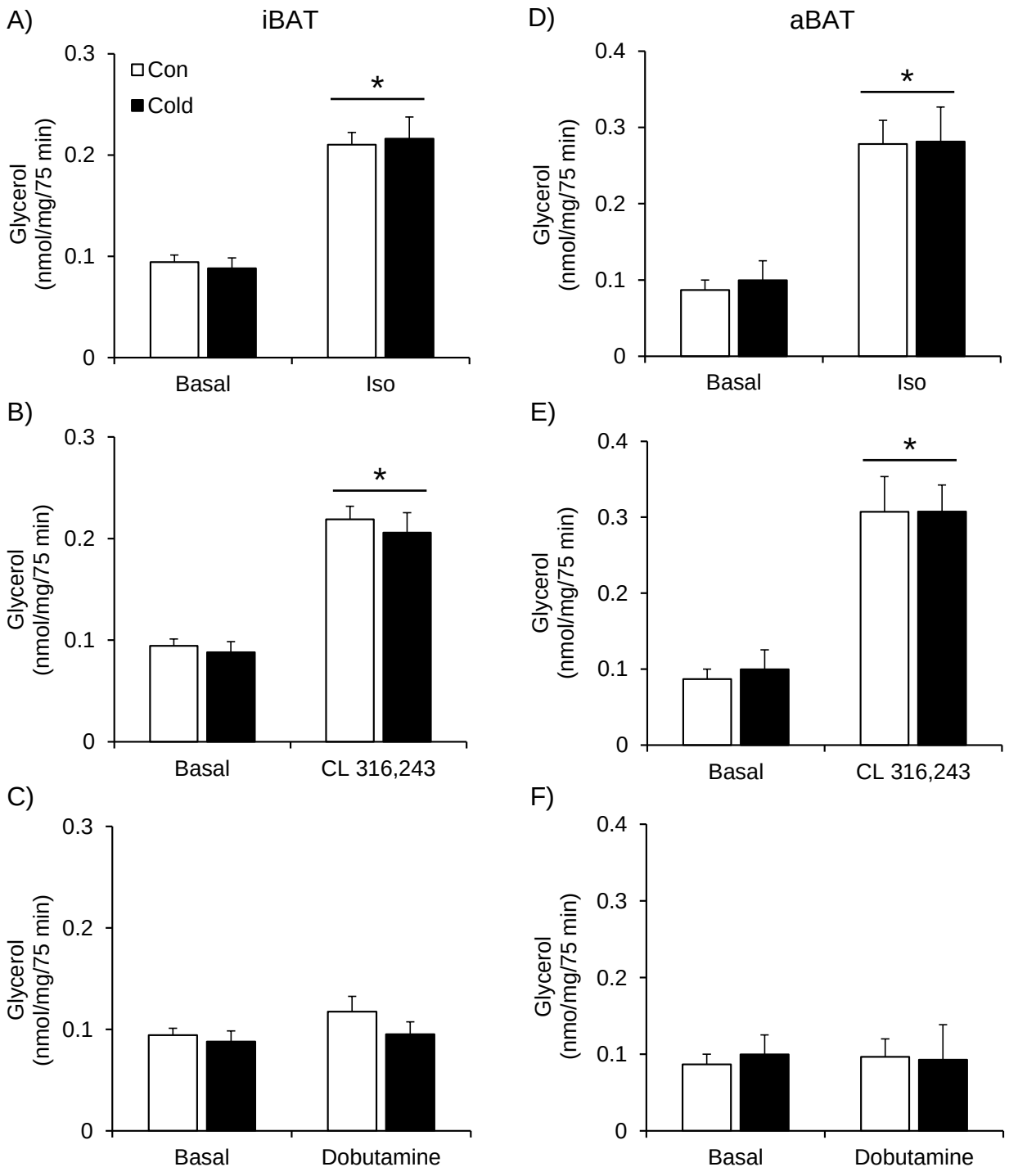

Figure A-0-3: Cold-induced effects on BAT lipolysis. Cold exposure has no effect on basal or stimulated rates of lipolysis in iBAT (A, B, C) and aBAT (D, E, F). Glycerol release was measured under basal conditions and also in the presence of isoproterenol, CL 316,243 or dobutamine for 75 minutes. Two-way ANOVA, n = 6. *p<0.05 vs. Basal.

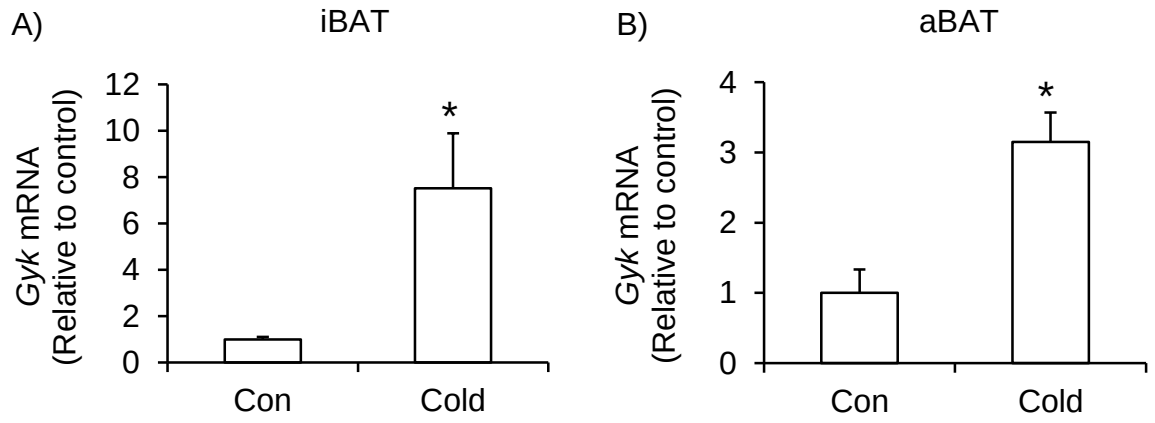

Figure A-0-4: Cold-induced changes in BAT *Gyk* gene expression. Cold exposure increases *Gyk* expression in both the iBAT (A) and aBAT (B). *p<0.05 vs. Con. Unpaired, two-tailed t-test, n= 9.

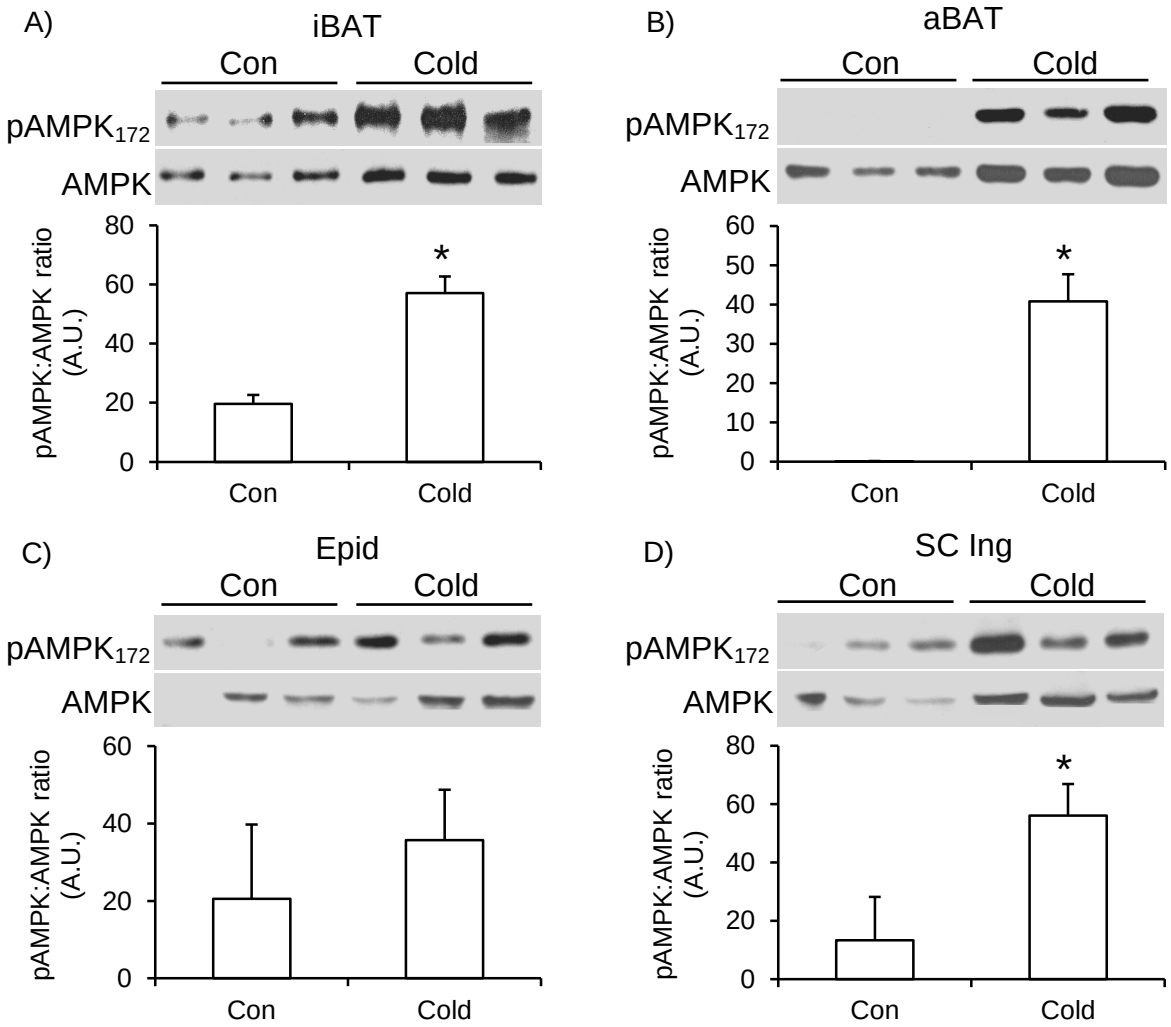

Figure A-0-5: AMPK phosphorylation in the BAT and WAT following cold exposure. Cold exposure increases the phosphorylation state of AMPK in the iBAT (A), aBAT (B) and SC Ing (D), but not the Epid (C). *p<0.05 vs. Con. Unpaired, two-tailed t-test, n= 9.

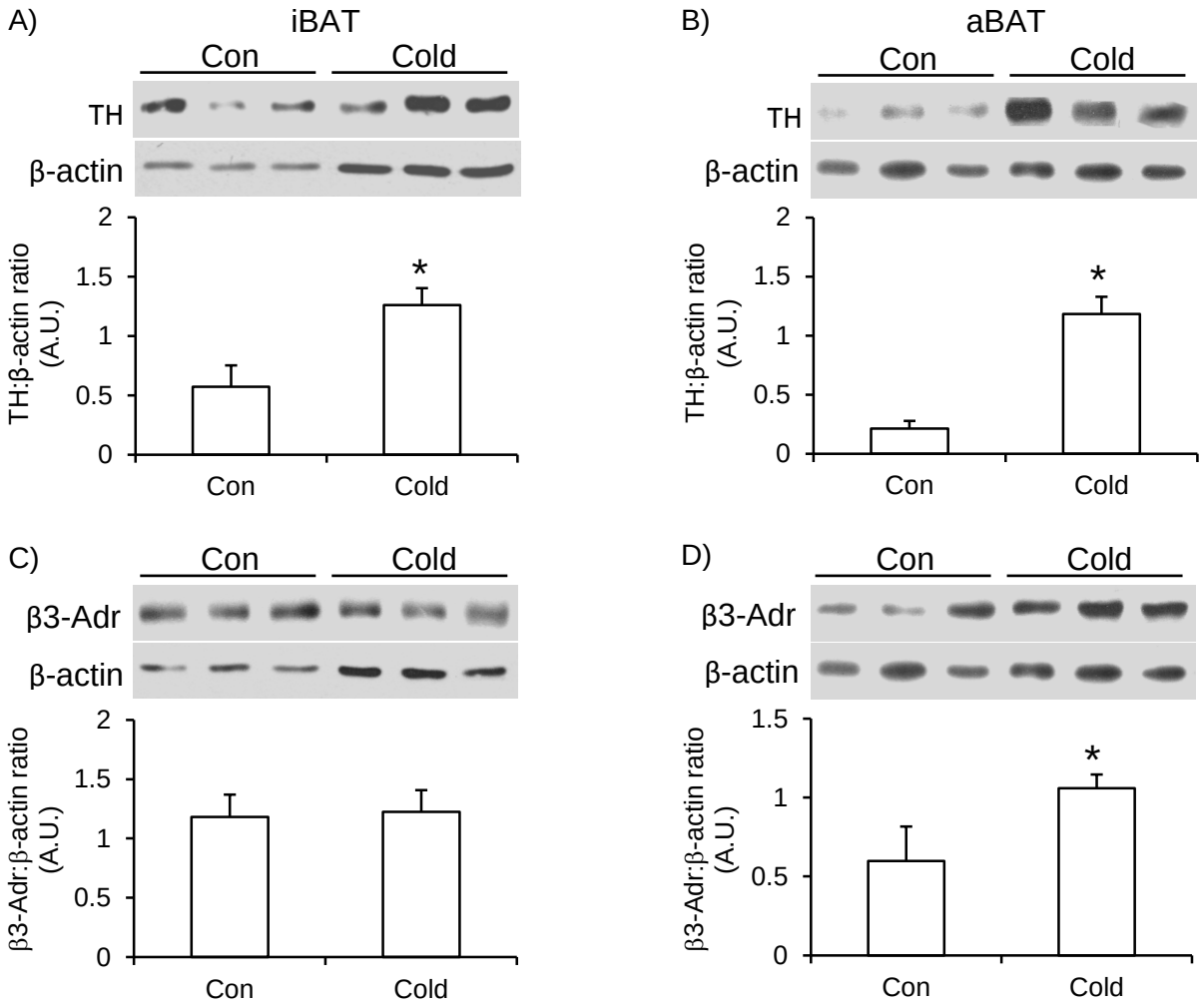

Figure A-0-6: Cold-induced changes in TH and β3-Adr content in the BAT. Cold exposure increases the content of TH in the iBAT (A) and aBAT (B), but only increases the content of the β3-adrenergic receptor in the aBAT (D). Age- and weight-matched animals were either kept at room temperature or cold exposed (4°C) for 7 days. Unpaired, two-tailed t-test, n = 9. *p<0.05 vs. Con.

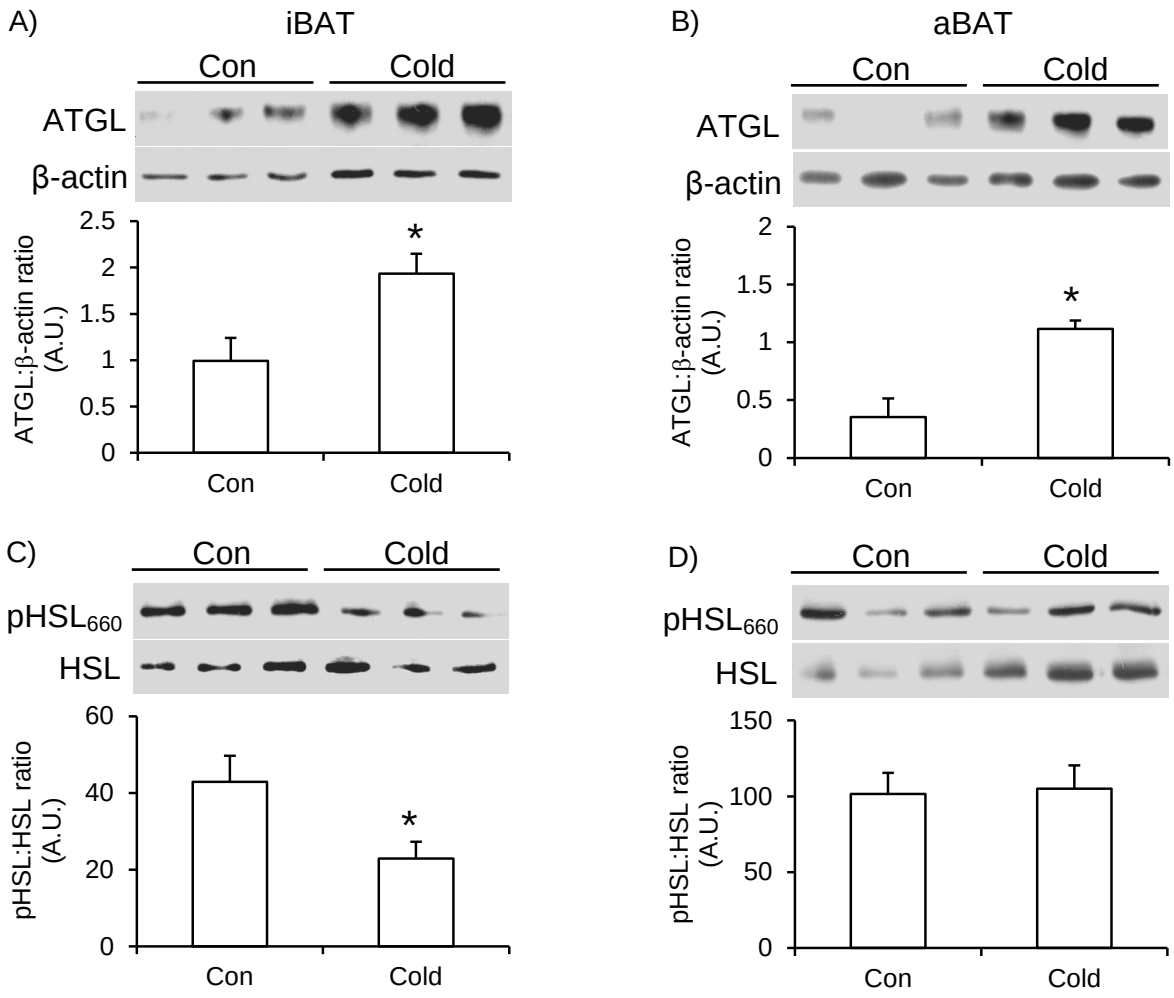

Figure A-0-7: ATGL and HSL content and phosphorylation in the BAT following cold exposure. Cold exposure increases the content of ATGL, but decreases or does not affect the phosphorylation state of HSL in the iBAT (A and C) and aBAT (B and D). Age- and weight-matched animals were either kept at room temperature or cold exposed (4°C) for 7 days. Unpaired, two-tailed t-test, n = 9. *p<0.05 vs. Con.

Table A-0-1: Rat Primer Sequences for BAT and WAT

Gene Name	Forward Primer	Reverse Primer
β-klotho	5'-GAC AGG TGC TGA ACT GGA TTA-3'	5'-CCG TGG TAT CTT CCG TCT TTA T-3'
Cd36	5'-ACG ACT GCA GGT CAA CAT ACT GGT-3'	5'-TGG TCC CAG TCT CAT TTA GCC ACA-3'
Fgf21	5'-GGT ACA CAT TGT ATC CGT CCT T-3'	5'-CAA CAA CCA GAT GGA ACT CTC TA-3'
Fgfr1	5'-CTC ACC TCT GTA CCT GGA AAT C-3'	5'-GTG CCG CTC TTC ATC TTG TA-3'
Gyk	5'-GGA GAC CAG CCC TGT TAA GCT-3'	5'-GTC CAC TGC TCC CAC CAA TG-3'
Lpl	5'-TTG AGA AAG GGC TCT GCC TGA GTT-3'	5'-TGC TTC TCT TGG CTC TGA CCT TGT-3'
Pgc-1α	5'-ACC GTA AAT CTG CGG GAT GAT GGA-3'	5'-ATT CTC AAG AGC AGC GAA AGC GTC- 3'

Table B-0-2: Rat Primer Sequences for Liver

Gene Name	Forward Primer	Reverse Primer
Acc	5'-ATA TGT TCG AAG AGC TTA TAT CGC CTA T-3'	5'-TGG GCA GCA TGA ACT GAA ATT-3'
Acot2	5'-GTG AGA TGG CTC AGT GAT AGT G-3'	5'-CTT GTC AGA GTT GGT TCT CTC C-3'
Cox6c	5'-TTG CTG CTG CCT ATA AGT TTG GCG-3'	5'-AGT TCA GGA ACA CAG GTC AGC AGT-3'
Cpt1	5'-ACG GAC CCT CGT GAT ACA AAC CAA-3'	5'-AGC CAA GGC ATC TCT GGA TGT AGT-3'
Crtc2	5'-AAACTGAGGAAAGGGAAGGG-3'	5'-GACCTCCAGACAGACGATTT-3'
Elovl3	5'-GGC CAA AGT GAA GCA TCC CAA CAT-3'	5'-AGC ACG AAG GAC CAG AAG AAG TGT-3'
Fas	5'-AAG GCA TCA CCA TAG CTA CAG CCT-3'	5'-TAT GCT TCT CAC AGT GGC CAC ACA-3'
Fbp1	5'-TCC ACC AGA AGG CAC CAG TTA TCA-3'	5'-CTA TCC GCG CTG TTG GGT TTG TTT-3'
Foxo1	5'-CCCAGTGAAGACACCTTTACA-3'	5'-AGGACACCCATCCTACCATA-3'
G6Pase	5'-AGA GCT GCA AAG GAG AAC TG-3'	5'-GCT TCA GCG AGT CAA AGA GA-3'
Gk	5'-ACA TGG AGA GGA CTT TCC AGG CAT-3'	5'-TGC TTG AAT AGT GCA GAG TGA GGC-3'
Hnf3β	5'-GAC CTT TGG TTC CCA CTA TGT-3'	5'-CTC TGT CAA CGA CAG CAA TAG A-3'
Hnf4α	5'-AAT GAA TAC GCC TGC CTC AAA GCC-3'	5'-AGT CAT ACT GCC GGT CGT TGA TGT-3'
Ir	5'-ATT TGC GTG TGT GTT GTG TCC AGG-3'	5'-AGG GCA CAA GCT CTC GGT TCA TAA-3'
Irs1	5'-ACG CCG AAA GAG GAT GGG TTT ACT-3'	5'-AAT ACT CTC TCC ACC CAA CGC GAA-3'
Irs2	5'-AAT GGC AAT GCA GCT GTC TTC CTG-3'	5'-TGC AGG AAG GGA AAC CTT GAG AGT-3'
Pdk4	5'-GAC TGG TGT ATC CCA AGT AAG G-3'	5'-GAC CCA CTT TGA TCC CGT AAA-3'
Pgc-1α	5'-ACC GTA AAT CTG CGG GAT GAT GGA-3'	5'-ATT CTC AAG AGC AGC GAA AGC GTC- 3'
Pparα	5'-CATACAGGAGAGCAGGGATTTG-3'	5'-GAAAGTAAGGATGTGGGAGGAG-3'
Pparγ	5'-GCCTAAGTTTGAGTTTGCTGTG-3'	5'-GCGGTCTCCACTGAGAATAATG-3'
Srebp-1c	5'-GGA CCA CAG AAA GGT GGA AT-3'	5'-GGC AGT TGA TGT AGA GGC TAA G-3'

Appendix B: Detailed Experimental Methods

B-1: Adipocyte Isolation

1. Collect Sc Ing and Epid fat depots. Remove connective tissue from Sc Ing depot. Thoroughly mince both tissues carefully without smashing tissue to avoid cell lysis.
2. Place the minced tissue into a urine vial with Krebs-ringer buffer (KRB) and collagenase (Type II, 1 mg/mL) and swirl to mix the minced tissue in with the buffer and collagenase. Incubate in orbital shaking water bath at 37°C for 30-45 minutes. Vigorously swirl the vials every 5-10 minutes to help with digestion.
3. Once digested, filter out any remaining pieces of connective tissue using a strainer (pore size 500 µm) and spin down the remaining solution in a 50 mL falcon tube for 30 sec at 1000 rpm.
4. When cells have settled (floating), carefully aspirate buffer only. Rinse the adipocytes by adding 10mL of fresh KRB down the side of the falcon tube, swirling to rinse cells in fresh buffer, and letting sit to allow adipocytes to float. Repeat this process 3 times.
5. Aspirate out the final volume of buffer and resuspend the cells in KRB or KRB-3.5% BSA depending on the subsequent assays you are running. Resuspend in 10-20 mL depending on the amount of cells you have.
6. Count the number of adipocytes.
    a. To measure the lipocrit, swirl the falcon tube to thoroughly mix the cells and buffer, take 300 µL of cell suspension and pipette into a skinny tube. Centrifuge this tube for 1 minute at 2000 rpm to separate the adipocyte layer from the buffer. Measure the height of the layer of adipocytes.
    b. To measure the diameter of adipocytes, take 15 µL of cell suspension and place on microscope slide. Add another 60 µL KRB to microscope slide to dilute cells. Diameters are measured on the microscope in the cell culture room.
    c. The number of cells in each sample of fat is calculated using the equations for the volume of a sphere (adipocyte) and the volume of a cylinder (lipocrit).
7. Calculate the number of cells in each sample of fat using the equations for volume of a sphere (using an average diameter of the adipocytes in the preparation) and volume of a cylinder (lipocrit).
8. Calculate the total number of cells needed for assay and distribute an appropriate volume of the cell suspension to the appropriate tubes/vials for each assay.

B-2: Complexation of Palmitate

1. Prepare 30 mL of medium or buffer (α-MEM, glucose-free KRB or SETH buffer) and add 3.75 g of FA-free BSA (Sigma Cat# A3803) to get a 12.5% solution. Stir to dissolve (but do not stir too hard to avoid the formation of bubbles).
2. Pre-heat the solution at 50°C.
3. Weigh out 160 mg of palmitate (Sigma Cat# P5585) into a 2 mL Eppendorf and add 100 µL of NaOH (10 N) and vortex the tube vigorously for 1-2 minutes.

4. Take the pre-heated medium with BSA and add the palmitate while stirring. Palmitate does not dissolve immediately, it precipitates initially.
5. Pour into a 50 mL falcon tube and wrap with foil to protect from light.
6. Incubate in 50°C water bath for 2-4 h or overnight with shaking at 150-200 rpm.
7. After the incubation period, filter solution to get chunks out using a 10 mL syringe and sterile strainer.
8. pH to 7.4.
9. Take a 50 µL of solution for measurement of NEFA (dilute 1:10 prior to measuring). Aliquot the remaining filtered medium (1 mL each) into tubes and freeze at -20°C.

B-3: Determination of FFA using Wako HR Series NEFA-HR kit

In addition to measuring palmitate in buffer, NEFAs can be measured in plasma or in media samples from lipolysis assays.

1. Dissolve reagent A into solvent A.
    a. Current Kit: 5.8 mg of reagent A per 1 mL of solvent A
2. Pipette appropriate amount of sample and standard into each cuvette.
3. Add 0.5 mL of reagent A solution into each cuvette and incubate for 5 min at 37˚C in water bath.
4. Dissolve reagent B into solvent B.
    a. Current Kit: 10.4 mg of reagent B per 1 mL of solvent B
5. Add 0.25 mL of reagent B solution into each cuvette and incubate for 5 min at 37˚C in water bath.
6. Read the absorbance at 550 nm.

Volumes of standard (Std) and sample

Cuvette #	Name	1mEq/L NEFA Std	H_2O
1	Blank	-	12.5 µL
2	Low Std	6.25 µL	6.25 µL
3	Std	12.50 µL	-
4 etc	Sample	12.50 µL	-

*Low Std is mainly used to help determine if the assay is working correctly (should see an appropriate increase in absorption according to Std concentration)

7. Calculate the NEFA concentration in each sample using the following equation: $C_s = A_s/A_{Std}*1$ (mEq/L) where C_s = concentration of sample, A_s = absorbance of

sample at 550 nm and A_{Std} = absorbance of the NEFA Std solution at 550 nm. The unit is mEq/L which is equivalent to mmol/L.

B-4: Palmitate and Glucose oxidation

This assay can be performed using isolated WAT adipocytes (2.5-5x10^5 cells), thoroughly minced BAT (~20 mg), or using thin strips of muscle (~20 mg) or liver (~30 mg). Muscle strips must be mounted on wire clips in order to maintain a resting muscle length during the assay.

For muscle and liver:

1. Pre-incubate samples prior to incubation with palmitate/glucose oxidation buffer. Weigh and mount thin strips of muscle onto wire clips. Weigh thin liver strips. Place samples in scintillation vials with 2 mL of KRB-3.5% BSA, cap with rubber stopper and incubate in a 37°C water bath with shaking for 1 h. Samples need to be gasified for the entire hour with O_2:CO_2- 95:5% (vol:vol).
2. Prepare buffer.
    a. Palmitate oxidation buffer: 0.2 µCi/ml of [1-^{14}C] palmitic acid and 200 µM non-labelled palmitate dissolved in KRB-3.5% BSA.
    b. Glucose oxidation buffer: 0.2 µCi/ml of D-[U-^{14}C] glucose dissolved in KRB-3.5% BSA (buffer already contains 5.5 mM glucose).
3. Following the 1 h pre-incubation, place sample in a new scintillation vial with 2 mL of the appropriate buffer. Using tweezers, add a 2 mL Eppendorf (with the lid removed) that contains a rolled up piece of filter paper. Wet the filter paper with 200 µL of 2-phenylethylamine/methanol (1:1, vol:vol). Cap the scintillation vial with a rubber cap and incubate in a 37°C water bath with shaking for 1 h. Samples are gassed with O_2:CO_2- 95:5% (vol:vol) for the entire during of the incubation.
4. Following the 1 h incubation, remove the skeletal muscle or liver sample. Rinse in PBS, blot dry and flash freeze in liquid nitrogen. The sample may then be digested for analysis of glycogen synthesis, or may be frozen at -80°C for any subsequent analysis.
5. To the scintillation vial add 200 µL of H_2SO_4 (5 N) to acidify the media and release any trapped CO_2. Incubate the vial for a further 1 h.
6. At the end of the incubation period, the filter paper may be removed and transferred to another scintillation vial for radioactivity counting.

For WAT and BAT:

1. Prepare buffer.
    a. Palmitate oxidation buffer: 0.2 µCi/ml of [1-^{14}C] palmitic acid and 200 µM non-labelled palmitate dissolved in KRB-3.5% BSA.
    b. Glucose oxidation buffer: 0.2 µCi/ml of D-[U-^{14}C] glucose dissolved in KRB-3.5% BSA (buffer already contains 5.5 mM glucose).
2. Isolate WAT adipocytes or thoroughly mince BAT. Pipette cells or weigh out minced tissue into scintillation vials.

3. Add 1.5-2 mL of the appropriate buffer. Using tweezers, add a 2 mL Eppendorf (with the lid removed) that contains a rolled up piece of filter paper. Cap the scintillation vial with a rubber cap and incubate in a 37°C water bath for 1 h. Gasify the samples with O_2:CO_2- 95:5% (vol:vol) for 15 seconds prior to the incubation. If testing inhibition using oligomycin, add 100 µM of oligomycin to the vials, swirl to mix, and let sit for 15 minutes, prior to the 1 h incubation.
4. After 1 h, use a needle to wet the filter paper with 200 µL of 2-phenylethylamine/methanol (1:1, vol:vol) without removing the rubber cap. Also add 200 µL of H_2SO_4 (5 N) to acidify the media and release any trapped CO_2. Allow the samples to incubate in the water bath for an additional 1 h.
5. At the end of the incubation period, the filter paper may be removed and transferred to another scintillation vial for radioactivity counting.

B-5: Glycerol Determination as a Measure of Lipolysis

1. Isolate WAT adipocytes and pipette a volume of cell suspension equal to $5x10^5$ cells into plastic vials. Mince BAT tissue and place ~20 mg into plastic vials with 600 µL of KRB-3.5% BSA. Take a 50 µL time zero media sample from the bottom of the vial. Add 100 nM of substrate of choice to appropriate vials (β3-adrenergic agonist CL 316,243; non-specific β-adrenergic agonist isoproterenol; β1-adrenergic agonist dobutamine). Gently swirl the sample to mix cells, media and substrate, and incubate in a 37°C water bath with gentle orbital shaking (50 orbital strokes/minute) for 75 minutes.
2. Allow the cells to settle after incubation and take 200 µL media sample (from the bottom of the vial) and analyze immediately or freeze at -80°C for future analysis.
3. Measure glycerol release in the media using the glycerol determination kit (Sigma Cat# FG0100).
4. Prepare the free glycerol reagent by dissolving the lyophilized powder in 40 mL of double distilled (dd) H_2O.
5. Label a set of cuvettes to measure a blank, a glycerol standard (Sigma Cat# G7793) and all of the samples. Pipette 10 µL of the blank, standard and samples into the appropriate cuvettes.
6. Pipette 0.8 mL of glycerol reagent into all cuvettes and incubate for 5 minutes at 37°C.
7. Record the absorbance (A) at 540 nm.
8. Calculate the glycerol concentration of the sample according to the following equation:
    a. Glycerol Content = $(A_{sample}-A_{blank})/(A_{standard}-A_{blank})$ x 0.26 mg/mL

B-6: Glucose or Glycerol Incorporation into Lipids

1. Isolate WAT adipocytes and pipette a volume of cell suspension equal to $5x10^5$-$1x10^6$ cells into scintillation vials.

2. Prepare buffer:
    a. Glucose incorporation into lipids: 0.2 µCi/ml of D-[U-^{14}C] glucose dissolved in KRB-3.5% BSA.
    b. Glycerol incorporation into lipids: 0.5 µCi/ml of [U-^{14}C] glycerol dissolved in KRB-3.5% BSA.
3. Add 1.5 mL of appropriate buffer to scintillation vials, cap with rubber stopper and incubate at 37°C for 1 h.
4. At the end of the incubation period, extract lipids from the cells. Add 5 mL of Dole's reagent (40:10:1 of isopropanol, heptane and 1 M H_2SO_4, vol:vol:vol) to the scintillation vials and vortex the samples for 15 seconds.
5. Add 3 mL of heptane and 3 mL of ddH_2O to the vials, cap and vortex for 15 seconds. Allow to sit for 20 minutes.
6. Remove 1 mL of the upper (heptane) phase and place into pre-weighed scintillation vials.
7. Leave to dry in the hood overnight.
8. The next day, re-weigh the scintillation vials, add 2 mL of scintillation fluid, shake and count the radioactivity.

B-7: Glycogen Synthesis

1. Digest pre-weighed strip of skeletal muscle in 500 µL of KOH (1 M) at 65°C for 30 minutes. Shake/vortex sample and remove 100 µL for glycogen content assay and 50 µL for protein determination.
2. Add 100 µL of carrier glycogen (stock solution 25 mg/mL) and boil samples for 5 minutes to denature proteins.
3. Add 80 µL of saturated Na_2SO_4 and 1.2 mL of cold 100% ethanol to each sample. Vortex and put in the -20°C freezer overnight for precipitation.
4. The next day, centrifuge tubes for 20 minutes at 3000 rpm at room temperature.
5. Discard the supernatant and dissolve the glycogen pellet in 500 µL of ddH_2O (use a warm water bath to help dissolve the glycogen pellet). Add 1.2 mL 100% ethanol, vortex and put the samples in the -20°C freezer for 20 minutes to precipitate and remove any impurities.
6. Centrifuge the tubes for 10 minutes at 3000 rpm at room temperature and discard the supernatant.
7. Dissolve the glycogen pellet in 500 µL of ddH_2O (use a warm water bath to help dissolve the glycogen pellet). Put 400 µL in scintillation vials with 2 mL scintillation fluid and measure the radioactivity. Use 400 µL of ddH_2O as the blank.

B-8: Glycogen Content

1. To the 100 µL of digested skeletal muscle or liver, add 10.2 µL of acetic acid (17.5 M), equivalent to ~10% of the volume. This decreases the pH to ~4.8 which is optimal for hydrolysis of glycogen by amyloglucosidase.

2. Prepare acetate buffer:
    a. 100 mL H_2O
    b. 480 µL acetic acid (98% pure)
    c. 975 mg sodium acetate
    d. Adjust pH to 4.8 and store at 4°C.
3. Add 500 µL of acetate buffer (pH 4.8) with 0.5 mg/mL amyloglucosidase (Sigma Cat# A7420) to each sample and incubate for 2 h at 40°C (with shaking) or on the bench overnight (no need to shake).
4. After incubation, neutralize the digested glycogen solution with 1/16 NaOH (5 N, ~37.5 µL). This will raise the pH to 7.4 which is the optimal pH for HK/G6PDH.
5. Centrifuge the samples for 5 minutes at 3000 rpm.
6. Prepare the hexokinase/glucose-6-phosphate dehydrogenase (HK/G6PDH):
    a. Resuspend 500 U HK/G6PDH (Sigma Cat# H8629) in 2 mL of 3.2 M ammonium sulfate (10 mL of 3.2 M ammonium sulfate is made by dissolving 4.23 g of ammonium sulfate in 10 mL H_2O).
7. Prepare the triethanolamine (TRA) buffer:
    a. Dissolve 5.6 g of TRA and 100 mg of $MgSO_4$ in 50 mL of H_2O. Add 12 mL of NaOH (1 N). Adjust pH to 7.5 and make up to 100 mL with ddH_2O.
    b. Add 50 µL of the HK/G6PDH suspension to 10 mL of TRA buffer.
    c. Add 6 mg ATP and 8 mg NADP to 10 mL of TRA buffer.
    d. TRA buffer with all components is only stable for 1 week at 4°C.
8. Collect 100 µL of the digested supernatant and place in cuvette. Add 1 mL of the TRA buffer (with all components) and incubate for 30 minutes on the bench at room temperature.
9. Read the absorbance at 340 nm.
10. Calculate µmoles of glucosyl units using the formula: Absorbance x 8.89.

B-9: Real-Time Quantified Polymerase Chain Reaction (qPCR)

RNA Isolation

1. Add 1 mL of Trizol™ reagent (Fisher Scientific Cat# 15596018) to 50-100 mg of tissue sample. 50 mg is sufficient for muscle, liver and BAT, 100 mg is required for WAT. Homogenize the sample. Incubate the homogenized sample for 5 minutes at room temperature.
2. Add 0.2 mL of chloroform and vortex the sample for 15 seconds.
3. Incubate the sample at room temperature for 3 minutes, then centrifuge at 13,000 rpm for 15 minutes at 4°C. The sample will separate into a lower red phenol-chloroform phase, an interphase and a colourless upper phase. Remove the aqueous upper phase and place in a new tube.
4. Add 0.5 mL of 100% isopropanol to the aqueous phase, invert to mix, and allow the sample to sit at room temperature for 10 minutes.
5. Centrifuge the sample at 13,000 rpm for 20 minutes at 4°C.
6. Remove the supernatant from the tube, leaving only the RNA pellet. Wash the pellet with 1 mL of 75% ethanol. Centrifuge the tube at 13,000 rpm for 20 minutes at 4°C. Discard the wash.

7. Vacuum or air-dry the RNA pellet for 10 minutes.
8. Resuspend the RNA pellet in RNAse-free water. Proceed to DNAse treatment.

DNAse Treatment (Fisher Scientific Cat# AM1906)

1. Add 0.1 x vol of 10X DNAse buffer + 1 µL rDNAse.
2. Incubate at 37°C for 30 minutes.
3. Add inactivation reagent (0.1 x vol).
4. Incubate for 2 minutes at room temperature while mixing throughout.
5. Centrifuge the sample at 10,000 rpm for 1.5 minutes and transfer the RNA to a new tube (inactivation reagent will pellet).
6. Measure the yield of RNA.

cDNA Synthesis using ABM EasyScript™ Reverse Transcriptase kit

1. In a RNAse-free tube, combine 2 µg RNA with 1 µL of 10 µM random primers and 1 µL of dNTP mix (10 mM each).
2. Heat mixture at 65°C for 5 minutes and incubate on ice for at least 1 minute.
3. Add 4 µL of 5X RT buffer, 0.5 µL of RNAseOFF Ribonuclease inhibitor and 1µL of EasyScript™ RTase to your sample.
4. Mix components and centrifuge briefly. Incubate the tube at 25°C for 10 minutes, 50°C for 50 minutes and 85°C for 5 minutes.
5. Store the cDNA at -20°C.

cDNA Synthesis using SuperScript™ II Reverse Transcriptase kit

1. In a RNAse-free tube, combine 5 µg RNA with 1 µL of 50-250 ng random primers and 1 µL of dNTP mix (10 mM each).
2. Heat mixture at 65°C for 5 minutes and incubate on ice for at least 1 minute.
3. Add 4 µL of 5X First-Strand buffer and 2 µL of 0.1 M DTT to your sample.
4. Mix components and centrifuge briefly. Incubate at 25°C for 2 minutes.
5. Add 1 µL of SuperScript™ II Reverse Transcriptase. Mix components and centrifuge briefly. Incubate the tube at 25°C for 10 minutes, 42°C for 50 minutes and 70°C for 15 minutes.
6. Store the cDNA at -20°C.

Real-Time qPCR

1. In a RNAse-free 96-well PCR plate combine cDNA, primers, water and qPCR mastermix. Each 20 µL reaction contains 4-5 µL cDNA (final amount = 10-100 ng), 0.4 µL primer solution (final concentration = 500 nM), 10 µL ABM EvaGreen qPCR Mastermix (Diamed, Mississauga, ON, Canada) and 4.6-5.6 µL of RNase free water.
2. Centrifuged the plate at 2500 rpm for 5 minutes at 4°C.
3. Complete real-time PCR analysis using the following amplification conditions: 95°C (10 min); 40 cycles of 95°C (15 s), 60°C (60 s).

4. Normalize genes a control gene such as GAPDH, TBP, or β-actin and determine relative differences in gene expression between treatment groups using the ΔΔCt method (226). Graph values as alterations relative to the control group.

B-10: Western Blotting

Western Blotting Buffers:

1. 10X Running Buffer (pH 8.3):
    a. 30.34 g Tris base
    b. 144 g Glycine
    c. 10 g SDS
    d. Dissolve contents in 1 L of ddH_2O and store at room temperature.

2. 1X Running Buffer (pH 8.3):
    a. 10% 10X running buffer
    b. 90% ddH_2O
    c. Mix solutions and store at room temperature.

3. 10X Transfer Buffer (pH 8.3):
    a. 30.3 g Tris base
    b. 144 g Glycine
    c. Dissolve contents in 1 L of ddH_2O and store at room temperature.

4. 1X Transfer Buffer (pH 8.3):
    a. 10% 10X transfer buffer
    b. 20% Methanol
    c. 70% ddH_2O
    d. Mix solutions and store at -20°C prior to use.

5. 10X Wash Buffer:
    a. 60.57 g Tris base
    b. 87.66 g NaCl
    c. Dissolve contents in 1 L ddH_2O and store at room temperature.

6. 1X Wash Buffer:
    a. 10% 10X wash buffer
    b. 90% ddH_2O
    c. Add 500 µL/L each of Tween-20 and NP-40. Mix solutions and store at room temperature.

7. Blocking Buffer:
    a. 3% BSA (w/v: 1.5 g/50 mL)
    b. Dissolve in 1X wash buffer, store at 4°C.

8. Antibody (Ab) Buffer:
    a. Primary Ab: 1 part blocking buffer + 2 parts 1X wash buffer + 0.02% sodium azide. Typically a 1:1000 dilution of primary Ab is appropriate, but may vary

depending on the strength of the signal and the abundance of the protein in the tissue.

b. Secondary Ab: 1 part blocking buffer + 2 parts 1X wash buffer (no sodium azide). Typically a 1:2000-1:5000 dilution of secondary Ab is appropriate, but may vary depending on the strength of the signal and the abundance of the protein in the tissue.

9. Resolving Gel Tris Buffer (1.5 M, pH 8.8):
    a. 90.86 g Tris base per 500 mL ddH_2O

10. Stacking Gel Tris Buffer (0.5 M, pH 6.8):
    a. 30.3 g Tris base per per 500 mL ddH_2O

11. 10% APS Solution:
    a. 10% (w/v) ammonium persulfate in ddH_2O. Weigh out 0.1 g and dissolve in 1 mL ddH_2O. Store at -20°C.

12. 10% SDS Solution:
    a. 10% (w/v) sodium dodecylsulfate in ddH_2O. Weigh out 1 g and dissolve in 10 mL ddH_2O. Store at room temperature.

13. Lysis Buffer for Protein Homogenization prior to Western Blot:
    a. Contains the following: 25 mM Tris-HCl, 25 mM NaCl (pH 7.4), 1 mM $MgCl_2$, 2.7 mM KCl, 1% Triton-X and 10% glycerol.
    b. Prepare stock of lysis buffer and store in aliquots at -20°C.
    c. Prior to use, add protease (cOmplete™ inhibitor cocktail tablets) and phosphatase (PhosSTOP™) inhibitors (Roche Diagnostics GmbH, Mannheim, Germany).

14. Laemmli Sample Buffer (2X) (BioRad Cat# 161-0737):
    a. For each mL of sample buffer: 950 µL Laemmli sample buffer and 50 µL β-mercaptoethanol.
    b. Store at room temperature. Dilute sample 1:1 with sample buffer and boil for 5 minutes prior to loading protein.

Preparation of Tissue Lysates:

1. The ratio of tissue to lysis buffer differs depending on the tissue being homogenized. For the WAT, weigh out 200 mg of tissue and homogenize in 250 µL lysis buffer. For the BAT, skeletal muscle and liver, weigh out 50 mg of tissue and homogenize in 250 µL lysis buffer.
2. Thoroughly homogenize the tissue. Sonicate the sample for 15 seconds. Centrifuge the homogenate for 5 minutes at 13,000 rpm at 4°C.
3. Remove the upper aqueous protein layer (may be located below a layer of fat for the WAT and BAT samples) and place in a new tube. For the WAT and BAT, an

additional centrifugation step may be necessary in order to remove all cellular debris.

4. Take an aliquot of each sample for protein determination by the Bradford method. Aliquot the remaining sample and store at -80°C until subsequent Western blot.
5. Prior to running the Western blot, dilute the sample 1:1 with 2X Laemmli sample buffer and boil for 5 minutes.

Western Blotting Protocol

Prepare the resolving and stacking gels according to the following recipes. Note that using a lower percentage resolving gel is appropriate when probing for larger proteins and a higher percentage resolving gel is appropriate when probing for smaller proteins.

Resolving Gel:	2 gels (8%)	2 gels (10%)
ddH_2O	8.05 mL	6.91 mL
30% Acrylamide (37:5:1)	4.53 mL	5.67 mL
Tris-HCL (1.5 M, pH 8.8)	4.25 mL	4.25 mL
10% SDS	0.17 mL	0.17 mL
TEMED	20 µL	20 µL
10% APS	100 µL	100 µL

Add TEMED and 10% APS immediately prior to pouring the gel into plates. Make sure the gels are mixed well. Pipette a thin layer of isopropanol over the top of the gel to accelerate the polymerization of the gel. Allow the gel to polymerize (~20 minutes).

Stacking Gel (4%)	2 gels
ddH_2O	3.92 mL
30% Acrylamide (37:5:1)	0.87 mL
Tris-HCL (0.5 M, pH 6.8)	1.63 mL
10% SDS	0.065 mL
TEMED	10 µL
10% APS	50 µL

Once the resolving gel is set, pour off the isopropanol and carefully blot any excess with filter paper. Pour stacking gel on top of resolving gel and put combs in place. Allow gel to set (~20 minutes).

Running the Gel

1. Take samples out of -80°C freezer. If required, dilute the sample 1:1 with 2X Laemmli sample buffer and boil for 5 minutes. Centrifuge samples to collect all the volume at the bottom of the tube.
2. Place gels into tanks and add 1X running buffer to fill the tanks.
3. Take out combs and pipette 6 µL protein ladder into the first well.

4. Add samples in the appropriate volumes and to the appropriate wells and top up 1X running buffer so that the tank is full.
5. Place lid on tank, matching the electrodes: black to black and red to red.
6. Turn on the voltage to 60 V for 30 minutes, then turn up the voltage to 110 V for approximately 1.5 h, or until the dye runs off the end of the gel.
7. While the gel is running, you can prepare the 1X transfer buffer according to the recipe. Store at -20°C until use.

Transferring the Gel onto the Membrane

1. Fill a large dish with cold transfer buffer.
2. Cut out equal-sized PVDF membranes and soak in methanol for 1 minute to activate. Also cut out equal-sized filter papers and gather the foam pads.
3. Place membranes in cold transfer buffer after activation.
4. Remove the gels from the tank and soak in transfer buffer. Carefully remove the glass plates.
5. Make the transfer sandwich:
    a. Place the black side of the cassette down in the dish with transfer buffer. Add a foam pad and two pieces of filter paper.
    b. Carefully place gel on top and in the centre of the filter paper. Make sure the gel is oriented so that the ladder will end up on the left side of the membrane when removed. (Transfers runs from negative (black) to positive (red). So this order of materials is important to ensure the proteins run from the gel to the membrane).
    c. Carefully place the membrane on top of the gel and roll out any bubbles. Place two filter papers on top of the membrane, and then a foam pad.
    d. Carefully close the cassette and place into transfer tank. Make sure the cassette is oriented black to black and red to red.
6. Place an ice pack in the transfer tank to keep the buffer cold. Fill the tank up with transfer buffer. Attach the lid by matching the electrodes. Surround the transfer tank with ice to keep cold.
7. Turn on the voltage to 120 V and run for 2 h. Alternatively, the transfer can be run at 20 V overnight.

Probing the membrane

1. Once transfer is finished, place the membranes in containers and cover with blocking buffer. Incubate at room temperature for 1 h.
2. Pour out blocking buffer and add primary Ab at the appropriate dilution. Incubate the membranes in primary Ab overnight at 4°C or for 2 h at room temperature. Membrane should be incubated with constant shaking.
3. Following primary Ab, wash the membranes for 1 h in 1X wash buffer, changing the buffer every 10-15 minutes. This removes any unbound primary Ab.
4. Incubate the membrane for 1 h in secondary Ab at room temperature.

5. Following secondary Ab, wash the membranes again for 1 h in 1X wash buffer, changing the buffer every 10-15 minutes. This removes any unbound secondary Ab.
6. Membranes are now ready to be developed.

Developing the membrane

1. Rinse the membranes in ddH_2O to remove any excess wash buffer. Incubate the membrane in 3 mL of chemiluminescence (Millipore Luminata Forte Western HRP Substrate Cat# WBLUF0500) for 3 minutes.
2. Dip the membranes in ddH_2O to rinse of any excess chemiluminescence and place on transparency inside the developing cassette.
3. In the dark room, place a piece of film in the cassette and expose film for desired amount of time. The timing will depend on the strength of the signal.
4. After the allotted time, place the film in developer solution until a signal appears. Dip into water and then into fixer solution to stop the reaction. Ensure ample fixing time.
5. Rinse with water and allow to dry.

B-11: ELISA kits for the determination of plasma insulin, glucagon, and FGF21

While the exact procedures may differ, the principle of the ELISA is the same for all proteins of interest. All assays use a quantitative sandwich enzyme immunoassay technique. The 96-well plate that is used is coated with a monoclonal antibody for the protein of interest. Standards, controls and samples are pipetted into the wells and any of the protein of interest present binds the antibody. After washing away any unbound substances, a second enzyme-linked polyclonal antibody is added that binds the protein of interest. A second wash removes any unbound substances, after which a substrate solution is added to the well. The enzyme reaction with the substrate produces a coloured product. The reaction is stopped by the addition of a stop solution, and the intensity of the colour produced is measured by spectrophotometer. The intensity of the colour is directly proportional to the amount of protein of interest in the sample.

Rat Insulin ELISA (Alpco Cat# 80-INSRT-E01, E10)

1. Prepare kit reagents. Note: all kit reagents must be equilibrated to room temperature prior to use.
    a. Dilute conjugate stock with 10 parts conjugate buffer.
    b. Dilute wash buffer concentrate with 20 parts ddH_2O.
    c. Reconstitute the controls in the appropriate amount of ddH_2O as listed on the certificate of analysis.
2. Pipette 10 µL of standard, control and undiluted rat plasma sample into the appropriate wells of the 96-well plate.
3. Pipette 75 µL of diluted conjugate into each well. Cover plate with a plate sealer and incubate for 2 h at room temperature with shaking.

4. Decant the contents of the plate and wash the plate 6X with diluted wash buffer. Use a wash bottle and fill the wells with adequate and equal force and discard all of the buffer in between washes. After the final wash, remove any residual wash buffer and bubbles from the wells by inverting the plate and firmly tapping on absorbent paper towels.
5. Pipette 100 µL of TMB substrate into each well. Cover the plate with a plate sealer and incubate for 15 minutes at room temperature with shaking.
6. Pipette 100 µL of stop solution into each well and gently shake the plate to mix the contents.
7. Read the absorbance at 450 nm.
8. To analyze the results, generate a 5 parameter standard curve using the standards in the assay, and use this curve to determine the concentration of your samples of interest. The final results are expressed in ng/mL.

Rat FGF21 ELISA (R&D Systems Cat# MF2100)

1. Prepare kit reagents. Note: all kit reagents must be equilibrated to room temperature prior to use.
    a. Reconstitute the control with 1.0 mL of ddH_2O.
    b. Dilute 20 mL of wash buffer concentrate with ddH_2O to produce a final volume of 500 mL wash buffer.
    c. Colour reagents A and B need to be mixed together in equal volumes within 15 minutes of use. Protect from light.
2. Prepare the standard curve. Reconstitute the lyophilized standard with ddH_2O and allow to sit for 5 minutes. Make the dilutions according to the following chart. Diluent RD6Z is used for analysis with serum/plasma samples and diluent RD5Y is used for analysis with cell culture supernatant samples.

Standard #	Standard Volume	Diluent	Concentrations
Stock	0 µL	1000 µL (ddH_2O)	20,000 pg/mL
#1	100 µL of Stock	900 µL	2000 pg/mL
#2	200 µL of #1	200 µL	1000 pg/mL
#3	200 µL of #2	200 µL	500 pg/mL
#4	200 µL of #3	200 µL	250 pg/mL
#5	200 µL of #4	200 µL	125 pg/mL
#6	200 µL of #5	200 µL	62.5 pg/mL
#7	200 µL of #6	200 µL	31.3 pg/mL

3. Prepare samples. Cell culture supernatant can be analyzed undiluted. Serum and plasma samples must be diluted 1:1 with diluent RD6Z.
4. Pipette 50 µL of assay diluent RD1-41 into each well.
5. Pipette 50 µL of standard, control or sample into each well. Cover the plate with a plate sealer and incubate for 2 h at room temperature with shaking.
6. Decant the contents of the plate and wash the plate 5X with diluted wash buffer. Use a wash bottle and fill the wells with adequate and equal force and discard all of the buffer in between washes. After the final wash, remove any residual wash

buffer and bubbles from the wells by inverting the plate and firmly tapping on absorbent paper towels.

7. Pipette 100 µL of conjugate into each well. Cover the plate with a plate sealer and incubate for 2 h at room temperature with shaking.
8. Repeat the wash as in step #6.
9. Pipette 100 µL of substrate solution into each well (needs to be made immediately prior to use). Cover the plate with a plate sealer and incubate for 30 minutes at room temperature with shaking. Protect from light.
10. Add 100 µL of stop solution into each well and gently shake the plate to mix the contents.
11. Read the absorbance at 450 nm.
12. To analyze the results, generate a 4 parameter logistic (4-PL) standard curve using the standards in the assay, and use this curve to determine the concentration of your samples of interest. Account for any sample dilutions. The final results are expressed in pg/mL.

Rat Glucagon ELISA (R&D Systems Cat# DGCG0)

1. Prepare kit reagents. Note: the conjugate must be kept cold during use. All other kit reagents must be equilibrated to room temperature prior to use.
    a. Dilute 100 mL of wash buffer concentrate with ddH_2O to produce a final volume of 1000 mL wash buffer.
    b. Colour reagents A and B need to be mixed together in equal volumes within 15 minutes of use. Protect from light.
2. Prepare the standard curve. Reconstitute the standard with ddH_2O and allow to sit for 30 minutes. Make the dilutions according to the following chart. Diluent RD5-59 is used for all dilutions except for the initial stock solution.

Standard #	Standard Volume	Diluent	Concentrations
Stock	0 µL	1000 µL (ddH_2O)	20,000 pg/mL
#1	100 µL of Stock	900 µL	2000 pg/mL
#2	500 µL of #1	500 µL	1000 pg/mL
#3	500 µL of #2	500 µL	500 pg/mL
#4	500 µL of #3	500 µL	250 pg/mL
#5	500 µL of #4	500 µL	125 pg/mL
#6	500 µL of #5	500 µL	62.5 pg/mL
#7	500 µL of #6	500 µL	31.3 pg/mL

3. Wash and aspirate the plate a total of two times with diluted wash buffer prior to use. Use a wash bottle and fill the wells with adequate and equal force and discard all of the buffer in between washes. After the final wash, remove any residual wash buffer and bubbles from the wells by inverting the plate and firmly tapping on absorbent paper towels.
4. Pipette 150 µL of assay diluent R1-110 into each well.

5. Pipette 50 µL of standard, control or undiluted plasma sample into each well. Cover the plate with a plate sealer and incubate for 3 h at room temperature with shaking.
6. Decant the contents of the plate and wash the plate 4X with diluted wash buffer. Use a wash bottle and fill the wells with adequate and equal force and discard all of the buffer in between washes. After the final wash, remove any residual wash buffer and bubbles from the wells by inverting the plate and firmly tapping on absorbent paper towels.
7. Pipette 200 µL of cold conjugate into each well. Cover the plate with a plate sealer and incubate for 1 h at 2-8°C with shaking. If running more than one plate, do not stack the plates.
8. Repeat the wash as in step #6.
9. Pipette 200 µL of substrate solution into each well (needs to be made immediately prior to use). Cover the plate with a plate sealer and incubate for 30 minutes at room temperature with shaking. Protect from light.
10. Add 50 µL of stop solution into each well and gently shake the plate to mix the contents.
11. Read the absorbance at 450 nm.
12. To analyze the results, generate a standard curve with a log/log curve fit using the standards in the assay, and use this curve to determine the concentration of your samples of interest. The final results are expressed in pg/mL.

B-12: TAG Quantification using a Colorimetric Kit (BioVision Cat# K622-100)

This kit quantifies TAG concentration by converting the TAG to FFAs and glycerol and then oxidizing the glycerol to generate a product that reacts with the kit probe to generate a colour that can be measured using a spectrophotometer.

1. Prepare kit reagents. Note: all kit reagents must be equilibrated to room temperature prior to use.
    a. If needed, re-dissolve the standard. Place in hot water bath (80-100°C) for 1 minute and vortex for 30 seconds. Repeat until the standard becomes clear.
    b. Warm the probe by placing in a water bath (37°C) for 1-5 minutes.
    c. Dissolve the enzyme mix in 220 µL of assay buffer.
    d. Dissolve the lipase in 220 µL of assay buffer.
2. Prepare the standard. Dilute 40 µL of the 1 mM standard into 160 µL assay buffer to generate 0.2 mM working standard.
3. Pipette 0, 10, 20, 30, 40 and 50 µL of the 0.2 mM standard into the appropriate wells and adjust the volume of the well to 50 µL with assay buffer to generate 0, 2, 4, 6, 8, 10 nmol/well.
4. For plasma samples, pipette 5 µL of undiluted sample into the appropriate wells. Pipette 45 µL assay buffer into each well so that the final volume in the well is 50 µL.
5. Pipette 2 µL of prepared lipase into each standard and sample well. Mix and incubate 20 minutes at room temperature.

6. Prepare the TAG reaction mix (enough for all the wells you are analyzing). You will need 46 µL of assay per well, 2 µL of probe per well and 2 µL of enzyme mix per well.
7. Add 50 µL of reaction mix to each well. Cover the plate with a plate sealer and incubate at room temperature for 60 minutes with shaking. Protect from light.
8. Measure absorbance at 570 nm. To analyze the results, generate a linear standard curve using the standards in the assay. Calculate the sample TAG concentration using the following formula: Concentration = B/V x D, where B = the amount of TAG determined from the standard curve (nmol), V = the sample volume added to the well (µL) and D = the sample dilution factor. Results are expressed in mM.

Appendix C: Additional Contributions

During my Doctural tenure, I made the following contributions not included in my Dissertation:

1. Pinho, R.A., **Sepa-Kishi, D.M.**, Bikopoulos, G., Wu, M.V., Uthayakumar, A., Mohasses, A., Hughes, M.C., Perry, C.G.R., and Ceddia, R.B. (2017) High-fat diet induces skeletal muscle oxidative stress in a fiber type-dependent manner in rats. *Free Radic Biol Med.* Epub 2017 Jul 6.

2. **Sepa-Kishi, D.M.**, and Ceddia, R.B. (2016) Exercise-mediated effects on white and brown adipose tissue plasticity and metabolism. *Exerc Sport Sci Rev.* **44**, 37-44.

3. Pistor, K.E., **Sepa-Kishi, D.M. (co-first author)**, Hung, S., and Ceddia, R.B. (2014) Lipolysis, lipogenesis, and adiposity are reduced while fatty acid oxidation is increased in visceral and subcutaneous adipocytes of endurance-trained rats. *Adipocyte.* **4**, 1-10.

Appendix D: Published Work

Am J Physiol Regul Integr Comp Physiol 311: R779–R787, 2016.
First published August 24, 2016; doi:10.1152/ajpregu.00243.2016.

Antilipolytic and antilipogenic effects of the CPT-1b inhibitor oxfenicine in the white adipose tissue of rats

Diane M. Sepa-Kishi, Michelle V. Wu, Abinas Uthayakumar, Arta Mohasses, and Rolando B. Ceddia
School of Kinesiology and Health Science, York University, Toronto, Ontario, Canada

Submitted 7 June 2016; accepted in final form 17 August 2016

Sepa-Kishi DM, Wu MV, Uthayakumar A, Mohasses A, Ceddia RB. Antilipolytic and antilipogenic effects of the CPT-1b inhibitor oxfenicine in the white adipose tissue of rats. *Am J Physiol Regul Integr Comp Physiol* 311: R779–R787, 2016. First published August 24, 2016; doi:10.1152/ajpregu.00243.2016.—Oxfenicine is a carnitine-palmitoyl transferase 1b (CPT-1b)-specific inhibitor that has been shown to improve whole body insulin sensitivity while suppressing fatty acid (FA) oxidation and increasing circulating FA. Because the white adipose tissue (WAT) is an organ that stores and releases FAs, this study investigated whether oxfenicine-induced inhibition of FA oxidation affected adiposity and WAT metabolism in rats fed either low (LF) or high-fat (HF) diets. Following 8 wk of dietary intervention, male Sprague-Dawley rats were given a daily intraperitoneal injection of oxfenicine (150 mg/kg body wt) or vehicle (PBS) for 3 wk. Oxfenicine treatment reduced whole body fat oxidation, body weight, and adiposity, and improved insulin sensitivity in HF-fed rats. All of these effects occurred without alterations in food intake, energy expenditure, and ambulatory activity. In vivo oxfenicine treatment reduced FA oxidation and lipolysis in subcutaneous inguinal (SC Ing) adipocytes, whereas glucose incorporation into lipids (lipogenesis) was significantly reduced in both SC Ing and epididymal (Epid) adipocytes. In summary, our results show that oxfenicine-induced inhibition of CPT-1b markedly affects WAT metabolism, leading to reduced adiposity through a mechanism that involves reduced lipogenesis in the SC Ing and Epid fat depots of rats.

fatty-acid oxidation; subcutaneous and visceral fat; insulin resistance; lipolysis and fatty acid metabolism; CPT-1b inhibition

OBESITY IS A PREVALENT METABOLIC disorder and major risk factor for Type 2 diabetes (T2D). In this context, strategies to prevent the development of insulin resistance and progression to T2D are of great therapeutic interest. Many theories exist attempting to mechanistically link obesity and T2D and identify appropriate targets for intervention, one of which is the Randle cycle of substrate interaction (21). The Randle cycle proposed that the increases in mitochondrial acetyl-CoA, NADH:NAD^+ ratio, and citrate that occur with increased fatty acid uptake and oxidation are responsible for inhibiting key enzymes and transporters involved in glucose oxidation and uptake (21). On the basis of this theory, it was hypothesized that inhibiting fatty acid oxidation would result in an increase in glucose uptake and oxidation. While it may seem counterintuitive to decrease rates of fatty acid oxidation in a state of obesity in which fat is abundant, studies have attributed the development of insulin resistance to an overload of fatty acid oxidation and have shown that decreasing it through genetic manipulation prevents the declines seen in insulin sensitivity (15). The concern was that inhibition of β-oxidation would lead to an accumulation of lipid derivatives, such as diacylglycerol (DAG) and ceramides in skeletal muscle, which have been previously shown to contribute to the development of insulin resistance (12, 29). However, beneficial effects of reduced β-oxidation have been reported, despite intracellular accumulation of DAG and ceramides (28, 30).

Reductions in fatty acid oxidation have been achieved through the inhibition of carnitine-palmitoyl transferase-1 (CPT-1). CPT-1 is the rate-controlling enzyme for mitochondrial β-oxidation, facilitating the import of long-chain (>12C) fatty acids (LCFAs) into the mitochondria (3). Located on the outer mitochondrial membrane, CPT-1 catalyzes the reaction between long-chain acyl-CoAs and carnitine to form acylcarnitine, which is then shuttled via the carnitine acylcarnitine translocase into the mitochondria, converted back into acyl-CoA (by CPT-2), and then released to undergo β-oxidation (3). Three isoforms of CPT-1 exist: liver (CPT-1a), heart and skeletal muscle (CPT-1b), and brain (CPT-1c) (3, 22).

Oxfenicine [*S*-2-(4-hydroxyphenyl)glycine] is considered a CPT-1b-specific inhibitor. It must be transaminated to its active form, 4-hydroxyphenylglyoxylate (4-HPG), which is competitive with carnitine, preventing the formation of acylcarnitines (23). Because CPT-1b shows the highest sensitivity to 4-HPG (23), inhibition of fatty acid oxidation by oxfenicine takes place selectively in those tissues that express this CPT isoform (3). Skeletal muscle, heart, and white and brown adipose tissues are the ones with the highest content of CPT-1b in the body (3). Therefore, these tissues are expected to be the ones most responsive to oxfenicine-induced inhibition of LCFA oxidation. The effects of oxfenicine in skeletal muscle have been studied and show positive metabolic outcomes. High-fat (HF)-fed mice given daily oxfenicine injections for 14 days had a reduced area under the curve for glycemia following a glucose tolerance test compared with HF-fed control animals, indicating an improvement in whole body insulin sensitivity (14). Further analysis of the gastrocnemius muscle revealed an increased phosphorylated Akt to total Akt ratio, as well as an increase in GLUT 4 content (14).

An additional metabolic outcome of inhibiting fatty acid β-oxidation is an increase in circulating nonesterified fatty acids (NEFAs), which must find an alternate metabolic fate to oxidation. In this context, we hypothesized that the adipose tissue would undergo metabolic changes to accommodate and adjust for these excess nonoxidized fatty acids. It could do so by reducing its rates of lipolysis to prevent the further release of NEFAs, and/or by increasing rates of lipogenesis to promote the storage of excess fatty acids as triacylglycerols. These, however, have never been previously investigated. Additionally, since the adipose tissue itself also expresses CPT-1b (3), pharmacological inhibition could also have direct effects on lipid metabolism in this tissue. Importantly, metabolic differ-

Address for reprint requests and other correspondence: R. B. Ceddia, School of Kinesiology and Health Science-York Univ., 4700 Keele St., North York, ON, Canada M3J 13P3 (e-mail: roceddia@yorku.ca).

ences clearly exist between the visceral (e.g., epididymal, Epid) and the subcutaneous (SC) (e.g., SC inguinal, SC Ing) fat depots. The SC depot is considered to be metabolically protective (27) and more likely to change its metabolic function under various physiological conditions (7). However, it is currently unknown whether visceral and SC fat depots elicit distinct metabolic responses upon CPT-1b inhibition. Importantly, it has also been shown that oxidative capacity differs between the two depots (4, 11), which could significantly affect the response to inhibition of β-oxidation. Our study is the first to examine the in vivo and in vitro effects of oxfenicine-induced CPT-1b inhibition on adipocyte metabolism. We provide novel evidence that CPT-1b inhibition causes fat depot-specific adaptive metabolic responses that affect lipolysis, lipogenesis, and adiposity in rats.

MATERIALS AND METHODS

Reagents. Type II collagenase, isoproterenol, fatty acid-free BSA, palmitic acid, oxfenicine (4-hydroxy-L-phenylglycine), and free glycerol determination kit were obtained from Sigma (St. Louis, MO). [1-^{14}C] palmitic acid was from American Radiolabeled Chemicals (St. Louis, MO) and D-[U-^{14}C]glucose was from GE Healthcare Radiochemicals (Quebec City, QC, Canada). Protease (Complete Ultra Tablets) and phosphatase (PhosphoStop) inhibitors were from Roche Diagnostics (Mannheim, Germany). The NEFA kit was from Wako Chemicals (NEFA-HR kit, Richmond, VA).

Animals. Male albino rats (Sprague-Dawley strain) aged 50–55 days and weighing ~250 g (upon commencement of the diet) were housed individually at 22°C on a 12:12-h light-dark cycle and fed for 11 wk ad libitum either a low-fat (LF) (Control, 27%, 13%, and 60% of calories provided by protein, fat, and carbohydrates, respectively, energy density 3.43 kcal/g), or a high-fat (HF) diet [20%, 60%, and 20% of calories provided by protein (casein), fat (lard, soybean oil), and carbohydrates (amylodextrin/sucrose), respectively, energy density 5.24 kcal/g]. The LF control diet (standard chow catalog no. 5012) was purchased from LabDiet (St. Louis, MO) and the HF diet (cat. no. D12492) was purchased from Research Diets (New Brunswick, NJ). Food intake and body weight were measured for 2 wk prior to and every day during the oxfenicine treatment. At the end of treatment, animals were placed in the Comprehensive Laboratory Animal Monitoring System (CLAMS) from Columbus Instruments for 24 h for the measurement of in vivo metabolic parameters. The animals were allowed to acclimatize for 1 h prior to collection of data, as previously described (2). The protocol containing all animal procedures described in this study was specifically approved by the Committee on the Ethics of Animal Experiments of York University [York University Animal Care Committee (YUACC) permit no. 2012-03] and performed strictly in accordance with the YUACC guidelines. All surgery was performed under ketamine/xylazine anesthesia, and all efforts were made to minimize suffering.

In vivo treatment with oxfenicine. Following 8 wk of either LF or HF diets, rats were given a daily intraperitoneal injection of oxfenicine (150 mg/kg body wt) suspended in 1× PBS, or just PBS (control) for three consecutive weeks.

Determination of fasting plasma NEFAs and insulin and the procedure for the glucose tolerance test. Following treatment with oxfenicine (*week 11*), the animals were fasted overnight, and blood was collected by saphenous vein bleeding. The animals were then intraperitoneally injected with a 20% glucose solution (2 g/kg body wt), and saphenous blood samples were taken at 15, 30, 60, and 120 min postinjection. Glucose was measured by the glucose oxidase method using a OneTouch Ultra Mini monitor. Aliquots of blood were centrifuged for 10 min at 4°C, and plasma was stored at −80°C for subsequent analysis of NEFAs and insulin.

Adipocyte isolation. Animals were anesthetized (0.4 mg ketamine and 8 mg xylazine per 100 g body wt) in the fed state. Subcutaneous inguinal (SC Ing) and Epid fat pads were extracted and weighed. A sample of each fat pad was immediately frozen in liquid nitrogen and stored at −80°C for subsequent Western blot analysis. The remaining tissue was used for adipocyte isolation, as described previously (11). Briefly, the adipose tissue was finely minced in Krebs-Ringer buffer (0.154 M NaCl, 0.154 M KCl, 0.11 M $CaCl_2$, 0.154 M $MgSO_4$, 0.154 M KH_2PO_4, and 0.154 M $NaHCO_3$, pH 7.4) with 5.5 mM glucose and 30 mM HEPES (KRBH) supplemented with type II collagenase (1 mg/ml). The finely minced tissues were then incubated at 37°C with gentle agitation (120 orbital strokes/min) for ~30–45 min. Digested tissue was strained using a nylon mesh, and cells were transferred to 50-ml tubes, carefully washed three times and resuspended in KRBH containing 3.5% BSA (KRBH-3.5% BSA). To distribute an equal number of adipocytes in each treatment condition, cell diameters and numbers were measured, as described by DiGirolamo and Fine (5).

Determination of adipocyte lipolysis. Lipolysis was measured by incubating adipocytes (5×10^5 cells) either in the absence or presence of isoproterenol (100 nM). Triplicates for each condition were used, and the isolated adipocytes were incubated for 75 min at 37°C with gentle agitation (50 orbital strokes/min). Isoproterenol was used to stimulate lipolysis by acting as a nonspecific β-adrenergic agonist (1). After incubation, a 200-μl aliquot of media was taken for the determination of glycerol concentration.

Measurement of palmitate oxidation in adipocytes. Adipocyte oxidative capacity was assessed, as previously described, by measuring the production of $^{14}CO_2$ (11). Briefly, 2.5×10^5 cells were incubated in KRBH-3.5% BSA containing 0.2 μCi/ml of [1-^{14}C]palmitic acid and 200 μM nonlabeled palmitate for 1 h. The vials used for incubation had a centered well containing a loosely folded piece of filter paper. After the 1-h incubation period, the filter paper was moistened with 0.2 ml of 2-phenylethylamine/methanol (1:1, vol/vol), and the media were acidified with 0.2 ml of H_2SO_4 (5N). The flasks were maintained sealed at 37°C for an additional 1 h for the collection of CO_2 released from the cells and the media. At the end of the incubation, the filter paper was removed and transferred to a scintillation vial for radioactivity counting (8, 10).

Western blot analysis of content and phosphorylation of proteins. Adipose tissue collected from the Epid and SC Ing depots was homogenized in a buffer containing 25 mM Tris·HCl, 25 mM NaCl (pH 7.4), 1 mM $MgCl_2$, 2.7 mM KCl, 1% Triton-X, and protease and phosphatase inhibitors (Roche Diagnostics, Mannheim, Germany). Homogenates were centrifuged, the infranatant was collected, and an aliquot was used to measure protein by the Bradford method. Samples were diluted 1:1 (vol/vol) with 2 × Laemmli sample buffer, heated to 95°C for 5 min, subjected to SDS-PAGE, and transferred to PVDF membrane. Membranes were subsequently probed with primary antibodies (1:1,000 dilution), followed by horseradish peroxidase-conjugated anti-rabbit secondary antibody (dilution of 1:2,000). β-actin was used as a loading control. Blots were visualized using chemiluminescence (Luminata forte, Millipore, Billerica, MA) and were scanned directly into an image quantification program.

In vitro treatment of isolated adipocytes with oxfenicine. SC Ing and Epid adipocytes were isolated, as previously described, from LF-fed rats weighing ~250 g. Following isolation, cells were incubated in various concentrations of oxfenicine for 2 h at 37°C with gentle agitation. Assays for lipolysis, palmitate oxidation, and glucose incorporation into lipids were then performed as described in these METHODS.

Measurement of glucose incorporation into lipids in adipocytes. Following treatment with oxfenicine, glucose incorporation into lipids in adipocytes was assessed as previously described (20). Briefly, 1×10^6 cells were incubated in KRBH-3.5% BSA (containing 5 mM glucose) with 0.5 μCi/ml of D-[U-^{14}C]glucose under basal or insulin-stimulated (100 nM) conditions for 1 h at 37°C. The cells were then lysed by the addition of H_2SO_4 (5N) and 5 ml of Dole's reagent

(40:10:1 of isopropanol, heptane and 1 M H_2SO_4, vol/vol/vol) was subsequently added to the vial to extract total lipids. Radioactivity of the total lipid fraction was counted and corresponds to glucose conversion to TAG (6).

Statistical analyses. Normality was evaluated using the Kolmogorov-Smirnov normality test. For data that passed normality, statistical analyses were assessed by one-way and two-way ANOVAs with Bonferroni post hoc test. For data that did not pass normality, statistical analyses were assessed by Kruskal-Wallis test with the Dunn multiple-comparison test or Mann Whitney *U*-test, as indicated in the figure legends. Statistical significance was set at $P < 0.05$.

RESULTS

Oxygen consumption, ambulatory activity, respiratory exchange ratio, and fasting plasma NEFAs. To examine the in vivo effects of the oxfenicine treatment, animals were placed in the CLAMS for 24 h following oxfenicine treatment and their $\dot{V}O_2$, ambulatory activity, and respiratory exchange ratio (RER) were measured. Oxfenicine had no effect on $\dot{V}O_2$ (Fig. 1*A*) or ambulatory activity (Fig. 1*B*) during the light or dark cycles. Treatment with oxfenicine also had no effect on the RER of animals fed the LF diet, whereas those fed a HF diet had significantly higher RER values, particularly during the dark cycle (Fig. 1, *C* and *D*). This is indicative of the effectiveness of oxfenicine at inhibiting fatty acid β-oxidation, resulting in an increased reliance on carbohydrate oxidation. This was more pronounced during the dark cycle (1900 to 0700), when the animals were the most active and ate the most food (0.830 ± 0.00271 $\dot{V}CO_2/\dot{V}O_2$ vs. 0.796 ± 0.00244, $\dot{V}CO_2/\dot{V}O_2$, Fig. 1, *C* and *D*). Fasting plasma NEFAs were also 1.45- and 1.46-fold higher in the LF- and HF-fed animals, respectively, following 3 wk of oxfenicine treatment (Fig. 1*E*). An increase in circulating fatty acids provides further evidence of the effectiveness of the oxfenicine treatment in reducing fatty acid oxidation.

Fasting plasma insulin and glucose tolerance test. As expected, HF-fed animals had a 1.6-fold increase in fasting plasma insulin compared with controls, indicating that these animals were insulin resistant (Fig. 2*A*). Further analysis of the area under the curve (AUC) of the glucose tolerance test (GTT) showed that plasma glucose remained 1.3-fold higher in the HF-fed animals compared with the LF-fed controls, confirming the development of insulin resistance in HF-fed animals (Fig. 2, *B* and *C*). Oxfenicine treatment reversed the effects of the HF diet, returning fasting insulin and plasma glucose AUC levels to those seen in the control animals (Fig. 2). Oxfenicine

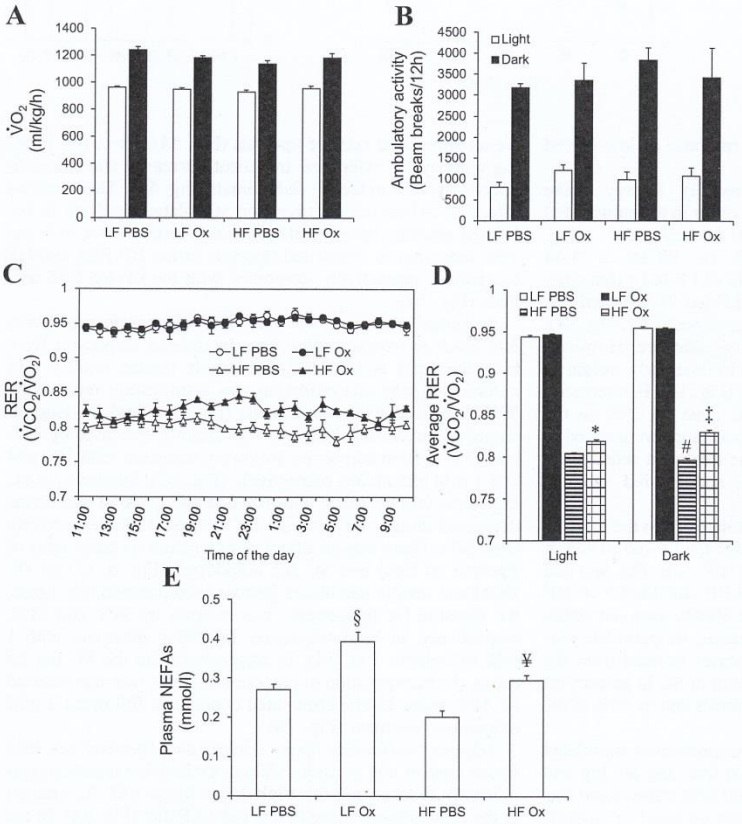

Fig. 1. Oxfenicine does not affect $\dot{V}O_2$ or ambulatory activity, but reduces whole body fat oxidation and increases circulating nonesterified fatty acids (NEFAs). The animals were fed high-fat (HF) or low-fat (LF) diets for 8 wk and then daily injected for 3 wk with either PBS (control) or oxfenicine (Ox; 150 mg/kg body wt). At the end of the oxfenicine treatment, rats were placed in the Comprehensive Laboratory Animal Monitoring System (CLAMS) for the determination of $\dot{V}O_2$ (*A*), ambulatory activity (*B*), and respiratory exchange ratio (RER) during a 24-h period (*C* and *D*). Subsequently, the animals were overnight-fasted, and blood was collected for the determination of NEFAs in the plasma (*E*). Kruskal-Wallis test, $n = 5$ for ambulatory activity. Mann-Whitney *U*-test, $n = 5$ for NEFAs. All other data were obtained by two-way analyses of variance (ANOVAS), $n = 5$. $^*P < 0.05$ vs. HF PBS in the light cycle. #$P < 0.05$ vs. HF PBS light cycle. ‡$P < 0.05$ vs. HF Ox light cycle and HF PBS dark cycle. §$P < 0.05$ vs. LF PBS. ¥$P < 0.01$ vs. HF PBS.

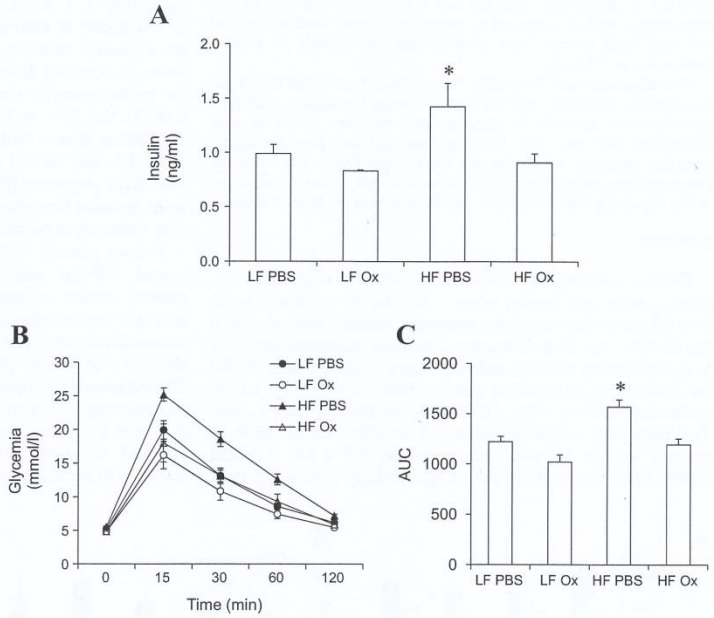

Fig. 2. Oxfenicine normalizes fasting insulin and improves insulin sensitivity. The animals were fed HF or LF diets for 8 wk and then daily injected for 3 wk with either PBS (control) or Ox (150 mg/kg body wt). *A*: at the end of the oxfenicine treatment, rats were fasted overnight, and blood was collected for the determination of insulin in the plasma. *B* and *C*: overnight-fasted rats then underwent an intraperitoneal glucose tolerance test. AUC, area under the curve. Mann-Whitney *U*-test, $n = 5$. *$P < 0.05$ vs. LF PBS and HF Ox.

treatment did not affect the glycemic response of low-fat-fed rats during the GTT.

Body weight, food intake, and adiposity. Energy intake during the oxfenicine treatment did not differ in the animals fed the LF (101.56 ± 5.68 vs. 94.45 ± 2.41 kcal·rat^{-1}·day^{-1}, Fig. 3*B*) or HF diet (100.40 ± 3.68 vs. 98.46 ± 4.44 kcal·rat^{-1}·day^{-1}, Fig. 3*B*). Body weight of LF-fed oxfenicine-treated rats was ~8% lower than the LF-fed PBS-treated rats (519.31 ± 9.64 g vs. 566.62 ± 24.05 g, respectively, Fig. 3*A*), although this did not reach statistical significance. However, there was a 10% significant reduction in final body weight in HF-fed animals treated with oxfenicine (Fig. 3*A*). Furthermore, oxfenicine treatment reduced Epid fat mass by 29% in the HF-fed animals (Fig. 3*C*). This effect was more pronounced in the SC Ing fat depot where oxfenicine treatment reduced fat mass by 43% and 37% in the LF- and HF-fed animals, respectively (Fig. 3*D*).

Palmitate oxidation. In adipocytes isolated from the Epid fat depot, palmitate oxidation was reduced in the LF-fed (0.965 ± 0.102 vs. 0.711 ± 0.056 nmol/h/2.5 × 10^5 cells, Fig. 4*A*) and HF-fed (1.092 ± 0.11 vs. 0.952 ± 0.101 nmol/h/2.5 × 10^5 cells, Fig. 4*A*) animals, although these effects were not statistically significant. This effect of oxfenicine on palmitate oxidation was more pronounced in adipocytes isolated from the SC Ing depot. In fact, palmitate oxidation in SC In adipocytes was decreased by 40% in the LF-fed animals and by 63% in the HF-fed animals (Fig. 4*B*).

Lipolysis. As expected, basal and isoproterenol-stimulated lipolysis differed in adipocytes isolated from the SC Ing and Epid fat depots (Fig. 5, *A* and *B*). In Epid adipocytes, there was no effect of diet or oxfenicine treatment on basal or isoproterenol-stimulated rates of lipolysis (Fig. 5*A*). However, in SC Ing adipocytes, oxfenicine treatment decreased stimulated lipolysis by 42% in the LF-fed animals (Fig. 5*B*). There was no effect of oxfenicine treatment on stimulated lipolysis in the HF-fed animals; however, the diet itself resulted in a 74% and 73% reduction in stimulated lipolysis in the HF PBS and HF Ox groups, respectively, compared with the LF-fed PBS animals (Fig. 5*B*).

Palmitate oxidation, lipolysis, and glucose incorporation into lipids in isolated adipocytes. In isolated adipocytes from both the Epid and SC Ing fat depots treated with 1 mM oxfenicine, palmitate oxidation was significantly reduced by 50% compared with control cells (Fig. 6, *A* and *B*). Isoproterenol-stimulated lipolysis was significantly decreased by 20% and 12% in Epid adipocytes following treatment with 100 μM and 1 mM oxfenicine, respectively (Fig. 6*C*). Similarly, in SC Ing adipocytes treatment with 100 μM and 1 mM of oxfenicine decreased stimulated lipolysis by 8% and 18%, respectively (Fig. 6*D*). There was no effect of oxfenicine on basal rates of lipolysis in Epid and SC Ing adipocytes (Fig. 6, *C* and *D*). Basal and insulin-stimulated glucose incorporation into lipids, the measure for lipogenesis, was reduced by 39% and 31%, respectively, in Epid adipocytes following treatment with 1 mM oxfenicine (Fig. 7*A*). In adipocytes from the SC Ing fat depot, the incorporation of glucose into lipids was also reduced by 41% under insulin-stimulated conditions, following 1 mM oxfenicine treatment (Fig. 7*B*).

Adipose triglyceride lipase content and hormone sensitive lipase content and phosphorylation. Oxfenicine treatment significantly reduced adipose triglyceride lipase (ATGL) content in the Epid adipose tissue in rats fed a LF diet (Fig. 8*A*). In the

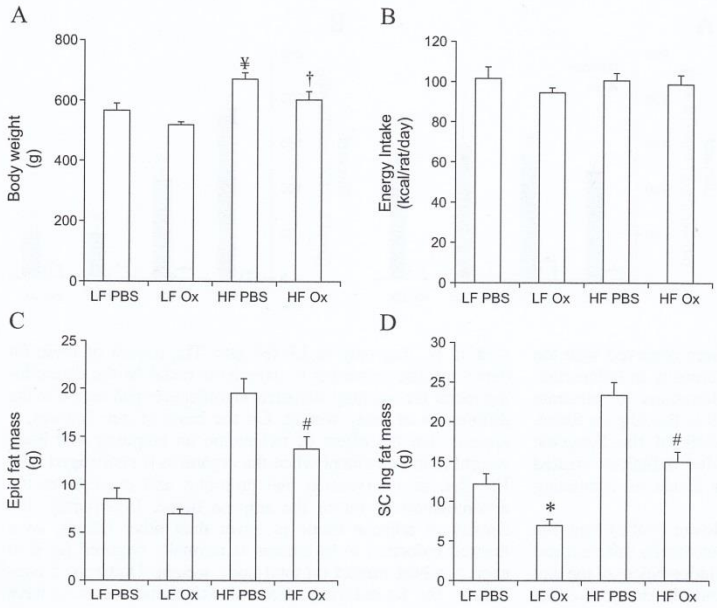

Fig. 3. Oxfenicine does not affect energy intake (*B*), but reduces body weight (*A*) and epididymal (Epid; *C*), and SC Ing (*D*) fat pad mass. Rats were fed a LF or HF diet for 8 wk and treated with either PBS or Ox (150 mg/kg body wt) for 3 wk. Kruskal-Wallis test, $n = 5$ for energy intake. All other data, two-way ANOVAs, $n = 5$. ¥$P < 0.01$ vs. LF PBS. †$P < 0.05$ vs. HF PBS and LF Ox. *$P < 0.05$ vs. LF PBS. #$P < 0.01$ vs. HF PBS.

HF-fed animals, there was no effect of oxfenicine; however, the diet itself resulted in a significant decrease in ATGL content in this fat depot (Fig. 8*A*). In contrast, ATGL content in the SC Ing adipose tissue was significantly increased with a HF diet in the PBS control animals, with no effect of oxfenicine treatment evident in rats fed either the LF or HF diet (Fig. 8*B*). There was no difference in phosphorylation of hormone sensitive lipase $(HSL)_{660}$ in either fat depot with diet or oxfenicine treatment (Fig. 8, *C* and *D*).

DISCUSSION

Here, we report the novel findings of depot-specific alterations in adipose tissue and adipocyte metabolism following pharmacological selective inhibition of CPT-1b. The effects were characterized by a reduction in isoproterenol-stimulated lipolysis in adipocytes from the SC Ing fat depot following 3 wk of daily oxfenicine injection, indicating an increased sensitivity to oxfenicine in this fat depot. In vitro incubation of adipocytes from both fat depots with oxfenicine also resulted in a reduction in stimulated rates of lipolysis. This suggests that fat cells adjusted their metabolism to compensate for the increased circulating NEFAs seen with inhibition of β-oxidation. We also expected glucose incorporation into lipids to be increased with oxfenicine treatment to promote storage of the excess lipids, resulting from CPT-1b inhibition. Contrary to our original hypothesis, basal and insulin-stimulated glucose incorporation into lipids was significantly reduced in Epid and SC Ing adipocytes directly treated with oxfenicine. This reduction likely contributed toward sustaining elevated levels of circulating NEFAs seen in oxfenicine-treated rats. It also, at least partially, explains the decrease in Epid and SC Ing fat mass observed in oxfenicine-treated animals, as no alterations

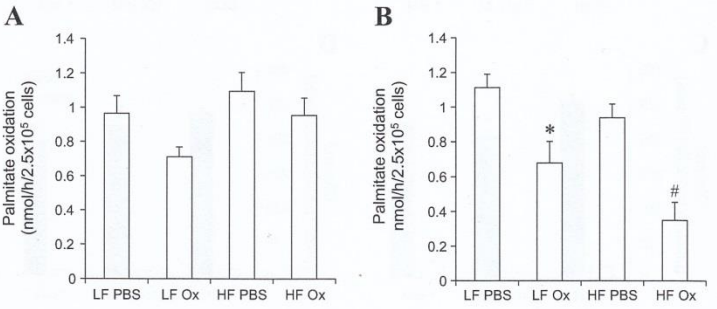

Fig. 4. Administration of oxfenicine reduces palmitate oxidation in epididymal (*A*) and subcutaneous inguinal (*B*) adipocytes. Rats were fed LF or HF diets for 8 wk and then either injected with PBS or Ox (150 mg/kg body wt) for 3 wk. Two-way ANOVAs, $n = 5$. *$P < 0.05$ vs. LF PBS. #$P < 0.01$ vs. HF PBS.

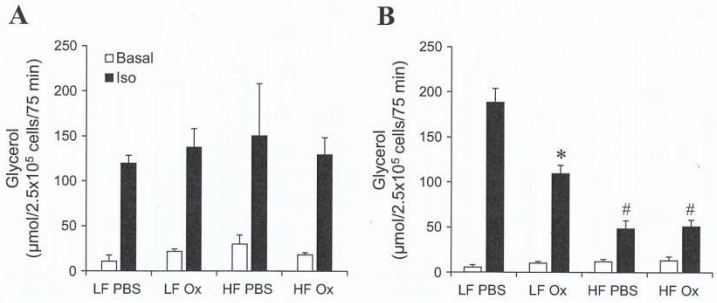

Fig. 5. Glycerol release is reduced in subcutaneous inguinal (*B*) but not in epididymal (*A*) adipocytes from LF- or HF-fed rats either injected with PBS or Ox (150 mg/kg body wt). Two-way ANOVAs, $n = 5$. *$P < 0.001$ vs. LF PBS, HF PBS, and HF Ox. #$P < 0.001$ vs. LF PBS and LF Ox.

in food intake or ambulatory activity were observed with the treatment. This suggests that reduced adiposity in oxfenicine-treated rats was mainly driven by alterations in substrate partitioning, preventing the storage of fat in the adipose tissue. This could be attributed to lower levels of the lipogenic hormone insulin in the plasma of HF-fed oxfenicine-treated rats, which is compatible with higher levels of circulating NEFAs in oxfenicine-treated rats.

Body weight of LF Ox was slightly lower (~8%) than that of LF PBS rats; however, this was not statistically different and did not characterize that rats lost weight independent of the diet following oxfenicine treatment. This could be due to the fact that in LF-fed rats treated with oxfenicine only the SC Ing fat pad was significantly reduced (43%) in its mass (Fig. 3*C*), whereas in HF-fed rats oxfenicine treatment caused a marked reduction in both Epid (29%) and SC Ing fat (37%) masses. Combining the effect of oxfenicine on Epid and SC Ing fat depots adds up to a 66% reduction in adiposity as opposed to 43% in SC Ing only in LF-fed rats. The impact of these fat depot-specific responses to oxfenicine could be the determining factor for reaching statistical significance with regard to the differences of body weight. On the basis of our findings, it appears that the effect of oxfenicine on adiposity and body weight is more evident when the organism is challenged by a HF diet, an intervention that promotes and exacerbates the accumulation of fat in the adipose tissue. Importantly, the density of adipose tissue is lower than other tissues, so a marked reduction in its content is normally required for it to exert a robust impact on total body weight. Under such conditions, the fat-reducing effect of oxfenicine seems to have caused a more pronounced effect on total body weight in HF-fed rats, and likely allowed statistical significance to be reached in this group.

The effectiveness of our pharmacological inhibition on CPT-1b was evaluated by placing the animals in the CLAMS for 24 h and measuring RER as an indication of substrate

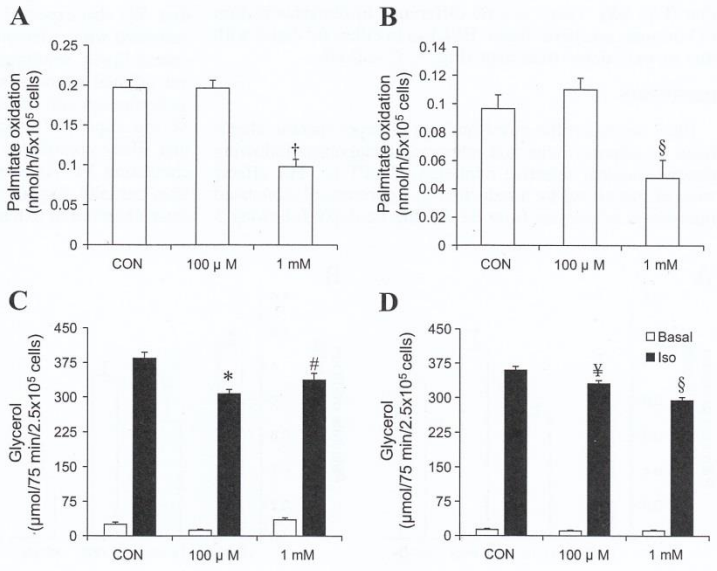

Fig. 6. Treatment with 1 mM oxfenicine reduces palmitate oxidation and isoproterenol (ISO)-stimulated lipolysis in epididymal (*A* and *C*) and subcutaneous inguinal (*B* and *D*) adipocytes. Adipocytes were extracted from lean rats and exposed to Ox (100 μM or 1 mM) in vitro for 2 h and then assayed for glycerol and palmitate oxidation. Two-way and one-way ANOVAs, $n = 5$. §$P < 0.01$ vs. CON and 100 μM. †$P < 0.0001$ vs. CON and 100 μM. *$P < 0.001$ vs. CON. #$P < 0.01$ vs. CON. ¥$P < 0.05$ vs. CON.

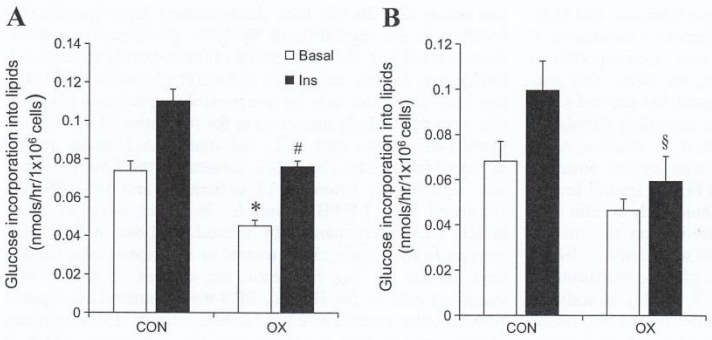

Fig. 7. Oxfenicine reduces glucose incorporation into lipids in epididymal (*A*) and subcutaneous inguinal (*B*) adipocytes. Adipocytes were extracted from lean rats and exposed to Ox (1 mM) in vitro for 2 h and then assayed for glucose incorporation into lipids. Two-way ANOVAs, $n = 5$. *$P < 0.001$ vs. Con Bas. #$P < 0.001$ vs. Con Ins. §$P < 0.05$ vs. Con Ins.

oxidation. There was a significant increase in RER in HF-fed, oxfenicine-treated animals during both the light and dark cycles, indicating a shift toward carbohydrate metabolism. Similarly to previous work (14, 30), the effect was more pronounced during the dark cycle, as this was when the animals were eating the most food and were the most active, requiring an increase in energy metabolism. Interestingly, there was no change in RER in animals fed the LF diet and treated with oxfenicine in either the light or dark cycles. Oxfenicine still seems to be exerting its inhibitory effects on β-oxidation in these animals, as plasma NEFAs are increased following treatment, to a similar extent as that seen in the HF-fed animals. It is possible that any changes in RER are masked in the LF-fed animals, as they are consuming a diet relatively low in fat that provides 60% of its energy content from carbohydrates. Under such conditions, carbohydrate is the main substrate for oxidation, so inhibition of fat oxidation does not affect RER in these animals. $\dot{V}O_2$ and ambulatory activity were also measured in vivo in the CLAMS and was not different between any of the groups, suggesting that these variables did not have an effect on the RER and adiposity data.

Previous studies examining the effects of CPT-1b inhibition have focused mainly on the metabolic improvements in skeletal muscle in animals fed a HF diet. Keung et al. (14) treated HF-fed mice with daily injections of oxfenicine for 4 wk, which resulted in an increase in the phosphorylated Akt:total Akt ratio, as well as an increase in GLUT 4 content in the gastrocnemius muscle. This was accompanied by a reduction

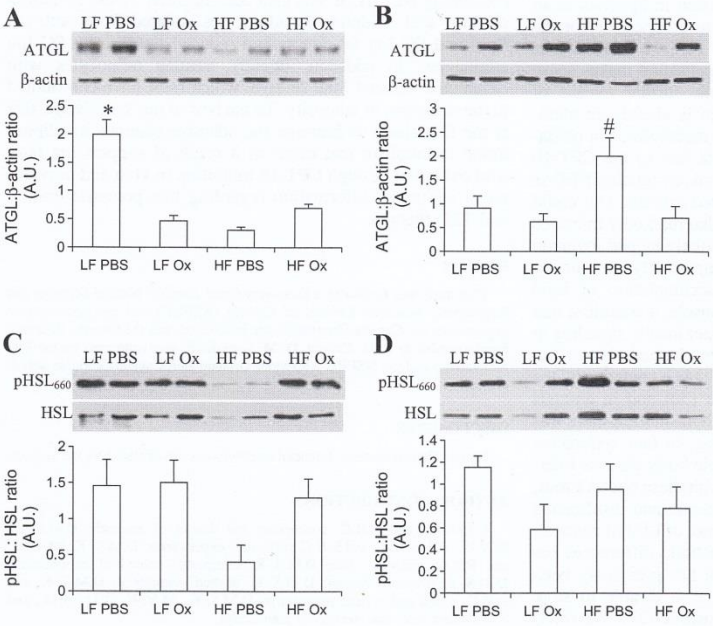

Fig. 8. Effects of oxfenicine on content of ATGL and content and phosphorylation of hormone sensitive lipase (HSL) in epididymal (*A* and *C*) and subcutaneous inguinal (*B* and *D*) adipose tissue. Animals were fed either a LF or HF diet for 8 wk, followed by 3 wk of treatment with PBS or Ox (150 mg/kg body wt). Mann-Whitney *U*-test; $n = 3$. *$P < 0.05$ vs. LF Ox and HF PBS. #$P < 0.05$ vs. all other groups.

in AUC for glycemia following a glucose tolerance test (14). Treatment of HF-fed mice with daily injections of etomoxir, a broad CPT-1 inhibitor, for 8 days has also been reported to improve whole body glucose tolerance, an effect that was accompanied by increases in phosphorylated Akt and in GLUT 4 content in the tibialis anterior muscle of mice (28). Similar to this work, we also observed a reduction in glucose AUC following a GTT in our HF-fed, oxfenicine-treated animals. This was accompanied by a reduction in fasting insulin levels, indicating an overall improvement in whole body insulin sensitivity. The effects of fatty acid inhibition on the insulin signaling pathway and whole body insulin sensitivity are likely secondary to increases in skeletal muscle glucose oxidation, as has been observed in numerous studies (17, 18, 21). In addition to the beneficial effects on glucose metabolism, we also found that oxfenicine treatment reduced body weight and adiposity in HF-fed animals. This is in line with data from Wicks et al. (30) in which a reduction in body weight and adiposity was reported in mice with muscle-specific deletion of CPT1b (Cpt1b$^{m-/-}$). Unlike our study, reduction in body weight in Cpt1b$^{m-/-}$ mice could be partially explained by a reduction in food intake (30); however, the reduction in food intake began 3–4 wk after the initial decrease in body weight and adiposity occurred, suggesting that another variable could have contributed to the decrease in weight. Our study provides evidence that a reduction in lipogenesis in the fat depots could be this alternative variable, which could at least partially explain the reduction in adiposity induced by the suppression of CPT-1b activity.

A further effect of oxfenicine treatment was the reduction in stimulated lipolysis in adipocytes isolated from the SC Ing fat depot of LF- and HF-fed animals. Stimulated lipolysis was also reduced in adipocytes that were directly treated with 1 mM oxfenicine. We expected to find a reduction in lipolysis as an adjustment made by the adipose tissue to compensate for the increased circulating NEFAs seen with CPT-1b inhibition in both LF- and HF-fed animals. The compensation makes sense physiologically, as it would prevent the further release of NEFAs into the circulation, where there is already an abundance. These NEFAs are not able to be metabolized in oxidative tissues, such as the skeletal muscle due to the CPT-1b inhibition. Despite the decrease in lipolysis, circulating NEFAs were still elevated in the oxfenicine-treated animals. This could be due to the fact that lipogenesis was also markedly inhibited in oxfenicine-treated adipocytes, which likely helped maintain elevated levels of circulating NEFAs. Importantly, chronically elevated NEFAs could result in an accumulation of lipid species in tissues such as the skeletal muscle, a condition that has been demonstrated to negatively impact insulin signaling in this tissue (13). Previous studies have, indeed, shown an increase in intramyocellular lipid and DAG contents in the skeletal muscle of the Cpt1b$^{m-/-}$ mice (30) and in animals treated with etomoxir (28). However, in both studies, there was no detrimental effect on insulin signaling. In fact, oxfenicine treatment led to an improvement in whole body glucose tolerance (28, 30). Our data are also in line with these observations, since oxfenicine treatment reduced glycemia and insulinemia in HF-fed animals to values similar to those of LF-fed controls.

Our novel results emphasize the metabolic differences between fat depots. The SC Ing fat depot has previously been shown to be metabolically protective, as it is able to store excess lipid, while remaining insulin sensitive (27). We (8, 9) and others (24, 26, 27) have demonstrated depot-specific differences in the regulation of lipolysis; however, the mechanisms underlying these differences remain poorly understood. Differences in HSL expression and activity between the SC Ing and Epid fat depots may be one possible explanation (24, 26). We were particularly interested in the regulation of ATGL, the main TAG lipase, and HSL, the main DAG lipase, in the different fat depots. The ATGL content in the Epid fat depot was significantly lower in LF-oxfenicine and HF-PBS rats compared with LF-PBS controls. However, none of these effects were accompanied by altered lipolysis in Epid adipocytes from animals either treated or nontreated with oxfenicine. In the SC Ing fat depot, the content of ATGL was increased only in the HF-fed, PBS-treated animals compared with all other groups, whereas no difference in HSL phosphorylation at serine-660 was found between any groups. ATGL is regulated by an activator, comparative gene identification-58 (16), and the full activation of both ATGL and HSL has been shown to require the phosphorylation of perilipin A (19, 25). Therefore, it is possible that lipolysis is being regulated at other proteins besides ATGL and HSL, and additional studies are required to test these possibilities.

Perspectives and Significance

Chronic CPT-1b inhibition has been shown to significantly improve whole body and skeletal muscle insulin sensitivity, making it a potential obesity and T2D therapy. In our study, we present novel findings showing that oxfenicine treatment also altered lipid metabolism in adipose tissue, resulting in a reduction in fat mass in animals fed a HF diet. A daily dose of oxfenicine for 3 wk was sufficient to increase RER and circulating NEFAs. It was also accompanied by the inhibition of fatty acid oxidation in adipocytes isolated from both the Epid and SC Ing fat depots and reduced lipolysis in SC Ing adipocytes. In addition, directly treating adipocytes with oxfenicine reduced lipid storage, which must have contributed to the reduction of adiposity. To the best of our knowledge, this is the first study to examine the adaptive changes in adipose tissue metabolism that occur as a result of suppressing fatty acid oxidation through CPT-1b inhibition in vivo and provides novel additional information regarding this potential obesity and T2D therapy.

GRANTS

This study was funded by a Discovery Grant from the Natural Sciences and Engineering Research Council of Canada (NSERC) and by infrastructure grants from the Canada Foundation for Innovation and the Ontario Research Fund awarded to R. B. Ceddia. D. M. Sepa-Kishi was supported by the Elia Scholarship and the NSERC Alexander Graham Bell Canada Graduate Scholarship.

DISCLOSURES

No conflicts of interest, financial or otherwise, are declared by the authors.

AUTHOR CONTRIBUTIONS

D.M.S.-K. and R.B.C. conception and design of research; D.M.S.-K., M.V.W., A.U., A.M., and R.B.C. performed experiments; D.M.S.-K., M.V.W., and R.B.C. analyzed data; D.M.S.-K. interpreted results of experiments; D.M.S.-K. prepared figures; D.M.S.-K. drafted manuscript; D.M.S.-K. and R.B.C. edited and revised manuscript; D.M.S.-K., M.V.W., A.U., A.M., and R.B.C. approved final version of manuscript.

REFERENCES

1. **Ahlquist RP.** Present state of α- and β-adrenergic drugs I. The adrenergic receptor. *Am Heart J* 92: 661–664, 1976.
2. **Araujo RL, Andrade BM, Padrón AS, Gaidhu MP, Perry RLS, Carvalho DP, Ceddia RB.** High-fat diet increases thyrotropin and oxygen consumption without altering circulating 3,5,3′-triiodothyronine (T3) and thyroxine in rats: the role of iodothyronine deiodinases, reverse T3 production, and whole-body fat oxidation. *Endocrinology* 151: 3460–3469, 2010.
3. **Ceccarelli SM, Chomienne O, Gubler M, Arduini A.** Carnitine palmitoyltransferase (CPT) modulators: a medicinal chemistry perspective on 35 years of research. *J Med Chem* 54: 3109–3152, 2011.
4. **Deveaud C, Beauvoit B, Salin B, Schaeffer J, Rigoulet M.** Regional differences in oxidative capacity of rat white adipose tissue are linked to the mitochondrial content of mature adipocytes. *Mol Cell Biochem* 267: 157–166, 2004.
5. **DiGirolamo M, Fine JB.** Cellularity measurements. *Methods Mol Biol* 155: 65–75, 2001.
6. **DiGirolamo M.** Measurements of glucose conversion to its metabolites. In: *Methods in Molecular Biology. Adipose Tissue Protocols*, edited by Ailhaud G. Totowa, NJ: Humana Press, vol. 155, 2001, p. 181–192.
7. **Frontini A, Cinti S.** Distribution and development of brown adipocytes in the murine and human adipose organ. *Cell Metab* 11: 253–256, 2010.
8. **Gaidhu M, Anthony N.** Dysregulation of lipolysis and lipid metabolism in visceral and subcutaneous adipocytes by high-fat diet: role of ATGL, HSL, and AMPK. *Am J Physiol Cell Physiol* 298: C961–C971, 2010.
9. **Gaidhu MP, Bikopoulos G, Ceddia RB.** Chronic AICAR-induced AMP-kinase activation regulates adipocyte lipolysis in a time-dependent and fat depot-specific manner in rats. *Am J Physiol Cell Physiol* 303: C1192–C1197, 2012.
10. **Gaidhu MP, Fediuc S, Anthony NM, So M, Mirpourian M, Perry RLS, Ceddia RB.** Prolonged AICAR-induced AMP-kinase activation promotes energy dissipation in white adipocytes: novel mechanisms integrating HSL and ATGL. *J Lipid Res* 50: 704–715, 2009.
11. **Gaidhu MP, Frontini A, Hung S, Pistor K, Cinti S, Ceddia RB.** Chronic AMP-kinase activation with AICAR reduces adiposity by remodeling adipocyte metabolism and increasing leptin sensitivity. *J Lipid Res* 52: 1702–1711, 2011.
12. **Itani SI, Ruderman NB, Schmieder F, Boden G.** Lipid-induced insulin resistance in human muscle is associated with changes in diacylglycerol, protein kinase C, and IκB-α. *Diabetes* 51: 2005–2011, 2002.
13. **Jornayvaz FR, Shulman GI.** Diacylglycerol activation of protein kinase Cε and hepatic insulin resistance. *Cell Metab* 15: 574–584, 2012.
14. **Keung W, Ussher JR, Jaswal JS, Raubenheimer M, Lam VHM, Wagg CS, Lopaschuk GD.** Inhibition of carnitine palmitoyltransferase-1 activity alleviates insulin resistance in diet-induced obese mice. *Diabetes* 62: 711–720, 2013.
15. **Koves TR, Ussher JR, Noland RC, Slentz D, Mosedale M, Ilkayeva O, Bain J, Stevens R, Dyck JRB, Newgard CB, Lopaschuk GD, Muoio DM.** Mitochondrial overload and incomplete fatty acid oxidation contribute to skeletal muscle insulin resistance. *Cell Metab* 7: 45–56, 2008.
16. **Lass A, Zimmermann R, Haemmerle G, Riederer M, Schoiswohl G, Schweiger M, Kienesberger P, Strauss JG, Gorkiewicz G, Zechner R.** Adipose triglyceride lipase-mediated lipolysis of cellular fat stores is activated by CGI-58 and defective in Chanarin-Dorfman Syndrome. *Cell Metab* 3: 309–319, 2006.
17. **Li J, Stillman JS, Clore JN, Blackard WG.** Skeletal muscle lipids and glycogen mask substrate competition (Randle cycle). *Metabolism* 42: 451–456, 1993.
18. **Lillioja S, Bogardus C, Mott DM, Kennedy AL, Knowler WC, Howard BV.** Relationship between insulin-mediated glucose disposal and lipid-metabolism in man. *J Clin Invest* 75: 1106–1115, 1985.
19. **Miyoshi H, Perfield JW, Souza SC, Shen WJ, Zhang HH, Stancheva ZS, Kraemer FB, Obin MS, Greenberg AS.** Control of adipose triglyceride lipase action by serine 517 of perilipin A globally regulates protein kinase a-stimulated lipolysis in adipocytes. *J Biol Chem* 282: 996–1002, 2007.
20. **Pistor KE, Sepa-Kishi DM, Hung S, Ceddia RB.** Lipolysis, lipogenesis, and adiposity are reduced while fatty acid oxidation is increased in visceral and subcutaneous adipocytes of endurance-trained rats. *Adipocyte* 4: 22–31, 2014.
21. **Randle PJ, Garland PB, Hales CN, Newsholme EA.** The glucose fatty-acid cycle- Its role in insulin sensitivity and the metabolic disturbances of diabetes mellitus. *Lancet* 1: 785–789, 1963.
22. **Schreurs M, Kuipers F, van der Leij FR.** Regulatory enzymes of mitochondrial beta-oxidation as targets for treatment of the metabolic syndrome. *Obes Rev* 11: 380–388, 2010.
23. **Stephens TW, Higgins AJ, Cook GA, Harris RA.** Two mechanisms produce tissue-specific inhibition of fatty acid oxidation by oxfenicine. *Biochem J* 227: 651–660, 1985.
24. **Sztalryd C, Kraemer FB.** Differences in hormone-sensitive lipase expression in white adipose tissue from various anatomic locations of the rat. *Metabolism* 43: 241–247, 1994.
25. **Sztalryd C, Xu G, Dorward H, Tansey JT, Contreras AJ, Kimmel AR, Londos C.** Perilipin A is essential for the translocation of hormone-sensitive lipase during lipolytic activation. *J Cell Biol* 161: 1093–1103, 2003.
26. **Tavernier G, Galitzky J, Valet P, Remaury a Bouloumie a Lafontan M, Langin D.** Molecular mechanisms underlying regional variations of catecholamine-induced lipolysis in rat adipocytes. *Am J Physiol Endocrinol Metab* 268: E1135–E1142, 1995.
27. **Tchkonia T, Thomou T, Zhu Y, Karagiannides I, Pothoulakis C, Jensen MD, Kirkland JL.** Mechanisms and metabolic implications of regional differences among fat depots. *Cell Metab* 17: 644–656, 2013.
28. **Timmers S, Nabben M, Bosma M, van Bree B, Lenaers E, van Beurden D, Schaart G, Westerterp-Plantenga MS, Langhans W, Hesselink MKC, Schrauwen-Hinderling VB, Schrauwen P.** Augmenting muscle diacylglycerol and triacylglycerol content by blocking fatty acid oxidation does not impede insulin sensitivity. *Proc Natl Acad Sci USA* 109: 11711–11716, 2012.
29. **Ussher JR, Koves TR, Cadete VJJ, Zhang L, Jaswal JS, Swyrd SJ, Lopaschuk DG, Proctor SD, Keung W, Muoio DM, Lopaschuk GD.** Inhibition of de novo ceramide synthesis reverses diet-induced insulin resistance and enhances whole-body oxygen consumption. *Diabetes* 59: 2453–2464, 2010.
30. **Wicks SE, Vandanmagsar B, Haynie KR, Fuller SE, Warfel JD, Stephens JM, Wang M, Han X, Zhang J, Noland RC, Mynatt RL.** Impaired mitochondrial fat oxidation induces adaptive remodeling of muscle metabolism. *Proc Natl Acad Sci USA* 112: E3300–E3309, 2015.